

**FREQUENCY SCALING IN MILLIMETRE-WAVE RAIN
ATTENUATION ESTIMATION FOR SATELLITE LINK
IN TROPICAL REGIONS**

BY

NUR HANIS SABRINA BINTI SUHAIMI

**A thesis submitted in fulfilment of the requirement for the
degree of Doctor of Philosophy in Engineering**

**Kulliyyah of Engineering
International Islamic University Malaysia**

APRIL 2023

ABSTRACT

The congestion at the lower frequency bands is pushing the demands for the usage and operation in the higher bands. The bands above 10 GHz are now required to satisfy the tremendously increasing needs in satellite communication (SatCom) systems. The biggest problem in deploying frequencies above 10 GHz in tropical-equatorial regions is that such areas will experience acute degradation of signal quality due to heavy rainfall throughout the year. A reliable estimation of rain attenuation is required. Dependable fade margins are required in mitigating the harsh signal losses. It is found that data validation for rain attenuation estimation using the frequency scaling technique is not available in any previous studies conducted in tropical regions. It has been suggested that instead of using the conventional method of predicting rain attenuation using the point rainfall rate information, an applicable non-meteorological technique should also be established. A frequency scaling technique can be the alternatives mean to predict rain attenuation when rainfall data is not available. The objectives of the research entail rain-induced attenuation studies for SatCom in tropical regions. They comprise identifying the best fade margin for rain attenuation at various links, formulating a new frequency scaling model with improved accuracy, and validating the proposed model. The methodologies involved in the study encompass the processing of the beacon signals into first-order statistics of rain attenuation. This, later, leads to the generation of monthly and annual rain attenuation Cumulative Distribution Functions (CDFs). The worst month analysis for rain intensity and rain attenuation was also carried out. The signal loss is expected to be appalling in the worst month because of the high occurrence of rain events. The required fade margin was determined from an exceedance at a specific point from the annual CDF. In brief, the frequency scaling model was derived based on the correlation between the attenuation ratio of a higher and lower frequency against the attenuation at a lower frequency. The newly developed formulation was utilized to generate new CDFs of attenuation at different frequencies. The proposed model offers a lower RMSE value and percentage error of 2.8 and 11.3% respectively. In contrast, the generic method suggested by the ITU-R only managed to perform prediction with RMSE value and percentage errors of 28.3 and 28% accordingly. The new model was validated using data set from alternative years and alternate locations. In conclusion, the results from the research demonstrate a model that can be used in the tropical-equatorial region in a way denoting the achievement of fulfilling the stated objectives. The satellite signal performance can be improved by applying developed mitigation techniques with an economically viable cost where dependable fade margins can be attained. The newly developed frequency scaling technique can offer the right margin to achieve the required quality of service (QoS) for future SatCom in supporting near-future 5G communication. Consistent connectivity for high-speed broadband communication demand in delivering digital and internet applications during heavy precipitation can be attained.

خلاصة البحث

يؤدي الازدحام في نطاقات التردد المنخفضة إلى زيادة الطلب على استخدام وتشغيل نطاقات التردد الأعلى. لذلك، فإنّ النطاقات فوق 10 جيجاهرتز مطلوبة الآن لتلبية الاحتياجات المتزايدة بشكل كبير في أنظمة اتصالات الأقمار الاصطناعية (SatCom). ولكنّ أكبر مشكلة في نشر الترددات فوق 10 جيجاهرتز في المناطق الاستوائية المدارية هي أن هذه المناطق ستشهد تدهوراً حاداً في جودة الإشارة بسبب هطل الأمطار الغزيرة على مدار العام. فمن المطلوب تقدير موثوق للتوهين الناجم عن المطر. وكذلك، هناك حاجة لهوامش تلاشي موثوقة للتخفيف من الخسائر الحادة في الإشارة. لقد وجد أن التحقق من صحة البيانات لتقدير التوهين الناجم عن المطر باستخدام تقنية تعديل التردد (Frequency Scaling) لم يرد في أي دراسات سابقة أجريت في المناطق المدارية. لذا يقترح هذا البحث أنه بدلاً من استخدام الطريقة التقليدية للتنبؤ بالتوهين الناجم عن المطر باستخدام معلومات معدل هطل المطر النقطي، ينبغي أيضاً إنشاء تقنية قابلة للتطبيق غير متعلقة بالأرصاد الجوية. ويمكن أن تكون تقنية تعديل التردد هي الوسيلة البديلة للتنبؤ بالتوهين الناجم عن المطر عندما لا تتوفر بيانات هطل الأمطار. تتضمن أهداف البحث دراسات التوهين الناجم عن المطر لاتصالات الأقمار الاصطناعية (SatCom) في المناطق المدارية. وتشمل تحديد أفضل هامش تلاشي للتوهين الناجم عن المطر في وصلات مختلفة، وصياغة نموذج جديد لتعديل التردد بدقة محسنة، والتحقق من صحة النموذج المقترح. كما تشمل المنهجيات المتضمنة في الدراسة معالجة الإشارات المرسله للحصول على إحصائيات أولية للتوهين الناجم عن المطر. ويؤدي هذا لاحقاً إلى توليد دوال توزيع تراكمي (CDFs) للتوهين الناجم عن المطر شهرية وسنوية. كما تم إجراء تحليل الشهر الأسوأ لكثافة المطر والتوهين الناجم عن المطر. حيث من المتوقع أن تكون خسارة الإشارة مروعة في أسوأ شهر بسبب ارتفاع معدل هطل المطر. وقد تم تحديد هامش التلاشي المطلوب من خلال تجاوز الحد الأقصى عند نقطة معينة من (CDF) السنوي. باختصار، تم اشتقاق نموذج تعديل التردد بناءً على الارتباط بين نسبة التوهين لتردد أعلى وتردد أدنى مقابل التوهين عند تردد أدنى. كما تم استخدام الصيغة المطورة حديثاً لتوليد (CDFs) جديدة للتوهين عند ترددات مختلفة. يقدم النموذج المقترح قيمة (RMSE) ونسبة خطأ بمقدار 2.8 و 11.3% على التوالي. وعلى النقيض من ذلك، فإن الطريقة العامة التي اقترحها قطاع الاتصالات الراديوية (ITU-R) لم تتمكن إلا من التنبؤ بقيمة (RMSE) ونسبة خطأ بمقدار 28.3 و 28% على التوالي. تم التحقق من صحة النموذج الجديد باستخدام مجموعة بيانات من سنوات مختلفة ومواقع مختلفة. وفي الختام، تظهر نتائج البحث نموذجاً يمكن استخدامه في المنطقة الاستوائية المدارية بطريقة

تدل على تحقيق الأهداف المذكورة. يمكن تحسين أداء إشارة القمر الاصطناعي من خلال تطبيق تقنيات تخفيف مطورة بتكلفة مجدية اقتصادياً، حيث يمكن تحقيق هوامش تلاشي موثوقة. ويمكن أن توفر تقنية تعديل التردد المطورة حديثاً الهامش الصحيح لتحقيق جودة الخدمة (QoS) المطلوبة لاتصالات الأقمار الاصطناعية (SatCom) المستقبلية في دعم اتصالات الجيل الخامس (5G) في المستقبل القريب. كما يمكن تحقيق اتصال ثابت لتلبية حاجة اتصالات النطاق العريض عالي السرعة في تقديم التطبيقات الرقمية وتطبيقات الإنترنت أثناء هطل الأمطار الغزيرة.



APPROVAL PAGE

The thesis of Nur Hanis Sabrina Binti Suhaimi has been approved by the following:

Ahmad Fadzil bin Ismail
Supervisor

Khairayu bt Badron
Co-Supervisor

Md Rafiqul Islam
Co-Supervisor

Yasser Asrul bin Ahmad
Co-Supervisor

Mashkuri Yaacob
Internal Examiner

Jafri Bin Din
External Examiner

Asadullah Shah
Chairman

DECLARATION

I hereby declare that this dissertation is the result of my investigations, except where otherwise stated. I also declare that it has not been previously or concurrently submitted as a whole for any other degrees at IIUM or other institutions.

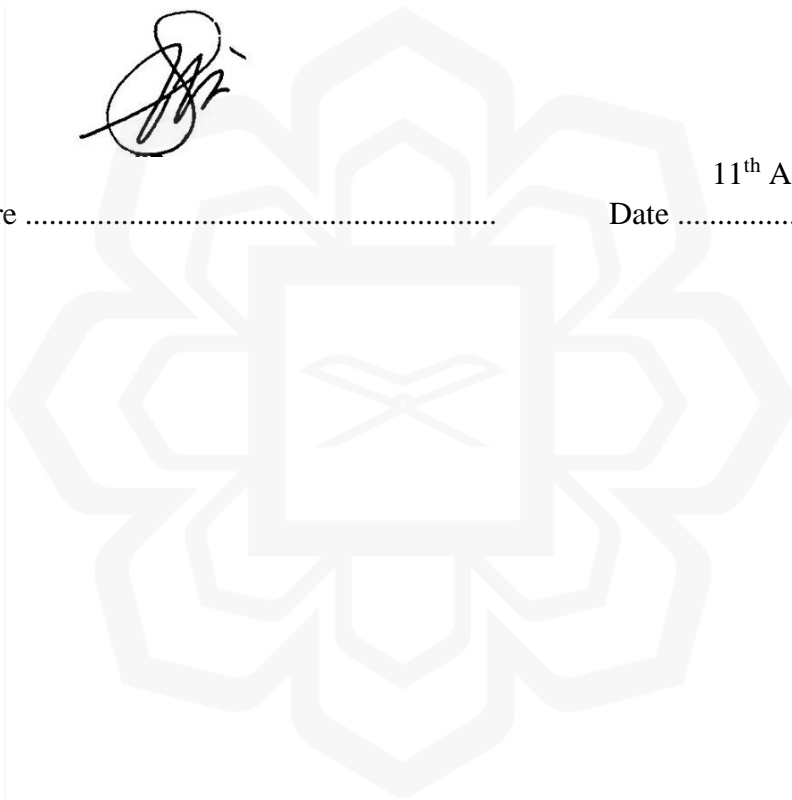
Nur Hanis Sabrina Binti Suhaimi



Signature

11th April 2023

Date



INTERNATIONAL ISLAMIC UNIVERSITY MALAYSIA
DECLARATION OF COPYRIGHT AND AFFIRMATION OF
FAIR USE OF UNPUBLISHED RESEARCH

FREQUENCY SCALING IN MILLIMETRE-WAVE RAIN
ATTENUATION ESTIMATION FOR SATELLITE LINK IN
TROPICAL REGIONS

I declare that the copyright holder of this thesis/dissertation are jointly owned by the student and IIUM.

Copyright © 2023 Nur Hanis Sabrina binti Suhaimi and International Islamic University Malaysia. All rights reserved.

No part of this unpublished research may be reproduced, stored in a retrieval system, or transmitted, in any form or by any means, electronic, mechanical, photocopying, recording or otherwise without prior written permission of the copyright holder except as provided below.

1. Any material contained in or derived from this unpublished research may only be used by others in their writing with due acknowledgement.
2. IIUM or its library will have the right to make and transmit copies (print or electronic) for institutional and academic purpose.
3. The IIUM library will have the right to make, store in a retrieval system and supply copies of this unpublished research if requested by other universities and research libraries.

By signing this form, I acknowledged that I have read and understand the IIUM Intellectual Property Right and Commercialization policy.

Affirmed by Nur Hanis Sabrina Binti Suhaimi.



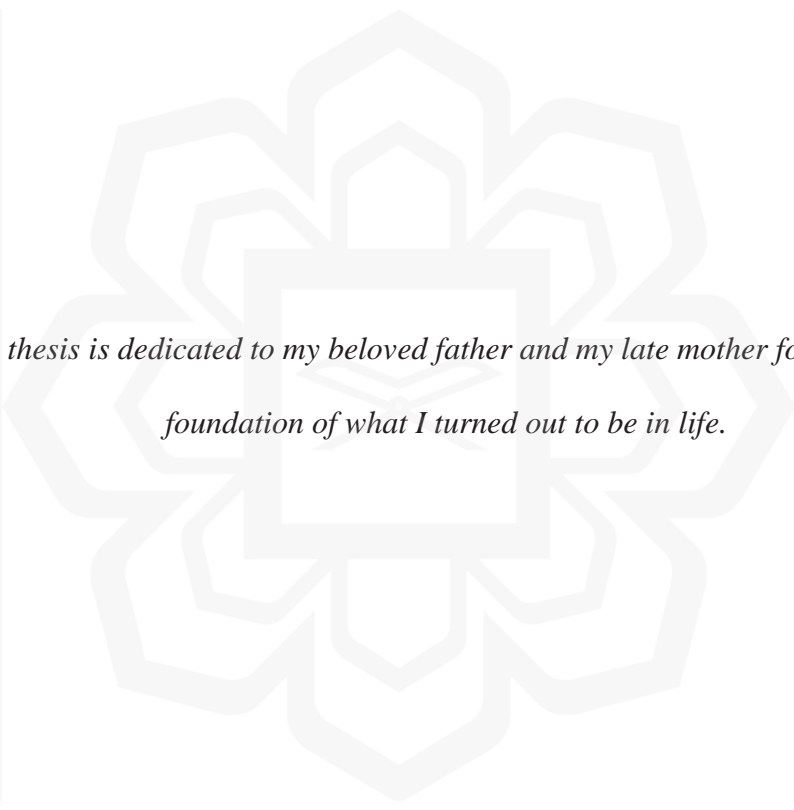
.....

Signature

11th April 2023

.....

Date



*This thesis is dedicated to my beloved father and my late mother for laying the
foundation of what I turned out to be in life.*

ACKNOWLEDGEMENTS

Praise to Allah SWT, The Most Gracious and Most Merciful, for granting me opportunities to complete this dissertation, and for blessing me throughout the years upon seeking knowledge in this PhD journey. Without the grace, mercy and blessings from Allah SWT, this achievement would be impossible. His Mercies and Blessings on me ease the difficulty of completing this journey.

I would like to express my sincerest gratitude to my supervisor Prof. Ir. Dr Ahmad Fadzil Ismail for his continuous courage and guidance for me in completing the research. I am most indebted to him for his highly committed characteristics, kindness, and thoroughness attitude have led to the successful completion of my work. His detailed comments and suggestions have improved this thesis and made this thesis well-written. His vast knowledge, patience and wisdom have been thorough and of great assistance to me in completing my study. Despite his very busy commitments, he always makes time to attend to me whenever requested. His moral support and high cooperation are the boosters that helped me in writing this research work.

I would also like to extend this act of gratitude to my co-supervisors Dr Khairayu bt Badron, Prof. Md Rafiqul Islam and Dr Yasser Asrul bin Ahmad throughout this journey of knowledge-seeking, for their guidance, assistance, fruitful discussions and their never-ending encouragement, have had motivated me to accelerate on the completion of this study. Besides that, I want to deliver my acknowledgement towards MEASAT Satellite System Sdn. Bhd. (MEASAT), MEASAT Broadcast Network System Sdn Bhd (ASTRO) and the Department of Irrigation and Drainage, Malaysia for the collaboration in providing the data for this research. Special thanks to Mr Mohd Akmal Yahaya and Mr Ahmad Faiz Yahaya as well, for their assistance in supplying the massive raw data on rain attenuation for this research.

It is with great pleasure to dedicate this achievement to my beloved dad, Suhaimi bin Abas, the vital backbone that has been continuously supporting and guiding me with his knowledge and experience in the field throughout my research completion journey. To my lovely family; my husband Alang, and my dearest children; Amni, Ali, and Aleesa whose unwavering faith in my capability and effort to accomplish the research made me work even harder and perform my best in completing my study, I owe each and every achievement to all of them. Their endurance and understanding when I am struggling in completing this study is the most valuable gift.

Last but not least, I would also like to extend my appreciation and gratitude to families and friends who have contributed their effort and supported this work, directly or indirectly, be it financial, time, as well as moral support, they have been the source of my strength and motivation to complete this research, and that they are truly cherished for a lifetime.

Table of Contents

Abstract	ii
Abstract in Arabic	iii
Approval Page.....	v
Declaration	vi
Copyright Page.....	vii
Acknowledgements	ix
Table of Contents	x
List of Tables	xiii
List of Figures	xv
CHAPTER ONE: INTRODUCTION	1
1.1 Background of the Study	1
1.2 Problem Statement	5
1.3 Purpose of the Study	10
1.4 Research Objectives.....	11
1.5 Research Questions.....	11
1.6 Theoretical Framework.....	12
1.7 Research Scope	13
1.8 Research Philosophy.....	14
1.9 Research Hypotheses	15
1.10 Significance of the Study.....	15
1.11 Limitations of the Study	16
1.12 Definition of Terms	17
1.13 Organization of the Thesis	18
1.14 Chapter Summary	19
CHAPTER TWO: LITERATURE REVIEW	21
2.1 Introduction.....	21
2.1.1 Satellite Communication System.....	22
2.1.2 Terrestrial Communication System	23
2.2 Importance of Satellite Communication System	24
2.3 Distribution of Frequencies Spectrum	27
2.3.1 Microwave Bands (C, X and Ku-bands).....	29
2.3.2 Millimetre Wave (Ka, Q and V-bands).....	30
2.4 Classification of Tropical Climate.....	31
2.4.1 Distribution of Equatorial Climate	32
2.4.2 Malaysia's Climate	32
2.4.3 Precipitation Type in Tropical Regions	36
2.5 Propagation Impairment in Satellite-Earth Link at Higher Frequencies	37
2.6 Fade Margin Requirement for Good Quality of Services (QOS)	39
2.7 Rain Attenuation Prediction for Earth-Space Telecommunication System.....	42

2.7.1 Approaches for the Prediction of Rain Attenuation	44
2.7.2 ITU-R Prediction Method of Determining Rain Attenuation.....	44
2.7.3 Meteorological Technique.....	46
2.7.4 Non-meteorological Technique.....	48
2.7.4.1 Frequency Scaling.....	49
2.7.4.2 Elevation Scaling	49
2.7.4.3 Path Length Scaling	50
2.7.4.4 Polarization Scaling	51
2.8 Frequency Scaling Technique	52
2.8.1 Statistical Frequency Scaling	54
2.8.2 Instantaneous Frequency Scaling	56
2.8.3 Previous Model of Frequency Scaling	58
2.8.3.1 ITU-R 618-13 Model (2017)	59
2.8.3.2 Hodge’s Model (1977).....	59
2.8.3.3 Battesti’s Model (1982)	60
2.8.3.4 Kheirallah’s Model (1980).....	61
2.8.3.5 CCIR (1980).....	62
2.8.3.6 Simple Power Law (SPL) Model (1974-1995).....	62
2.8.3.7 Boithias’s Model (1989)	63
2.8.3.8 Zhou’s Model (1999)	64
2.8.4 Previous Related Research	64
2.8.5 Research Gap.....	69
2.9 Worst Month Analysis	70
2.10 Chapter Summary.....	73
CHAPTER THREE: METHODOLOGY.....	74
3.1 Introduction.....	74
3.2 Measurement Setup.....	77
3.2.1 C-band Beacon Measurement Setup.....	82
3.2.2 Ku-band Beacon Measurement Setup.....	85
3.2.3 Ka-band Beacon Measurement Setup.....	87
3.2.4 Rain Gauge Measurement Setup.....	90
3.3 Collection of Data.....	92
3.4 Data Processing.....	92
3.4.1 Extraction & Conversion of Raw Data into Rain Attenuation Data	93
3.4.2 Generation of Probability Density Function (PDF)	94
3.4.3 Generation of Cumulative Density Function (CDF).....	95
3.4.4 Generation of Time Exceedance	95
3.4.4.1 Monthly.....	96
3.4.4.2 Annual.....	96
3.5 Data Analysis.....	97
3.5.1 Time Exceedance Analysis for C, Ku & Ka-band	98
3.5.2 Technique to Extrapolate the Ka-band Attenuation Data	102
3.5.3 Selection of The Best Extrapolation Technique to Determine Ka-band.....	104
3.5.4 Comparison with ITU-R.....	105
3.5.5 Determination of Worst Month	105

3.6 Determination of Frequency Scaling Technique	106
3.6.1 Proposed Frequency Scaling Model	106
3.7 Validation of the Model	107
3.8 Summary	107
CHAPTER FOUR: RESULT	109
4.1 Introduction.....	109
4.2 Diurnal Time-Series Analysis.....	110
4.2.1 Monthly Analysis.....	117
4.2.1.1 Rainfall Rate	117
4.2.1.2 Rain Attenuation	120
4.2.2 Annual Analysis.....	130
4.2.2.1 Rainfall Rate	130
4.2.2.2 Rain Attenuation at the C-band.....	132
4.2.2.3 Rain Attenuation at the Ku-band	134
4.2.2.4 Rain Attenuation at the Ka-band.....	137
4.2.2.5 Extrapolation of Rain Attenuation at the Ka-band	139
4.3 Determination of Fade Margin	144
4.4 Comparison With ITU-R	148
4.5 Worst Month Analysis	151
4.6 Frequency Scaling.....	158
4.6.1 ITU-R 618-13 Frequency Scaling.....	158
4.6.2 Hodge.....	159
4.6.3 Battesti	161
4.6.4 Kheirallah.....	162
4.6.5 CCIR	163
4.6.6 Simple Power Law	164
4.6.7 Boithias	167
4.6.8 Zhou	168
4.7 Proposed Frequency Scaling Technique.....	170
4.8 Implementation of Frequency Scaling Technique for Q-band and V-band	179
4.9 Validation of Proposed Frequency Scaling Technique.....	182
4.10 Summary	190
CHAPTER FIVE: DISCUSSION AND CONCLUSION.....	192
5.1 Discussion	192
5.2 Conclusion and Future Works	195
REFERENCES.....	197
APPENDIX I: SAMPLE PDF OF KA-BAND RAIN ATTENUATION	213
APPENDIX II: SAMPLE CDF OF KA-BAND RAIN ATTENUATION	214
APPENDIX III: EXTRAPOLATIONS FORMULA FOR THE KA-BAND LINK	215

LIST OF TABLES

Table 2.1	Comparison of Frequency Scaling Technique in Predicting Rain Attenuation for the Satellite Communication Link	65
Table 2.2	Limitation of Frequency Scaling Technique in Predicting Rain Attenuation for the Satellite Communication Link	68
Table 2.3	Q_l and β for Various Propagation Effects and Areas in Tropical Regions	72
Table 3.1	C-band Beacon Signals Receiving Setup	83
Table 3.2	Ku-band Beacon Signals Receiving Setup	86
Table 3.3	Ka-band Beacon Signals Receiving Setup	88
Table 3.4	Vaisala Weather Transmitter WXT520 Specifications	91
Table 3.5	Rain Detected at Different Rain Gauge Locations in January 2016	101
Table 4.1	Total Precipitations in Cyberjaya for the Year 2016	120
Table 4.2	Rainfall Rate at 0.01% of Time Exceedance for C-band Rain Attenuation at 0.1%, 0.3%, 0.01% and 0.03% of Time Exceedance	122
Table 4.3	Rainfall Rate at 0.01% of Time Exceedance with Ku-band Rain Attenuation at 0.1%, 0.3%, 0.01% and 0.03% of Time Exceedance	124
Table 4.4	Rainfall Rate at 0.01% of Time Exceedance with Ka-band Rain Attenuation at 0.1%, 0.3%, 0.01% and 0.03% of Time Exceedance	128
Table 4.5	Annual Rainfall Rate and Annual Rain Attenuation of the C-band at 0.1%, 0.3%, 0.01% and 0.03% of Time Exceedance	134
Table 4.6	Annual Rainfall Rate and Annual Rain Attenuation of the Ku-band at 0.1%, 0.3%, 0.01% and 0.03% of Time Exceedance	135
Table 4.7	Annual Rainfall Rate and Annual Rain Attenuation of Ka-band at 0.1%, 0.3%, 0.01% and 0.03% of Time Exceedance	138
Table 4.8	Summary of Techniques Used to Determine the Best Extrapolation Graph for Extended Ka-band	142
Table 4.9	Comparison of Measured Rain Attenuation at 0.1%, 0.01% and 0.001% of Time Exceedance with Ahmad's (2019) Model and ITU-R 618-13 (2017)	143

Table 4.10	Fade Margins for C, Ku And Ka-band Links Operating at 99.70%, 99.90%, 99.97% and 99.99% in 2016	147
Table 4.11	Measured Values and Proposed Values for Q_1 and β in Tropical Regions for Slant Path and Rain Rate Propagation	156
Table 4.12	RMSE and Percentage Error of Available Model over the Interval [0.001% to 1%]	169
Table 4.13	RMSE and Percentage Error Obtained after Testing the Proposed Model over the Intervals [0.001% to 1%]	177
Table 4.14	Comparison of Statistical Parameters between the Proposed Frequency Scaling Model and the ITU-R Frequency Scaling Method	179
Table 4.15	Tabulated Values of Scaled Attenuation at Ka, Q and V-band links	181
Table 4.16	Comparison Values of V-band Rain Attenuation at 99.9% and 99.99% of Link Availability Between the Existing Model and the New Model.	182
Table 4.17	RMSE and Percentage Error Value of Rain Attenuation Predicted at Cyberjaya in the year 2015 using the Proposed Model	184
Table 4.18	RMSE and Percentage Error Value of Rain Attenuation using the Proposed Model Predicted at Rawang in the year 2016	186
Table 4.19	RMSE and Average Percentage Error Value of Rain Attenuation at the V-band (40 GHz) Predicted in Nigeria using the Proposed Model	188
Table 4.20	RMSE Percentage Improvement for the Ka-band using the Proposed Model as compared to the ITU-R Frequency Scaling Technique	189
Table 4.21	RMSE Percentage Improvement for Estimating V-band Rain Attenuation using the Proposed Model as compared to the ITU-R Rain Attenuation Prediction Model	190

LIST OF FIGURES

Figure 1.1	Map of Tropical Regions (IEEI, 2014)	4
Figure 1.2	Overview of System Setup for the C & Ku-bands	8
Figure 1.3	Miniature Model of Measat-3 Satellite	8
Figure 1.4	Overview of System Setup for the Ka-band	9
Figure 1.5	Miniature Model of Measat-5 Satellite	9
Figure 1.6	Theoretical Framework of Statistical Frequency Scaling Study	13
Figure 2.1	Satellite Communication (SatCom) System (Walter, 2018)	23
Figure 2.2	Terrestrial Communication System (Yee et al., 2007)	24
Figure 2.3	Wavelength Designation for Frequency Band	28
Figure 2.4	Climate Region (Mustafa et al., 2017)	31
Figure 2.5	Total Rainfall in Malaysia in 2016 (MMD, 2016)	35
Figure 2.6	Schematic Diagram of an Earth-Space Input Parameter Needed in the Attenuation Prediction Process (ITU-R P.618-13, 2017)	45
Figure 2.7	The Research Gap Identified in the Study	70
Figure 3.1	Overview of the Research	75
Figure 3.2	Research Flow Chart	76
Figure 3.3	Earth Stations at the MEASAT Teleport and Broadcast Centre	77
Figure 3.4	Receiver Station at the ASTRO Broadcast Centre	78
Figure 3.5	MEASAT-3 Specifications and Footprints (MEASAT, 2022)	79
Figure 3.6	MEASAT-5 Specifications and Footprints (MEASAT, 2022)	79
Figure 3.7	MEASAT-3 and MEASAT-5 in reference to their Earth Stations	80
Figure 3.8	Earth-Space Link Design	81
Figure 3.9	C/Ku-band Configuration	84
Figure 3.10	C-band Antenna (General Dynamics SATCOM Technologies)	84

Figure 3.11	Ku-band Antenna (General Dynamics SATCOM Technologies)	86
Figure 3.12	Digital Tracking Receiver for Ku and C-band	87
Figure 3.13	Ka-band Configuration	88
Figure 3.14	Ka-band Antenna	89
Figure 3.15	Digital Tracking Receiver for Ka-band	89
Figure 3.16	ASTRO Rain Sensor	91
Figure 3.17	Flow Chart of Processing Data	93
Figure 3.18	Steps in Generating Time Exceedance for C, Ku and Ka-band Beacon Signals, and Rainfall Rate Data.	97
Figure 3.19	Time-Series for Rain Event on 6th February 2016	98
Figure 3.20	Attenuation Time-Series of Ka-band for One Day on 6th February 2016	99
Figure 3.21	Location of Rain Gauge at Paya Indah, Puncak Niaga, and Earth Station at Cyberjaya	100
Figure 3.22	Time-Series of Rain Attenuation of Ka-band on 4th January 2016	102
Figure 3.23	Plot of Annual Rain Attenuation of Ka-band versus Annual Rainfall Rate	103
Figure 4.1	Time-Series Plots of Rainfall Intensity and Attenuation During Rainfall on 20 th May 2016	111
Figure 4.2	Time-Series for Rain Events on 6 th February 2016	112
Figure 4.3	Time-Series of C-band Attenuation for the Entire Day of 6 th February 2016	113
Figure 4.4	Time-Series of C-band Attenuation during Rainfall on 6th February 2016	113
Figure 4.5	Time-Series of Ku-band Attenuation for One Day (6 th February 2016)	114
Figure 4.6	Time-Series of Ku-band Attenuation during Rainfall on 6 th February 2016	115
Figure 4.7	Rain Attenuation Time-Series of Ka-band on 6 th February 2016	116
Figure 4.8	Time-Series of Rainfall on 4 th January 2016	117
Figure 4.9	Monthly Rain Intensity of Time Exceedance in 2016	119

Figure 4.10	Monthly Distribution of the C-band Rain Attenuation at Cyberjaya in 2016	121
Figure 4.11	Monthly Distribution of the Ku-band Rain Attenuation at Cyberjaya in 2016	123
Figure 4.12	Histogram of Certain Attenuation Thresholds and Monthly Time Exceedance	125
Figure 4.13	The Probability of Specific Rain Attenuation Thresholds at the Ku-band Link	126
Figure 4.14	Monthly Distribution of Rain Attenuation of Ka-band at Cyberjaya in 2016	127
Figure 4.15	Histogram of a Specific Threshold of Attenuation is Exceeded Monthly at the Ka-band Link	129
Figure 4.16	Probability of Specific Thresholds of Rain Attenuation Exceedance at the Ka-band Link	130
Figure 4.17	Annual CDF of Rain Intensity for 2016 in Cyberjaya	131
Figure 4.18	Annual CDF of C-band Rain Attenuation for 2016 in Cyberjaya	132
Figure 4.19	C-band Rain Attenuation Correlated to Rainfall Rate in Cyberjaya's Rain Gauge	133
Figure 4.20	Annual CDF of Ku-band Rain Attenuation for 2016 in Cyberjaya	135
Figure 4.21	Ku-band Rain Attenuation Correlated to Rainfall Rate in Cyberjaya's Rain Gauge	136
Figure 4.22	Annual CDF of Ka-band Rain Attenuation for 2016 in Cyberjaya	137
Figure 4.23	Ka-band Rain Attenuation Correlated to Rainfall Rate in Cyberjaya's Rain Gauge	138
Figure 4.24	Measured Plotted Values with Linear Extrapolation Model	139
Figure 4.25	Measured Plotted Values with First-Order Power Law Extrapolation Model	140
Figure 4.26	Measured Plotted Values with Second-Order Power Law Extrapolation	140
Figure 4.27	Measured Plotted Values with Second-Degree Polynomial Extrapolation Model	141
Figure 4.28	Measured Plotted Values with Ahmad's (2019) Extrapolation Model	141

Figure 4.29	Extrapolated Ka-band Rain Attenuation Correlated to Rainfall Rate in Cyberjaya's Rain Gauge	144
Figure 4.30	Annual CDF of C-band Rain Attenuation	145
Figure 4.31	Annual CDF of Ku-band Rain Attenuation	145
Figure 4.32	Annual CDF of Measured Ka-band Rain Attenuation	146
Figure 4.33	Annual CDF of Extrapolated Ka-band Rain Attenuation	146
Figure 4.34	Annual CDF of the Measured Rain Rate Value in 2016 compared to ITU-R 837-7 Rainfall Prediction	149
Figure 4.35	Annual CDF of Measured Values compared to ITU-R Prediction Values of Rain Attenuation for C, Ku and Ka-band Links	150
Figure 4.36	The Probability of a Specific Threshold of Rainfall Rate Exceeded for the year 2016 at Cyberjaya	151
Figure 4.37	Annual and Worst Month Rain Rate Exceedance Curve	152
Figure 4.38	Q as a Function of Annual Rainfall Rate Exceedance Percentage	153
Figure 4.39	Q as a Function of Annual Rain Attenuation at Ku-band Exceedance Percentage	154
Figure 4.40	Worst Month Model Comparison of Ku-band Rain Attenuation	155
Figure 4.41	Q as a Function of Annual Rain Attenuation at Ka-band Exceedance Percentage	157
Figure 4.42	Worst Month Model Comparison of Ku-band Rain Attenuation	158
Figure 4.43	ITU-R 618-13 Frequency Scaling	159
Figure 4.44	Hodge Frequency Scaling Model	160
Figure 4.45	Battesti Frequency Scaling Model	161
Figure 4.46	Kheirallah Frequency Scaling Model	162
Figure 4.47	CCIR Frequency Scaling Model	163
Figure 4.48	Simple Power Law Frequency Scaling for Pairs Ku-band/C-band and Ka-band/C-band	164
Figure 4.49	Simple Power Law Frequency Scaling for Pairs Ka-band/Ku-band	165
Figure 4.50	Drufuca Frequency Scaling Model	166
Figure 4.51	Boithias Frequency Scaling Model	167

Figure 4.52	Zhou Frequency Scaling Model	168
Figure 4.53	Time Percentage Exceedance Curve of Measured Rain Rate and Rain Attenuation of C, Ku and Ka-band Links for 2016	170
Figure 4.54	RAS for the Year 2016 as a Function of Lower Frequency Attenuation for the Frequency Pairs of 20/12 GHz	171
Figure 4.55	Graph of Attenuation at the Ku-band versus Attenuation at the Ka-band	172
Figure 4.56	Graph of Attenuation at the Ku-band versus Attenuation at the C-band	173
Figure 4.57	Graph of Attenuation at the Ka-band versus Attenuation at the C-band	174
Figure 4.58	Comparison of Scaled-up Ka-band Rain Attenuation Using the Proposed Frequency Scaling Model with Measured Rain Attenuation at the Ka-band in 2016	175
Figure 4.59	Comparison of the Derived Frequency Scaling Technique and Available Frequency Scaling Models, including ITU-R at Frequency Pair of Ka/Ku-band	176
Figure 4.60	Scale-up of Ka, Q and V-band links using the Proposed Frequency Scaling Model	180
Figure 4.61	Comparison of Measured Rain Attenuation of the Proposed Model at Cyberjaya in 2015	183
Figure 4.62	Comparison of Measured Rain Attenuation of the Proposed Model at Rawang in 2016	185
Figure 4.63	Comparison of the Proposed Model with the Measured Rain Attenuation at the V-band Link in Nigeria	187
Figure 4.64	RMSE Comparison between the New Model and ITU-R model	189

CHAPTER ONE

INTRODUCTION

1.1 BACKGROUND OF THE STUDY

The Covid-19 global pandemic has caused serious problems for the world's leading satellite industries. They faced several challenges in delivering reliable link availability of satellite-Earth signals. Since the start of the pandemic, broadband connectivity provided by satellite operators had drastically increased from 15% to 70% in network usage. Satellites can instantly connect isolated communities and offer connectivity to unreachable and remote areas. However, the main challenge experienced by satellite industries is providing consistent internet connection in places that experience frequent heavy precipitation where severe impairment of satellite signal reception occurs. Precipitation like rain prominently degrades the quality of satellite signals. When signals travel from satellites to the Earth's receivers, they pass over unpredictable rain along their propagation paths. The signal power may weaken before reaching its destination, especially when longer slant paths and lower elevation angles are involved (Igwe et al., 2019; Nazrul et al., 2013). These factors affect link availability, leading to negatively impacting consumer satisfaction which further damages and causes a tumble in the reputation of satellite providers.

The International Telecommunication Union's (ITU) Radio Regulations (RR) defined satellite links as radio links transmitting between Earth stations to satellite receivers and vice versa. An "uplink" refers to an Earth-to-satellite propagation, and a "downlink" implies transmission from the satellite to a receiving Earth station. Radio frequencies that have wavelengths (λ) ranging between 1 mm to 10 mm in satellite-Earth links are referred to as millimetre-wave frequencies. Communication satellites facilitate human connection regardless of location (Badron et al., 2015). Satellite communication (SatCom) is then considered the best option for addressing user demands for areas not economically reachable by terrestrial links, such as for

developing countries with vast lands or in the middle of the ocean. Numerous requirements in the telecommunication and broadcasting industries have prompted an increase in demand for high-speed broadband communication, especially for multimedia services. These have subsequently led to the growing demands for greater bandwidth (Yussuff et al., 2019). Although the rollout of fibre in South Africa significantly enhanced the speed of home broadband in the year 2014, satellite infrastructures continue to fulfil a crucial role in providing communication access to rural, remote and inland areas throughout the continent and across the globe as well. The fast growth in telecommunications, increasing bandwidth demands, congestion in lower frequency bands, and miniaturisation of communication equipment have forced designers to employ higher frequency bands such as the Ku (12 to 18 GHz), Ka (26.5 to 40 GHz) and V (40 to 75 GHz) (Kamruzzaman & Islam, 2014). Unfortunately, higher operating frequency bands are very susceptible and vulnerable to tropospheric conditions that impair and reduce signal quality (Sujimol et al., 2015).

The proposed satellite television broadcast for home reception is called Direct Broadcast Satellite (DBS) or Direct-to-Home (DTH). It enables the easy access to live television channels from other countries. Various multimedia applications are offered by satellite communication which all require extremely high data rate transmissions, including videoconferencing, broadcasts, data broadcasts that include High Definition (HD) television broadcasts, bandwidth on demand, intranet works and telemedicine. Such applications lead to spectrum congestion in lower frequency bands. Shifting to higher frequency bands is one option for achieving better services in satellite communication applications since these bands support high data-rate broadcasts and internet applications. SatCom systems are now moving towards the use of Ka-bands (20/30 GHz). In future, the shift to higher frequency bands, such as the Q/V (40/50 GHz), will undoubtedly occur to accommodate larger bandwidth requirements. High radio frequency offers several advantages such as larger spectrum availability, smaller equipment size requirements and less interference for SatCom (Samat & Singh, 2020).

High Throughput Satellites (HTS) are communication satellites with higher throughput than traditional Fixed Satellite Services (FSS) which give advantages in frequency reuse and multiple spot beams. High throughput is important because of its high-speed information delivery (bits/sec). It can be influenced by frequency reuse and

channel efficiency. The first commercial HTS in Asia is the IPSTAR (Thaicom-4) operating in the Ku-band and is now developing to operate in the Ka-band (ITU-R P.618-13, 2017). The main purpose of these satellites is fast internet connectivity. The commercial HTS, IPSTAR, was launched by Thaicom in 2005. This satellite was designed for FSS, which is a two-way communication over an Internet Protocol (IP) platform with a maximum capacity throughput of 45 Gbps, a user download speed of up to 5 Mbps and an upload speed of 4 Mbps.

Today, the IPSTAR is licensed to operate in 14 countries in the Asia Pacific areas, which directly allows service providers and operators to deliver real-time broadband internet access via satellite. In May 2011, Thaicom began selling some parts of its satellite capacity to Malaysia. Malaysia's satellite operator, MEASAT, signed a contract for a specific capacity on the IPSTAR. MEASAT Satellite Systems Sdn. Bhd. purchased access to seven IPSTAR spot beams under a decade contract for delivering a total of 3.3 Gbps, representing 7% of the satellite's total capacity. The bandwidth was known and marketed in Malaysia as MEASAT-5 (Christensen, 2012).

The idea of deploying a new satellite system in the Ka-band frequency started to evolve and gain attention in countries with tropical environments. The areas between the Earth's latitudes of 23°27' North and 23°27' South are identified as tropical regions, as shown in Figure 1.1. The propagation impairments are quite critical in locations with tropical weather. This is due to the occurrence of frequent heavy rain which severely affects high-frequency radio wave signals. The rain can cause severe signal fading as well as interference (Yeo et al., 2009a). The dominant factor for signal impairment of satellite links at higher frequencies is rain, and this depends on the rain rate, the raindrop size and raindrop density (Kamruzzaman & Islam, 2014; Islam et al., 2018). Raindrops absorb and scatter radio waves with shorter wavelengths, hence resulting in signal attenuation as well as reducing system availability and reliability (Mom et al., 2021). The attenuation due to rain on any path depends on several parameters, such as the specific attenuation in dB/km, frequency, polarization, temperature, path length and latitude. As it is known rain attenuation causes a reduction of the received signal level, therefore, upon designing dependable Ka-band satellite communication systems, rain attenuation must be considered as an important propagation element to ensure signal quality. The conventional quality of service (QoS) criterion in Malaysia for broadcasts

is 99.99% availability (MCMC, 2022). The QoS requirement recommended by the ITU-R Telecommunication Standardisation is 99.9% link availability for communication services (ITU-T G.1028, 2016).



Figure 1.1 Map of Tropical Regions (IEEI, 2014)

Rain attenuation is typically assumed as a product of specific attenuation (dB/km) and the effective propagation path length (km). The effective path length is the product of the path reduction factor and the physical path length of a microwave link (Islam et al., 2012). Rain is the most destructive source of signal propagation on these bands. The consequence of rain attenuation on band signal quality, especially in tropical countries such as Malaysia, requires comprehensive research. The appropriate fade margins must be identified to ensure successful implementation in all provinces throughout Malaysia.

Several methods can be used for identifying and estimating rain attenuation. The frequency scaling technique is one suggested approach (Ulaganathan et al., 2013). Frequency scaling of attenuation is the prediction of rain attenuation at the desired frequency derived from attenuation values at another frequency (Laster & Stutzman, 1995; Ramana, 2015; Ulaganathan et al., 2013). The method can be used to obtain an estimation of the attenuation statistics at the desired frequency from attenuation values measured at a lower frequency. This is very much applicable where and when reliable long-term rain attenuation statistics are available. Numerous scaling models have been developed either from theory, from empirical data of various propagation experiments or from both (Islam et al., 1999).

Generally, statistical models (such as ITU-R) are suitable for establishing fade margins to mitigate the impairment of transmitted signals. However, it has been highlighted by various research that the proposed margin cannot cater to large attenuations and acute impairments in tropical regions (Ismail et al., 2013; Sujimol et al., 2015; Yaccop et al., 2016). The design and deployment of satellite systems in tropical regions for higher frequencies require an accurate and precise prediction of impairment statistics. The statistics must have the smallest error margin to employ several adaptive techniques at the receiver system. This applies to Malaysia, a country with a tropical climate with persistent heavy rainfall every year. The research outcomes will help in solving the relevant problems and setting an appropriate link budget when designing new satellite networks. Appropriate allocation of higher power transmission can be deployed to overcome rain fade endured by higher frequency satellite-Earth links.

1.2 PROBLEM STATEMENT

The terrestrial network has a serious limitation in terms of offering mass coverage for rural areas and isolated locations. This can be complemented by satellite-Earth

communication that delivers broadband connectivity to unreachable locations. Implementing SatCom in the mentioned areas would be more effective for investment cost and installation time. Numerous sectors were affected by the Movement Control Order (MCO) during the Covid-19 pandemic. For example, the education and employment sectors were unable to continue physical operations and had to run online. The efficiency and effectiveness of work and learning processes during that period were largely impaired. Parallel to the rapid technological advancement in the terrestrial link (the 5G network application), SatCom has also shifted to operate in higher frequency bands. This is to manage traffic congestion issues that occur in lower frequency bands as well as to address the increasing demands for larger broadband connectivity. The most significant challenge of applying a high-frequency band in areas with frequent heavy precipitation, such as Malaysia, is the degradation of satellite signals due to rain.

Most established rain attenuation prediction models are considered to be capable of providing a good estimation for temperate regions. Nonetheless, they might be deemed unsuitable and even referred to as inaccurate when applied to tropical regions. In many rain attenuation models, both terrestrial and satellite-Earth paths are semi-empirical models. This is mainly due to the inadequate understanding of the physics of rain. These models do not incorporate detailed characterizations of various rain types that cause signal impairments. Propagation studies at higher frequencies in tropical regions are very scarce since numerous rain attenuation prediction models have been developed for temperate region measurement data (Yeo et al., 2009; Cuervo 2016). The parameters involving rain characteristics and statistics suggested in the ITU-R prediction model cannot be applied to tropical regions. The ITU-R model is implied to underestimate the rain attenuation in Malaysia. The predicted rain rates suggested by the ITU-R also do not consider the overall severity of rainfall in the country (Khairolanuar et al., 2015).

The prediction of rain attenuation in tropical regions has been widely examined. Most were derived from the general rain attenuation prediction methods that require localized rain rate data from a specific place or region. The actual performance of these propagation models for higher frequencies in tropical regions remains undefined (Cuervo et al., 2016). It is advisable to adopt a non-meteorological approach, such as the frequency scaling technique, as an alternative way to predict rain attenuation.

Scaling of rain attenuation statistics as a function of frequency is a useful method when appropriate measured attenuation data is available for a specific location. The technique predicts the attenuation statistics at one or more frequencies based on the measured attenuation statistics at a different frequency. Scaling methods are generally applicable in the statistical sense which apply to exceedance probabilities averaged over a considerable length of time.

The latest frequency scaling technique proposed by ITU-R was used to generate the long-term statistics of rain attenuation on Earth-space links in tropical regions (ITU-R P.618-13, 2017). Somehow, the proposed method by the ITU-R 618-13 seems to underpredict the rain attenuation values in tropical regions. Most previous studies related to frequency scaling techniques of rain attenuation were proposed based on data obtained from temperate regions. Rain attenuation in tropical regions cannot be accurately obtained from such procedures (Ulaganathan et al., 2016). The ITU-R P.311-15 proposed that in the effort of obtaining a high-accuracy model, the best prediction method should produce the smallest values of statistical parameters. Long-term statistical data, especially from tropical regions, are required to enhance the model's precision and accuracy. A comprehensive study is essential for exploring the frequency scaling technique to acquire a better rain attenuation prediction model.

Several studies on frequency scaling of long-term statistical methods were accomplished. The outcomes revealed that such techniques only have 10% accuracy for the probability range between 0.001% to 0.1% (COST, 2011; Toriola et al., 2021). This indicates that the application of frequency scaling methods from measured rain attenuation data is required to reliably predict rain attenuation. Instead of using measured rain rate data, it is advisable to utilize rain attenuation data for the desired location. It was observed that the scaling factor is more influenced by the year-to-year variability than by the site-to-site inconsistency. The same formula may therefore be used for different regions as well. The overview of the system setup for rain attenuation studies of the C and Ku-bands is shown in Figure 1.2, while the overview of the system setup for Ka-bands is shown in Figure 1.4. The miniature model of satellites Measat-3 and Measat-5 are displayed in Figures 1.3 and 1.5 respectively.

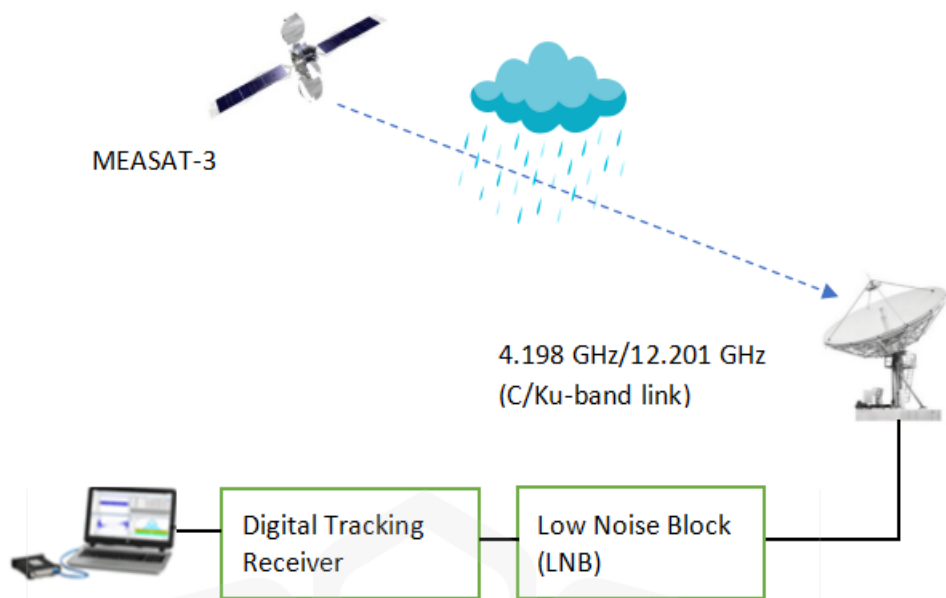


Figure 1.2 Overview of System Setup for the C & Ku-bands



Figure 1.3 Miniature Model of Measat-3 Satellite

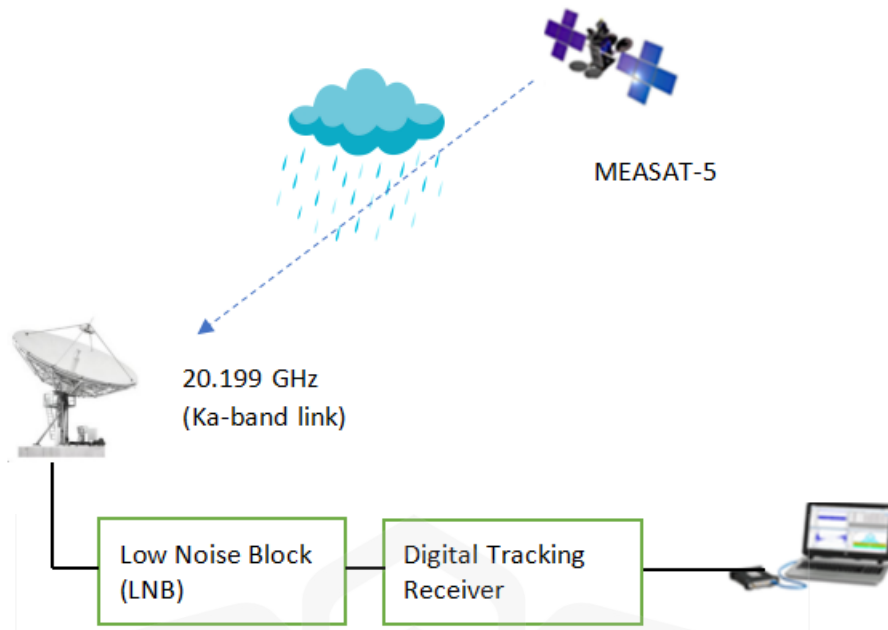


Figure 1.4 Overview of System Setup for the Ka-band



Figure 1.5 Miniature Model of Measat-5 Satellite

1.3 PURPOSE OF THE STUDY

This research aims to assess and identify a suitable frequency scaling formulation for satellite communication links in tropical-equatorial regions. The difference in terms of frequency scaling formulation from the ITU-R model when compared to the tropical or equatorial climate will help identify the improvement of rain attenuation prediction in the region. The new frequency scaling formula can be used to enhance the current rain attenuation prediction model. The cost to launch a satellite system is very high, therefore, accurate prediction for reliable satellite link availability is important. This is crucial for creating the best plan, the most cost-effective implementation and the fastest rollout for next-generation satellites or High-Throughput Satellite (HTS) systems.

The cost of installing and deploying millimetre-wave bands at the Earth terminal is also extremely high. Proper planning must be supported by significant and credible research. Satellite design requires a margin to resolve the anticipated fading within a link budget. To cater to the fading that is likely to occur for several hours during a year, greater transmission capacity, as well as enhanced antenna capability, may be required. This will entail tremendous capital investments. Alternatively, a smart power controller can be deployed along with adaptive processes, such as adaptive power regulation and adaptive encoding. The transmission power can be raised to compensate for the attenuation measured at the Earth station's receiver. Overall, understanding and determining accurate fade margins likely to be experienced by satellite-Earth links is extremely crucial.

Numerous researchers have attempted to implement frequency scaling using the empirical frequency scaling ratio. However, most had only focused on instantaneous frequency scaling (Luini et al., 2021; Acharya, 2020; Vidyarthi et al., 2017; Cuervo et al., 2017; Nessel et al., 2014). In this work, the proposed statistical frequency scaling technique involves the use of local attenuation data. It should also be applicable during the condition of rain along the signal path. The statistical frequency scaling technique offers a reliable fixed attenuation margin that can be used for link budget planning.

1.4 RESEARCH OBJECTIVES

The objective of this study is to expand the knowledge concerning propagation effects, climatological influences, refined propagation and attenuation modelling for satellite communication. These aspects also apply to satellite broadcasting systems that provide services in tropical regions.

The specific objectives of the study are summarised as follows:

1. To identify the best fade margin for rain attenuation at C, Ku and Ka-band radio frequencies at Cyberjaya, Malaysia.
2. To formulate a new frequency scaling model capable of accurately estimating the fade margin of millimetre-wave satellite links for desired availability in tropical regions.
3. To validate the frequency scaling technique in tropical regions with attenuation data from a different year as well as data from various countries in tropical areas.

1.5 RESEARCH QUESTIONS

The followings are the research questions of this study:

1. What is the monthly and annual time exceedance probability of less than 1% for the average rainfall rate in tropical-equatorial rain conditions?
2. What is the monthly and annual time exceedance probability of less than 1% for the average rain attenuation in satellite-Earth frequency bands such as C, Ku and Ka-bands for equatorial-tropical rain conditions?
3. What are the fade margin values of the Quality of Service (QoS) requirement for communication services and broadcasting applications?

4. Does the recommended frequency scaling method by ITU-R 618.13 provide a dependable rain attenuation prediction in tropical regions?
5. Does the derived frequency scaling model from equatorial-tropical regions able to improve the prediction of the rain attenuation model?

1.6 THEORETICAL FRAMEWORK

Statistical frequency scaling is the implementation of statistical values at a base frequency to predict attenuation statistics at the desired frequency. Ratio Attenuation Statistics (RAS) is the division of two statistical attenuation values (upper frequencies, A_2 , and lower frequencies, A_1) at the same percentage of time of occurrence, p . The RAS is easier to acquire compared to the Ratio Attenuation (RA) value for the m event, which is used by instantaneous frequency scaling.

Statistical frequency scaling techniques in satellite-Earth communication can be obtained by correlating the annual Cumulative Distribution Function (CDF) of rainfall rate with the annual CDF of rain attenuation. The relationship between attenuation at two different frequencies is also accomplished. Figure 1.6 describes the research framework for formulating the frequency scaling of rain attenuation in tropical regions.

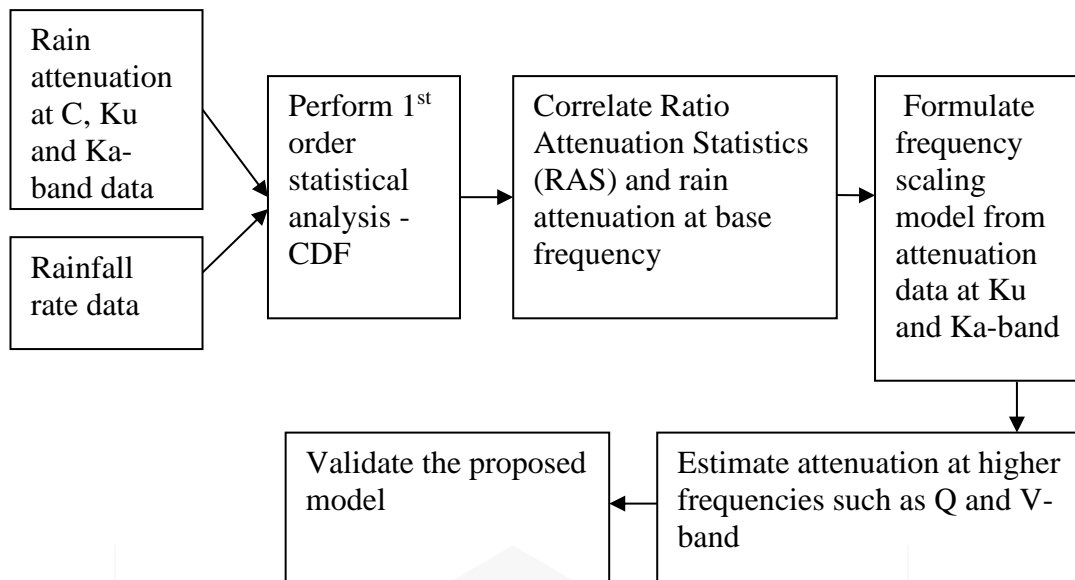


Figure 1.6 Theoretical Framework of Statistical Frequency Scaling Study

1.7 RESEARCH SCOPE

To obtain a better and more reliable rain attenuation prediction model that suits tropical climates, this study only covers tropical areas and excludes temperate regions. This study also only focuses on the propagation of satellite-Earth links and not terrestrial links. The measured satellite frequency bands are for the C, Ku and Ka-bands with values of 4.198 GHz, 12.201 GHz and 20.1998 GHz, respectively, originating from MEASAT-3 and MEASAT-5 which use beacon signals. The available rain attenuation data was retrieved from the Earth station located at Cyberjaya. It was processed only during rainy days as recorded by the rain gauge installed at Cyberjaya. The two years of data, from January 2015 to December 2016, were successfully processed. The attenuation data in 2016 was statistically processed to obtain a new frequency scaling formula. The attenuation data for the year 2015 was statistically employed for validation purposes.

The idea of frequency scaling can be expanded to involve other parameters of rain attenuation, such as polarisation scaling, elevation angle scaling and path length scaling. This is because attenuation is a function of the path length, elevation angle and frequency. However, the research only concentrated on attenuation as a function of frequency. Frequency scaling of attenuation can be implemented with statistical scaling and instantaneous scaling techniques. For this research, statistical scaling is highlighted instead of instantaneous scaling frequency. Instant frequency scaling is an attenuation of the reference frequency scaling to anticipate the attenuation in each unit period at the desired frequency. Scaling of statistic frequencies allows link budgets to be determined for new systems with a fixed attenuation margin.

1.8 RESEARCH PHILOSOPHY

This section discusses the research philosophy of the study, involving the investigations accomplished based on empirical analysis. A new formulation was developed from the data outcomes using empirical assessment. A frequency scaling technique for rain attenuation prediction on a given path was developed in the experimental methodology.

The empirical modelling produced in the research refers to the mathematically definable relationships of the system rather than computer designation based on empirical observations. To develop the empirical model and conduct statistical analysis based on the obtained data, software such as Microsoft Excel and MATLAB are applied in the study. The empirical formulation was developed according to the rainfall and rain attenuation data obtained from the Earth station in Cyberjaya for one year. The distribution pattern was examined, and the resultant equations were presented.

1.9 RESEARCH HYPOTHESES

Tropical regions, especially equatorial areas, experience severe rainfall on a daily basis. The general model of rain attenuation prediction is based on the utilisation of climatic data at a specific location or region for satellite communication links. However, there is a non-meteorological approach that can be deployed to predict rain attenuation. The technique is deemed capable of generating attenuation statistics at other frequencies from the measured attenuation statistics at a specific available frequency. The input variables applied to the formulation are frequency and attenuation values. An improved rain attenuation estimation can be derived from the formula of frequency scaling, which was accordingly revised to be the best analytical fit for tropical-equatorial attenuation data.

1.10 SIGNIFICANCE OF THE STUDY

Accurate formulation of the rain attenuation model involves longer data collection of rainfall rates in Malaysia. Further comprehensive analysis of the satellite system's performance in tropical regions will be of great concern. Tropical regions typically experience high rainfall intensity which is or should not be, affected by month-to-month variations. The analysis includes determining the rain attenuation of C, Ku and Ka-band links along the slant path in tropical regions. In the study, the direct measurements involving the rain attenuation information of C, Ku and Ka-bands are significant in investigating the statistical analysis of rain attenuation. A more reliable predicted value of attenuation is anticipated to be achieved with C, Ku and Ka-band propagation data collected during a one-year duration. The proposed frequency scaling model that estimates rain attenuation at other frequencies is the optional method offered when rainfall data is unavailable. Knowing the fade margin value at the required link availability in the system design is extremely important. It is required to overcome the

losses in signal strength due to rain over the path. The best performance of satellite communication services that can meet user satisfaction would be consistently delivered even during heavy rainfall.

The research outcome will contribute to the development of an alternative formula that accurately estimates rain attenuation in tropical regions. The proposed technique is a statistical frequency scaling model that can generate statistical attenuation values at a higher frequency. The model can also provide data for a higher frequency of slant path attenuation in tropical regions. The extrapolation technique was applied to the rain attenuation of the Ka-band. The worst month analysis was also accomplished in this research. The critical part of the study is the derivation of the frequency scaling method to estimate rain attenuation at higher frequencies. Throughout the research, one conference proceeding, one non-index journal and three indexed journals have been published. The research outcomes are expected to be beneficial for future enhancements of the fade margin in satellite links during rainfall in tropical regions. The cost of pre- and post-operations of satellite launches is high, therefore, this research will assist decision-makers and satellite designers to enhance cost efficiency, link availability and throughput. Hopefully, this decision will help to provide a better-received signal in broadcasting and telecommunication services. The databases made available from the measurement campaigns in Malaysia provide excellent opportunities to examine the propagation characteristics in tropical regions.

1.11 LIMITATIONS OF THE STUDY

The study employed the measurement data of the received beacon signals for the three frequencies previously mentioned in the scope of the research. The frequencies originated from two different satellites. The C and Ku-band signals were from MEASAT-3 and the Ka-band signal was from MEASAT-5. These satellites are in different orbit locations. There is a small difference in the elevation angle during the

measurement of the beacon signal. The rain gauge was installed at the ground station located in Cyberjaya. There were days when the rain gauge was deemed inoperable. As an alternative, rain attenuation was compared using a nearby alternative rain gauge owned by the Department of Irrigation and Drainage (DID). The sensor should have a similar coverage of rain conditions near Cyberjaya. The study's limitation is the all-inclusive availability of data. There were days where attenuations were observed but somehow no rain event was recorded in Cyberjaya. This is probably because the rainfall did not directly pour into the rain gauge due to the wind draft at the location. Attenuation was detected since the rain had occurred along the path of the satellite links, despite the rain did not localize in the Cyberjaya area. The rain attenuation data for the C-band during November 2016 was incomplete. The C-band data for December 2016 was also unavailable. It has been acknowledged that the ground station underwent a system downtime for technical maintenance purposes during these months. The data for November and December were then extrapolated using information from other available months. The attenuation data belongs to MEASAT and ASTRO. Acquiring the datasets was a complicated process. It required significant bureaucracy and security clearance procedures as well as official agreements. The rain attenuation data in 2016 was used for developing the frequency scaling technique due to the availability of concurrent rainfall data. The validation of the proposed model was accomplished on two measurement datasets. The first and second datasets include the rain attenuation data at Ka-band retrieved from an Earth station in Cyberjaya for the year 2015 and Rawang station for the year 2016, respectively.

1.12 DEFINITION OF TERMS

An electromagnetic wave is a medium that carries information between the ground and space for microwave communications, including terrestrial and satellite systems.

The electromagnetic spectrum is all frequencies from zero to infinity.

Frequency is the rate of reversing the polarity of electromagnetic waves in cycles per second. The unit is in hertz (Hz).

Wavelength is inversely proportional to frequency. The proportionality constant is the value of the speed of light.

The frequency band is a range of frequencies.

Radiofrequency (RF) is a part of the electromagnetic spectrum that permits the efficient generation of signal power, its radiation into free space and reception at a distant point.

The fade margin is the difference between the level of the unfaded received signal and the threshold of the receiver's sensitivity.

Link availability is the percentage of time that a link is available.

Time exceedance is time the exceeded time that involves a system outage.

Quality of Service (QoS) is the measurement of standard for the overall service performance to ensure that consumers attain the best service quality.

Rain attenuation is the amount of signal loss in dB, as detected at the receiver, due to rain (Ozuomba & Kalu, 2015).

1.13 ORGANIZATION OF THE THESIS

To produce plausible and well-organised research that covers the study aim and the methods employed, this thesis was divided into five chapters.

Chapter Two highlights a comprehensive literature review on the propagation impairment endured by satellite-Earth links, the classification of tropical climates, rain attenuation due to precipitation, fade margin requirement, rain attenuation prediction

model, frequency scaling technique and a summary of previous related research. The chapter begins with a brief explanation of propagation impairment in satellite-Earth links. Next, the classification of tropical climates and rain attenuation due to precipitation is discussed since Malaysia annually experiences high precipitation. The chapter continues to elaborate more on the fade margin and rain attenuation model, with a focus on frequency scaling techniques. Afterwards, previous related studies on frequency scaling techniques are reviewed, summarised and arranged accordingly.

Chapter Three focuses on raw data collection, extraction and conversion of data into first-order statistical rain attenuation information. The analysis is divided into three main parts. The first part involves the compilation of the monthly and annual Cumulative Distribution Functions (CDFs) for the rain attenuation data of the C, Ku and Ka-bands. The second part determines the worst month statistics. The third part covers the focus of the study, where it outlines the development of a new frequency scaling formulation as well as the validation of the proposed formula.

Chapter Four presents the results and findings, including the annual CDFs. The chapter explains the outcome of the proposed frequency scaling technique and its validation. Chapter Five highlights the discussion and conclusion of the overall project. It also features a framework and suggests improvements for future research.

1.14 CHAPTER SUMMARY

This chapter briefly discussed the background of the study. It highlighted the impact of rain attenuation in areas that experience frequent rainfall. The frequency scaling technique is an alternative method for predicting rain attenuation. The problem statements that led to accomplishing this research were highlighted. The research questions and hypotheses were briefly discussed. The theoretical framework was outlined, clearly showing how the research was managed and conducted. The scope and limitations were discussed to maintain the research focus. The chapter concluded with

the organization of the thesis. The study is crucial in predicting the fade margin of rain attenuation at a higher frequency band by using the frequency scaling technique. A more reliable fade margin value was identified from the annual availability of CDFs generated using data from tropical regions, making the research outcomes very significant. The main research contribution is the applicability of the new model in estimating rain prediction with increased accuracy as compared to the available model.



CHAPTER TWO

LITERATURE REVIEW

2.1 INTRODUCTION

Chapter Two introduces the relevant theoretical backgrounds which are considered essential for the research. The chapter also briefly discusses the classification of microwave communication systems. Several important pieces of knowledge in conducting the research including the propagation impairments in the satellite-Earth link, spectrum allocation to the satellite system, rain attenuation in tropical regions, and available frequency scaling techniques in predicting rain attenuation are described in this chapter. Rain attenuation becomes the main challenge in deploying the higher frequency bands in tropical regions that experience severe rain conditions. It leads to signal losses at the receiver and transmission power will be increased to overcome the loss of signal. The losses can be encountered if the margin is accurately determined. This chapter also explains the steps in performing the worst month analysis in tropical regions.

The transmission of signals through radio waves which utilize a series of radio wavelengths measured in small numbers of centimetres is defined as microwave communication (Mohamed & Nadir, 2005). A microwave radio system is usually used in broadcasting and telecommunications transmissions. Microwave communication systems can be divided into two types which are satellite systems and terrestrial systems (Mao, 2021). Both of these systems have transmitters and receivers to transmit and receive the signals. In general, the transmitter converts a baseband signal to a microwave signal. The microwave signal is converted back to the baseband signal via the receiver. The baseband signal is a multiplexed signal. The multiplexed signal carries several individual low bandwidth signals such as voice, data and video.

2.1.1 Satellite Communication System

A satellite communication (SatCom) system is a system that uses a microwave repeater station, permitting two or more users to deliver or exchange information with appropriate Earth stations. The basic elements of a communications satellite system are the space segment and ground segment (Elbert, 2008). The space segment consists of the spacecraft and launches mechanism. The ground segment comprises the Earth station and network control centre of the entire satellite system. Electromagnetic waves are used as carrier signals that carry information such as voice, audio, video, or any other data between ground and space and vice-versa.

SatCom consists of four major phases. The first step is when an uplink Earth Station transmits or beams the required signal to the satellite. The second step is when the onboard transponders at the satellite amplify the incoming signal and change the frequency to differentiate between incoming and outgoing signals. The transponder in the satellite system is used to provide connectivity between source and destination stations. The third step is when the satellite transmits the signal back to the Earth station. The last step is when the ground communication system at the Earth station receives the signal (Mitra, 2008). The transferred data usually refer to voice (telephone), video (television), and digital information. Figure 2.1 shows the satellite communication system.

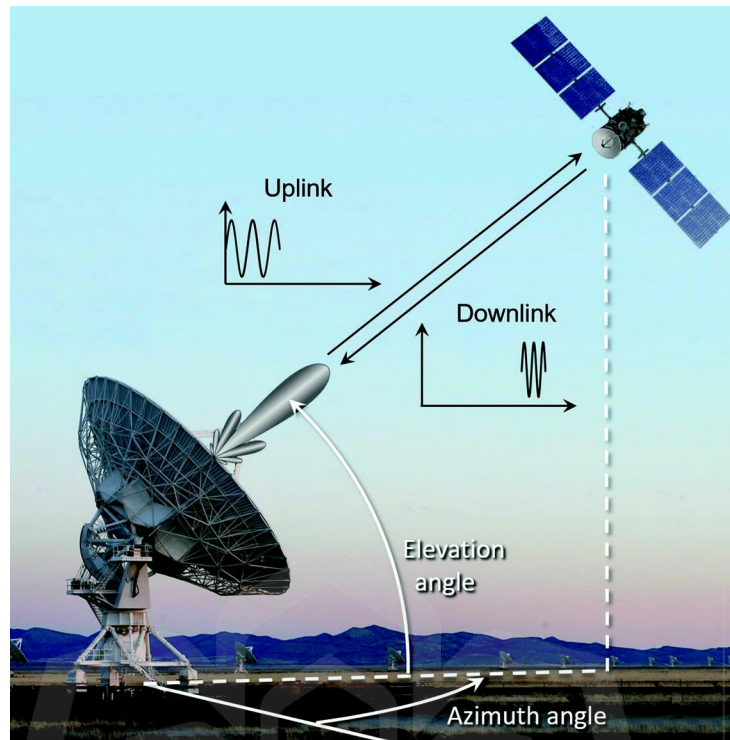


Figure 2.1 Satellite Communication (SatCom) System (Walter, 2018)

2.1.2 Terrestrial Communication System

In a terrestrial communication system, a microwave link consists of a transmitter and a receiver designed in a point-to-point link system. The transmitter and the receiver are each connected to their antenna respectively. The terrestrial system is affected by Line-Of-Sight (LOS) which microwave frequency gets attenuated due to buildings, trees as well as geographical locations (Yee et al., 2007). Besides, the ground distance is limited from one part of the Earth to the other as the long distance will reduce the power of transmission. Thus, multi-section relays or repeaters are used between sources and destination stations to extend the range of the terrestrial communication system. Figure 2.2 illustrates the terrestrial communication system.

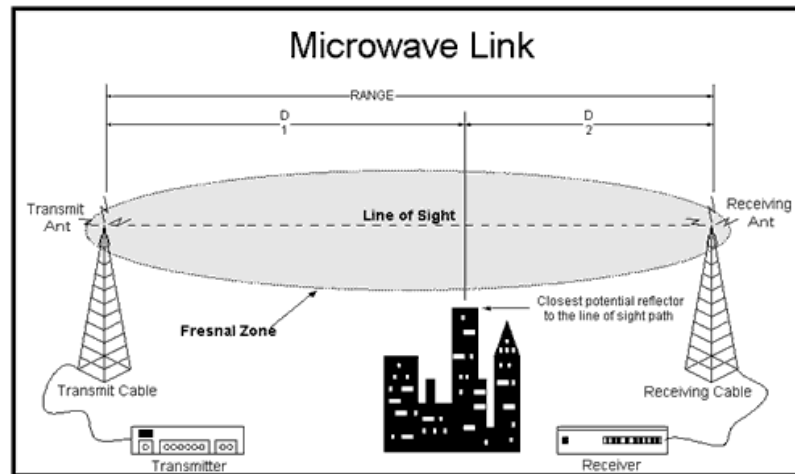


Figure 2.2 Terrestrial Communication System (Yee et al., 2007)

2.2 IMPORTANCE OF SATELLITE COMMUNICATION SYSTEM

The advancement of the SatCom system towards higher frequencies is parallel to the development of terrestrial technology in providing better communication system performance. SatCom system assists to deliver successful digital and internet applications in remote and unreachable locations. It accelerates the 5G technology expansion and sets new levels of performance for enterprise, telecommunication, defence system, telemedicine, and government broadband connectivity on land, air, and sea. SatCom system is important in areas which are broadcasting information across a wide region and allowing remote communications access to isolated places or rural areas (Lutz et al., 2004). Terrestrial communication develops tremendously in heavily built-up areas such as cities and suburban communities, despite the inability to cover rural areas since it is costly (Cuervo et al., 2016). The advancement of fibre optic networks has not weakened the importance of satellite communication systems, especially for rural, remote, and inland cities across the globe (Malinga et al., 2013). In regard to that, the government of Malaysia has come out with a national broadband initiative by executing the application of satellite in providing internet access to rural

areas (Ahmad et al., 2019). SatComs are developed to higher bands in delivering high-capacity data rates to accommodate all the demands. This is parallel to terrestrial communication that goes up to 5 GHz technology to furnish the technologies needed (Samat et al., 2019).

Satellite broadcasting delivers a bright future in terms of the economy if attractive content can be provided. All television coverages are covered by the SatCom system whereas the channel reaches directly to the home from space which is known as direct-to-home (DTH) multimedia services (Shrestha et al., 2017; Usha & Karunakar, 2020). It is similar to data communication applications in which users require all the data to carry out their business regardless of time and place. The necessity of having a telecommunication system to be connected is a trigger point for the majority of countries around the world to use SatCom. SatCom systems are also developing multimedia information and personal communication to reach many potential users. This leads to the quality improvement of the telephone network system (Malinga et al., 2013).

SatCom is the best option to reach in the area of emergency preparedness and response (Abubakar et al., 2019). SatCom has maintained reliable television broadcast and transmission around the nation in the event of all terrestrial long-distance lines out of the city being disconnected. It happened when the earthquake hit Mexico City in September 1985. Satellite communications were also utilized to facilitate disaster relief on the island of Sumatra after the December 2004 earthquake and subsequent tsunami (Lee & Winkler, 2011). With the implementation of the SatCom system, countries that are unreachable by terrestrial communication infrastructure can experience high-speed data communication services. This is very essential in critical applications such as telemedicine disaster monitoring as well as distance learning (Lee & Winkler, 2011). SatComs in general, offer alternative modes of transmission when terrestrial microwave, cable, or fibre networks cannot be applied. In addition to that, Satcoms also provide the following benefits:

- i. Wide area coverage and cost-effective

The costs for satellite-based transmission are more consistent, particularly for international or intercontinental communications across

long distances (Ahmad, 2019). It generally covers a wide area in a single setup, hence, is more cost-effective for rural areas, long-distance areas, or in any case of emergency.

ii. High Capacity

High carrier frequencies and huge information bandwidths are required for satellite communications networks. Typical communications satellites have capacities ranging from tens to hundreds of megabits per second (Mbps) and may support hundreds of video channels or tens of thousands of phone or data lines (Abubakar et al., 2019; Samat et al., 2019).

iii. Diverse user networks

The applications of satellite communications can be expanded into satellite-based air traffic management, personalized land mobile radio broadcasting, and aeronautical satellite communications due to the advantages offered (Lutz et al., 2004). Thus, higher demand for greater bandwidth of satellite communication will shift to higher frequency band deployment (Ghanim et al., 2018).

Even though the signal usually degrades when transmit through the atmosphere, especially in higher frequencies, there is a mitigation technique that can contribute to successful system performance (Acharya, 2019; Lyras et al., 2016; Saad et al., 2013; Yunus et al., 2016). Therefore, having an in-depth knowledge of the types of atmospheric effects that impact satellite communications in tropical regions is essential (Lwas et al., 2015), especially in designing satellite link budgets (Fadilah & Pratama, 2018; Yeo et al., 2014).

SatCom is essential for large populations that live outside the cities to keep up with the requirements of current global development. High Throughput Satellite (HTS) technology has changed the SatCom industry in recent years to facilitate a much higher capacity and reduce costs per Megabits per second (Mbps) so that it can be more affordable (Ahmad et al., 2019; Samat & Singh, 2020; Vidal et al., 2012). The HTS system has increased in the system capacity and data rates due to the use of multiple beams that apply frequency reuse (Widjanarko & Gunawan, 2017). The high availability of HTS allows for smaller terminals that support applications with

aeronautical and maritime mobility. HTS is beneficial in cellular use that requires data service in areas that are unreachable by cable or optical fibre networks (Samat & Singh, 2020). HTS satellite with high-speed internet is beneficial in providing better internet services to remote areas proving that the performance of HTS to conduit information is better than conventional satellites (Hidayat et al., 2019). Again, HTS is the best choice for providing high-speed satellite internet use for schools, health centres, police stations, and public facilities in remote areas.

2.3 DISTRIBUTION OF FREQUENCIES SPECTRUM

The design of satellite communication links depends on the frequency of operation (Jong et al., 2015). The satellite systems designer technically operates within the constraints of international and domestic radio frequency bands. Frequency bands are allocated for various purposes by the International Telecommunication Union (ITU), a specialized agency of the United Nations that has its headquarters in Geneva. Members of the ITU are responsible for assigning radio frequencies in allocated bands to domestic users (Kestwal et al., 2014). Because the RF spectrum is a limited resource, the ITU has allocated the same parts of the spectrum to many countries and for many purposes around the globe (Ahmad, 2019). The frequency band designation by wavelength is summarised in Figure 2.3.

Frequency	Wavelength		
3 Hz	10 ⁸ m	—	
30 kHz	10 ⁴ m	→	VLF Very Low Frequency
300 kHz	10 ³ m	→	LF Low Frequency
3 MHz	10 ² m	→	MF Medium Frequency
30 MHz	10 m	→	HF High Frequency
300 MHz	1 m	→	VHF Very High Frequency
3 GHz	10 cm	→	UHF UltraHigh Frequency
30 GHz	1 cm	→	SHF Super High Frequency
300 GHz	1 mm	→	EHF Extremely High Frequency

Figure 2.3 Wavelength Designation for Frequency Band (IEEE, 2002)

Various frequency bands are allocated to satellite transmission while some segments of the band can be transmitted easily and propagate through the atmosphere with less fading. The spectrum for space-to-Earth applications lies between about 1 and 4 GHz and is perfect for transmission since it is less affected by weather (Ahmad et al., 2022). The Super High Frequency (SHF) range has been divided into common usage into sub-bands with letter designations, the familiar L, S, C, X, Ku and Ka-bands being included. Generally, Ku-band and frequencies below 10 GHz are the most popular because of the relatively low cost of equipment and good propagation characteristics. Meanwhile, the Ka, V and Q-bands employ millimetre wavelengths and are potentially useful for very high-frequency bandwidth transmissions into small receiving antennas. Despite that, there are challenges in applying the millimetre-wave bands due to increased rain attenuation and hardware expenses (Singh & Saleh, 2021).

The VHF and UHF bands lie within the range from 30 to 300 MHz and from 300 to 3,000 MHz, respectively. The band within the range of 400 MHz and 1,000 MHz is for SatCom application purposes. However, that range already is highly congested for terrestrial wireless applications such as cellular, mobile data, and various radio systems

of government and emergency services. A system that employs VHF/UHF takes as random for fading and disruption in transmission (Albert, 2008).

The 1 GHz represents the starting frequency for satellite-Earth microwave applications. The L and S-bands are very effective in providing vast communications by way of mobile and transportable Earth stations. The antenna that has been used for two-way voice and data service is a small Yagi (TV-type antenna), a wire helix, and a quarter-wavelength rod. The size of the antenna is reduced by applying the high satellite transmit power for each channel of communication (voice or data) (Albert, 2008).

2.3.1 Microwave Bands (C, X and Ku-bands)

SatCom usually employs C, X and Ku-bands which lie between frequencies of 3 to 15 GHz. Compared to L and S-bands, these bands offer larger bandwidths. C-band is deployed in broadcasting industries such as cable TV in North America and satellite DTH in Asia. The C-band is also popular in domestic and international telephone services in large countries such as China, Russia, Brazil, and Mexico. X-band is a specially assigned medium for fixed services for government and military users. The ground terminals that have been developed for these applications are designed to operate under all types of weather by soldiers and security forces in many countries. Ku-band was first exploited in broadcasting such as in TV distribution and became the band of choice for DTH and VSAT networks in developed countries (Albert, 2008).

2.3.2 Millimetre Wave (Ka, Q and V-bands)

Since the C and Ku-bands tend to become congested, millimetre wave bands offer greater bandwidth and smaller wavelengths. Ka-band with its 30/20-GHz allocations and about 2.5 GHz of the available spectrum was first considered and after that, the frequencies above about 40 GHz which are known as Q and V-bands are evaluated for space and ground applications because of the wide bandwidths offered. Ka-band (30/20 GHz) was considered to be used for commercial applications in cases where C and Ku-bands are fully occupied. However, during rainy conditions, the applications that employ these frequencies must allow for some periods of total outage (Albert, 2008).

A Ka-band communication satellite is an alternative to an unreachable terrestrial communications network system, that is embattled in areas that are not covered by terrestrial communications networks. The primary Ka-band application comprises voice messaging services in remote areas, maritime and in-flight Internet connection services, community Internet services, emergency communications, TV broadcasting services, Internet of Things (IoT) data transmission, and company and government agency intranets (Kalaivaanan et al., 2020). Ka-band technology provides a new range of frequencies for the satellite communications market with the benefits of HTS (Christensen, 2012). HTS is more cost-effective for delivering higher quality, better performance, and higher speed services (Hidayat et al., 2019).

As now the world is in the Fourth Industrial Revolution (4th IR) and Internet of Things (IoT) data transmission, the demand to transfer data volume is increasing (Samad et al., 2021). The millimetre-wave (mm-wave) frequency is a feasible alternative for offering bandwidth to transfer the higher data volume (Choi, 2021). However, the mm-wave frequency is very vulnerable and susceptible to rain attenuation for terrestrial or satellite communications applications (Al-Samman et al., 2020). Thus, the wavelength of the signal determines the interaction effects of the atmosphere which leads to link path degradations and further affects the quality of services (QoS) (Osahenvemwen & Omorogiuwa, 2017).

2.4 CLASSIFICATION OF TROPICAL CLIMATE

The region of the Earth by the Equator lies in latitude by the Tropic of Cancer in the northern hemisphere at approximately 23°27' North and the Tropic of Capricorn in the southern hemisphere at 23°27' South is known as the tropics or tropical regions or torrid zones. Tropical regions comprise the tropical zone, equatorial zone, and sub-equatorial zone as shown in Figure 2.4. Tropical countries are including India, Bangladesh, Burma, Thailand, Indonesia, the Philippine Islands, South China, Central America, West India, Venezuela, Brazil, Nigeria, Singapore, and Columbia.

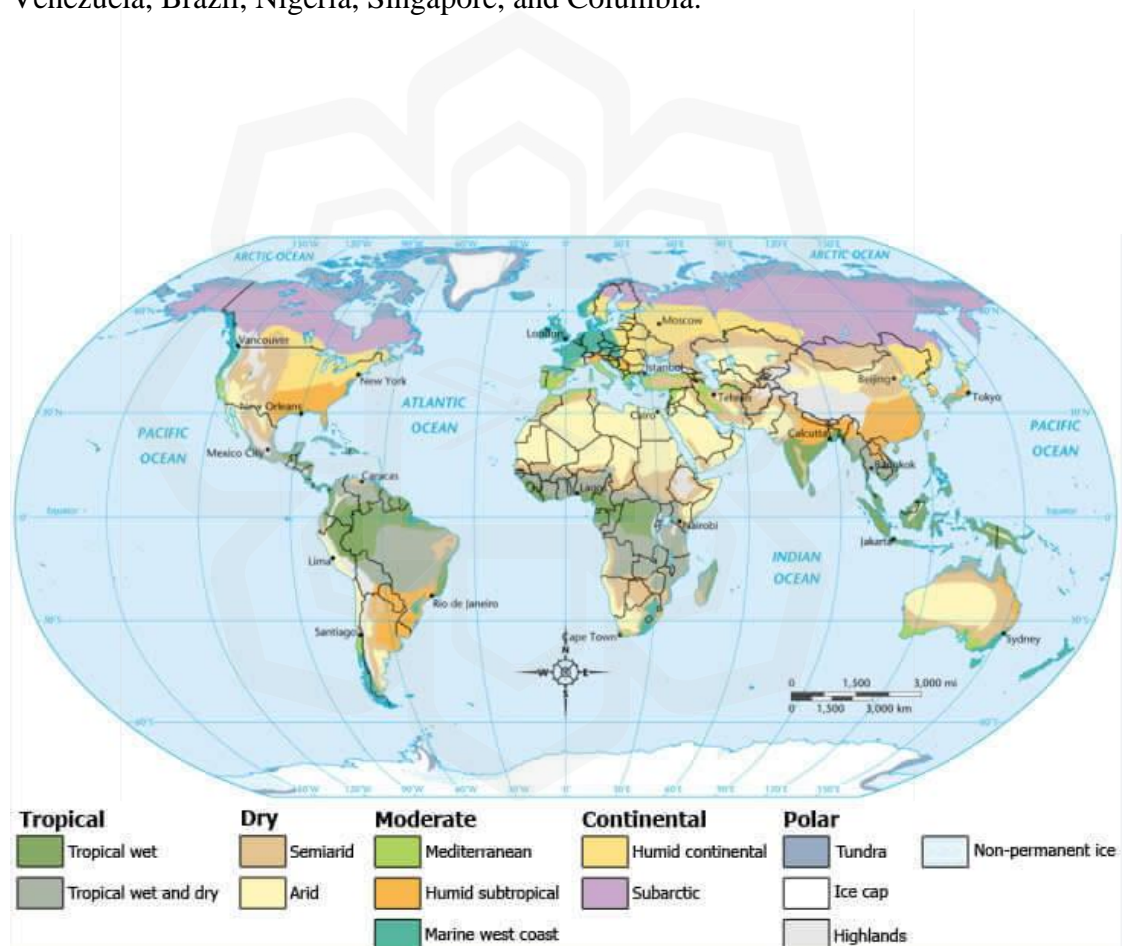


Figure 2.4 Climate Region (Mustafa et al., 2017)

2.4.1 Distribution of Equatorial Climate

The region that lies between 5° and 10° of North and South of the equator is known as the equatorial region with a hot and wet climate throughout the year. Equatorial regions comprise the lowlands of the Amazon, the Congo, Malaysia, and the East Indies. Indonesia, Vietnam, and Sri Lanka share a similar climate to Malaysia. Some of the Central and South American countries with equatorial climates are Colombia, Brazil, Venezuela, Nicaragua, Panama, Guyana, Suriname, and Peru. Tropical climates experience a dry season which is two months or more with less than 50 mm of total rain while equatorial climates possess no dry season. Equatorial climates show only little variation in temperature during the day and throughout the year (Green, 2004). Figure 2.4 shows the regions of the world which experience the hot and wet equatorial climate. Rainfall intensity in the equatorial region is very high, usually from 2,500 to 3,500 mm per year, and well distributed throughout the year. The average relative humidity is around 80% and there is no month without rain as well as a distinct experience of the dry season like those of the Savannah. The Equator region has a tropical rainforest climate, also known as an equatorial climate which has an average annual temperature of around 30 °C (86 °F) during the day and 23 °C (73 °F) at night.

2.4.2 Malaysia's Climate

Malaysia is located in the Southeast Asian region. Land borders are shared with Thailand, Indonesia, and Brunei, and maritime borders exist with Singapore, Vietnam, and the Philippines. Malaysia contains the southernmost point of continental Eurasia which is Tanjung Piai. Malaysia is located near the equator and has a tropical and equatorial climate. Malaysia is one of the Asian countries that is located just north of the equator in which the climate is equatorial. The Peninsula of Malaysia is situated between 3° and 7° North of the Equator as shown in Figure 2.4. Its position in the

equatorial zone guarantees a classic wet tropical climate with relative humidity levels usually around 95%.

Since Malaysia is completely located in the tropical zone and lies in the equatorial zone which is about 3.08° North of the equator as shown in Figure 2.4, its climate is influenced by consistent temperature, high humidity, and heavy rainfall (Abdulrahman et al., 2015; Cuervo et al., 2016; Samat & Singh, 2020). The average rainfall in Malaysia is around 2,500 mm (98 in.) and the intensity of rainfall rate in Malaysia is 222 mm/hr (Nizhanthi, 2012; Omotosho et al., 2017). This is because Malaysia often experiences heavy rainfall due to convective rain and thunderstorms (Chakraborty et al., 2021). The rains are caused by the monsoon regime since Malaysia is near the Equator and surrounded by the sea, therefore is no real dry season (Mandeep et al., 2008). The average daily temperature throughout Malaysia varies from 26 °C to 28 °C (MMD, 2016).

As Malaysia is divided into two parts which are the peninsula and East Malaysia, both climates are slightly different. The climates of the peninsula of Malaysia are directly affected by wind from the mainland, and more maritime weather affects east Malaysia. Typically, Malaysia's climate is affected by winds blowing from the Indian Ocean (South-west Monsoon Winds - from May to September) and the South China Sea (North-east Monsoon Winds - from November to March). From March to the end of April, the season is called inter-monsoon (Omotosho et al., 2017; Samat & Singh, 2020). According to the weather report prepared by the Malaysia Meteorological Department (MMD), the year 2016 was recorded as the warmest year in Malaysia's history with a mean temperature of 27.66 °C exceeding 27.60 °C, as recorded in 1998 (MMD, 2016). The average temperature of Malaysia was 0.78 °C above normal, which was the average daily temperature from 1981 until 2010. On the other hand, the average maximum daily temperature in Malaysia was 0.70 °C above normal, while the average minimum daily temperature was 1.03 °C above normal.

Malaysia's weather was strongly influenced by the natural climate variability of Super El Nino that took place until the middle of 2016, and the La Nina conditions that began in the third quarter of 2016 (MMD, 2016). Despite the relatively severe dry season between February and April, in general, most areas of the country received the

average annual rainfall (Samat & Singh, 2020). Significant effects on Malaysia during the change of climates besides the increase in sea levels and rainfall also increased flooding risks and led to large droughts (Mandeep & Ng, 2008; Samat & Singh, 2019). Although the rainfall pattern of the West Cost Peninsular Malaysia (WCPM) is influenced by monsoon winds and El Nino events, topographical features affect inter-annual rainfall patterns (Sany et al., 2018). The northeast monsoon contributes 41% of the total rainfall, while the southwest monsoon contributes a little less (37%) in the region.

The rainfall pattern over the west coast of Malaysia is classified into two periods of maximum and two periods of minimum rainfall. The maximum rainfall usually occurs near the end of the year during the northeast monsoon, while the secondary maximum rainfall occurs in April-May (the second inter-monsoon period). Minimum rainfall is observed in January-February, while the secondary minimum rainfall occurs in June-July. The highest monthly rainfall of 314 mm occurs in December, which contributes about 14% of the mean annual rainfall. The lowest monthly rainfall of 115 mm is observed in February, which is 14% of the mean annual rainfall. Thus, during the northeast monsoon (November-March), both the minimum and maximum monthly rainfalls occur. River discharge variation significantly correlates with rainfall patterns (MMD, 2016; Wong et al., 2009). The total rainfall for the year 2016 in Malaysia is shown in Figure 2.5.

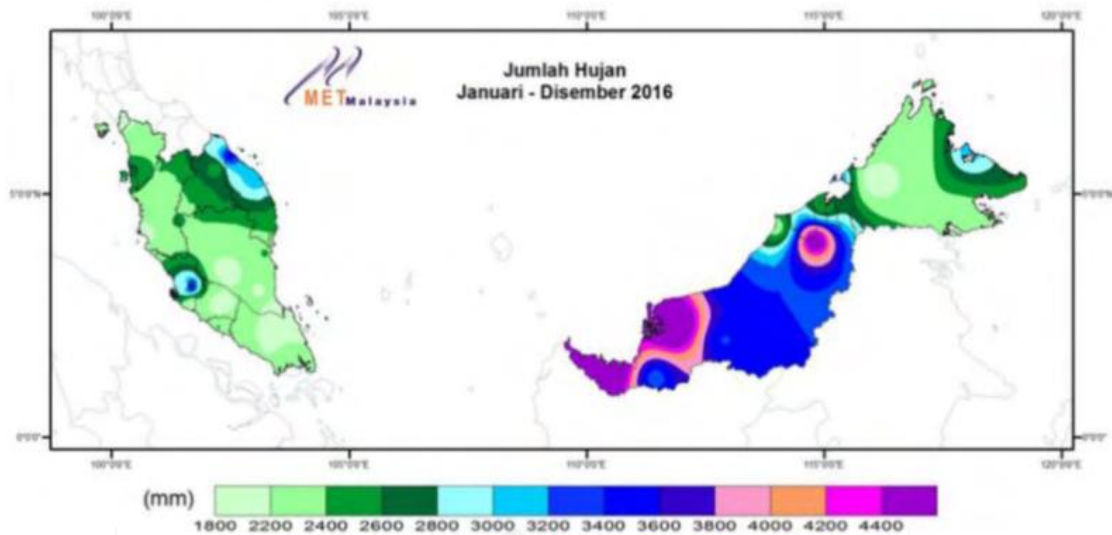


Figure 2.5 Total Rainfall in Malaysia in 2016 (MMD, 2016)

Precipitation is usually experienced by the propagation of a slant path of microwave and millimetre waves along tropical regions in the rain instead of snow or hail (Yussuff & Khamis, 2013). The precipitation characteristics in tropical regions are different compared to those in temperate regions. Rain attenuation is a significant impairment that produces a significant amount of loss compared to other environmental disturbances in terrestrial and satellite communications wave propagation links operating with microwave and millimetre-wave frequencies (Al-Saman et al., 2020; Grabner et al., 2017; Kalaivaanan et al., 2020; Samad et al., 2021). Rainfall is an inhomogeneous process in nature and a meteorological phenomenon with a complex structure attributable to its variability in duration, region, and occurrence frequency (Afahakan et al., 2016; Islam et al., 2018; Samat & Singh, 2020; Yussuff et al., 2019). The rain in tropical regions can be divided into two types which are stratiform and convective (Green, 2004; Lam et al., 2010; Osahenvemwen & Omorogiuwa, 2017; Yussuff & Khamis, 2014).

2.4.3 Precipitation Type in Tropical Regions

Convective rain is produced from clouds that are formed and stimulated by the strong movements of air masses due to differences in tropospheric pressure. Intense rainfall is defined as convective rain. Malaysia which is a tropical region experiences heavy rain throughout the year which is usually correlated with convective rain which is characterized as a high rainfall rate in short events with a limited region or smaller area (Das et al., 2013; Yussuff et al., 2014). Pek et al., (2016) claimed that convective rain is a rain rate exceeding 10 mm/h.

Stratiform rain, which is larger in the area is caused by the formation of small ice particles in the upper tropospheric layers. The small particles merge and produce bigger nuclei upon falling, and turn into raindrops upon reaching the Earth's surface, as the nuclei become unstable while passing through the melting tropospheric layer. During continuous rain events, a stratiform structure develops and spreads over larger areas with smaller intensities. According to Lee & Winkler (2011), the stratiform rain event happens at 30.5 hours for 15 minutes with a peak rainfall rate of 12 mm/hr. Meanwhile, the convective rain event happens in 32.4 hours for a duration of 3 to 4 minutes with a peak rainfall rate of 48 mm/hr. Badron et al., (2015) claimed that stratiform rain is determined by medium and low-rate events that occur for a longer period.

Rainfall in tropical and equatorial regions is also categorized into three types which are thunderstorms, showers, and drizzle according to their degree of intensity (Ulaganathen et al., 2013). Rainfall intensity is varying with time and location (Abubakar et al., 2019; Durodola et al., 2017; Nalinggam et al., 2012; Suryana et al., 2005). Rainfall in temperate regions is significantly different from tropical regions (Oluwayemisil et al., 2019).

A nucleus of rain, varying in diameter but with high precipitation, intensity forms a rain cell whose size increases as the intensity of the rainfall increases. (Albendag & Zain, 2020; Chakraborty et al., 2021). Distinctive dimensions of heavy rain rate cells are identified through radar measurements within the range from 2 to 5

km. The lifespan of each cell is short which is about 10 to 20 minutes but intense rainfall has a longer lifetime (Green, 2004). Rainstorms have a longer period of an event due to the tendency of forming new rain cells adjacent to existing ones. The propagation impairments in tropical regions are severe since the regions receive abundant rainfall throughout the year (Chakraborty et al., 2021). The propagated radio waves at the satellite-Earth link in tropical regions are seriously attenuated due to the convective rain which is heavy rainfall intensity (Samat & Singh, 2020).

2.5 PROPAGATION IMPAIRMENT IN SATELLITE-EARTH LINK AT HIGHER FREQUENCIES

The propagation impairments consist of signal attenuation, fading, crosstalk, inter-system interference, increase in sky noise temperature, and variation in the signal angle of arrival (Green, 2004). Propagation impairment in the 10 GHz and above on satellite-Earth paths in tropical and equatorial regions is very severe (Chakraborty et al., 2021). In microwave satellite-Earth link communication, reduction of energy and decrease in amplitude occurs when the signal propagates from satellites to Earth which are approximately 36,000 km. At the Earth station, the received signal is usually affected by propagation impairment from the tropospheric effect such as tropospheric scintillation, gaseous absorption, clouds, and rain distortion (Kubista et al., 2000). While travelling to receivers with longer slant paths and lower elevation angles, signals are passing over an occurrence of rain along their propagation paths and lead to rain attenuation (Nazrul et al., 2013).

Since equatorial and tropical regions experience abundant rainfall, the dominant impairment in the satellite-Earth link in tropical and equatorial regions is rain attenuation (Cuervo et al., 2016; Kalaivaanan et al., 2020; Momin et al., 2021; Yunus et al., 2016). Rain attenuation causes a decrease in the received strength of a signal due to a large number of losses along the transmission link (Yeo et al., 2014). The received

power of signals reduces before reaching their destinations leading to a reduction system's performance (Ahmad, 2019; Omotosho et al., 2017; Sujimol et al., 2019). Subsequently, link availabilities will reduce and consumer satisfaction levels also decrease (Abdulrahman et al., 2015).

There are two types of attenuation sources along signal propagation which are in clear conditions and rain conditions. During clear sky conditions, radio waves are disturbed by multipath, scintillation, gaseous absorption, atmospheric water vapour, and reflection (De & Maitra, 2020; Ozuomba & Kalu, 2015). Radio waves are more vulnerable to severe weather compared to clear conditions. Rain dominantly disturbs satellite signals, especially in a higher frequency band that has a short wavelength (Singh & Saleh, 2021). As frequency increases, the wavelength decrease becomes comparable in size to the particles with which the wave interacts. This decrease in wavelength makes the waves particularly susceptible to impairment from fog, clouds, dirt, and especially rain (Al-Saman et al., 2020).

An electromagnetic wave passes through raindrops on the propagation due to its shorter wavelength (Nizhanthi, 2012; Singh & Saleh, 2021; Toriola et al., 2021). The signal quality is reduced as the decrease of received signal level due to the scattering and absorption phenomenon. Scattering is a physical process due to the diffraction or refraction of radio waves that deviate the direction of radio waves from their original path as they pass through raindrops. As a consequence, the energy of the signal is scattered from its travel direction. Besides that, when a signal passes through raindrops, the water molecules in the rain droplet will absorb half of all of the signal energy. Higher interaction between radio waves with shorter wavelengths and water molecules causes energy losses. The polarization of the electromagnetic waves that are being changed by rain as it propagates through it leads to a reduction in the quality of the received signal. Reduction in the quality of the received signal is defined as rain attenuation (Acharya, 2017; Albendag & Zain, 2020; Patra & Mitra, 2020; Singh et al., 2018; Singh & Saleh, 2021).

The main parameters such as raindrops size, rain temperature, drop velocity, polarization, raindrop orientation, as well as transmitting frequency of the communication systems will affect the level of rain attenuation (Malinga et al., 2013;

Samad et al., 2021; Singh & Saleh, 2021; Toriola et al., 2021). Thus, satellite communication systems operating at frequencies above 10 GHz in tropical and equatorial regions will experience low signal quality due to higher rainfall rates and larger raindrop sizes compared to temperate regions (Abdulrahman et al., 2015; Igwe et al., 2019; Singh & Saleh, 2021; Tashan et al., 2021; Yussuff et al., 2019).

2.6 FADE MARGIN REQUIREMENT FOR GOOD QUALITY OF SERVICES (QOS)

In the SatCom system, a sufficient fade margin in the satellite link is required to overcome path fading that weakens the radio signal. The fade margin is defined as how much margin in decibels (dB) between the received signal and the receiver sensitivity and it is directly proportional to link availability. Link availability refers to the percentage of time that the link is functional. As the fade margin increases, the available link is increasing, and the link will experience fewer system outages or less time exceed. Therefore, a higher fade margin will increase the reliability of the link (Patra & Mitra, 2020; Shrestha & Choi, 2018).

The reliable link will achieve the required quality of services (QoS) and increase the performance of the system. A greater fade margin will cause a link to experience fewer system outages. Ozuomba & Kalu (2015) explained the statistically available time of expression in the following:

$$P_{ot} = 100\% - P_{at} \quad (2.1)$$

P_{ot} : a percentage time exceedance or outage time or total unavailability time of the link.

P_{at} : the percentage of the available time of the link.

T_{at} : the total number of hours or minutes or seconds in the year when the link is available or simply known as the total available time of the link per year.

T_{ot} : the total number of hours or minutes or seconds in a year when the link is not available or simply known as the total outage time or time exceedance or total unavailable time of the link per year.

For instance, the total number of hours in a year of 365 days is $365 \times 24 = 8760$ hours/year.

$$T_{at} = \frac{P_{at} \times \text{Total number of hours in a year}}{100} = \frac{P_{at} \times 8760}{100} \text{ (hours/year)} \quad (2.2)$$

$$T_{ot} = \text{Total number of hours in a year} - T_{at} = 8760 - T_{at} \text{ (hours/year)} \quad (2.3)$$

$$T_{ot} = \frac{P_{ot} \times \text{Total number of hours in a year}}{100} = \frac{P_{ot} \times 8760}{100} \text{ (hours/year)} \quad (2.4)$$

For example, if the link availability, P_{at} is 99.97%,

$$P_{ot} = 100\% - 99.97\% = 0.03\% \quad (2.5)$$

$$T_{at} = \frac{99.97 \times 8760}{100} = 8757.372 \text{ (hours/year)} \quad (2.6)$$

$$T_{ot} = \frac{0.03 \times 8760}{100} = 2.628 \text{ (hours/year)} \quad (2.7)$$

Thus, unavailable total hours per year for link availability of 99.99% or time exceedance or time outage of 0.01%, is 2.628 hours which is equal to 157.68 minutes in one year if that year is not a leap year. Link availability or time exceedance at a particular point can be determined from the annual cumulative distribution of the rain attenuation (Badron et al., 2011). Samad et al., (2021) presented attenuation at 0.1% and 0.01% of time exceedance, corresponding to the typical link availability of 99.9% and 99.99% over time to highlight the maximum availability of the radio links. Sudarshana & Samarasinghe (2011) claimed that the link availability performance of the direct-to-home application, IS-DTH services is 99.98%.

The percentage of time exceedance help in providing guideline in radio network planning to determine link budget availability in satellite-Earth link designs (Samad et al., 2021). Fade mitigation techniques (FMTs) have been proposed as a solution to obtain the high availability of satellite links (Karagiannis et al., 2013). Abubakar et al., (2019) emphasized that an underestimation of rain attenuation will affect the link

availability of the system and leads to higher cost estimation. A deeper rain attenuation study in tropical and equatorial regions is essential in determining reliable signal attenuation estimations.

The computation of rain attenuation in a particular area is important to estimate the link margin required by the satellite-Earth link (Fadilah & Pratama, 2018; Sujimol et al., 2019). A sufficient fade margin can be included in the link budget analysis (Yaccop et al., 2016). Reliable fade margin determination is very important in assuring the reliability of the system for new satellite link planning (Badron, et al., 2015). A reliable fade margin can be determined from long-term rain attenuation data analysis. The satellite system designers have to determine a suitable time margin for high data rate communication with higher link availability to maintain a lower fade margin and for further enhancement of rain compensation methods or fade mitigation techniques (Das et al., 2013; Shrestha & Choi, 2018). For instance, the rainfall rate exceeding 0.01% of the time is essential in predicting attenuation statistics to surmount the fade margin due to rain so that the satellite communication links obtain 99.99% of link availability (Balotra & Hudiara, 2004).

Evaluation of the performance of the main element with their technical cost is the best way to ensure the reliable network cost in implementing new technology. Risk analysis should be performed to ensure a proper level of technology maturity for a particular application. Technology maturity cannot be ensured but in such higher-demand situations, at least one or more alternatives can be identified early on to provide what could be called an escape route or mitigation technique. To overcome the deterioration of system performance and increase link availability of severe rain attenuation conditions, the satellite beacon data are processed into first-order statistical analysis which CDF. From the CDF analysis, the fade margin can be determined.

The data also may be scaled up, using appropriate coefficients to predict up-link performance and determine the need for appropriate countermeasures. The up-link availabilities of the average year and the worst month which are 99.99% and 99.93% respectively are relevant. Three fade countermeasure techniques are power control, space diversity, and time diversity. These are significant to the physical link on a satellite broadcast system. While power control and site diversity are eminent

techniques for application to broadcast up-links (Badron, et al., 2015; Samat & Singh, 2020; Singh et al., 2018), time diversity is a recent technique that is suitable for satellite downlinks as well as significant to radio-return path systems (Hassan et al., 2021).

2.7 RAIN ATTENUATION PREDICTION FOR EARTH-SPACE TELECOMMUNICATION SYSTEM

The earlier satellite networks operate at lower frequency bands which are L, S, C and X-bands, while the recent ones start operating at higher frequency bands which are Ku, K, Ka, Q and V-bands since the radio spectrum is congested at lower frequency bands. Advancements in communication technology including increasing demand for broadband services and telecommunication networks caused the increase in demand for higher frequency band usage (Haule et al., 2019; Kamruzzaman & Islam, 2014; Mandeep et al., 2011; Osahenvenwen & Omorogiuwa, 2017; Samad et al., 2021; Toriola et al., 2021; Vilhar & Hrovat, 2016). Shifting to a higher frequency band is required to accomplish tremendous growth in communication systems such as supporting Industrial Revolution (IR) 4.0, Internet of Things (IoT), and telemedicine to unreachable locations by the terrestrial network. Among the advantages of telecommunications systems operating at higher frequencies are such as having large bandwidth, increased frequency reuse, small device size, and a wide range of spectrum availability which are suitable for HTS technology to be applied (Bahri et al., 2013; Luini et al., 2021; Malinga et al., 2013; Maruddani et al., 2014; Renju et al., 2021; Vidyarthi et al., 2017; Yussuff et al., 2019). However, the major obstacle in deploying the satellite-Earth links at higher frequency ranges is rain (Abubakar et al., 2019; Badron et al., 2015; El-Shami et al., 2015; Grabner et al., 2017; Kestwal et al., 2014; Momin et al., 2021; Oluwayemisi et al., 2019; Singh et al., 2018).

The presence of rain in satellite communication links causes the degradation of signals, especially for frequencies above 10 GHz (Abdulrahman et al., 2015; Ahmad et

al., 2019; Panagopoulos & Arapoglou, 2004; Badron et al., 2015; Das & Maitra, 2015; Das et al., 2010; Ojo & Rotimi, 2015; Osahenvenwen & Omorogiuwa, 2017; Singh et al., 2018; Singh & Saleh, 2021; Yaccop et al., 2013; Yagasena & Hassan, 2000). In tropical regions, electromagnetic waves at millimetre-wave bands passing through raindrops will be absorbed or scattered, which constitutes severe rain attenuation. For example, the effect of rain attenuation is more severe at the Ka-band (20-30 GHz) frequency than at the Ku-Band (10-15 GHz) frequency. The impacts of rain rate along the satellite path in Malaysia, where tropical and equatorial climates demand special attention concerning rain attenuation modelling. Rain attenuation, A in dB is the product of specific attenuation, γ in dB/km, and the propagation path length, d in km along transmitter to receiver. The following equation represents rain attenuation (Mishra et al., 2020; Ozuomba & Kalu, 2015);

$$A (dB) = \gamma \left(\frac{dB}{km} \right) \times d(km) \quad (2.8)$$

The specific attenuation is obtained from the rain rate exceeded at percentage, p of the time as shown in the equation below:

$$\gamma_{(p\%)} \left(\frac{dB}{km} \right) = k \times R_{(p\%)} \left(\frac{mm}{h} \right)^\alpha \quad (2.9)$$

where k and α are constants that depend on the polarization and frequency of the electromagnetic wave. The constants can be referred to in the recommendation tables (P.838-3, 2005). In general, the rain attenuation to the satellite-to-Earth radio link depends on many parameters including point rain rate, frequency, elevation angle, 0° isotherm height as well as the height of the Earth station from the mean sea level.

Commonly, in rain attenuation analysis along satellite-to-Earth links, attenuation of the signal is directly affected by the intensity of rain that occurred (Momin et al., 2021). Since rain attenuation is depending on the rainfall that varies in place and time, rain attenuation prediction based on temperate regions data is not accurate to be applied to tropical regions (Das & Maitra, 2015; Jong et al., 2015; Kestwal et al., 2014; Mandeep et al., 2011; Singh et al., 2018; Yagasena, 2016; Yeo et al., 2014).

2.7.1 Approaches for the Prediction of Rain Attenuation

There are two approaches to the prediction of rain attenuation for a given path which are physical and semi-empirical (Mandeep, 2009; Ojo, 2008; Shrestha & Choi, 2018; Usha & Karunakar, 2020). The physical approach of rain attenuation prediction measured the path attenuation in terms of all individual increments of rain attenuation caused by the drops that come across along the path. However, it is impossible to measure rain along the path accurately without an extensive meteorological database, as an extensive meteorological database technically does not exist in most regions of the world including Malaysia (Mandeep et al., 2011; Usha & Karunakar, 2020). Mostly all inputs needed for physical approach analysis are not available.

The semi-empirical approaches that are mostly deployed by most prediction models are depending on two factors which are the rain rate at a point on the surface of the Earth and the effective path length over the rain that is considered to be homogeneous (Shrestha & Choi, 2018; Usha & Karunakar, 2020). The less understanding of the physical mechanisms as well as the lack of adequate characterization of the various sources generating the impairments along the path is the factor that most prediction models prefer semi-empirical approaches (Malinga et al., 2013; Mandeep et al., 2010; Rahim et al., 2020).

2.7.2 ITU-R Prediction Method of Determining Rain Attenuation

In predicting rain attenuation, two parameters have to be considered; the rainfall rate distribution across a given region and specific attenuation (Islam et al., 2017; Mandeep et al., 2010; Shrestha & Choi, 2017b). Figure 2.6 illustrates the schematic presentation of an Earth-space path obtained from ITU-R (ITU-R P.618-13, 2017). In the figure, A

and B represent the frozen precipitation area and rain height respectively. C represents the liquid precipitation and D is a line that illustrates the Earth-space path.

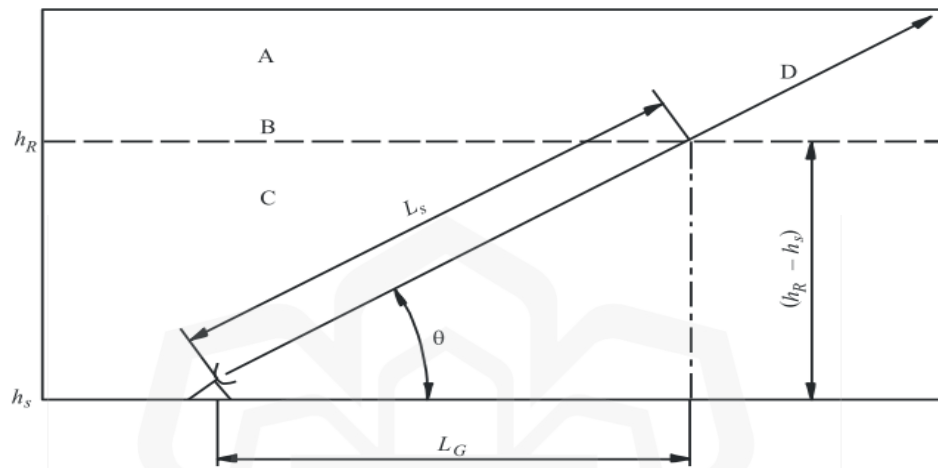


Figure 2.6 Schematic Diagram of an Earth-Space Input Parameter Needed in the Attenuation Prediction Process (ITU-R P.618-13, 2017)

where other parameters are;

h_R : rain height,

h_s : the height of the ground station above sea level,

L_S : slant path length,

L_G : horizontal projection of slant path,

θ : elevation angle.

2.7.3 Meteorological Technique

The general method to predict attenuation due to rain along a slant propagation path is presented in this section. This method can be performed if no reliable rain attenuation data is available, by using rainfall data, the rain attenuation prediction can be determined. The estimation of rain attenuation along a slant path in a satellite link requires an understanding of the rain height (Ahmad et al., 2019; Choi, 2021; Haule et al., 2019).

Long-term rain attenuation statistics from the point rainfall rate proposed by (ITU-R P.618-13, 2017) are presented in Eq. (2.10)-(2.20): The annual average in tropical and equatorial regions especially Malaysia for a probabilistic value, $p < 1\%$ and $|\varphi| < 360$ and $\theta > 250$ is shown as follows:

$$A_{p\%} = A_{0.01} \frac{p}{0.01}^{-(0.6555+0.033 \ln(p)-0.045 \ln(A_{0.01})-\beta(1-p)\sin\theta)} \quad (2.10)$$

where;

coefficient β and attenuation at 0.01% of time exceedance are shown as follows:

$$\beta = -0.005 (|\varphi| - 36) \quad (2.11)$$

$$A_{0.01} = \gamma_R \times L_E \quad (2.12)$$

γ_R : specific attenuation,
 L_E : the effective path length.

The provided method is used to estimate the long-term statistics of the slant-path rain attenuation at a given location for frequencies up to 55 GHz. The following parameters are required:

$R_{0.01}$: rainfall rate for 0.01% of an average year (mm/h)
 h_S : height above mean sea level of the Earth station (km)
 θ : elevation angle (degrees)
 f : frequency (GHz)
 φ : latitude of the Earth station (degrees)

R_E :	effective radius of the Earth (8 500 km)
h_R :	mean annual rain height above mean sea level
L_S :	the slant path length
L_G :	the horizontal projection of the slant path length
$r_{0.01}$:	the horizontal reduction factor for 0.01% of the time
$v_{0.01}$:	the vertical adjustment factor

If data for the earth station height above mean sea level, h_S is not available, an estimation can be used from the maps of topographic altitude given in Recommendation ITU-R P.1511. In tropical and equatorial climates, the vertical dimensions of the rain event may be different from the 0° isotherm in altitudes compared to the temperate climate in which rain is most widespread. The assumption for temperate climates is that the rain cells extend vertically up to the height of the 0° isotherm (Badron et al., 2011; Yussuff et al., 2019). The elevation angle, θ is the view angle from the Earth station to the satellite which is the geostationary satellite in orbit. The azimuth angle is the angle from the north that will complement the view angle and direction of the satellite in the geostationary orbit from the ground station location. Usually, the elevation angle, θ is available from the website of the satellite operator and also can be found using the application (SatFinder, 2018).

This method provides an estimation of the long-term statistics of rain attenuation on a global scale. Somehow, previous research had proven that this model was not accurate for rain attenuation prediction in tropical regions (Ahmad et al., 2019; Dao et al., 2011; Islam et al., 2017; Kalaivaanan et al., 2020; Khairolanuar et al., 2015; Shrestha & Choi, 2019; Yeo et al., 2009b). After performing statistical analysis of rain attenuation of the measured rain attenuation in Malaysia and comparing them to the ones measured using ITU-R standards, it is concluded that the ITU-R model did not accurately predict attenuation in tropical regions, specifically for higher frequencies and rainfall rates. The ITU-R model was designed based on data collected from temperate regions of the world which experience less rain compared to tropical regions (Kalaivaanan et al., 2020; Lwas et al., 2015; Yagasena, 2016). Since tropical regions have high rainfall rates compared to temperate regions, the ITU model underestimated the rainfall rate and produced a less accurate result (Lwas et al., 2015; Nuroddin et al., 2013; Semire et al., 2013; Ulaganathen & Assis, 2015). Previous research also added that the ITU- R model was

not suitable for the prediction of rain attenuation at elevation angles higher than 54° (Samat et al., 2019).

2.7.4 Non-meteorological Technique

The scaling technique is a non-meteorological technique to predict rain attenuation which no rain data or known also as meteorological data required. Scaling of the rain attenuation is preferable rather than using the general method if reliable long-term statistical attenuation data are available (ITU-R P.618-13, 2017). The available data were measured at an elevation angle and a frequency different from the prediction data is needed. The scaling techniques of rain attenuation in rainy conditions for the radio wave link are categorized into four types which are elevation angle scaling, frequency scaling, path length scaling, and polarization scaling (Samad & Choi, 2021). Rain attenuation, A can be represented as attenuation in a function of the following parameters:

$$A = A(L, f, \theta, R, \text{polarization})$$

where;

- L : path length in the rain,
- f : operating frequency,
- θ : the elevation angle,
- R : the rainfall rate.

However, the scaling of the rain attenuation model comprising all of the above parameters has not been developed. Among these parameters, four parameters: frequency, elevation angle, path length, and polarization scaling techniques are explained in the literature.

2.7.4.1 Frequency Scaling

Frequency scaling can be used when rain attenuation at one frequency is available to predict rain attenuation at another frequency. This technique can be applied in predicting attenuation in a dual-frequency use of a satellite communication system. This scaling technique is explained in detail in section 2.8.

2.7.4.2 Elevation Scaling

The elevation scaling can be defined as the change in the rain attenuation at distinct probability levels as a function of the elevation change (Tomaz et al., 2018). The elevation scaling of rain attenuation can generally be written as:

$$A(\theta_1) \sin \theta_1 = A(\theta_2) \sin \theta_2 \quad (2.13)$$

where θ_1 and θ_2 are elevation angles, and $A(\theta_1)$ and $A(\theta_2)$ are rain attenuations at a particular frequency at respective elevation angles θ_1 and θ_2 .

There are three techniques to determine the scaling factor for elevation scaling which are power law techniques, cosecant rule techniques, and synthetic time series techniques (Das & Maitra, 2015; Jong et al., 2017; Samad & Choi, 2021). The power law-based technique describes that an elevation angle scaling is the ratio of rain attenuation at the zenith and the slant paths for elevation angles are from 1^0 to 89^0 . The scaling factor, $SF(\theta)$ for power law-based is:

$$SF(\theta) = 1.741 \times \theta^{-0.6015} + 0.8931 \quad (2.14)$$

This technique can predict slant link attenuation accurately from $5^0 \leq \theta \leq 90^0$.

Cosecant-rule-based technique exhibits a scaling factor (SF[P, θ]) is defined as the proportion of the attenuation across θ and attenuation from the zenith path using the simple cosecant law:

$$SF(P, \theta) = \frac{A_{dB}(P, \theta)}{CSC(\theta) \times A_{dB}(P, 90^\circ)} \quad (2.15)$$

The time-series-based technique is applied when a single rain cell intercepts the propagated signal from the Earth station antenna. The elevation angle scaling with the rainy time series generation technique is:

$$F = (h_r - h_a)/(h_{r,1} - h_{a,1}) \times (\sin(\theta_1)/\sin(\theta_2)) \times (f_2/f_1)^{1.72} \quad (2.16)$$

where the subscripts “1” are used for the reference measured and “2” are used for desired datasets, h_r (km) is the rain height and h_a (km) is the antenna height. Both heights are concerning the sea level. θ is the elevation angle, and f is the frequency in GHz. However, this scaling is not valid when multiple rain cells exist.

2.7.4.3 Path Length Scaling

The path length scaling techniques can be combined with frequency scaling (Samad et al., 2021). The cumulative distribution of rainfall from the particular reference path for the frequencies employed can be recalculated to other paths as follows:

$$A_1 = U \times V \quad (2.17)$$

$$U = k_1 L_1 / (1 + \frac{L_1}{d_o}) \quad (2.18)$$

$$V = (A_2 \times (1 + \frac{L_2}{d_o})) / k_2 L_2^{\frac{a_1}{a_2}} \quad (2.19)$$

where;

A_1 : the attenuation on the reference path,

- A_2 : the attenuation on the desired path,
 k_1 and k_2 : coefficients dependent on the frequency for the reference path and the desired path,
 L_1 : the reference link's path length,
 L_2 : the desired link's path length,
 d_0 : the path reduction factor.

This method can be applied only to operating frequencies from 38 GHz to 58 GHz (Kvicera et al., 2012a).

2.7.4.4 Polarization Scaling

Polarization scaling is used to predict attenuation as a function of polarization for which attenuation is unknown in a given region at a particular polarization (Choi, 2021; Samad et al., 2021). Polarization in radio waves is the orientation of electric and magnetic fields including horizontal, vertical, left-hand circular, and right-hand circular. For instance, the ITU-R model can predict horizontal polarization attenuation if long-term attenuation statistics in vertical polarization are available and vice versa for a particular link (P.530-18, 2021). However, this polarization scaling cannot be deployed in circular polarization. Polarization scaling in determining rain attenuation can be described in the equation below:

$$A_{Ve} = \frac{300 \times A_{Ho}}{335 + A_{Ho}} (dB) \quad (2.20)$$

$$A_{Ho} = \frac{300 \times A_{Ve}}{335 + A_{Ve}} (dB) \quad (2.21)$$

where A_{Ho} is the rain attenuation of the horizontal links, and A_{Ve} is the rain attenuation of the vertical links. The scaling of polarization is used to predict the type of polarization of attenuation at a specific frequency in particular areas (Lin & Chen, 2002). The ITU-

R model can estimate the vertical polarization attenuation due to the availability of long-term attenuation data (Mohamed & Nadir, 2005).

2.8 FREQUENCY SCALING TECHNIQUE

Frequency scaling is the prediction technique of propagation effects such as rain attenuation at the desired frequency with known information at a different or reference frequency (Nuroddin et al., 2013; Samad et al., 2021; Samad & Choi, 2021; Toriola et al., 2021). The frequency scaling technique is an alternative method to predict rain attenuation at different frequencies quickly when rainfall data is not available (Pinder et al., 1999; Usha & Karunakar, 2020). Statistics frequency scaling predicts attenuation values at another frequency by scaling previously measured attenuation at a reference frequency. The reference frequency attenuation is known from the previous analysis. For instance, in a particular area, the rain attenuation information is well-known at a specific frequency, using that frequency and related information as a reference, the attenuation at other frequencies can be predicted.

Typically, the frequency of the predicted rain attenuation is higher than the frequency of the known rain attenuation (Kvicera et al., 2012b). The frequency scaling technique helps to determine rain attenuation prediction for another desired frequency band accurately even if the attenuation statistics at the desired frequency are unavailable. The ratio between the rain attenuation at both frequencies can vary during a rain event. Generally, the ratio increases as the rain attenuation increases. In addition, to scale the value of rain attenuation which will occur at the desired frequency, the known value of rain attenuation at the based frequency has to pass through the same rainfall (Hodge, 1977). The applications of frequency scaling are useful in determining predicted attenuation at different frequencies as well as in a dual-frequency use of satellite communication systems, discovering the magnitude of rain-induced attenuation at higher frequencies, and predicting rain attenuation on uplink/downlink based on

measured rain attenuation in downlink/uplink (Cuervo et al., 2016; Montera et al., 2008; Samad et al., 2021; Toriola et al., 2021).

Most of the prediction methods of rain attenuation for satellite communication applications are based on measured rain rate as the main input parameter which is called rain-induced attenuation. However, when measured attenuation data is available at one frequency, frequency scaling techniques become an alternative method for estimating measured rain attenuation at the other frequencies. Frequency scaling techniques can be helpful to estimate the attenuation at another frequency band for the quick management of slant links and real-time frequency attenuation scaling can be used in adaptive fade mitigation systems (Laster & Stutzman, 1995; Ramana, 2015; Samad et al., 2021; Samad & Choi, 2021). A good estimation of rain attenuation is very important to predict an accurate level of signal loss to be compensated for during satellite radio propagation (Afahakan et al., 2016). Thus, accurate link budgeting with effective cost in satellite communication system planning can be attained (Toriola et al., 2021; Yeo et al., 2014). Consequently, frequency scaling rain attenuation prediction techniques can save time for the immediate operation of a slant path link in a communication system (Samad et al., 2021).

There is little research that has been done on terrestrial frequency scaling (Islam et al., 1999; Islam et al., 2004; Kvicera et al., 2012b; Ulaganathen et al., 2015; Ulaganathen et al., 2013). There are differences between the terrestrial and slant links which are complex non-rainy atmospheric elements, such as clouds, gasses, and turbulence that appear in slant links. Thus, frequency scaling models for terrestrial links cannot be applied to slant links without proper parameter considerations and validations (Samad et al., 2021).

Frequency scaling can be carried out through two techniques which are statistical and instantaneous mechanisms. In other words, the rain attenuation scaling technique in terms of frequency can be categorized into long-term (statistical) and short-term (instantaneous) applications (ITU-R P.618-13, 2017; Samad & Choi, 2021). Some models can predict short-term or instant attenuation and some of the models for long-term or statistical attenuation applications.

2.8.1 Statistical Frequency Scaling

Statistical scaling methods require long-term attenuation statistics. Statistical frequency scaling uses statistics from the first measures at a reference frequency to estimate the rain attenuation statistics at the desired frequency (Ramana, 2015). Typically, reference or based frequency and desired frequency are represented by f_1 and f_2 respectively. The main input parameter in the numerous statistical scaling methods is frequency. The ratio of the rain attenuation at two frequencies for the same time percentage of occurrences is provided by the long-term frequency scaling (Acharya, 2017).

The Statistical Attenuation Ratio (SAR) method considers statistical attenuation analysis in terms of the percentage of time exceeding the corresponding rain rate. In this technique, many researchers perform empirical relationships of a satellite link for two frequencies by determining the fraction of f_2 and f_1 for different frequency bands in GHz to identify the ratio where the f_2 value is higher than the f_1 value (Choi, 2021). The model that presents the SAR through a mathematical model is the CCIR model (IRCC, 1986). SAR from the model is the model that relates to the ratio of rain attenuation model on both frequencies instead of directly depending on frequency value. This model acquires attenuation values that can form a ratio to estimate SAR for a given pair of frequencies (Choi, 2021). The equation is as below:

$$\text{SAR}(f_1, f_2, p\%) = \frac{\text{SA}_{CA}(f_2, p\%)}{\text{SA}_{CA}(f_1, p\%)} \quad (2.22)$$

where;

SA_{CA} : the statistical attenuation with clear air

$P\%$: the percentage of time exceedance of the occurring rain event for particular frequencies f_1 and f_2 .

The SAR is computed from three models which are raindrop size distribution (DSD)-based path-averaged rain rate, DSD-based specific attenuation ratio, and the spatial rain rate profile or known as the simple atmospheric model, SAM. The rain attenuation is significantly influenced by the distribution of the raindrop size rather than the rain rate but the specific attenuation is affected by the rain rate (Cuervo et al., 2016).

Some researchers present statistical and physical raindrop size distribution models in Malaysia (Lam et al., 2015). The limitation of this model is that it requires a sophisticated device to record the drop size of rain. However, DSD-based information is not available in rain attenuation datasets.

The SAR that is derived from DSD-derived attenuation is as follows:

$$\text{SAR}_{DSD} = \frac{A_{DSD}(f_2)}{A_{DSD}(f_1)} \quad (2.23)$$

where A_{DSD} is attenuation with DSD information at the frequency of f_1 and f_2 .

Besides that, the specific attenuation factor can be identified for the frequency f_1 (GHz) and f_2 (GHz) as γ_{f1} and γ_{f2} accordingly (Luini et al., 2021). The SAR represents the ratio of two specific attenuations as follows:

$$\text{SAR}_{f_1, f_2} = \frac{\gamma_{f_1}}{\gamma_{f_2}} \quad (2.24)$$

where the product of SAR_{f_1, f_2} is constant.

The constant SAR_{f_1, f_2} , and the specific attenuation of a baseline link can be used to estimate rain attenuation at the desired link. The application of this model is to estimate the specific attenuation of a satellite's downlink channel using the specific attenuation of the uplink channel.

The simple atmospheric model, SAM highlights the spatial rain distribution by adopting the exponential rain cell distribution (Acharya, 2019; Stutzman & Dishman, 1982). The basic idea is to provide the geographical rain rate profile for the rainfall rates when the rain rate can be recorded. The SAM represents the rainfall rate's spatial profile as exponential and varies as:

$$R(t, h) = R_0(t) \quad \text{for } R_0 \leq 10\text{mm/hr} \quad (2.25)$$

$$R(t, h) = R_0(t) \times \exp(-\gamma \times \ln(\frac{R_0}{10}) \times h) \quad \text{for } R_0 > 10\text{mm/hr} \quad (2.26)$$

where;

$R(t, h)$: the rain rate at a range of h ,

- h : projection or height of the slant link to the rainy region from the receiver at any time,
- $R_0(t)$: the point of rain rate at the receiver located at the corresponding time.

Instead of ratio-based scaling like SAR, the non-ratio scaling rule formulation derives that scaling rule is performed from an empirical formula that conveys the relationship of the physical influence of scaling (Samad et al., 2021; Shrestha & Choi, 2017a; Zhou et al., 2000).

In the scaling method based on the empirical formula, the link between the desired and base/reference frequency attenuation is determined by quantifying the relationship between A_{f1} and A_{f2} through empirical relationships (Ahmad et al., 2019). There are two ways of predicting frequency scaling through empirical studies which are single-frequency and dual-frequency implementations. The models of the single-frequency empirical method include International Consultative Committee (CCIR), Kheirallah, Hodge, and ITU-R (Pinder et al., 1999).

2.8.2 Instantaneous Frequency Scaling

For instantaneous frequency scaling in terms of ratio-based, the scaling is related to the ratio of attenuation due to clear air (ACA) at high and low frequencies in a particular sample time (Acharya, 2019; Laster & Stutzman, 1995). Instantaneous frequency scaling helps to estimate real-time attenuation on a link from attenuation measured on another link that can be used for fade mitigation techniques (Ebert et al., 2015; Ramana, 2015). Matricciani & Paraboni (1985) developed instantaneous frequency scaling in 0.8 seconds of resolution and Bertorelli and Paraboni derived instantaneous frequency scaling by using a Gaussian generator (Acharya, 2019). The relationship between simultaneous attenuation at different frequencies can be investigated through instantaneous frequency scaling (Brisseau et al., 2006; Brisseau et al., 2003; Montera et

al., 2008). The proposed method to determine attenuation, A in the range of 20 to 30 GHz is given as:

$$A = (k \times R\alpha) \times (1 - \exp[-\gamma_c \times \alpha \times h_r \times \text{CSC } \theta] / \gamma_c \times \alpha] \quad (2.27)$$

where;

- γ_c : the specific attenuation coefficient,
- R : rainfall rate,
- k and α : the coefficient,
- h_r : the height of the receiver,
- θ : is the elevation angle.

The specific attenuation coefficient, γ_c can be determined by deploying the non-linear least squares approach. The advantage of this model is better options for real-time applications based on spatial variation via specific attenuation. The limitation of this technique is the non-uniformity of rain rate distribution and the DSD of the rain along its path link (Samad et al., 2021). Sampling techniques were used to determine the short-term scaling. The instantaneous time limit is within 5 minutes. Thus, the scaling factor is not constant as an instantaneous factor is vary for each frequencies pairs (Laster & Stutzman, 1995)

For the non-ratio instantaneous frequency scaling technique, the instantaneous rain attenuation is executed using the spatial rain rate distribution. The spatial rain rate distribution is determined via the SAM rain rate distribution (Acharya, 2019; El-Shami et al., 2018; Samad et al., 2021; Yunus et al., 2018). The hysteresis attenuation behaviour is shown at two frequencies in different frequency bands and the impact is severe (Kvicera et al., 2007). The mean, standard deviation, and covariance parameters of the two frequencies were defined by using the cumulative distribution function of the rain attenuation graph. The resulting covariance parameter indicates the correlation of the frequencies. The equation develops as:

$$A_2 = A_1 \times \left(\frac{f_2}{f_1}\right)^{1.72} \times \exp [\Delta a \times \xi] \quad (2.28)$$

where Δa is a log-normal variable with zero mean ($\mu = 0$)

σ_{depend} and σ_{independ} are the standard deviations (STD) of a link's attenuation depending on any other radio links respectively.

The reduction coefficient (ξ) is the ratio of two STDs as follows:

$$\zeta = \frac{\sigma(\text{depend})}{\sigma(\text{independ})} = 0.3548 \times \left(\frac{f_2}{f_1} - 1 \right)^{0.1676} \quad (2.29)$$

where f_2 is derived for the pair of frequencies if f_1 is known and vice versa (Bertorelli & Paraboni, 2007). This model supports frequency ranges from 1 to 100 GHz and considers rain as inhomogeneity. The relation between peak precipitation and attenuation values is considered important (Karagiannis et al., 2013).

2.8.3 Previous Model of Frequency Scaling

In this section, several available models relating to statistical frequency scaling techniques were discussed. The models are including the frequency scaling method proposed by the ITU-R, Hodge, Battesti, Kheirallah, CCIR, Simple Power Law, Boithias and Zhou (Nuroddin et al., 2013; Pinder et al., 1999; Toriola et al., 2021; Zhou et al., 2000). The frequency scaling developed by the CCIR, Drufuca, and Dintelmann generated lower values than the measured data. The Simple Power Law and ITU-R frequency scaling model, on the other hand, produced higher values than the measurements in tropical regions (Nuroddin et al., 2013). Zhou model was then developed for the terrestrial link. The Hodge and Kheirallah models were developed based on the United State of America (USA) measurement data; a temperate region that experienced less rainfall.

2.8.3.1 ITU-R 618-13 (2017) Model

If reliable attenuation data measured at one frequency are available, the ITU-R model has proposed a frequency scaling technique with the following empirical formula giving statistical attenuation ratio directly as a function of frequency and attenuation (ITU-R P.618-13, 2017). This technique was applied for frequency scaling on the same path in the frequency range of 7 to 55 GHz:

$$A_2 = A_1(\varphi_2/\varphi_1)^{1-H(\varphi_1,\varphi_2,A_1)} \quad (2.30)$$

where;

$$\varphi(f) = \frac{f^2}{(1 + 10^{-4}) \times f^2} \quad (2.31)$$

$$H(\varphi_1, \varphi_2, A_1) = 1.12 \times 10^{-3} \times (\varphi_2/\varphi_1)^{0.5} (\varphi_1 \times A_1)^{0.55} \quad (2.32)$$

where A_1 and A_2 were the rain attenuations at given time exceedance for frequencies f_1 and f_2 (GHz), respectively. For frequency scaling of attenuation, reliable long-term measured attenuation data was preferred to be used instead of long-term measured rain data. This model was then proposed for satellite-Earth propagation links. Previous studies had used this technique in tropical regions, but the result was not validated.

2.8.3.2 Hodge's Model (1977)

Hodge's proposed method included a correction factor for rain inhomogeneity and took into account the high correlation between peak rainfall rate and attenuation. The rainfall along the attenuation path was represented by the Gaussian function of position along the path which:

$$R(x) = R_0 \times e^{\frac{(-x)^2}{l_0}} \quad (2.33)$$

where;

R_0 : a peak of rainfall rate along the rain path,

x : position on the path,

l_0 : length of rainfall.

The ratio between attenuation for two frequencies, f_1 and f_2 was described in the equation below.

$$\frac{A_2}{A_1} = \frac{a_2}{a_1} \left(\frac{A_1}{a_1} x \sqrt{\frac{b_1}{\pi}} \right)^{\left(\frac{b_2-1}{b_1} \right)} x \sqrt{\frac{b_1}{b_2}} \quad (2.34)$$

The constant coefficients a and b were taken from the specific attenuation-rain rate relationship in the equation below and referred to in (P.838-3, 2005).

$$\gamma = a x R^b \quad (2.35)$$

where γ is the specific attenuation expressed in decibels/kilometres and R is the rain rate expressed in millimetres/hour. A_1 and A_2 are rain attenuations at f_1 and f_2 respectively.

2.8.3.3 Battesti's Model (1982)

A linear model based on rain attenuation statistics was proposed by Battesti Segal in Canada for terrestrial microwave links which emphasized on attenuation is proportional to the linear function of frequency (Pinder et al., 1999). This model was obtained from observing specific attenuation in uniform rain events with typical drop size distribution (DSD) where a statistical attenuation ratio of f_2 and f_1 was determined. The frequency scaling techniques have three conditions applied which are:

$$\text{If } f_1, f_2 \leq 20 \text{ GHz, } \frac{A_{f_2}}{A_{f_1}} = \frac{f_2-6}{f_1-6} \quad (2.36)$$

$$\text{If } f_1, f_2 \geq 20 \text{ GHz, } \frac{A_{f_2}}{A_{f_1}} = \frac{f_2-10}{f_1-10} \quad (2.37)$$

$$\text{If } f_1 < 20 \text{ GHz}, f_2 > 20 \text{ GHz}, \frac{A_{f_2}}{A_{f_1}} = 1.4 \times \frac{f_2^{-10}}{f_1^{-6}} \quad (2.38)$$

A_{f_1} and A_{f_2} are rain attenuations at f_1 and f_2 respectively. The model was used to scale up the frequency from 20 GHz to 27 GHz.

2.8.3.4 Kheirallah's Model (1980)

Kheirallah frequency scaling technique was derived from ITU-R's rain attenuation model with the assumption of path length, L and reduction factor, r is the same for both frequencies (Kheirallah et al., 1980). Thus, the equation was proposed as below:

$$\frac{A_{f_2}}{A_{f_1}} = \frac{A_{s_2} L_2 r_2}{A_{s_1} L_1 r_1} = \frac{A_{s_2}}{A_{s_1}} \quad (2.39)$$

where;

A_{f_1} and A_{f_2} are rain attenuations at f_1 and f_2 respectively,

A_{s_1} and A_{s_2} are specific rain attenuations at f_1 and f_2 respectively.

$$A_s = a \times R^b \quad (2.40)$$

where a and b are the regression coefficients dependent on frequency and the drop size distribution (DSD). Kheirallah proposed the model below:

$$A_2 = a_2 \left(\frac{A_1}{a_1} \right)^{\frac{b_2}{b_1}} \quad (2.41)$$

2.8.3.5 CCIR (1980)

The International Consultative Committee (CCIR) has concluded that the statistical attenuation ratio (RAS) has a non-linear relationship with frequency. It does not require any parameter that relates to DSD or the intensity profile of rainfall. CCIR has proposed a model that can be applied within the range of 7 to 30 GHz, however, if the region with a low rainfall rate is less than 50 mm/hr, the model can be used up to 50 GHz. The equation as below:

$$RAS_{CCIR} = \frac{A(f_2)}{A(f_1)} = \frac{\Phi(f_2)}{\Phi(f_1)} \quad (2.42)$$

$$\text{where, } \Phi(f) = \frac{f^{1.72}}{1 + 3 \times 10^{-7} \times f^{3.44}} \quad (2.43)$$

$A_{(f_1)}$ and $A_{(f_2)}$ are rain attenuations at f_1 and f_2 respectively.

2.8.3.6 Simple Power Law (SPL) Model (1974-1995)

One of the well-known frequency scaling models for rain attenuation prediction is the power over the ratio of frequencies and statistical attenuation ratio (RAS). This model assumes that the attenuation ratio is directly proportional to the square of frequencies ratio. The SPL is shown in the equation below:

$$RAS_n = \frac{A(f_2)}{A(f_1)} = \left(\frac{f_2}{f_1}\right)^n \quad (2.44)$$

A_1 and A_2 are the values of rain attenuation in decibels which correspond to the frequencies f_1 and f_2 , respectively, at desired time exceedance in gigahertz. Previous research has proposed various values of n for different frequency ranges and locations. Drufuca (1974) had found empirically that rain attenuation scales were according to the

frequency range of approximately 11 to 19 GHz with an n value of 1.72. This method was proposed in Ohio, United States. Drufuca's (1974) model is suitable for a homogeneous rainfall of 1 mm/h and progressively worse as the rainfall differs in its exponents from 1 mm/h, particularly for high rain rates. In tropical regions, a high rainfall rate with inhomogeneous rainfall will cause inaccuracy in this model. Owalabi and Ajayi (1982) proposed that the value of an n is equal to 2 after investigating specific attenuation for a Laws and Parson drop size distribution, DSD. This model was designed for a range of over 10 to 20 GHz and found a trend of decreasing with increasing rain rates (Pinder et al., 1999). Dintelman (1992) proposed an n value equal to 1.8 based on experimental German propagation for the frequency range of 12 to 30 GHz.

The power law relation derived from the Virginia Tech data proposed n value equal to 1.9 based on OLYMPUS satellite data for the frequency range of 12 GHz to 30GHz (Brisseau et al., 2006; Ulaganathen et al., 2013). Some authors found that the frequency scaling ratio is very susceptible to the distribution of raindrop diameters (DSD). Besides, frequency scaling ratio measurements performed using the Olympus data demonstrated that changes and hysteresis effects occurred during some rain events since variations in raindrop size distribution (DSD) during the event is very essential (Brisseau et al., 2006; Cuervo et al., 2017; Laster & Stutzman, 1995).

2.8.3.7 Boithias's Model (1989)

A more complicated model modification to ITU-R 618-13 that includes base attenuation as well as the frequency was proposed by Boithias frequency scaling (Toriola et al., 2021). It provided an empirical expression for a scaling factor that produces an attenuation ratio directly as a function of frequency and measured attenuation as below:

$$\frac{A_2}{A_1} = \left(\frac{\varphi_2}{\varphi_1} \right)^{1-H(\varphi_1, \varphi_2, A_1)} \quad (2.45)$$

$$\varphi(f) = \frac{f^2}{1 + 10^{-4} x f^2} \quad (2.46)$$

$$H(\varphi_1, \varphi_2, A_1) = 1.12 \times 10^{-3} \times \left(\frac{\varphi_2}{\varphi_1}\right) \times (\varphi_2 \times A_1)^{0.55} \quad (2.47)$$

where φ is a function of frequency-dependent, and H is a function in terms of frequency and base attenuation dependent. A_1 and A_2 are the measured attenuation and predicted attenuation respectively.

2.8.3.8 Zhou's Model (1999)

The most commonly implemented formula, which is CCIR was proved to be inaccurate to be applied in Singapore's tropical region (Zhou et al., 1999). The frequency scaling model was proposed in Singapore for terrestrial or line-of-sight communication as in the equation below:

$$A_2 = 4.8 + 1.61 \times A_1 \quad (2.48)$$

where A_1 and A_2 are the measured attenuation and predicted attenuation respectively.

2.8.4 Previous Related Research

Most of the available frequency scaling techniques were comprehensively studied. Various methods had been employed in deriving statistical and instantaneous frequency scaling models. Most research focused on the techniques used in the terrestrial link. It has been found fewer studies conducted on exploring a technique that applies to the satellite-Earth link in tropical regions. Therefore, this study focuses on the relevant frequency scaling technique to be used for the satellite-Earth link in heavy rainfall areas. This study also concentrates on statistical frequency scaling since it is a suitable

technique for acquiring a reliable fade margin for operation at higher frequency bands. The instantaneous frequency scaling is used to estimate real-time attenuation on a link from attenuation measured on another link that can be used for fade mitigation techniques. Previous studies regarding frequency scaling techniques in estimating rain attenuation for satellite-Earth communication links were summarised in Table 2.1. The limitations of the available frequency scaling technique for the SatCom link are shown in Table 2.2.

Table 2.1 Comparison of Frequency Scaling Technique in Predicting Rain Attenuation for the Satellite Communication Link

No	Source	Methodology	Frequency bands	Location	Types of frequency scaling	Findings
1	Toriola et al., (2021)	Applied Boithias frequency scaling model and ITU-R rain attenuation prediction model	F ₁ (Ku-band) 12.245 GHz and F ₂ of 16, 20, 30, and 40 GHz	Nigeria	Statistical frequency scaling	Attenuation by frequency scaling at 16, 20, 30, and 40 GHz were 28.36 33.95, 42.17 and 46.07 dB respectively.
2	Samad et al., (2021)	Applied Artificial Neural Network (ANN)-based scaling	F ₁ (Ku-band) 12 GHz and F ₂ (Ka-band) 20 GHz	South Korea	Frequency and vertical polarization frequency	ITU-R frequency scaling model overestimated the measured value of 20 GHz at 0.1

						and 0.01% of time exceedance.
3	Luini et al., (2021)	Performed total attenuation frequency scaling (TAFS) and simplified TAFS (S-TAFS) first	F ₁ (Ka-band) 19.701 GHz and F ₂ (Q-band) 39.402 GHz	Italy	Instantaneous frequency scaling	Additional information on radiometric data and the raindrop size distribution (DSD) were required. Good accuracy in scaling the total attenuation from Ka- to Q-bands in Italy in terms of first-order statistics and time series
4	Acharya (2020)	Used a simple atmospheric model (SAM)	F ₁ (Ka-band) 20 GHz and F ₂ (Q-band) 30 GHz	India	Instantaneous frequency scaling	The model produced an error of 2.5 dB
5	Usha & Karunakar (2019)	ITU-R 618-13 frequency scaling model	F ₁ (Ka-band) 20 GHz and	India	Statistical frequency scaling	Frequency scaling attenuation values for 30.5 GHz at

			F ₂ (Q-band) 30 GHz			polarization PH, PV, MH, and MV was 18.77, 18.29, 15.55, and 15.14 dB respectively.
6	Vidyarthi et al., (2017)	Proposed frequency scaling model, $A_{\text{uplink}} = 1.818509 \times A_{\text{downlink}}$	F ₁ (Ka-band) 20 GHz and F ₂ (Q-band) 30 GHz	India	Instantaneous frequency scaling	Rain attenuation at 20 GHz and 30 GHz were 10 and 19 dB respectively.
7	Cuervo et al., (2017)	Applied frequency scaling ITU-R 618-12 model	F ₁ (Ka-band) 19.7 GHz and F ₂ (Q-band) 39.4 GHz,	Austria	Instantaneous frequency scaling	Frequency scaling overestimated the measured value
8	Shreshta & Choi (2017)	Applied frequency scaling ITU-R 618-12 model	F ₁ (Ku-band) 12.7 GHz and F ₂ (Ka-band) 20.73 GHz,	South Korea	Statistical frequency scaling	At 0.01% of time exceedance, the measured rain attenuation and frequency scaling rain attenuation were 13 dB and 27 dB

9	Nessel et al., (2014)	Applied frequency scaling derived from DSD	F ₁ (Ka-band) 20 GHz and F ₂ (Q-band) 40 GHz,	Italy	Instantaneous frequency scaling	The average errors and RMS values produced were 0.86 and 2.4 respectively
10	Maruddani et al., (2014)	Applied frequency scaling ITU-R 618-10 model	F ₁ (Ku-band) 12.7475 GHz and F ₂ (Ka-band) 18.9 GHz,	Indonesia	Statistical frequency scaling	At 0.01% of time exceedance, measured rain attenuation and frequency scaling rain attenuation was 17 dB and 36 dB respectively.

Table 2.2 Limitation of Frequency Scaling Technique in Predicting Rain Attenuation for the Satellite Communication Link

No	Author	Year	Limitations
1	Toriola et al.,	2021	Applied the Boithias model and no validation was done on the result in tropical regions.
2	Samad et al.,	2021	The model was developed in South Korea which had four seasons of weather.
4	Luini et al.,	2021	Additional information on radiometric data and the raindrop size distribution (DSD) were required as

			this technique was meant for the instantaneous method.
3	Acharya	2020	The SAM model was suitable for the instantaneous model, not for the statistical model.
4	Usha & Karunakar	2019	ITU-R 618-13 frequency scaling model was applied and there was no data validation for the obtained result.
5	Vidyarthi et al.,	2017	A simple model was developed for the instantaneous technique.
6	Cuervo et al.,	2017	The frequency scaling ITU-R 618-12 model was applied and the model overestimated the measured value.
7	Shreshta & Choi	2017	The ITU-R 618-13 frequency scaling model was applied and there was no data validation for the obtained result.
8	Nessel et al.,	2014	A simple model was developed for the instantaneous technique.
9	Maruddani et al.,	2014	The ITU-R 618-13 frequency scaling model was applied and there was no data validation for the obtained result.

2.8.5 Research Gap

Based on the existing studies on the frequency scaling technique that is applicable to the satellite-Earth link, it is found that data validation is not available in any studies conducted in tropical regions. Regarding that, this study focuses on the statistical scaling technique with a validation step to enhance the reliability of the existing

methods used in tropical regions. Figure 2.7 shows the research gap identified for the study to be conducted.

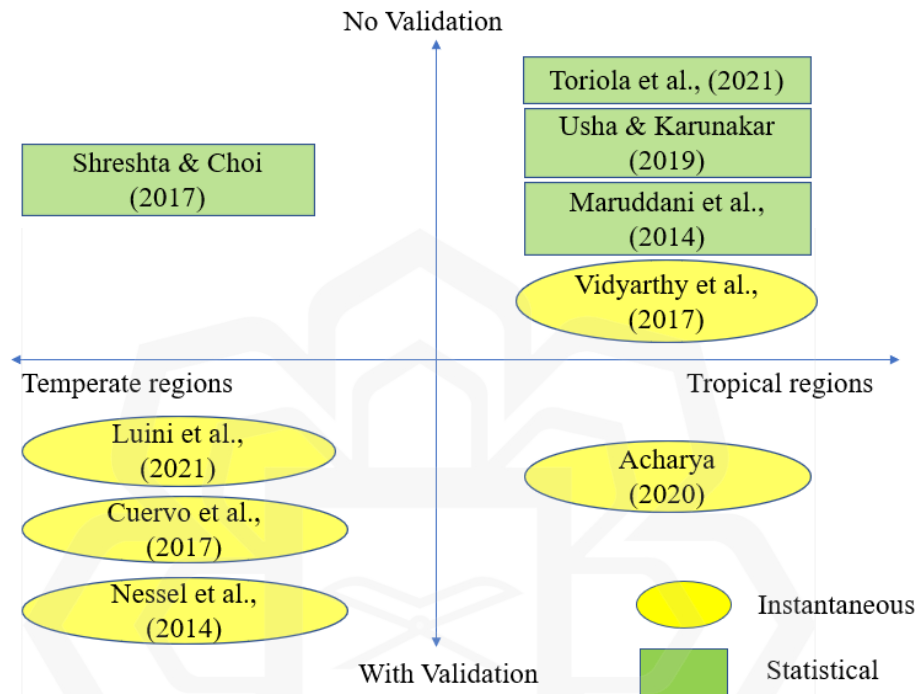


Figure 2.7 The Research Gap Identified in the Study

2.9 WORST MONTH ANALYSIS

The worst-month analysis is very useful to design satellite-to-Earth because the required fade margin must be contented in any given month throughout the year. Therefore, performing analysis for the worst month data is crucial for telecommunication system designers (Abubakar et al., 2019; Chebil, 2003; Mandeep & Ng, 2008; Yagasena & Hassan, 2000). The annual worst-month statistic is determined by choosing the worst CDF at the occurrence level computed during twelve sequential months. Comparing the

monthly CDF at a particular level is recognized as the worst month which is representing the month with the highest probability of exceeding that threshold within the particular period (Badron et al., 2011; Ismail et al., 2012; Pontes et al., 2015; Ting & Mandeep, 2014). The annual worst month is the month in the particular year in which the threshold has been exceeded for the longest time (Abubakar et al., 2019).

The concept of the worst month given in has provided a solution to help the designer who is confronted with high-quality communication network intention based on any month (Ismail et al., 2012; Samat et al., 2019). It is also recommended that the worst month concepts can be applied to different types of quantities such as rain rate, rain attenuation, and cross-polarization (Chebil, 2003; Mandeep & Ng, 2008; Ting & Mandeep, 2014; Yagasena & Hassan, 2000). Some researchers agreed that the worst month is not the same for all threshold levels (Pontes et al., 2015; Abubakar et al., 2019; Chebil, 2003). The model for the conversion of annual statistics to worst-month statistics is represented by the conversion factor, which is given below (Durodola et al., 2017; P.841-6, 2019; Ting & Mandeep, 2014).

$$Q = \frac{P_w}{P_{av}} \quad (2.49)$$

where P_w is the probability of the average worst-month and P_{av} is the probability of average annual rainfall intensities for the same threshold. Q is the conversion factor for converting from the average annual per cent to the average annual worst month time percentage in the function of the occurrence level and the climatic region. Regions with the same climatic categories will have alike values of Q . The factor Q is also defined by the power law relationship in the parameters of Q_1 and β (P.841-6, 2019):

$$Q = Q_1 \times P_{av}^{-\beta} \quad (2.50)$$

By inserting equation 2 into equation 1, the probability of the average worst month can be defined as:

$$P_w = Q_1 \times P_{av}^{1-\beta} \quad (2.51)$$

For rain attenuation effect on slant path in global purpose, the value of parameters Q_1 and β suggested by the ITU are 2.85 and 0.13, respectively. While, for the rain rate in

tropical regions, the values of Q_I and β are 2.82 and 0.15 respectively. The values of Q_I and β for various propagation effects and regions in the world are given in ITU-R P.841-6 (2019). Previous researchers also proposed several values of Q_I and β for various propagation effects and regions in tropical regions as tabulated in Table 2.3.

Table 2.3 Q_I and β for Various Propagation Effects and Areas in Tropical Regions

No	Source	Country	Propagation Effect	β	Q_I
1.	(Durodola et al., 2017)	i) Akure, Nigeria ii) Jos, Nigeria	Rain rate	i) 0.372 ii) 0.207	i) 1.06 ii) 2.042
2.	(Marzuki et al., 2016)	Kotabang, Indonesia	Rain rate	0.24	1.39
3.	ITU-R P.841-4	Indonesia	Rain rate	0.22	1.7
4.	(Ting & Mandeep, 2014)	USM, Nibong Tebal, Penang	Slant path rain attenuation i) 60 samples ii) 4 years	i) 0.097 ii) 0.07	i) 1.7952 ii) 1.6769
5.	(Ismail et al., 2012)	UTM, Johor Malaysia	Terrestrial rain attenuation	0.219	1.69
6.	(Mandeep & Ng, 2008)	USM, Nibong Tebal, Penang	i) Slant path rain attenuation ii) Rain rate	i) 0.10 ii) 0.39	i) 1.695 ii) 1.343

7.	(Islam et al., 2003)	Skudai, Johor	i) Slant path rain attenuation ii) Rain rate	i) 0.3 (Ku-band) ii) 0.32 (Ka-band)	i) 0.945 ii) 0.9078
8.	(Chebil, 2003)	Malaysia	Rain rate	0.27	1.32
9.	(Yagasena & Hassan, 2000)	Tronoh, Perak, Malaysia	i) Slant path rain attenuation ii) Rain rate	i) 0.3041 ii) 0.293	i) 1.3862 ii) 1.397

2.10 CHAPTER SUMMARY

This chapter presents and discusses in terms of definition and importance of satellite communication as well as the development of HTS satellites which will be operating in Malaysia as MEAST-3d has been launched recently. This chapter also elaborates on the distribution of frequency spectrum in microwave communication. As the higher frequency is highly affected by precipitation, the climate of Malaysia located in tropical-equatorial regions has been highlighted in this chapter. The type of precipitation is also being discussed as precipitation such as rain is the main propagation impairment affecting space communications in tropical regions. There has also been a review on the requirement of fade margin to sustain good Quality of Services (QoS) for better link availability of the system's performance. A comprehensive literature on frequency scaling with the frequency scaling classification was also discussed by presenting the previous research related to the frequency scaling technique in predicting rain attenuation. Besides that, the worst-month analysis is also being covered as the worst-month analysis is important in designing a satellite-Earth communication system. A parameter required in the frequency scaling technique is also being analysed. Finally, the frequency scaling techniques in predicting rain attenuation for a satellite-Earth link in tropical-equatorial regions were summarised in this chapter.

CHAPTER THREE

METHODOLOGY

3.1 INTRODUCTION

The chapter highlights the methodologies that were carried out throughout the study. The approaches used in the research were empirical and evidence-based. Data collections used in the study were the C, Ku, and Ka-band beacon signals during rainy conditions transmitted from the MEASAT-3 and MEASAT-5 satellites. Both satellites are located in their fixed geostationary orbits. The beacon signals from MEASAT-3 and MEASAT-5 transponders were retrieved using the respective Earth stations' receiving systems. At the same time, rainfall intensity data were collected using a dedicated rain sensor. The rain attenuation data at C, Ku, and Ka-band alongside the rainfall information were analysed, assessed, and evaluated in statistical form. From the statistical analysis, the enhanced frequency scaling model was produced. In this chapter, the methodological processes of the study were presented in detail. The overview and synopsis of the research methodology are illustrated in Figure 3.1.

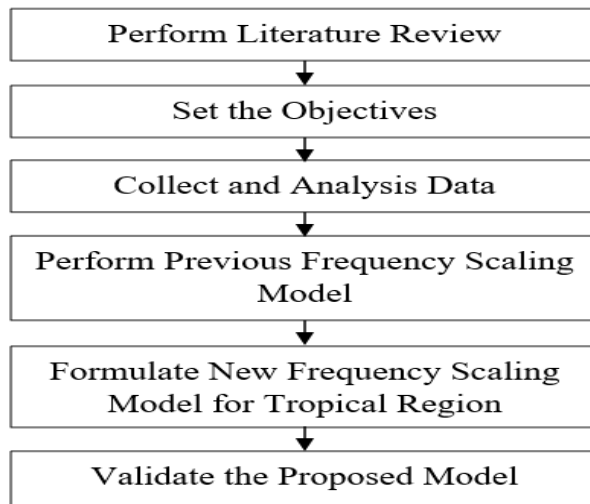


Figure 3.1 Overview of the Research

The cumulative distribution function (CDF) was constructed from the time series of rain attenuation data acquired during the rain events. The frequency scaling techniques proposed by previous studies were presented in this chapter for reference and comparison. The flow chart of the methodologies carried out in the research is shown in Figure 3.2.

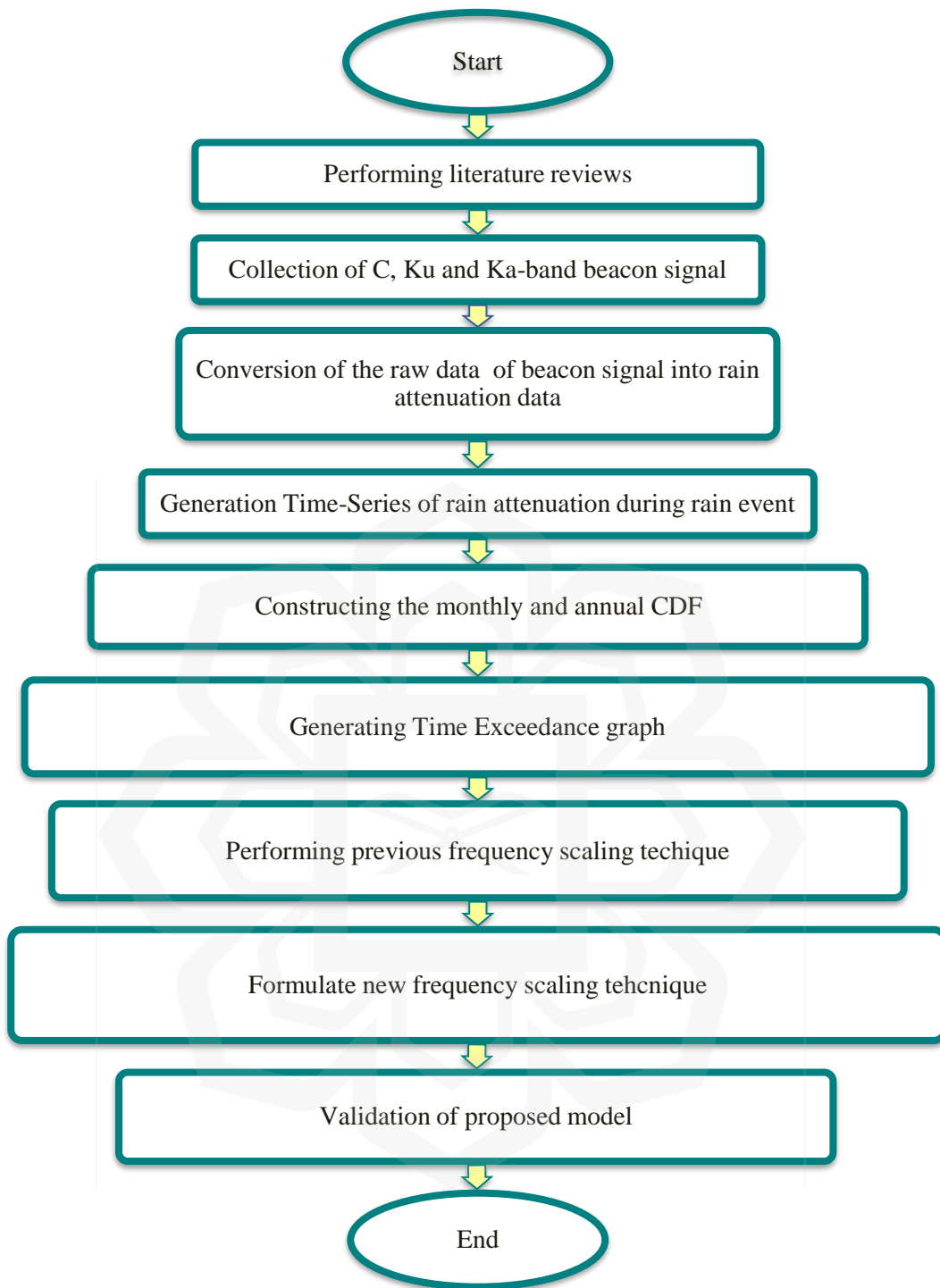


Figure 3.2 Research Flow Chart

3.2 MEASUREMENT SETUP

The determination of rain attenuations was based on the measured beacon signals data of the C-band and Ku-band links broadcasted from the MEASAT-3 satellite. The Ka-band data originated from the MEASAT-5 satellite also known as IPSTAR (Thaicomm-4). The C-band and Ka-band Earth stations are located at MEASAT Teleport and Broadcast Centre. Figure 3.3 shows the Earth station at the MEASAT location. The Ku-band Earth station is located at the ASTRO Broadcast Centres. Figure 3.4 portrays the receiver station at the ASTRO site.



Figure 3.3 Earth Stations at the MEASAT Teleport and Broadcast Centre

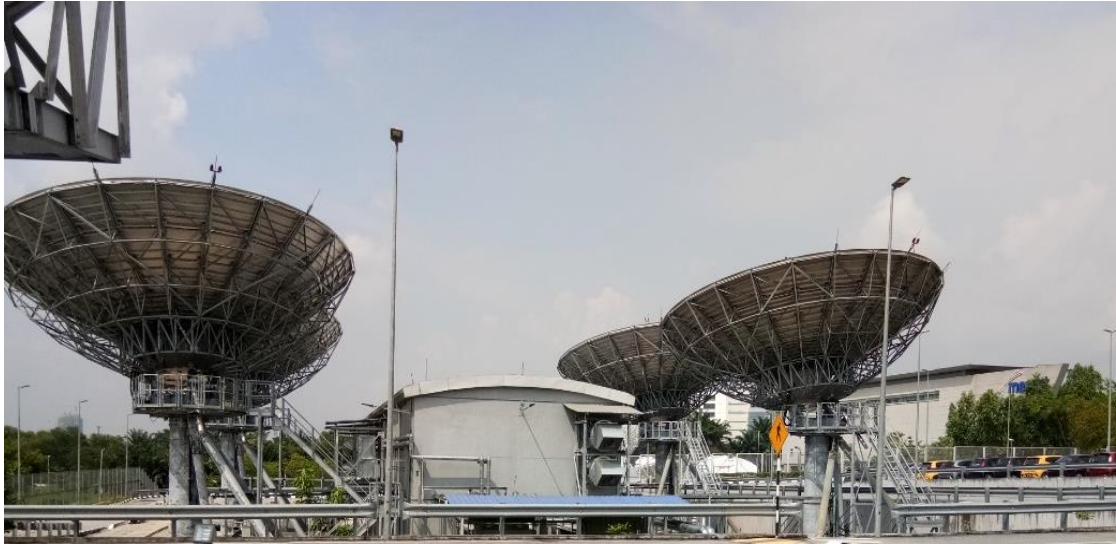


Figure 3.4 Receiver Station at the ASTRO Broadcast Centre

Both centres can be considered neighbouring to each other in Cyberjaya, Malaysia with latitude and longitude information of 2.935° N and 101.658° E. The Earth stations were constructed on an area of about 20 m above sea level. The locations of the MEASAT-5 and MEASAT-3 satellites are at 119.5° E and 91.5° E respectively. The beacon signal frequencies of the C, Ku, and Ka-band are 4.198 GHz, 12.201 GHz, and 20.198 GHz accordingly. The footprints and specifications for MEASAT-3 and MEASAT-5 are shown in Figures 3.5 and 3.6.

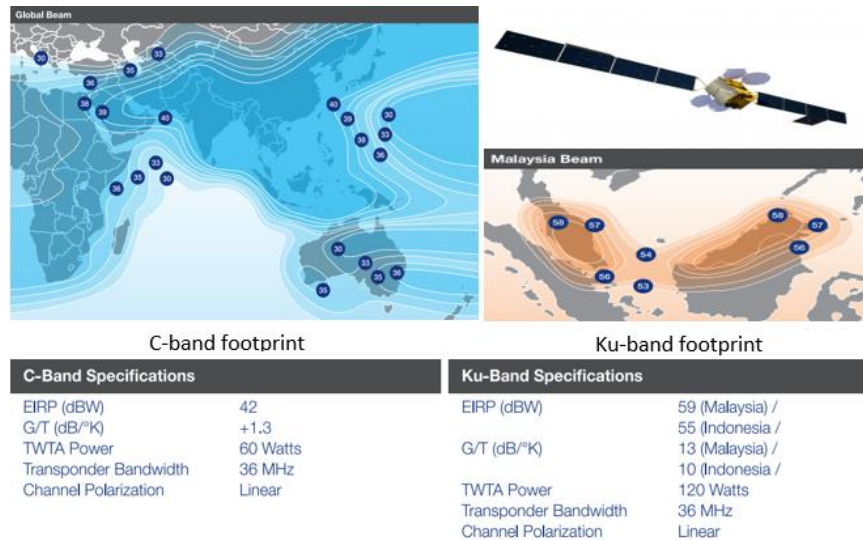


Figure 3.5 MEASAT-3 Specifications and Footprints (MEASAT, 2022)

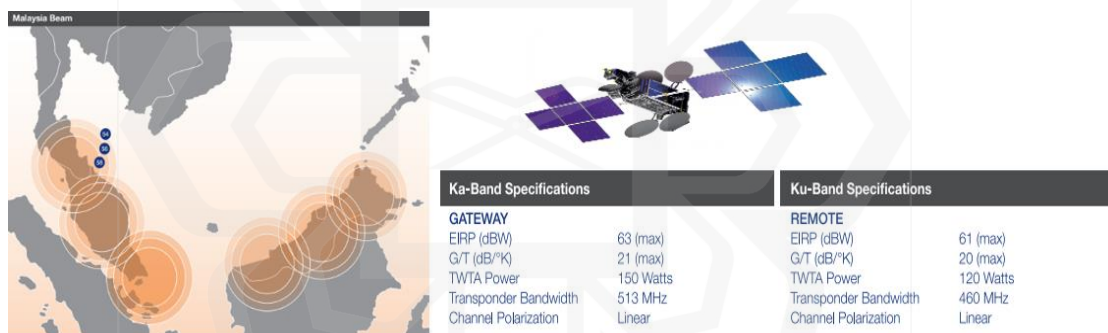


Figure 3.6 MEASAT-5 Specifications and Footprints (MEASAT, 2022)

The elevation and azimuth angle values of C and Ku-band antennas are 77.5° , and 245.05° respectively as both antennas point to the same satellite; MEASAT-3. The Ka-band antenna points toward the MEASAT-5 satellite with an elevation angle of 68.77° and an azimuth angle of 99.04° . Both MEASAT-3 and MEASAT-5 are geostationary satellites and are about 36000 km away from the Earth. The difference between the elevation angle of the Ka-band and the C/Ku-band is small and can be considered insignificant. There is also a difference in slant path calculation during rain

events, however, the difference is also very small. At a rain height of 5.36 km as proposed by the ITU (ITU-R P.618-13, 2017), the slant path lengths for the C/Ku-band and Ka-band link are 5.47 km and 5.72 km respectively. The difference of 0.25 km can be assumed negligible and can be disregarded. The locations of the satellites in reference to the Earth stations are shown in Figure 3.7.

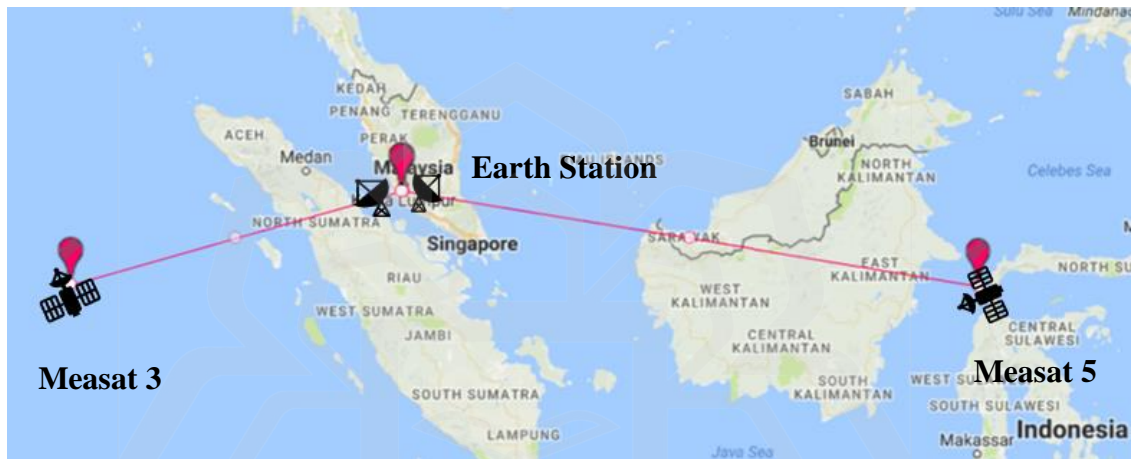


Figure 3.7 MEASAT-3 and MEASAT-5 in reference to their Earth Stations

The observation and recording of satellite beacon signals were continuously carried out using the tracking and ranging subsystems at the Earth station. The tracking and ranging subsystems enable the accurate provision of the beacon signals measurement. A predefined level for the beacon signals received power was determined by the subsystems. The predefined level of received power is denoted as the clear sky signal value. The peak signal strength of the beacon was constantly monitored by the automatic ranging measurement device. The received strength of beacon signals will determine the pointing direction of the antenna at the Earth station.

Rain events cause signal losses. The signal losses or rain attenuations were attained by measuring the difference between received signal levels during rain events

and information collected in clear-sky conditions. Figure 3.8 portrays the Earth-space link design used in the research for the determination of rain attenuation.

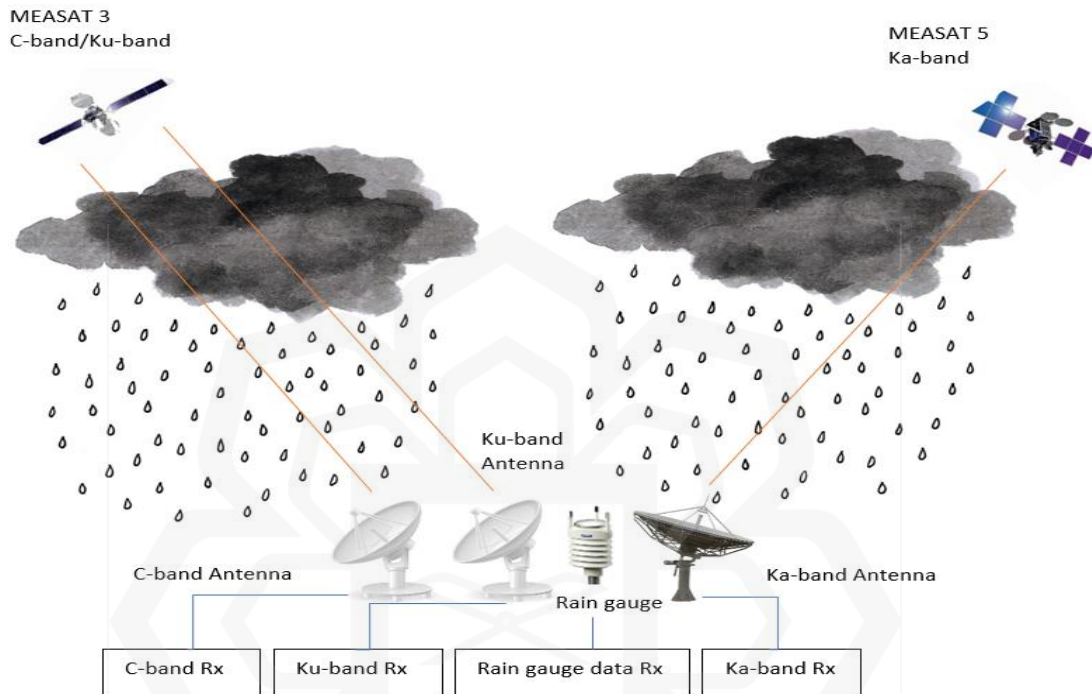


Figure 3.8 Earth-Space Link Design

A thorough understanding of the statistical characteristics of rainfall intensity as well as rain attenuation in heavy rainfall areas such as tropical regions is critical. Those pieces of knowledge are beneficial for better planning of any millimetre-wave SatCom system. Every different frequency band measurement has its experimental setup consisting of the antenna and its digital track receiver (beacon receiver) for monitoring and recording the satellite signals.

The low noise amplifier (LNA) amplifies the power of every received signal by the antenna. The final signal power, therefore, is increased according to the set gain

value. The beacon's original frequency is down-converted to an intermediate frequency (IF), making it possible for the digital tracking receiver to detect and record the beacon signals. In the research, two years of beacon data from January 2015 until December 2016 were acquired from the C, Ku, and Ka-band Earth stations. The details of the measurement for each beacon are discussed in sections 3.2.1 to 3.2.3.

3.2.1 C-band Beacon Measurement Setup

The receiver system measures 4.198 GHz C-band beacon signals. The C-band receiver consists of a Cassegrain antenna with an 11.1 m diameter and it is linearly polarized. The antenna was manufactured by General Dynamics Satcom Technologies from the USA. The reflector of the antenna is designed from precision-formed panels, truss radials, and hub assembly that uses matched tooling for interchangeable components. The advantages of the antenna are high antenna efficiency, low noise temperature, high gain, as well as excellent rejection of noise and microwave interference due to its feed and sub-reflector design. The reflector is supported by a galvanized elevation over an azimuth kingpost pedestal that provides the required stiffness for accurate pointing and tracking purposes. The antenna is easy to install on the ground or rooftop since the pedestals are designed for full orbital arc coverage. The antenna system consists of an LNA with a high Gain over Temperature (G/T) performance of 33 dB/K. The received signals are amplified by the LNA and then down-converted to the IF of 1.5 GHz.

The beacon tracking receiver is made by General Dynamics Satcom Technologies USA. The tracking receiver is a Digital Signal Processor (DSP) based receiver that is developed for satellite tracking and uplink power control. It receives wideband Radio Frequency (RF) inputs, selects frequency, and processes the selected signal in digital form using the Direct Digital Synthesis (DDS) technique to facilitate 1 kHz frequency resolution. The maximum power level of the tracking receiver is – 10 dBm in conditions where the input signal levels are within the range of – 40 dBm to -

110 dBm. The recording of the beacon signals is performed by data interfaces of RS/422 with a PC. Table 3.1 shows the parameters set up for the C-band receiver extracted from the antenna and beacon/tracking receiver datasheets.

Table 3.1 C-band Beacon Signals Receiving Setup

Parameters	Specification
Antenna Type	Cassegrain Antenna
Diameter	11.1 m
Antenna Polarization	Linear
G/T	33 dB/K
Antenna Material	36 Precision Formed Aluminium
Antenna Mount	Elevation over Azimuth Pedestal
Tracking Receiver Input Signal Level	-40 to -110 dBm (nominal)
Tracking Receiver Input Frequency	3.4 – 4.8 GHz
Receiver Tuning Resolution	1 kHz
Minimum Carrier over Noise (C/N ₀)	35 dB-Hz
Tracking Sensitivity	1 V/dB
Data Interface	RS-232 / RS-422

The reference level of the C-band beacon signals receiving system is 0 dB. Figure 3.9 shows a simplified block diagram of measurement at C-band and Ku-band links. Figure 3.10 shows the picture of the C-band antenna.

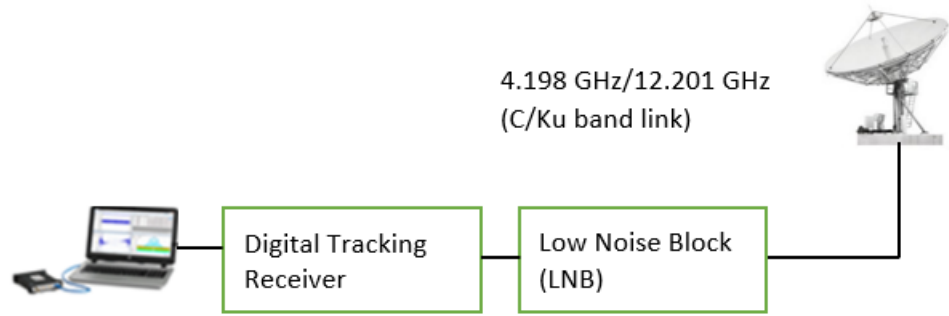


Figure 3.9 C/Ku-band Configuration



Figure 3.10 C-band Antenna (General Dynamics SATCOM Technologies)

3.2.2 Ku-band Beacon Measurement Setup

The Ku-band antenna is of the Cassegrain type with a diameter of 13.1 m. The size of the Ka-band's antenna is larger than the C-band to provide a better link margin for Broadcasting Satellite Services (BSS) operations, particularly during high precipitation conditions. A large centre hub provides wider space for proper equipment mounting. The antenna was manufactured for full orbital arc coverage use. The precision-formed panels, truss radials, and hub assembly was designed for the antenna's reflector. The antenna also has the ability in providing the required stiffness for pointing and tracking accuracy. The characteristics and specifications of the Ku-band antenna are somewhat similar to the C-band antenna except for the dish size and the gain. The size of the Ku-band antenna is bigger than the C-band antenna to provide better performance in terms of G/T which is 40.5 dB/K. The LNA intensifies the power of the Ku-band beacon-received signals. Table 3.2 lists the parameters of the Ku-band receiver, retrieved from the General Dynamics documentation. The 13.1m Ku-band antenna is provided by General Dynamics Satcom Technologies from the USA.

The signals were down-converted to an IF with a value of 1.5 GHz. The beacon tracking receiver is a product from General Dynamics Satcom Technologies USA. The tracking receiver can receive L, S, C, X, Ku and Ka-band. The input range of the tracking receiver is configured at the factory. The system which is interfaced with a PC via RS/422 is capable of recording all beacon signals. The predetermined level or the clear sky signal is set to -76 dBm in the Ku-band beacon receiver system. Figure 3.11 shows the picture of the 13.1 meters diameter of the Ku-band antenna while Figure 3.12 shows the digital tracking receiver that is being used for Ku and C-band measurement setups.

Table 3.2 Ku-band Beacon Signals Receiving Setup

Parameters	Specification
Antenna Type	Cassegrain Antenna
Diameter	13.1 m
Antenna Polarization	Linear
G/T	40.5 dB/K
Antenna Material	50 Precision Formed Aluminium
Antenna Mount	Elevation over Azimuth Pedestal
Tracking Receiver Input Signal Level	-40 to -110 dBm (nominal)
Tracking Receiver Input Frequency	10.7 – 13 GHz
Receiver Tuning Resolution	1 kHz
Minimum Carrier over Noise (C/N ₀)	35 dB-Hz
Tracking sensitivity	1 V/dB
Data interface	RS-232 / RS-422



Figure 3.11 Ku-band Antenna (General Dynamics SATCOM Technologies)



Figure 3.12 Digital Tracking Receiver for Ku and C-band

3.2.3 Ka-band Beacon Measurement Setup

The Ka-band antenna system is located within the vicinity of the C-band as well as the Ku-band antenna. The main purpose of the deployment of the Ka-band antenna system is to provide a better internet connection, especially to remote places in Malaysia. Ka-band should be capable of accomplishing such tasking due to its characteristic which is high-frequency bands with high throughput. High-speed data connection services in Malaysia using satellite communication can be achieved since Ka-band has greater data transmission capacity with low latency.

The ground station uses an 8.1 m dual reflector Gregorian antenna. The antenna selection involving a smaller diameter compared to the low-frequency antennas was due to economic reasons and flexible reception services purposes. The reflector consists of 20 segments from precision-formed aluminium. The antenna is mounted on an elevation over azimuth and pedestal so that it will be stable during conditions of strong wind and rain. The Ka-band receiver system has a gain of 21 dB/K to receive Ka-band beacon signals from the satellite. The specifications of the Ka-band parameters are shown in Table 3.3. Figure 3.13 portrays a simplified block diagram of measurement at the Ka-band link.

Table 3.3 Ka-band Beacon Signals Receiving Setup

Parameters	Specification
Antenna Type	Dual Reflector Gregorian
Diameter	8.1 m
Antenna Polarization	Linear
G/T	20.1 dB/K
Antenna Material	20 Precision Formed Aluminium
Antenna Mount	Elevation over Azimuth Pedestal
Tracking Receiver Input Signal Level	-30 to -90 dBm (nominal)
Tracking Receiver Input Frequency	930 to 2300 MHz
Receiver Tuning Resolution	10 kHz
Minimum Carrier over Noise (C/N ₀)	45 dB-Hz
Tracking Sensitivity	0.5 V/dB
Data Interface	RS-232 / RS-422

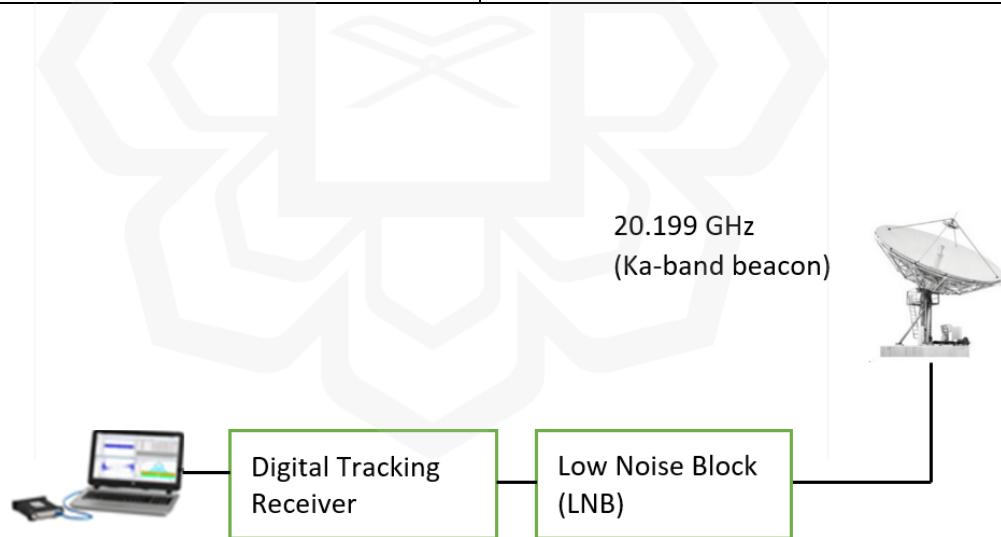


Figure 3.13 Ka-band Configuration

The LNA was used to increase the power of the Ka-band received signals. The 20 GHz frequency was also down-converted to an IF of 1.5 GHz. The clear sky signal or

predetermined level was set manually in section 3.4.1. Figure 3.14 shows the picture of the Ka-band antenna. The digital tracking receiver being used for the Ka-band measurement setup is portrayed in Figure 3.15.



Figure 3.14 Ka-band Antenna

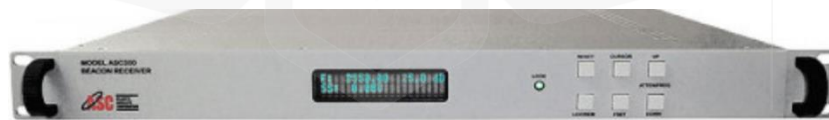


Figure 3.15 Digital Tracking Receiver for Ka-band

3.2.4 Rain Gauge Measurement Setup

To measure and monitor the rainfall rate, a rain gauge or rain sensor is required. A rain sensor installed at ASTRO Broadcast Centre was used to monitor the rain events in Cyberjaya. When a rain event occurs, lower received signals are detected where such an instance specifies the attenuation in the link because of rain. In this measurement setup, the Vaisala Weather Transmitter WXT520 model is used as the rain sensor. Covering an area of 60 cm², the sensor has an accuracy of 95% with a resolution of 0.001 inches. The units of the rainfall reading by the sensor are in millimetres and inches. The sensor comprises two parts which are the steel cover and a piezoelectrical sensor. The piezoelectric sensor is mounted on the bottom surface of the cover. The detection of size and impact of individual raindrops are measured as raindrops.

The volume of the drops produces proportional signals and is converted to the accumulated rainfall rate. Rain amount is referring to the detection of every individual drop. Rain intensity with high resolution also can be computed. After every 10 seconds, the current rain intensity is updated. The transmitter automatically sends a precipitation/rain message every 10 seconds after recognition of the first drop and the messages are continuously sent until the rain stops. After every sixth measurement, the one-minute integration time is generated. The general specification of the Vaisala Weather Transmitter WXT520 rain sensor is summarised in Table 3.4. The rain sensor that has been installed at ASTRO Broadcast Centre is shown in Figure 3.16.

Table 3.4 Vaisala Weather Transmitter WXT520 Specifications

Parameters	Specification
Wind speed measurement	0 - 60 m/s ($\pm 3\%$ @ 10 m/s)
Wind direction measurement	0 - 360° ($\pm 3\%$, response time <250 m/s)
Rainfall accumulation	Resolution of 0.01 mm ($\pm 5\%$ uncertainty)
Rainfall duration	Counts each ten-second increment when droplets detected
Rainfall intensity	0 - 200 mm/h (one-minute running average in ten-second steps)
Barometric pressure measurement	600 - 1100 hPa (± 0.5 hPa at 0 - 30 °C)
Digital output options	SDI-12, RS232, RS485, RS422, USB adapter
IP65 design	Up to IP66 with mounting kit option (for pole installation)
Lightening protection	Optional bird spike and WSP150 surge protection



Figure 3.16 ASTRO Rain Sensor

3.3 COLLECTION OF DATA

The data of the C, Ku and Ka-band beacon signals were collected from receivers at the respective ground stations for twenty-four months from 2015 to 2016. The rainfall data were retrieved from the rain sensor for one year in 2016. Both rain attenuation and rainfall data were processed into first-order statistics and analysed thoroughly.

3.4 DATA PROCESSING

Figure 3.17 shows the flow chart of the overall analysis process in the research. Firstly, the attenuation data of the C, Ku, and Ka-band as well as rainfall information were gathered.

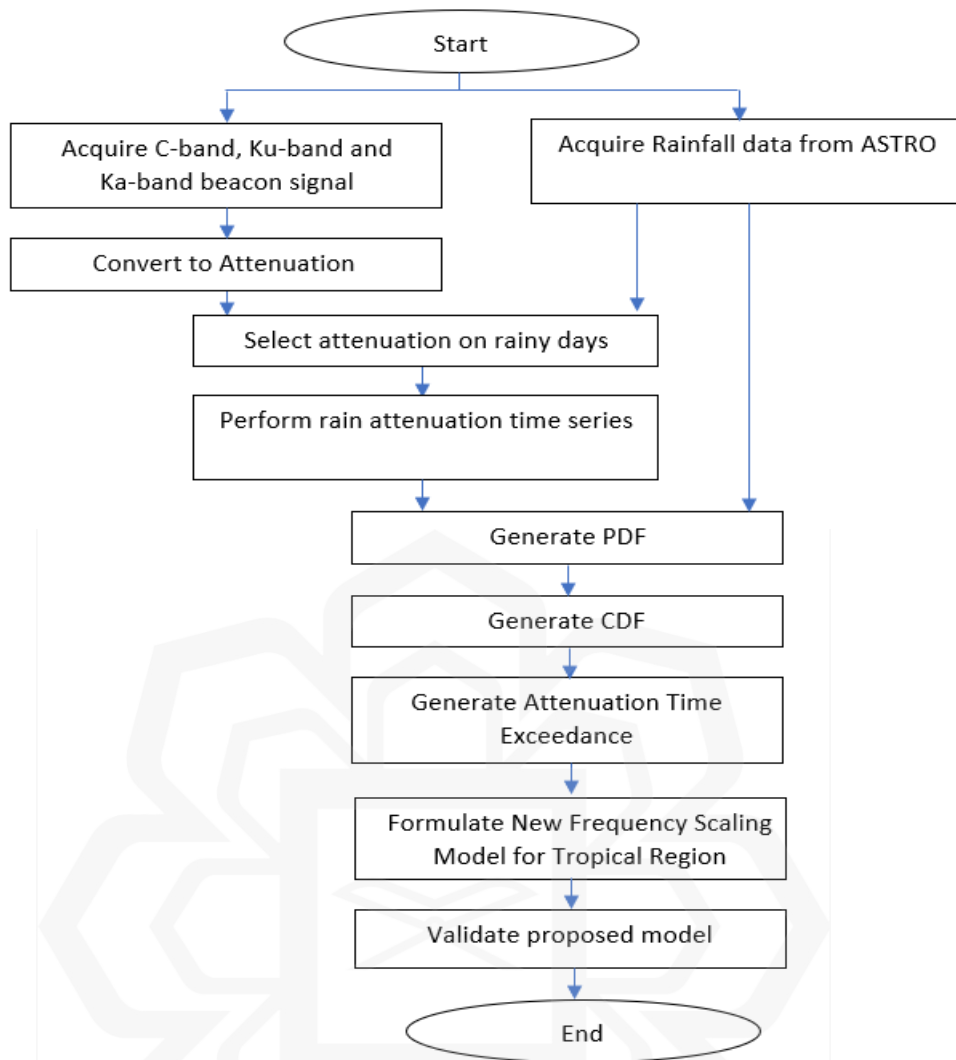


Figure 3.17 Flow Chart of Processing Data

3.4.1 Extraction & Conversion of Raw Data into Rain Attenuation Data

The following approaches have been applied to achieve the first objective of the research. The rain attenuation and rainfall data were processed to obtain first-order statistics which are the cumulative distribution function (CDF). The CDF of the Ku and Ka-band is important as an input parameter for developing a frequency scaling model. The raw data of the Ka-band beacon signals were collected in text document type (.txt)

format. The data were imported into Microsoft Excel format. The raw data of C-band and Ku-band was already in Microsoft Excel format. For Ku-band, the predetermined level of the digital tracking receiver was set at -76 dBm in the Ku-band beacon receiver system. The data collected for C-band were recorded in terms of Delta (in dB) concerning 0 dBm which presents the attenuation value itself. The beacon signals data of the Ka-band were registered in terms of beacon signal level in dBm. The beacon signals have to be subtracted by a clear sky value to produce attenuation data. The clear sky value for Ka-band was derived manually.

The received signal strength from the beacon signal, during the clear sky, was individually compared for each day to determine the minimum value received signal. The average received signal minimum value acquired during non-rainy days from 12 months throughout the year 2016 was then denoted as a clear sky value. The clear sky value was deducted from the received signal strength values to obtain the attenuation value. The clear sky value for the Ka-band beacon received signal was determined as 66.7 dB. The time-series graphs for rain attenuation of C, Ku, and Ka-band correlated with concurrent rainfall rates were generated. The attenuation data of the C, Ku, and Ka-band were analysed in detail related to the time of the rain on rainy days.

3.4.2 Generation of Probability Density Function (PDF)

The rain attenuation and rainfall were accumulated to obtain their frequencies of occurrence and probability density function (PDF). The PDF is a method for calculating the likelihood that a variable value falls within the same interval. For a continuous function, the PDF is the probability that the variate has the value x , and the probability at a single point is zero. It can be expressed in terms of integration between two points. In the research, the PDF was created using Microsoft Excel's pivot table feature. The sample of the PDF for the Ka-band beacon signals is attached in Appendix I.

3.4.3 Generation of Cumulative Density Function (CDF)

The CDF is a function whose value represents the chance that a related continuous random variable has a value less than or equal to the argument of the function. The CDF is used to determine the likelihood that a random observation taken from the population will be less than or equal to a particular value. The CDF is generated from PDF. The CDF is the most competent way to present data for a very long period. In this research, the CDF curve was plotted to evaluate the probability of rainfall rate exceeding a percentage of time and the time exceedance for signal link loss due to rain. The sample of the CDF for the Ka-band beacon signals is attached in Appendix II.

3.4.4 Generation of Time Exceedance

After the PDF was transformed into the CDF, the time percentage of exceedance was calculated in obtaining a probabilistic value. The percentage of time exceedance for rain attenuation was established from the obtained CDF. The formula to determine time exceedance is given:

$$\text{Time exceedance} = \frac{\text{CDF}}{24 \times 60 \times n} \times 100\% \quad (3.1)$$

Parameter n refers to how many days are in a particular month/year. For example, for a one-year duration, at 0.01% of time exceedance for the one-minute based rain attenuation and rainfall intensity, the required value of samples is $0.01 \times 60 \times 24 \times 365 / 100$ amounting to 53 minutes. From the time exceedance graph, the fade margin capable of achieving the required QoS of the link can be determined. A fade margin on annual basis can be obtained. The monthly and annual experimental data were plotted for the year 2016.

3.4.4.1 Monthly

Monthly CDF in the form of time exceedance is presented as the equation as follows:

$$\text{Time exceedance} = \frac{\text{Monthly CDF}}{24 \times 60 \times n_m} \times 100\% \quad (3.2)$$

where;

- n_m : 31 days for January, March, May, July, August, October, and December,
- n_m : 30 days for April, June, September, and November,
- n_m : 28 days for February of the year 2016,
- n_m : 29 days for February of the year 2015.

3.4.4.2 Annual

Annual CDF in the form of time exceedance is presented as the equation as follows:

$$\text{Time exceedance} = \frac{\text{Annual CDF}}{24 \times 60 \times n_a} \times 100\% \quad (3.3)$$

where;

- n_a : 365 days for the year 2016,
- n_a : 366 days for the year 2015.

The summarised flow chart of generating time exceedance for rainfall and rain attenuation in 5 steps is illustrated in Figure 3.18 to achieve the first objective. The annual CDF is very important in determining the best and most reliable fade margin to be applied in the communication link designs. These five steps were performed on the rainfall and rain attenuation data in 2016 and 2015 for analysis and validation purposes respectively. The validation process was executed by using rain attenuation data from 2015 due to the limitation of data.

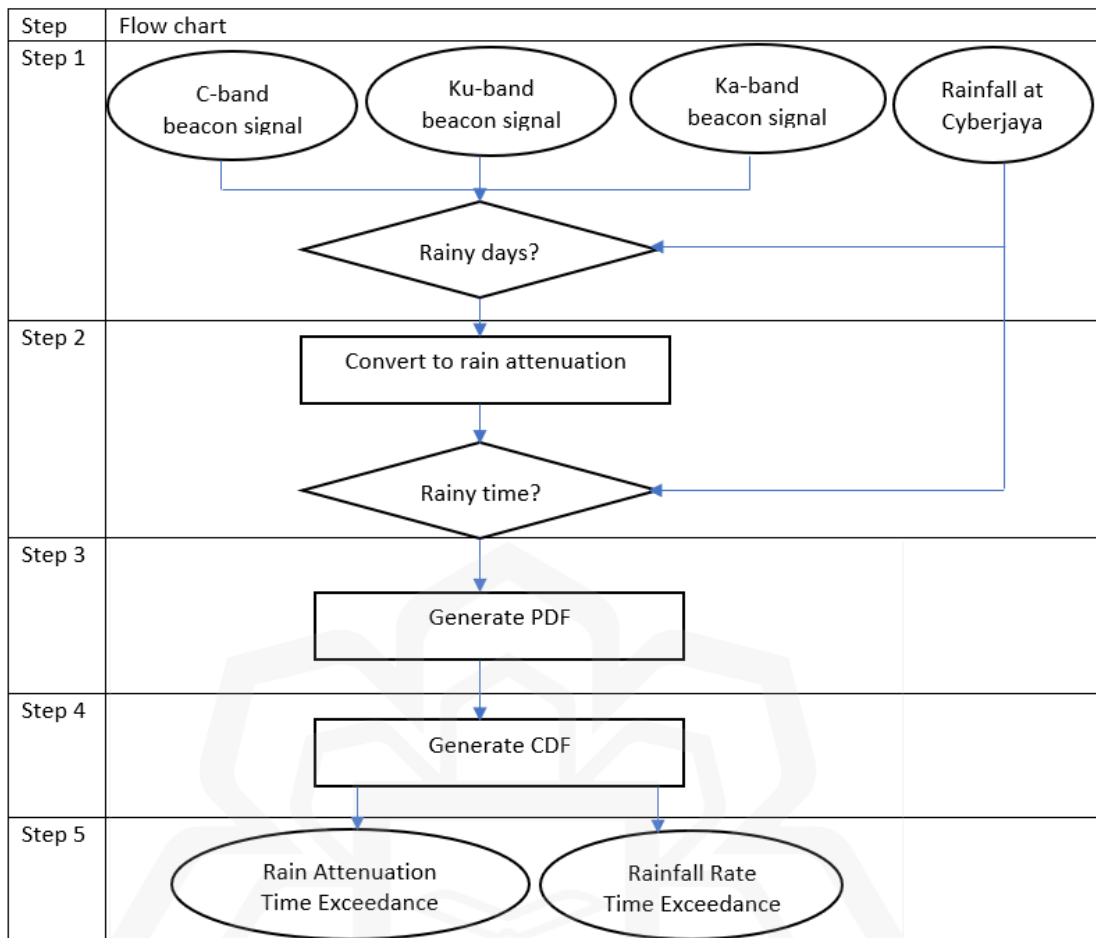


Figure 3.18 Steps in Generating Time Exceedance for C, Ku and Ka-band Beacon Signals, and Rainfall Rate Data.

3.5 DATA ANALYSIS

The rain attenuation data were analysed daily, monthly, and annually.

3.5.1 Time Exceedance Analysis for C, Ku & Ka-Band

For daily analysis, the attenuation values at C, Ku and Ka-band were extracted accordingly from all recorded rain events throughout the day. A time-series graph was generated for every rain event during rainy days for all frequencies. The time frames for C and Ku-band were the same since both rain attenuation measurements were retrieved from MEASAT-3. The results of the time-series plots were presented in Chapter Four.

The timestamp for rain attenuation of the Ka-band link was different from those of the C-band and Ku-band highlighted previously. The timestamp was in GMT (Greenwich Mean Time) where the time difference was at +8 hours. Kuala Lumpur is located east of Greenwich town, thus having GMT+8 time zone. The received signal of the Ka-band beacon was 8 hours earlier from the Malaysian time zone. The time frame had to be adjusted so that the attenuation would overlap with the rainfall event timestamp. The rainfall rate and Ka-band rain attenuation time-series graphs for one day were presented in Figures 3.19 and 3.20 accordingly.

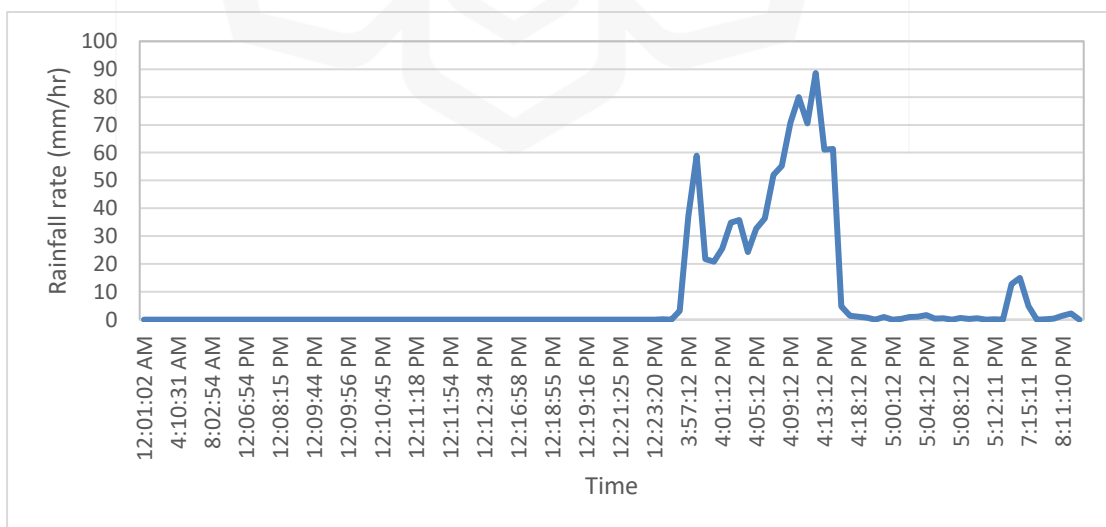


Figure 3.19 Time-Series for Rain Event on 6th February 2016

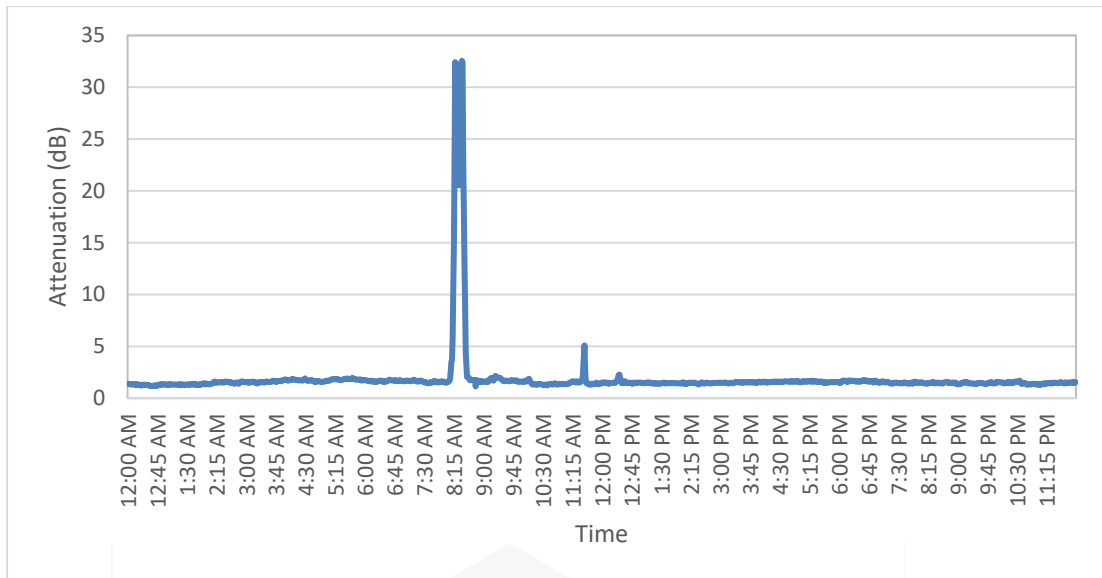


Figure 3.20 Attenuation Time-Series of Ka-band for One Day on 6th February 2016

There were several days where rain attenuation values were registered at the Ka-band, however, no rain was detected and recorded in the Cyberjaya area. The attenuation data were then compared with alternative rainfall rate data retrieved from other rain sensors installed nearby the Ka-band Earth station. These substitute rain gauges are located at Paya Indah (2.8789, 101.6192) and Puncak Niaga (2.9111,101.6972) as shown in Figure 3.21.



Figure 3.21 Location of Rain Gauge at Paya Indah, Puncak Niaga, and Earth Station at Cyberjaya

Paya Indah and Puncak Niaga sites are located 5 km and 9.2 km away from Cyberjaya Earth station respectively. Table 3.5 tabulates the rain detected at different locations on the rain gauge in January 2016. From Table 3.5, on 12th January 2016, there was no rain detected at Cyberjaya yet somehow the attenuation with a value of 34.3 dB was registered. It can be observed from the table that there was rain detected in Paya Indah and Puncak Niaga. Based on the literature and physical observation, it has been acknowledged that the clouds consisting of a rain cell can be repositioned from one place to another place by a wind gust. The new rain cells were produced at the new location. The collected rain data along the ground path should be counted into consideration for rain attenuation comparison. However, the research only focuses on rainfall data from Cyberjaya as a concerned parameter since the rain gauge is located nearest to the Earth station.

Table 3.5 Rain Detected at Different Rain Gauge Locations in January 2016

Month	Date	Rain Attenuation of Ka-band link (2.95,101.678)	Rain at Paya Indah (2.8789, 101.6192)	Rain at Puncak Niaga (2.9111, 101.6972)	Rain at Cyberjaya (2.95, 101.678)
January	3-Jan	21.4 dB		YES	
	4-Jan	31.9 dB	YES	YES	YES
	5-Jan	9 dB	YES		YES
	6-Jan	11.2 dB	YES		
	12-Jan	34.3 dB	YES	YES	
	14-Jan	17.4 dB	YES	YES	
	15-Jan	33 dB	YES	YES	YES
	17-Jan	31.7 dB	YES	YES	
	18-Jan	12.6 dB			
	19-Jan	32.3 dB	YES		YES
	28-Jan	22.5 dB	YES	YES	YES
	29-Jan	31.5 dB	YES	YES	YES

From Figure 3.22, the attenuation value experienced by the Ka-band link was capped at 33 dB due to the limited receiver sensitivity level. Due to the limitation, the higher attenuation values (>33 dB) of the Ka-band needed to be extrapolated to produce a better graph. The rain attenuation graph at the frequency is very essential in further analysis in the research which is to develop the frequency scaling model. The applied extrapolation techniques were explained in detail in section 3.5.2.

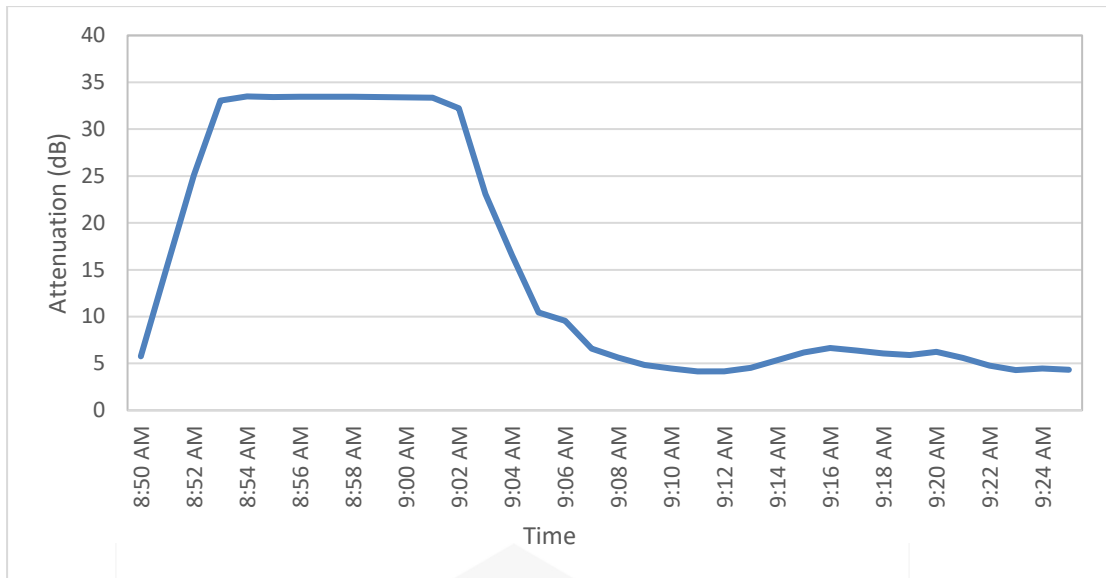


Figure 3.22 Time-Series of Rain Attenuation of Ka-band on 4th January 2016

3.5.2 Technique to Extrapolate the Ka-band Attenuation Data

Since the annual rain attenuation of the Ka-band link was capped at 33 dB, the extrapolation formula was developed based on the rainfall data obtained from the rain gauge installed at ASTRO Broadcast Centre. The available data was within the range of time exceedance percentages from 0.6% to 0.05%. The extrapolation formula was used to calculate the attenuation exceedance at other percentages of time between 0.04% and 0.001%. Several techniques had been applied for extrapolation methods such as the linear, power, and polynomial approaches. The following steps were used to evaluate the extrapolation techniques. The most suitable technique for extrapolating rain attenuation at the Ka-band link had been identified as follows:

1. Correlate annual rainfall rate with annual rain attenuation data of Ka-band by plotting the graph of Ka-band rain attenuation versus rainfall rate for the same probabilities of time exceedance in EXCEL shown in Figure 3.23.

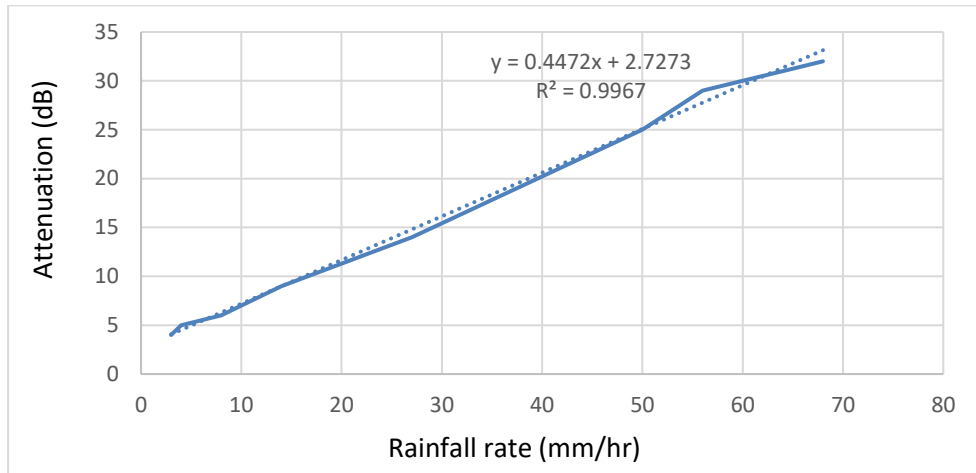


Figure 3.23 Plot of Annual Rain Attenuation of Ka-band versus Annual Rainfall Rate

2. Apply the linear curve fit equation to the graph.

The linear model equation by EXCEL is shown as follows:

$$A = 0.4472 \times (R_{\%}) + 2.7273 \quad (3.4)$$

A denotes attenuation, $R_{\%}$ represents rainfall rate at desired time exceedance.

3. Apply the curve fit tool to the graph and evaluate a few extrapolations formulas using MATLAB such as linear, first-order power law, second-order power law, and second-degree polynomial as attached in Appendix III.

The variables m and n were used in MATLAB to represent the annual rain attenuation of the Ka-band versus the annual rainfall rate of the year 2016 at the same percentage of time exceedance respectively. The data for Ka-band rain attenuation was also extrapolated by using Ahmad's model (Ahmad, 2019). The applied extrapolation techniques are:

- i) The linear model equation by MATLAB is as follows:

$$A = p1 \times (R_{\%}) + p2 \quad (3.5)$$

where $p1$ is 0.4472 and $p2$ is 2.727.

ii) The first-order Power Law equation by MATLAB is as follows:

$$A = a \times (R_{\%})^b \quad (3.6)$$

with constants of a and b of 0.2038 and 0.8704 respectively.

iii) The second-order Power Law equation by MATLAB is as follows:

$$A = a \times (R_{\%})^b + c \quad (3.7)$$

with constants of a , b , and c of 0.4638, 0.9917, and 2.659 respectively.

iv) The second-degree polynomial equation by MATLAB is as follows:

$$A = (a \times R_{\%}^2) + (b \times R_{\%}) + c \quad (3.8)$$

with the constants of a , b and c are -0.0004, 0.4717, and 2.5305 respectively.

v) Applying ITU-R 618-13 rain attenuation prediction with specific attenuation proposed by (Ahmad, 2019), k is 0.1454173 and a is 1 and $R_{0.01\%}$ is 102 mm/hr.

3.5.3 Selection of The Best Extrapolation Technique to Determine Ka-band

After that, the best extrapolation model was selected. All the extrapolation models were analysed using R-square, RMSE, and percentage error. The best-predicted methods produced the smallest value of RMSE. If the R-squared of the model is equal to 1, it indicates that the predicted model fits perfectly with measured data. Thus, the better model should yield a smaller RMSE and higher R-squared which is approaching 1 value. The findings are presented in section 4.2.2.5.

3.5.4 Comparison with ITU-R

During the data analysis, the ITU-R analysis was also conducted for comparison purposes. The results of the ITU-R analysis of rain attenuation and rain rate are presented in Chapter Four.

3.5.5 Determination of Worst Month

Since the worst month analysis is also important in the planning of the satellite-Earth system, the attenuation value exceeded for a time percentage of the worst month, p_w was determined in the research. The following steps were used to evaluate the attenuation exceedance for a particular percentage of the worst month.

- i. Step 1: Acquire the desired worst-month time percentage, p_w , corresponding to the annual time percentage, p_a , throughout the year.
- ii. Step 2: Obtain the conversion factor, Q from equation 2.34 which is the ratio of p_w and p_a .
- iii. Step 3: Plot the conversion factor, Q versus the average annual time percentage of rain attenuation, p_a to obtain parameters of Q_I and β . The least-square method is one of the methods to obtain regression parameters Q_I and β with the measured rainfall rate and rain attenuation data.
- iv. Step 4: The estimated attenuation for a percentage of the worst month, p_w is acquired from attenuation exceeded for the resulting annual time percentage, p_a . The results of the worst month analysis are included in Chapter Four.

3.6 DETERMINATION OF FREQUENCY SCALING TECHNIQUE

In this section, the methods that had been deployed to carry out the second objective are elaborated. The available techniques on frequency scaling were tested on the sample set of rain attenuation data. The accuracy of the models was investigated. The tested model included the ITU-R 618-13 frequency scaling model, Hodge Model, Drufuca Model, Battesti Model, Kheirallah Model, CCIR Model, Simple Power Law Model, and Boithias Model. Based on the ITU-R guidelines, in developing the frequency scaling of the rain attenuation model, reliable long-term measured attenuation data was preferred to be applied instead of long-term measured rain data. The ITU-R suggests that the accuracy is obtainable from the smallest statistic parameters. The prediction accuracy can be improved with the implementation of long-term statistical data in tropical regions. All the models mentioned in section 2.8.3 had been tested on attenuations at the equiprobable values of the excess rain attenuation at pairs (f_2/f_1) for 12.201 (Ku-band) GHz/4 GHz (C-band) and 20.199 GHz (Ku-band)/12.201 GHz (Ka-band). The results are presented in section 4.6.

3.6.1 Proposed Frequency Scaling Model

Long-term rain attenuation data is required to develop a frequency scaling model. The research used one-year rain attenuation data of the C, Ku, and Ka-band. The employment of statistical rain attenuation data at different operating frequency bands was essential in the frequency scaling studies. In the research, the CDFs of rain attenuation measurements at C, Ku, and Ku-band were obtained and the rain path was considered consistent. A new frequency scaling model that depends on rain attenuation was derived based on the relationship between RAS and attenuation at base frequency. The correlation between attenuation at upper frequency and attenuation at lower

frequency was also considered. The new model was developed by adopting the curve fitting technique to the correlation graph.

3.7 VALIDATION OF THE MODEL

The validation of the model is very critical in providing reliable results and a dependable new frequency scaling technique. In ensuring that the model can be trustworthily applied in tropical regions, authentication was done by comparing the proposed frequency scaling model with the measured rain attenuation data of alternative years and locations, as well as the ITU-R frequency scaling model. The first phase of validation of the proposed model was performed with two sets of measurement data. The first dataset is rain attenuation data of Ka-band retrieved from Earth station in Cyberjaya in 2015. Another set of data was rain attenuation data of the Ka-band in 2016 which was obtained from the MEASAT backup station located in Rawang, Selangor. The backup station had the same specification as the station in Cyberjaya.

The proposed model was utilized to scale up the possible attenuation at V-band. The scaling data was validated with V-band rain attenuation data in Akure, Nigeria. All the validation methods were carried out to achieve the last objective of the research. The validation results were presented and detailed in the result section in Chapter Four.

3.8 SUMMARY

This chapter elaborates in detail on the methodology conducted throughout the research, including the data processing and analysis as well as correlation approaches. The method involved in the processing and analyzing of the twelve months of rain

attenuation data was thoroughly presented. The step required in generating CDFs for C, Ku, and Ka-band were also explained. The steps of determining the worst month were also detailed. Several previous models of existing frequency scaling were also tested to evaluate their performance efficiency. The regression analysis from the scaling ratio was performed to acquire the best frequency scaling model deemed suitable for tropical-equatorial regions.

The proposed frequency scaling technique was deployed to obtain potential rain attenuation data of Ka, Q, and V-band. The scaled Ka-band data was validated with the two sets of measured Ka-band data with changed years and another area in tropical regions. The outcomes were compared with the frequency scaling model of the ITU-R. The estimation of the V-band values from the proposed model was justified using measured data from the Nigerian communication satellite, NigComSat. The accuracy was compared with the one that has been tested with the ITU-R rain attenuation prediction model. All results of the research are presented, analysed, and discussed in detail in Chapter Four.

CHAPTER FOUR

RESULT

4.1 INTRODUCTION

The research results are presented and discussed in this chapter. This is to fulfil all the mentioned objectives. The results were obtained from the conducted methodologies, as extensively explained in Chapter Three. The statistical analysis of the twelve-month continuous data of rainfall rates and rain attenuation from January to December 2016 in Cyberjaya was carried out. The findings on the rain attenuation data for the C, Ku and Ka-band links were presented in first-order statistics format. The outcomes also include the relationship between attenuation and rainfall intensity in tropical regions. The time exceedance of each Cumulative Distribution Function (CDF) for C, Ku and Ka-bands rain attenuation and rainfall rate data were depicted on a monthly and annual basis. The CDF analysis is the most effective method to present one-year attenuation data. This is very important in providing the best link margin for proper system operations as well as service configuration. The CDF of the Ka-band rain attenuation was extrapolated for the development of a new frequency scaling technique. The best extrapolation technique with the smallest RMSE and the highest R-squared value was selected. An error analysis was performed on the existing frequency scaling techniques for comparison purposes. A new frequency scaling method was derived based on rain attenuation data in Malaysia. The newly developed frequency scaling model was presented and discussed. This is to determine a more accurate rain attenuation prediction method in tropical regions. The proposed model was evaluated using the RMSE value and relative percentage error. Acquiring the RMSE value is the right method for determining whether the model will fit the available dataset for tropical regions. The essential findings in this chapter consist of:

1. The statistical analysis of rain attenuation for C, Ku and Ka-bands in tropical regions.

2. The correlation between the rainfall rate and the measured rain attenuation in developing a frequency scaling model for tropical regions.
3. The validation of the proposed model in determining a reliable technique for estimating rain attenuation that is applicable in tropical regions.

4.2 DIURNAL TIME-SERIES ANALYSIS

This chapter presents the time-series plots for the rainfall rate and rain attenuation for C, Ku and Ka-bands. It was noted that 160 rain events occurred in Cyberjaya throughout the year 2016. Figure 4.1 displays an example of a time-series plot for rainfall intensity and rain attenuations on the satellite-Earth link at the C, Ku and Ka-bands. The rain attenuation data were obtained from the MEASAT databases on 20th May 2016. The rainfall intensity measurements and the MEASAT satellite signal attenuation of the C, Ku and Ka-band links are simultaneously represented in Figure 4.1. The peak of the time-series graph represents the highest level of attenuation values, which are concurrent with the highest values of rainfall rates. This was demonstrated by the Ku and Ka-band rain attenuation graphs. The C-band rain attenuation plots indicate that the C-band link is less likely influenced by rain. A good and definite correlation between rain attenuation and the intensity of rainfall can be observed in the time-series plots.

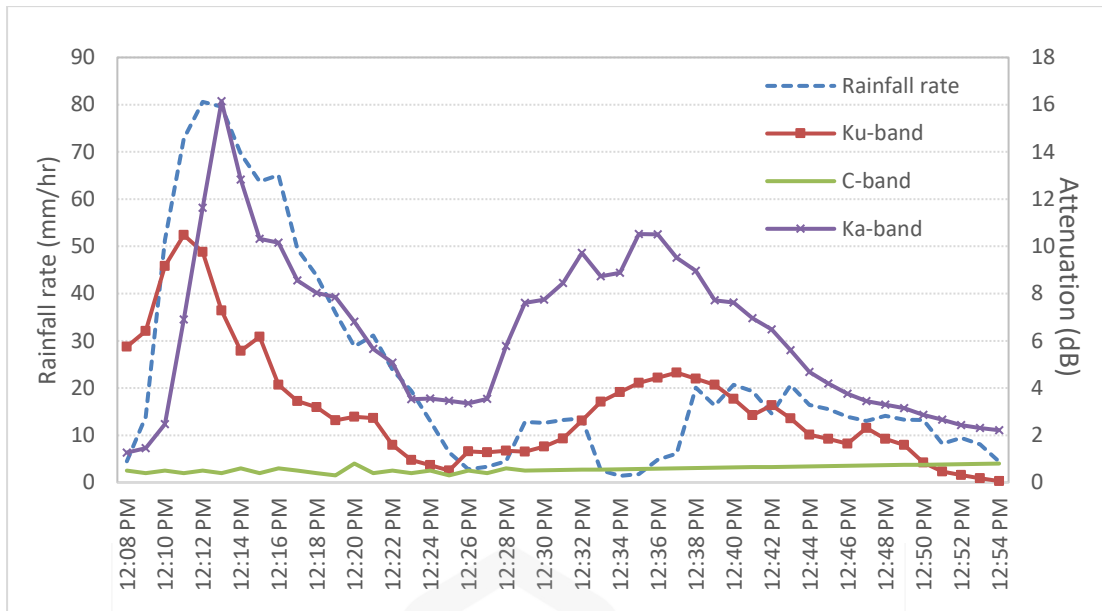


Figure 4.1 Time-Series Plots of Rainfall Intensity and Attenuation during Rainfall on 20th May 2016

Figure 4.2 shows another example of the time-series graph of rainfall rates during rainfall registered on the 6th of February 2016. In the figure, the peak in the time-series graph represents the heavy rainfall rate experienced on that day. The rain occurred during the evening between 3.56 p.m. to 4.16 p.m. The heaviest rainfall rate was detected at 4.12 p.m. where the value almost reached 90 mm/hr. There was light rainfall during the late evening at approximately 7.14 p.m. where the rainfall rate was about 10 mm/hr. According to the rainfall rate recorded in Cyberjaya throughout the year 2016, most of the downpours occurred in the evening. A rainfall intensity of more than 60 mm/hr is classified as convective rain or very heavy rain condition by the Department of Irrigation and Drainage (DID), Malaysia. A rainfall rate of 10 mm/hr and below is considered a light rain condition. The rainfall rates within the range of 11 mm/hr to 30 mm/hr and 30 mm/hr to 60 mm/hr are categorised as moderate and heavy rain events, respectively.

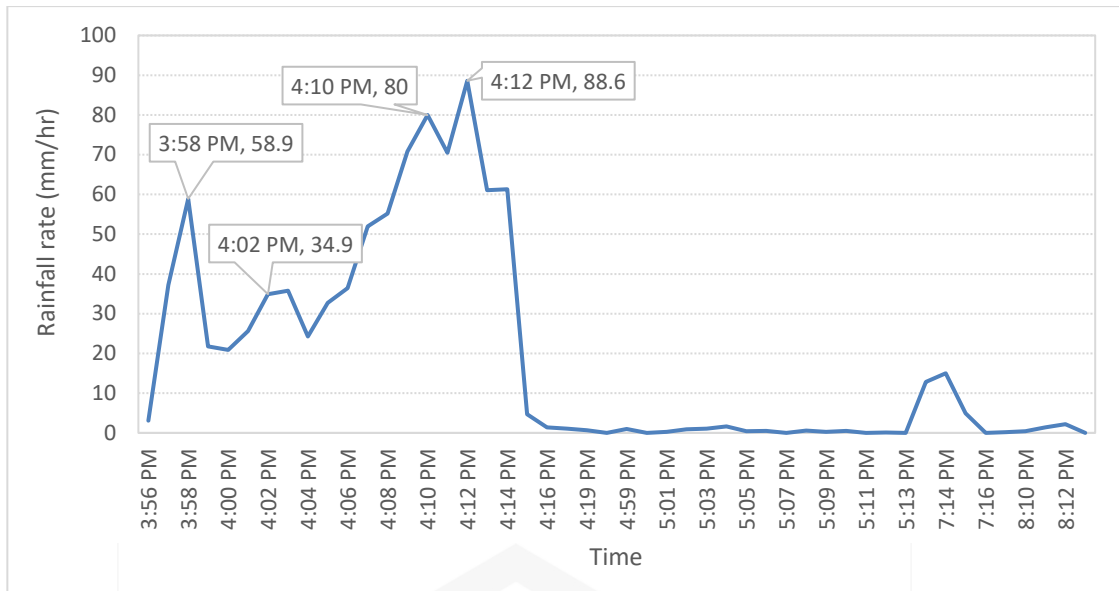


Figure 4.2 Time-Series for Rain Events on 6th February 2016

Figure 4.3 shows the C-band attenuation for the day in a time-series presentation. The peak of attenuation was detected in the morning with an approximate value of 1.2 dB. There was no rain spotted at that time. Attenuation may be due to clouds or scintillation since rain is not the only factor that causes attenuation in the satellite-Earth link. Based on Figure 4.4, the attenuation of the C-band varies from the value of 0.3 dB to 0.6 dB during rainfall. It is shown that rain has a limited effect on the C-band link. It is also evident that the wavelength of C-band frequencies, which is 74.8 mm, can tolerate rain in signal propagation. It is 10 to 50 times larger than a raindrop diameter in tropical regions, varying from 1.2 mm to 7.0 mm. The observation indicates that the C-band link is probably not significantly affected by the rain's particle scattering and absorption. The signal can pass through the rain by enduring relatively small attenuation which can be considered negligible.

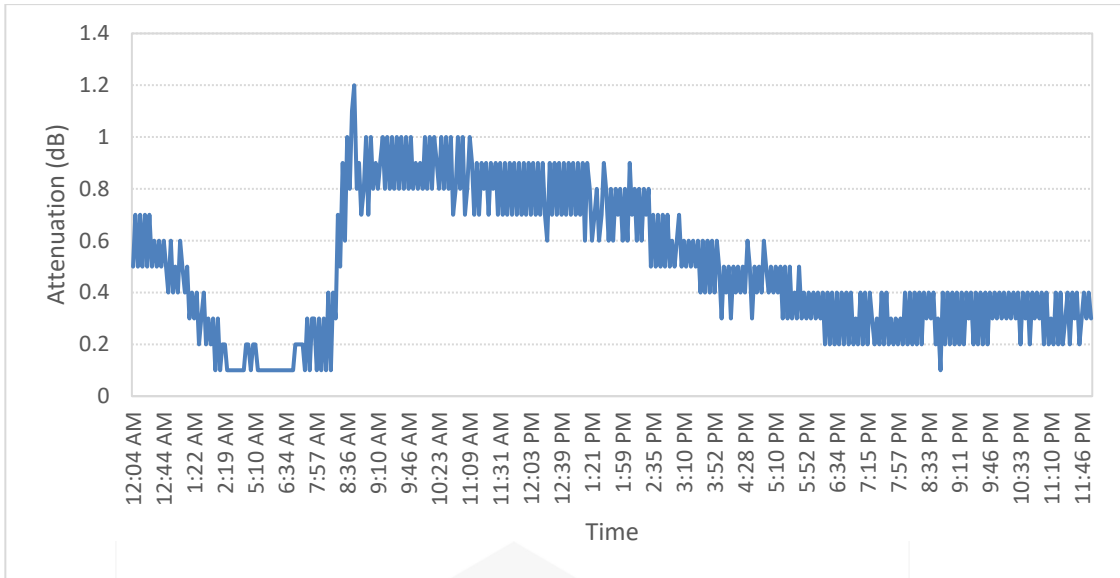


Figure 4.3 Time-Series of C-Band Attenuation for the Entire Day of 6th February 2016

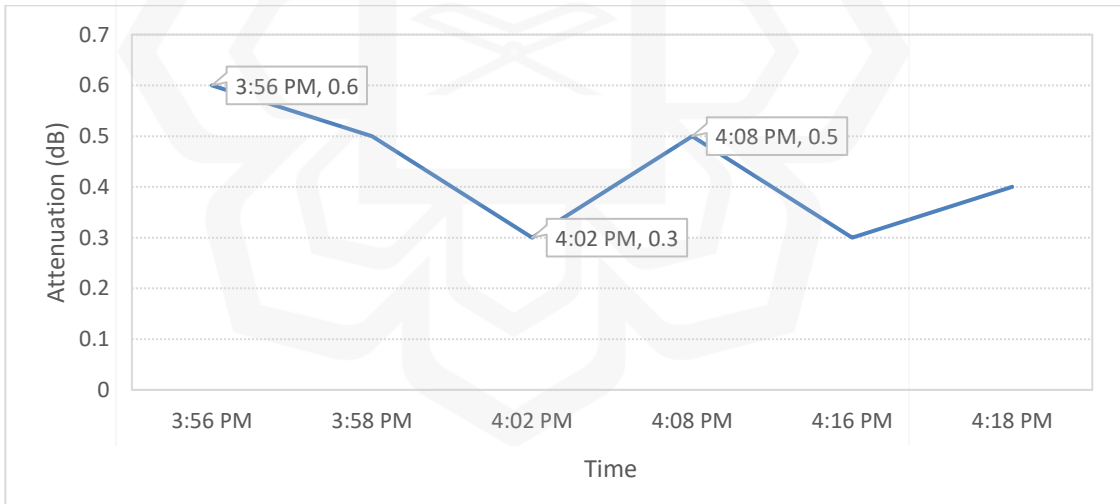


Figure 4.4 Time-Series of C-Band Attenuation during Rainfall on 6th February 2016

Figure 4.5 presents the time series of the Ku-band attenuation for the entire day. The attenuation occurred from 3.55 p.m. to 4.16 p.m. From Figure 4.6, the highest

attenuation level of the Ku-band link was 22.4 dB on the 6th of February 2016. The rainfall rate was registered during the first rainfall rate peak, which was 59 mm/hr, as depicted in Figure 4.2. From Figure 4.6, it can be seen that the values of Ku-band attenuation are 11.06 dB and 13.61 dB when experiencing rainfall intensity of 34.9 mm/hr and 80 mm/hr, respectively. The Ku-band link is considered to be more susceptible to heavy rainfall compared to the C-band link since it has higher rain attenuation values. When the value of 5 dB attenuation was considered, the Ku-band link attenuation began at 3.54 p.m. and disappeared at 4.13 p.m., parallel to rain occurrence at Cyberjaya. It was noted that the attenuation level of the Ku-band varies from 0 to 1 dB during light rainfall or no recorded rainfall. If a 5 dB amount of attenuation is considered a threshold in the Ku-band link system, the link outage should be about 19 minutes. It was also noted that attenuation at the Ku-band link is quite severe during heavy rainfall. The wavelength of the Ku-band signal is 24.5 mm. In areas with heavy rain, rain droplets tend to become larger, leading to more induced attenuation. The Ku-band signal was severely degraded by heavy rain since the signal power was absorbed and the particles were scattered by the rain droplets.

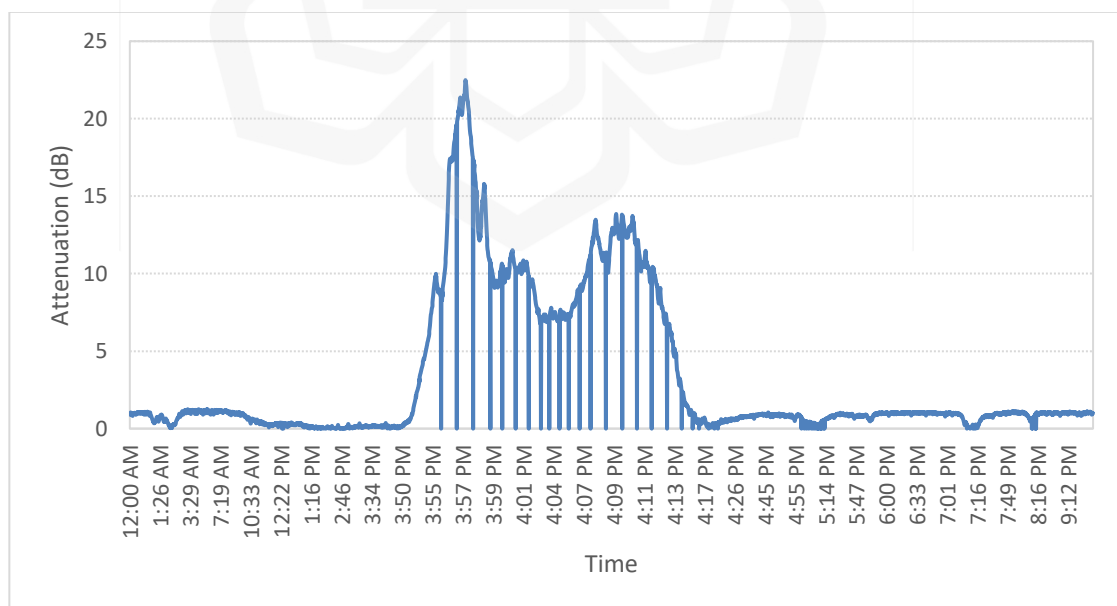


Figure 4.5 Time-Series of Ku-Band Attenuation for One Day (6th February 2016)

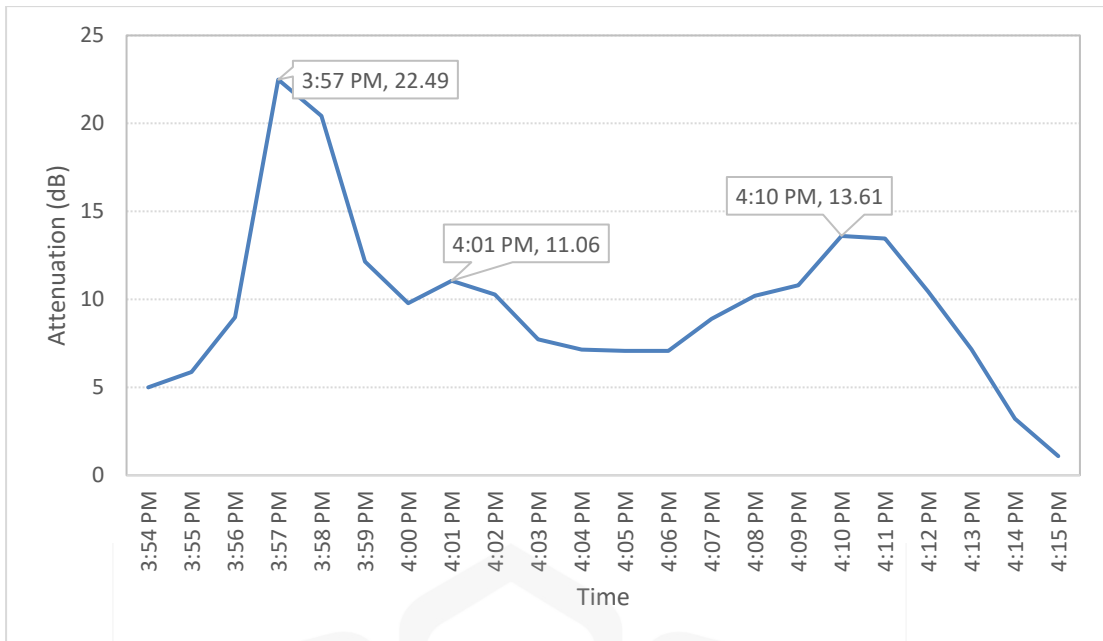


Figure 4.6 Time-Series of Ku-Band Attenuation during Rainfall on 6th February 2016

The peak of the Ka-band rain attenuation time-series graph denotes the highest attenuation value recorded on that day. Figure 4.7 shows the time-series plots of the Ka-band rain attenuation during rainy conditions. From the figure, the highest rain attenuation value noticed on that day was 32 dB. Since the time was unavailable, it was estimated at approximately 20 minutes when the value of 5 dB attenuation was considered as a threshold for the Ka-band link. The attenuation amounts fluctuate from 21 dB to 33 dB during rainfall. This indicates that the Ka-band link suffers a much more severe rain attenuation effect compared to the Ku-band link for the same rain conditions. In contrast to the Ku-band, the Ka-band link also seems to suffer from high attenuation during both light and heavy rainfall. The wavelength of the Ka-band frequency is 14.8 mm, which is 5 times shorter than the C-band and almost half the value of the Ku-band's wavelength. It was noted that the Ka-band frequencies are very sensitive to rain. Their shorter wavelength is close to the raindrop size, allowing the signal strength to be easily absorbed and scattered by the rain droplets.

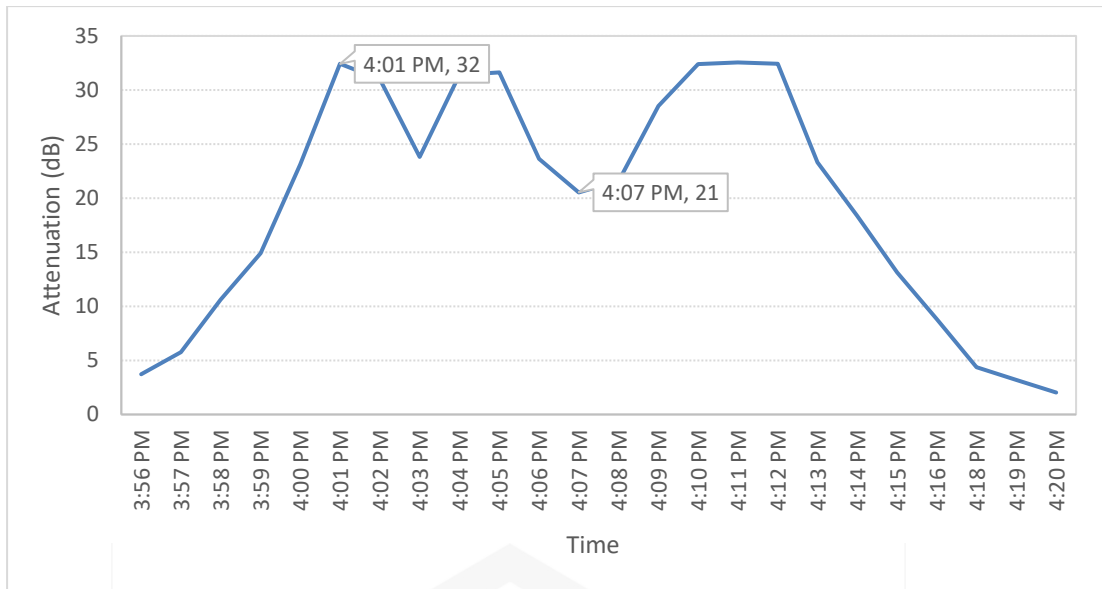


Figure 4.7 Rain Attenuation Time-Series of Ka-band on 6th February 2016

The maximum attenuation value of the Ka-band link was a cause for concern. The high values of Ka-band attenuation encountered saturation. This was capped at 33 dB due to the limitation of the receiver's sensitivity. Higher attenuation values of more than 33 dB (>33dB) cannot be identified. Figure 4.8 presents a different time series where the rain attenuation peak of the Ka-band was capped at about 9 minutes. Figure 4.8 clearly shows that the attenuation value of the Ka-band link was saturated at 33 dB. The actual highest value of attenuation on that day cannot be determined. Extrapolation techniques must be performed to solve this problem. This issue is extensively discussed in Section 4.2.2.5.

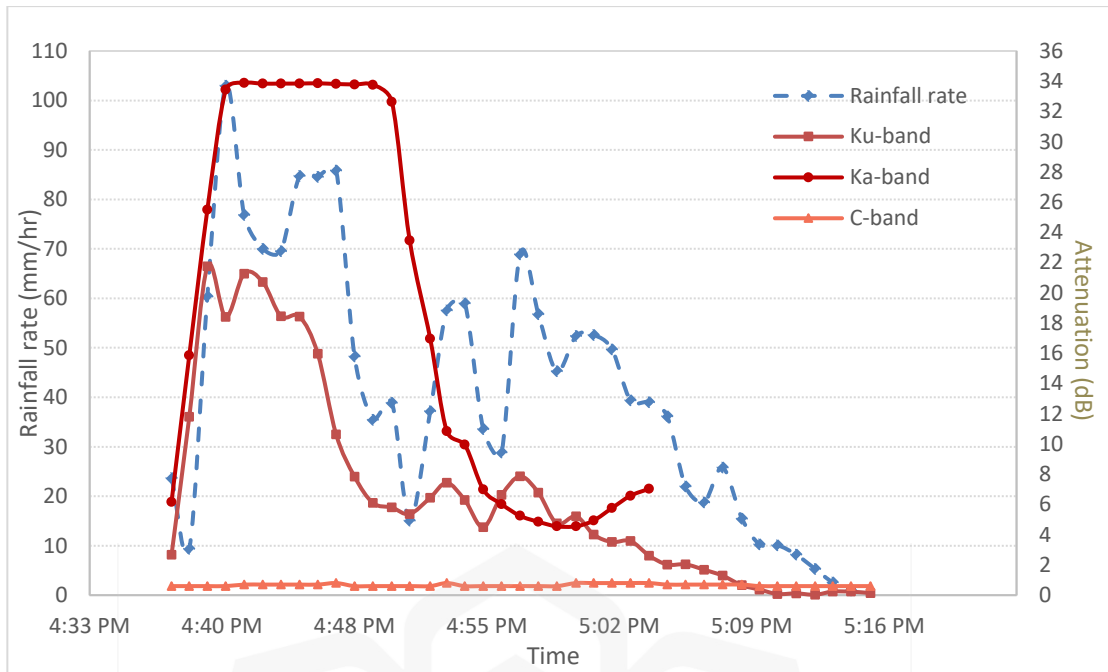


Figure 4.8 Time-Series of Rainfall on 4th January 2016

4.2.1 Monthly Analysis

The various time series of rainfall, as well as rain attenuation, were generated into the monthly CDF for twelve consecutive months.

4.2.1.1 Rainfall Rate

The CDF of rain intensity for the year 2016 was examined. Equatorial regions endure far more precipitation values than what is experienced by temperate regions. High precipitation conditions significantly influence Earth-space propagation,

particularly at frequencies above 10 GHz. This leads to relentless link impairment due to rain. Determining an accurate rain rate at the desired probability is critical in predicting reliable rain attenuation values. The local measured rain rate at 0.01% of time exceedance was applied as an input parameter to predict rain attenuation while adhering to the ITU-R P.618-13 recommendation.

Figure 4.9 presents the monthly CDF of the recorded rainfall rate acquired from the rain sensor. From the figure, November experienced the heaviest rainfall intensity, followed by March, May and January at 0.1% of time exceedance with values of 80 mm/hr, 67 mm/hr, 67 mm/hr and 60 mm/hr, respectively. From the monthly statistics, September experienced the least rainfall rates with a value of only 10 mm/hr at the same time exceedance. At 0.01% of time exceedance, November and March experienced rainfall rates of 122 mm/hr. The month of May underwent 109 mm/hr of rain intensity, and January suffered 106 mm/hr of rain condition. Throughout the year 2016, June experienced the least rainfall rate with a value of 64 mm/hr at the same time exceedance. It was observed that the average, rain intensity is higher in January, March, May and November. The rain distribution in Malaysia is typically affected by two main monsoon seasons; the southwest monsoon and the northeast monsoon. The southwest monsoon occurs in the months of May, June, July, August and September. The northeast monsoon occurs in November, December, January, February and March.

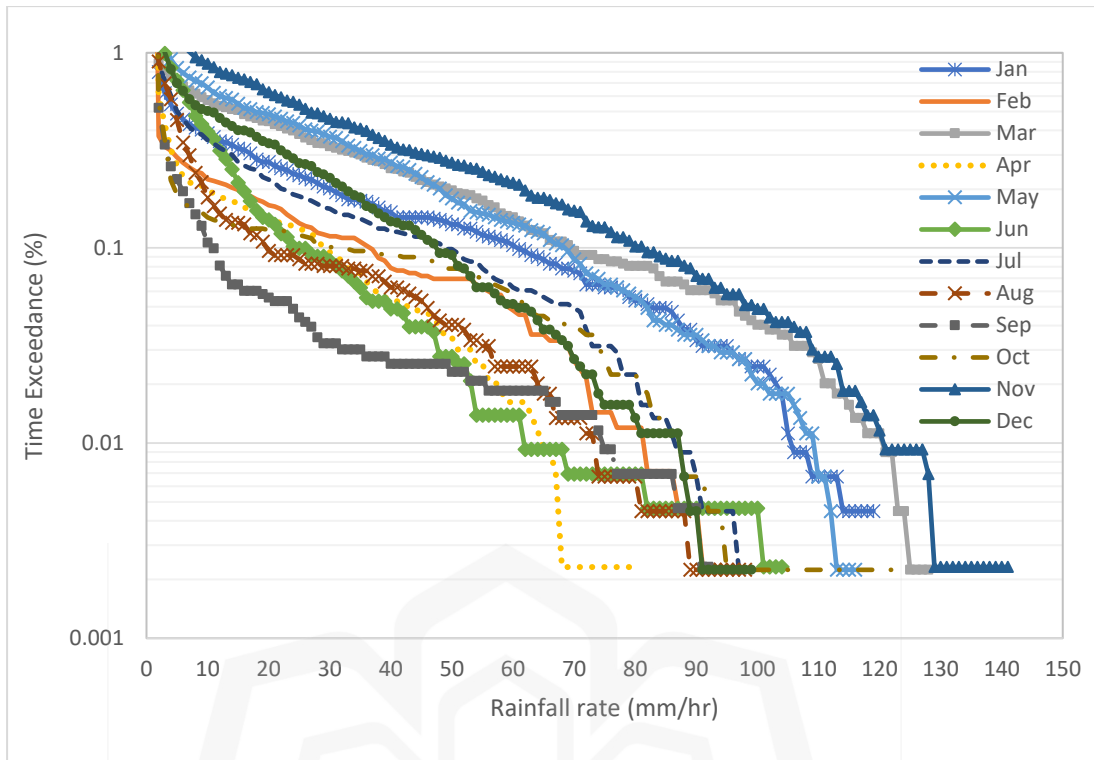


Figure 4.9 Monthly Rain Intensity of Time Exceedance in 2016

Table 4.1 lists the total precipitation values recorded at Cyberjaya with the number of rainy days. The month of November suffered the highest total precipitation followed by May, March and December with values of 276.10 mm, 201.45 mm, 190.19 mm and 131.40 mm, respectively. This is because March, November and December were affected by the northeast monsoon that struck peninsular Malaysia. The heavy rain that occurred in May was influenced by the southwest monsoon. The month of September experienced the lowest rainfall rate with a value of 30.58 mm, and it had the fewest number of rainy days. The maximum rainfall rate and the highest total monthly rainfall were detected in November 2016 with a value of 140 mm/hr and 276.1 mm, respectively. The lowest rainfall rate of that year occurred in April with a value of 78 mm/hr.

Table 4.1 Total Precipitations in Cyberjaya for the Year 2016

Months	Millimetres (mm)	No. of Rainy Days	Maximum rainfall rate (mm/hr)
January	124.60	6	118.00
February	61.05	3	89.80
March	190.19	8	126.70
April	50.41	4	78.30
May	201.45	8	115.40
June	78.26	4	102.60
July	100.83	4	97.00
August	58.97	4	97.40
September	30.58	2	90.60
October	59.27	3	122.80
November	276.10	9	140.20
December	131.40	5	92.80
The year 2016	1363.18	60	140.20

4.2.1.2 Rain Attenuation

The CDFs of C, Ku and Ka-bands rain attenuation from Cyberjaya were plotted for each month. In each frequency band, the monthly CDFs for twelve consecutive months were grouped to present a one-year observation.

4.2.1.2.1 Rain Attenuation at the C-band

Figure 4.10 shows the monthly distribution of C-band attenuation in 2016. The value of attenuation is below 2 dB for all percentages of time exceedance. The highest rain attenuations measured at time exceedance of 0.01% and 0.001% are 1.2 dB and 1.6 dB, respectively. These instances were detected in January 2016. The lowest rain attenuations at time exceedance of 0.01% and 0.001% were recorded in September 2016 with 0.1 dB and 0.3 dB, respectively. The C-band link impairment due to rain was insignificant and therefore the resulting attenuation can be considered negligible. Table 4.2 presents the rainfall rate at 0.01% time exceedance for each month for the C-band rain attenuation.

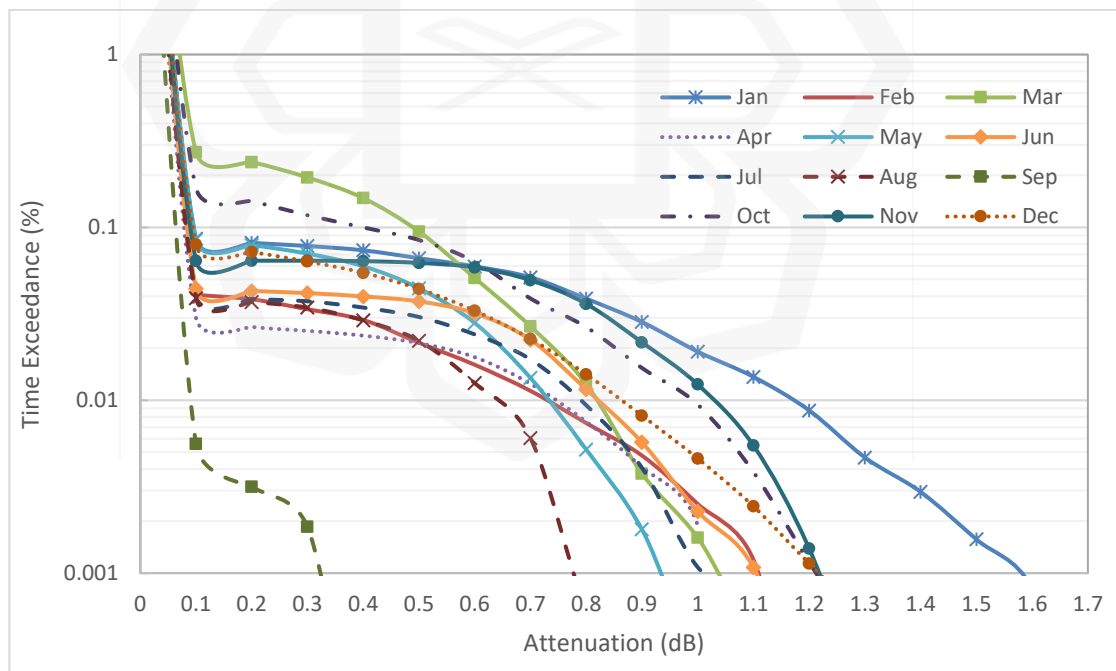


Figure 4.10 Monthly Distribution of the C-band Rain Attenuation at Cyberjaya in 2016

Table 4.2 Rainfall Rate at 0.01% of Time Exceedance for C-band Rain Attenuation at 0.1%, 0.3%, 0.01% and 0.03% of Time Exceedance

Month	Rainfall rate, R _{0.01%} (mm/hr)	Attenuation (dB)			
		0.01 %	0.03 %	0.1 %	0.3 %
Jan	105	1.2	0.9	0.1	0.1
Feb	81	0.7	0.4	0.1	0.1
Mar	118	0.8	0.7	0.5	0.1
Apr	64	0.7	0.2	0.1	0.1
May	109	0.7	0.6	0.1	0.1
June	67	0.8	0.6	0.1	0.1
Jul	86	0.8	0.4	0.1	0.1
Aug	73	0.6	0.4	0.1	0.1
Sep	75	0.1	0.1	0.1	0.1
Oct	84	1	0.8	0.4	0.1
Nov	120	1.1	0.8	0.1	0.1
Dec	82	0.8	0.6	0.1	0.1

4.2.1.2.2 Rain Attenuation at the Ku-band

The monthly statistics for Malaysia were compiled accordingly. From the monthly CDF graph of rain attenuation for the Ku-band, as shown in Figure 4.11, the month of May experienced the highest attenuation values of 18 dB, 42 dB and 46 dB at 0.1%, 0.01% and 0.001% of the time exceedance, respectively. May is one of the months with a higher value of total rainfall rate and the number of rainy days in the year 2016. September has the lowest attenuation values of 1 dB, 10 dB and 14 dB at 0.1%, 0.01% and 0.001% of time exceedance, respectively. This is because September experienced the least rainy days throughout the year. Even though December is one of the months which experienced high total rainfall in the year, it did not have the highest value of Ku-

band rain attenuation at any percentage of time exceedance due to the low amount of rainfall intensity at 0.1% and 0.01% of time exceedance. The maximum rainfall rate detected in that month was also small, only 92 mm/hr. The results demonstrate the principle that attenuation differs from the variation of rainfall characteristics, which includes the intensity, duration, total amount and frequency of rainfall.

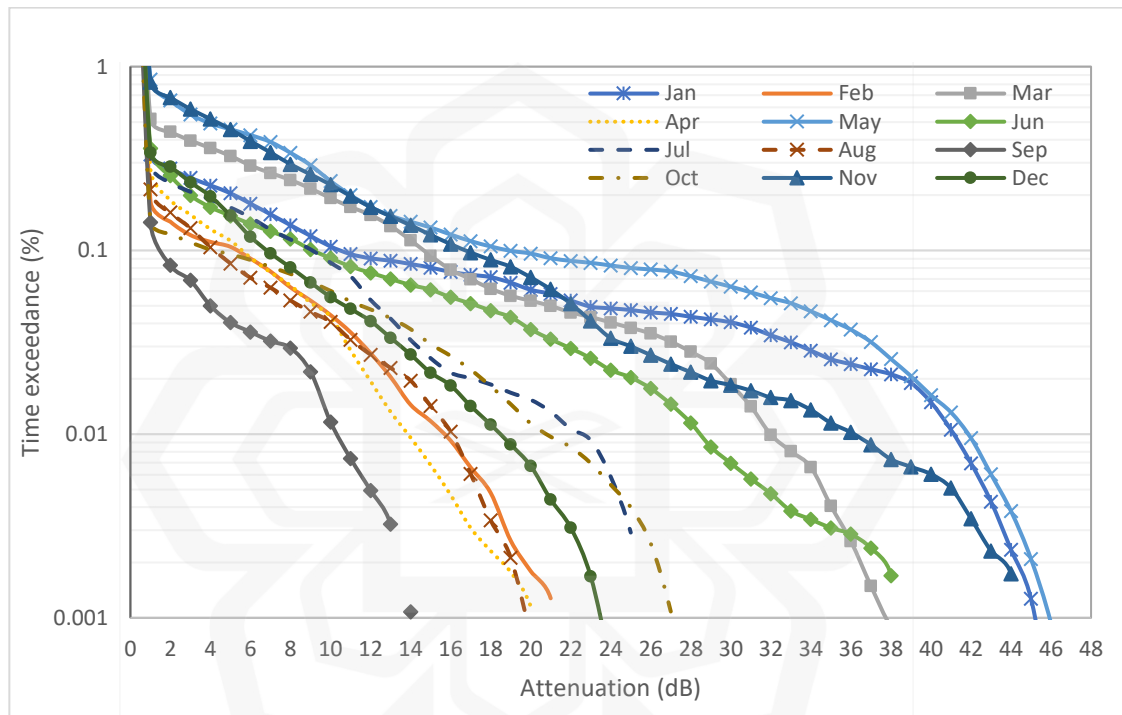


Figure 4.11 Monthly Distribution of the Ku-band Rain Attenuation at Cyberjaya in 2016

Table 4.3 presents the monthly rainfall rate at 0.01% of time exceedance for rain attenuation of the Ku-band at 0.1%, 0.3%, 0.01% and 0.03% of time exceedance. From the table, it can be seen that attenuation becomes higher than the value of 30 dB when the rainfall rate increases, approaching a value of more than 100 mm/hr. It was noted that attenuation becomes higher as the rainfall rate increases, but the severity of rain

attenuation is not limited to the rain attenuation value at 0.01% of time exceedance, $R_{0.01}$. Table 4.3 displays the Ku-band rain attenuation at 0.1%, 0.3%, 0.01% and 0.03% of time exceedance with the rainfall rate at 0.01% of time exceedance. As shown in Table 4.3, only the month of September experienced small rain attenuation of less than 10 dB at 0.1%, 0.3%, 0.01% and 0.03% of time exceedance. The rest of the months experienced a considerably high value of rain attenuation which is more than 10 dB at 0.01% and 0.03% of time exceedance.

Table 4.3 Rainfall Rate at 0.01% of Time Exceedance with Ku-band Rain Attenuation at 0.1%, 0.3%, 0.01% and 0.03% of Time Exceedance

Month	Rainfall rate, $R_{0.01\%}$ (mm/hr)	Attenuation (dB)			
		0.01 %	0.03 %	0.1 %	0.3 %
Jan	105	41	33	10	1
Feb	81	15	12	5	1
Mar	118	32	27	14	5
Apr	64	14	11	5	1
May	109	42	37	18	8
Jun	67	28	21	9	1
Jul	86	22	14	9	1
Aug	73	16	11	4	1
Sep	75	10	8	2	1
Oct	84	20	14	4	1
Nov	120	36	25	17	7
Dec	82	18	13	6	1

Figure 4.12 presents a bar chart of rain fades at the selected thresholds of 5, 10, 15, 20, 25, 30, 35 and 40 dB monthly exceedance in the year 2016. From the figure, the

attenuation level of 5 dB and 10 dB were constantly detected for each month. This indicates that 5 dB and 10 dB attenuation were not influenced by the monthly variation. The 40 dB level was detected in January, May and November since those months endured heavy rainfall. Severe fading can be seen in May. Each year, the monsoon winds hit Peninsular Malaysia, particularly Cyberjaya, in January, March and May as well as in November and December since heavy rainfall was detected during that period. The attenuation amounts in these months were the highest compared to the other months.

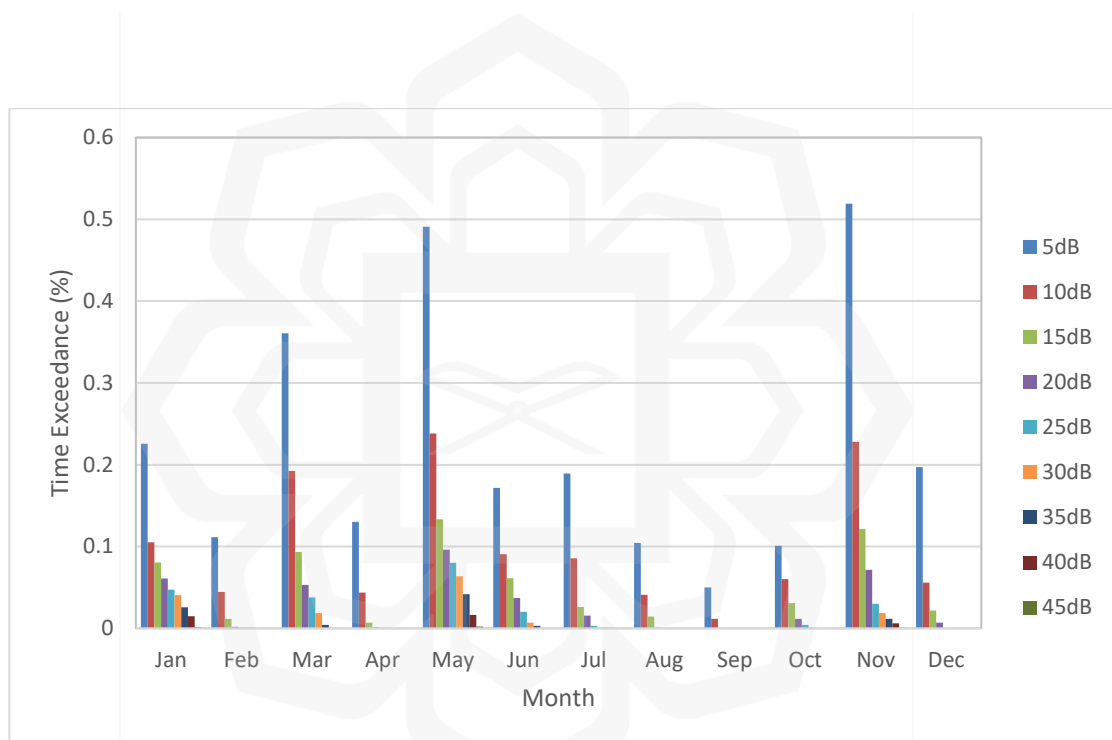


Figure 4.12 Histogram of Certain Attenuation Thresholds and Monthly Time Exceedance

The lowest point of selected attenuation values over a year is extensively presented to highlight the severity of rain attenuation suffered by tropical regions. The results in Figure 4.13 represent the probability of exceeding a specific threshold of a particular attenuation level statistics. The probability of the highest attenuation level

was detected in May. The presence of the ‘worst month’ of attenuation was verified by the probability that the attenuation level will exceed 45 dB. The month of May experienced the highest probability of high attenuation levels. The attenuation level with the lowest value was observed in September. The month of September had very limited rain-induced attenuation where the probability of attenuation levels exceeding 5 dB and 10 dB are 0.05% and 0.01%, respectively.

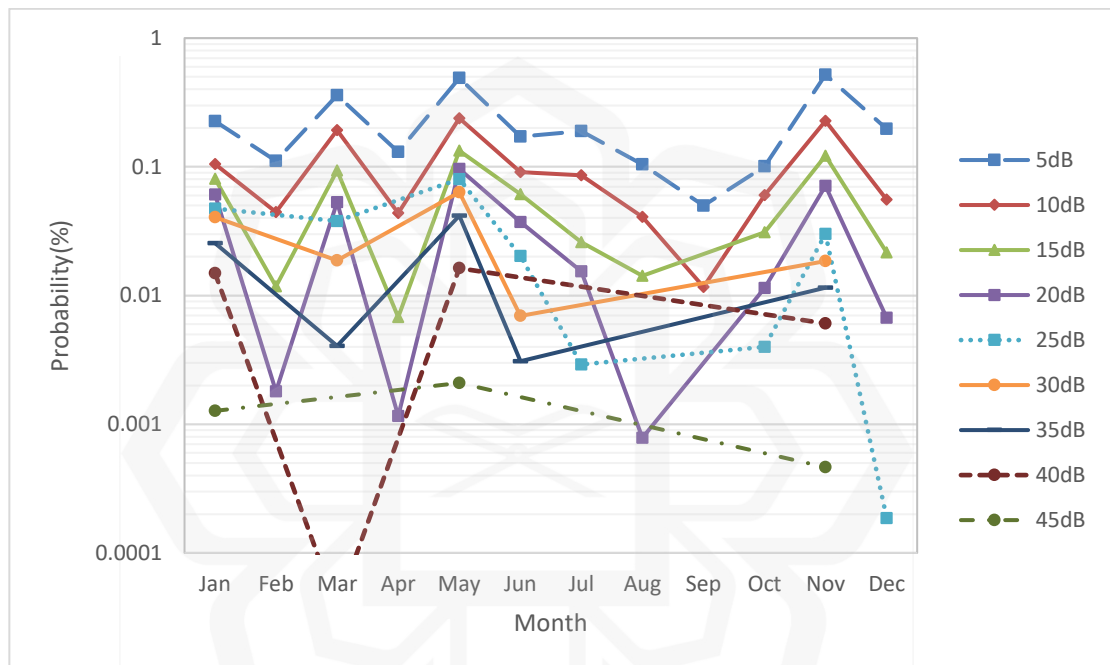


Figure 4.13 The Probability of Specific Rain Attenuation Thresholds at the Ku-band Link

4.2.1.2.3 Rain Attenuation at the Ka-band

The recorded attenuation data of the Ka-band were compiled on a monthly basis. Figure 4.14 portrays the CDF for the measured beacon signal of the Ka-band for each month. January, May and March experienced the highest rain attenuation values for the time

exceedance of 0.1% (which is 32 dB), followed by April with an attenuation value of 30 dB. These months experienced higher rainfall intensity. However, the rain attenuation for time exceedance of 0.01% could not be obtained since the graph shows saturation at the value of 33 dB. September experienced the lowest attenuation value for the time exceedance of 0.1% and 0.01% with attenuation values of 12 dB and 22 dB, respectively. Table 4.4 presents the rain attenuation for the Ka-band at 0.1%, 0.3%, 0.01% and 0.03% of time exceedance with a rainfall rate of 0.01% of time exceedance for each month. The NA value in the table refers to “Not Available” since no data was available at that percentage of time exceedance.

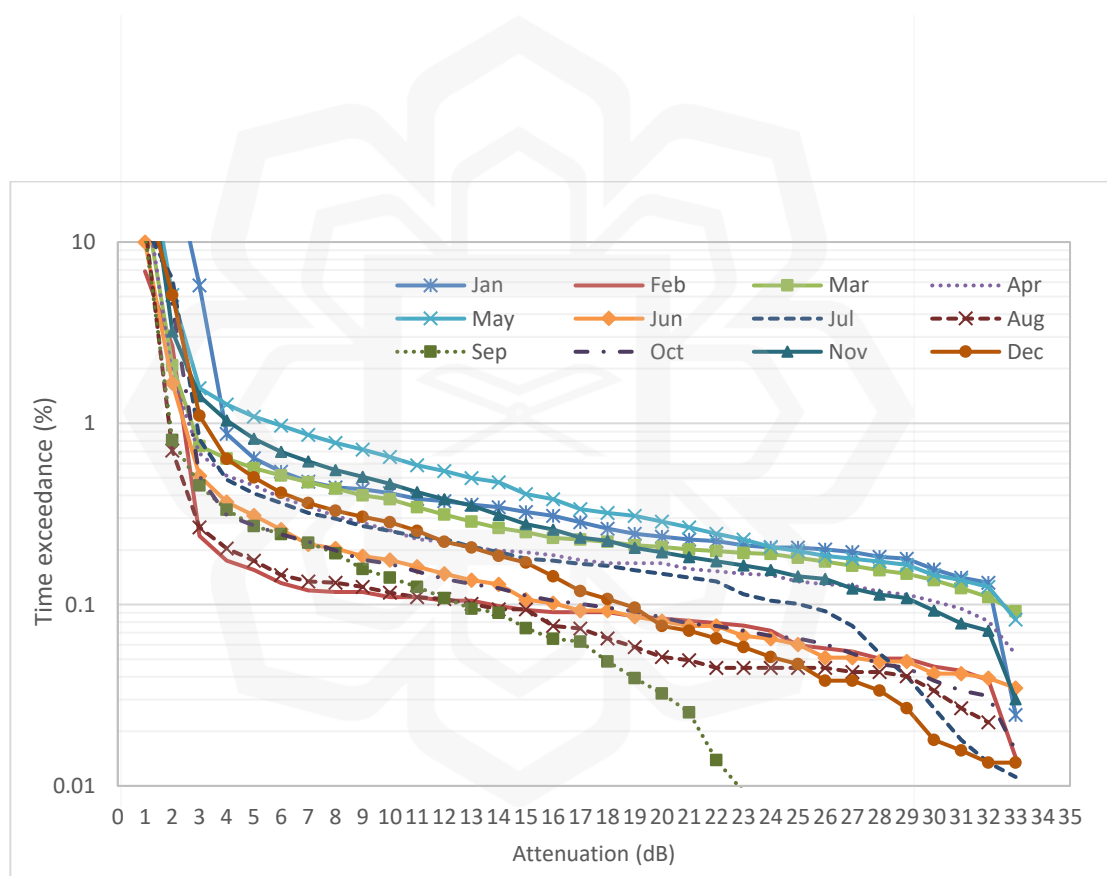


Figure 4.14 Monthly Distribution of Rain Attenuation of Ka-band at Cyberjaya in 2016

Table 4.4 Rainfall Rate at 0.01% of Time Exceedance with Ka-band Rain Attenuation at 0.1%, 0.3%, 0.01% and 0.03% of Time Exceedance

Month	Rainfall rate, R _{0.01%} (mm/hr)	Attenuation (dB)			
		0.01 %	0.03 %	0.1 %	0.3 %
Jan	105	NA	33	32	16
Feb	81	NA	29	14	3
Mar	118	NA	NA	32	12
Apr	64	NA	NA	30	8
May	109	NA	NA	32	19
Jun	67	NA	NA	16	6
Jul	86	NA	31	25	8
Aug	73	NA	31	13	3
Sep	75	22	20	12	4
Oct	84	NA	33	16	4
Nov	120	NA	33	29	14
Dec	82	NA	29	19	9

Figure 4.15 represents a bar chart of rain fades at the selected thresholds of 5, 10, 20, 25, 30 and 33 dB of monthly exceedance for each month, from January 2016 to December 2016. The attenuation levels of 5, 10, 15 and 20 dB can be noticed for each month. All months experienced attenuation levels of up to 25 dB and 30 dB, except for the month of September. From the figure, May is the dominant month that endured the most severe fading in the year 2016. September had fewer detected fading instances throughout the year.

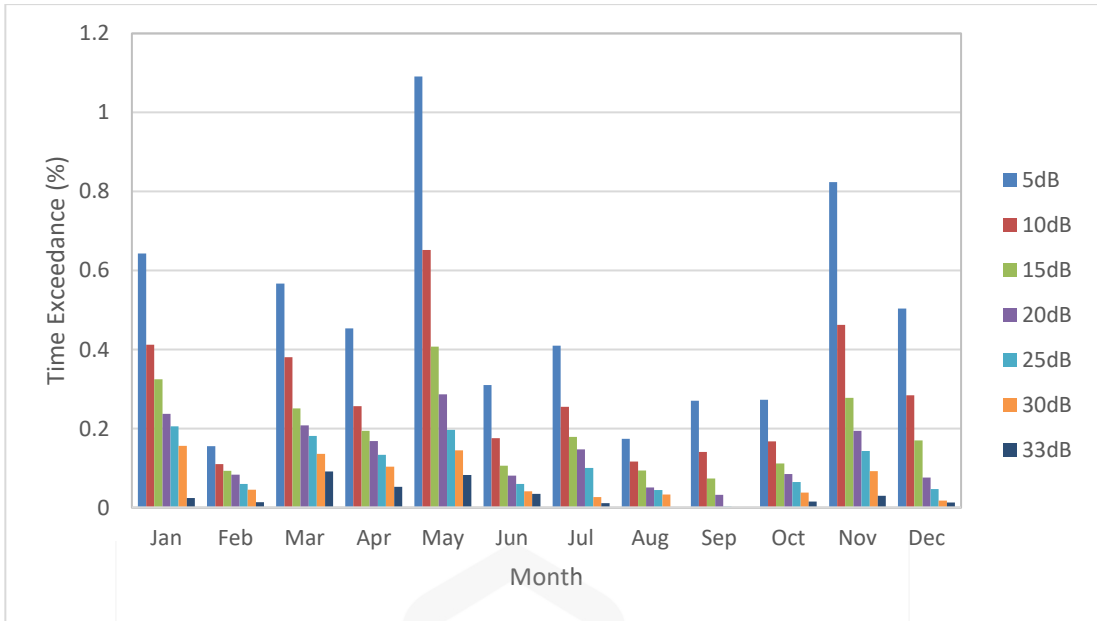


Figure 4.15 Histogram of A Specific Threshold of Attenuation is Exceeded Monthly at the Ka-band Link

It was noted in Figure 4.16 that the probability of the highest attenuation levels was detected in March. March experienced the highest probability of attenuation amounts of 33 dB and was denoted as the ‘worst month’ for Ka-band rain attenuation. The attenuation level with the lowest value was apparent in September. September can be described as the ‘best month’ since the attenuation level at 30 dB was not detected.

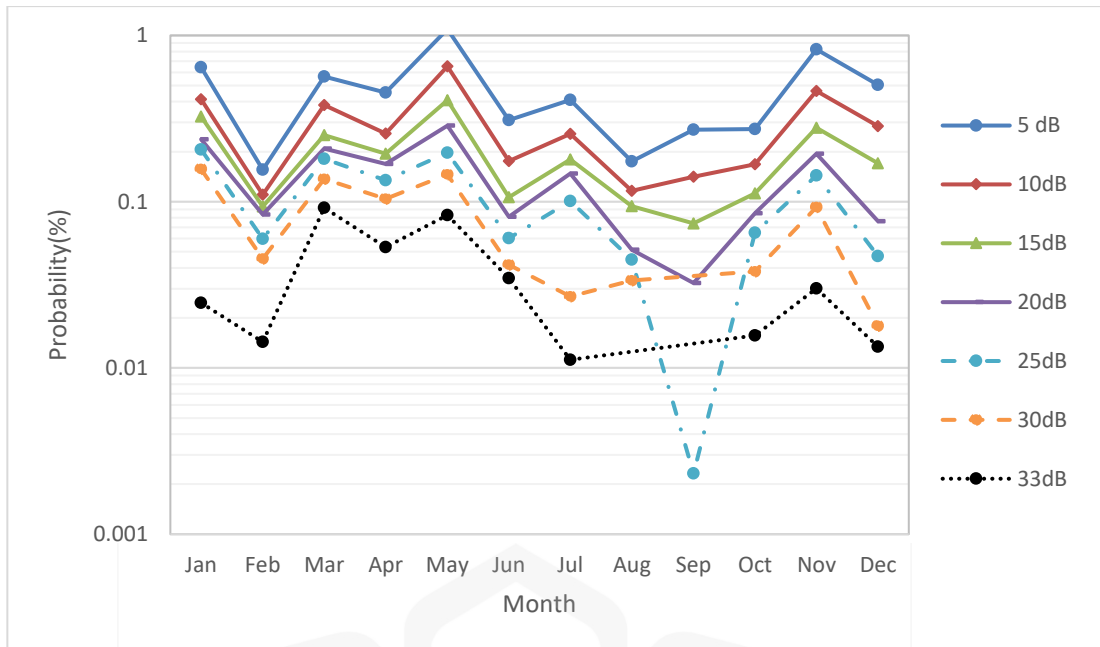


Figure 4.16 Probability of Specific Thresholds of Rain Attenuation Exceedance at the Ka-band Link

4.2.2 Annual Analysis

The monthly CDF for twelve consecutive months of rainfall rate and rain attenuation were then compiled to produce an annual CDF. The annual CDF represents one-year observation data.

4.2.2.1 Rainfall Rate

The annual CDF of rainfall rate for the year 2016 was analysed. Figure 4.17 presents the CDF for the year 2016. For annual analysis, 0.1% and 0.01% of time exceedance of

rainfall rates at Cyberjaya was 50 mm/hr and 103 mm/hr, respectively. The typical average annual precipitation at Cyberjaya is 1493.0 mm, based on weather reports of rain collected from 2005 to 2015 at Sultan Abdul Aziz Shah-Subang, which is 26 kilometres from Cyberjaya (Timeanddate, 2022). The total rainfall amount observed in 2016 was only 1363.18 mm. The rainfall amount in the year 2016 can be considered slightly low compared to other years. It was recorded that only 60 out of 365 days experienced rain in the year 2016. Compared to other regions in tropical areas, the rainfall rate at 0.01 % of time exceedance recorded in Singapore and Thailand was 106 mm/hr and 100 mm/hr respectively is very close to the one recorded in Cyberjaya (Yeo et al.,2014; Singh & Saleh, 2021).

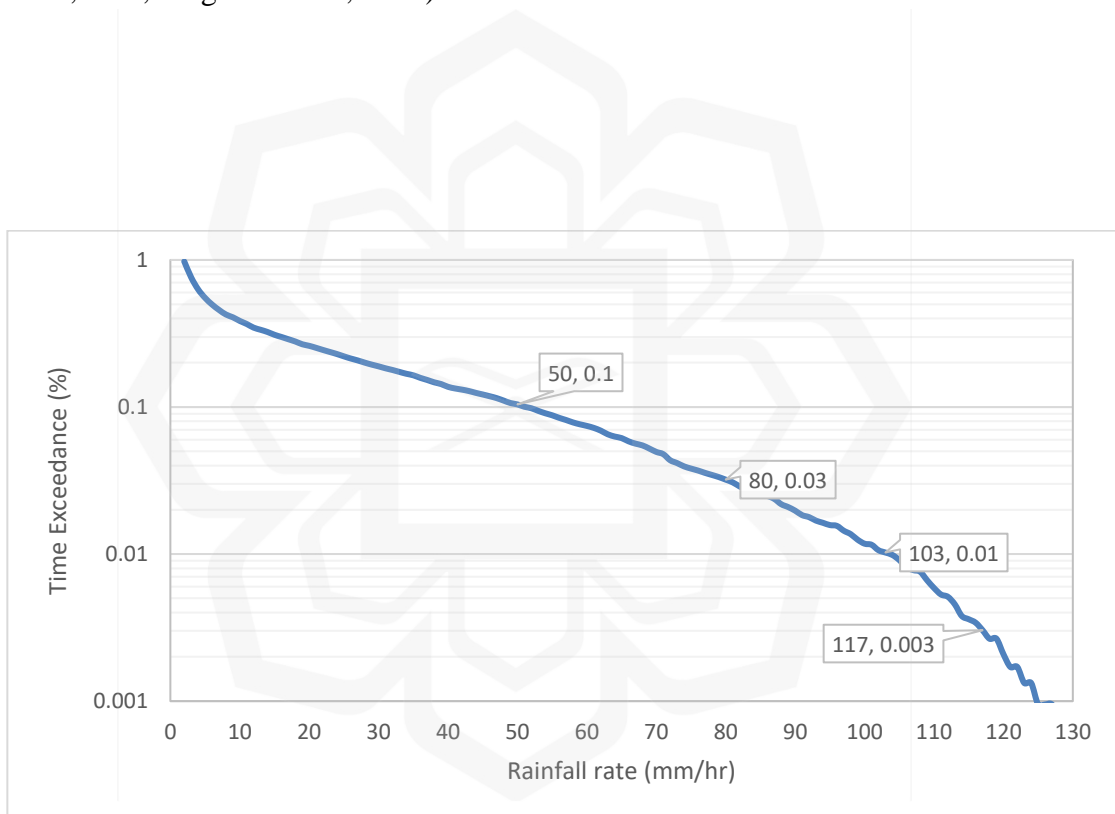


Figure 4.17 Annual CDF of Rain Intensity for 2016 in Cyberjaya

4.2.2.2 Rain Attenuation at the C-band

The annual CDF of rain attenuation for the C-band in the year 2016 is plotted in Figure 4.18. The annual rain attenuations at time exceedance of 0.01% and 0.001% are 0.8 dB and 1.2 dB, respectively. The attenuation value of 1.2 dB can be considered low attenuation in tropical regions.

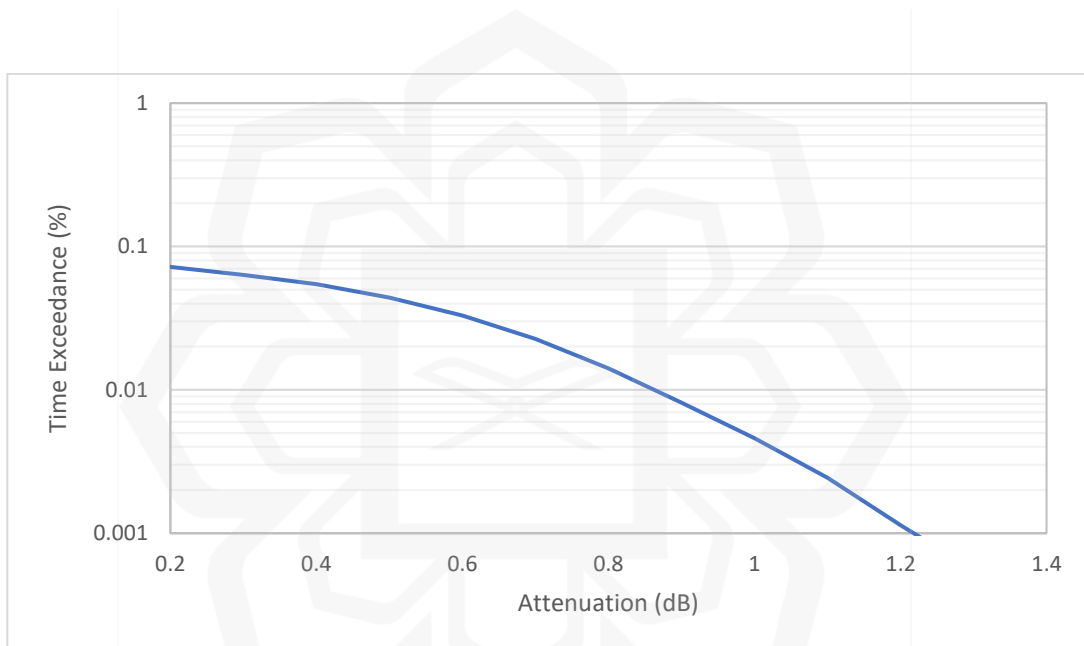


Figure 4.18 Annual CDF of C-band Rain Attenuation for 2016 in Cyberjaya

The measured C-band rain attenuation and rainfall rate in Cyberjaya were correlated in a graph by equalising the time exceedance of rainfall rate and rain attenuation. The correlation graph is shown in Figure 4.19. It was noted that the C-band rain attenuation begins to increase when the rainfall rate is higher than 60 mm/hr. Attenuations are considerably low (less than 1 dB) for rainfall rates below 112 mm/hr.

As rainfall rates approach 123 mm/hr, the C-band link experiences a value of 1.2 dB rain attenuation.

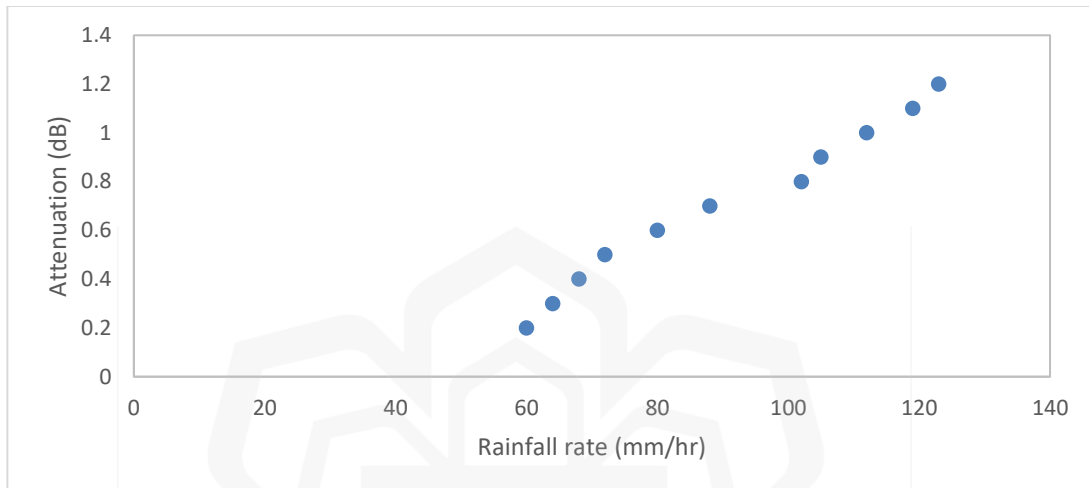


Figure 4.19 C-band Rain Attenuation Correlated to Rainfall Rate in Cyberjaya’s Rain Gauge

From the annual CDF, the rain attenuation at 0.01%, 0.03%, 0.1% and 0.3% of time exceedance means that the rain-induced attenuation would exceed 0.01%, 0.03%, 0.1% and 0.3% of the time for that particular year. In the year 2016, the duration is about 52.6 minutes, 157.7 minutes, 525.6 minutes and 1576.8 minutes, respectively. From Table 4.5, it was noticed that 0.6 dB and 0.8 dB of losses of C-band occurred at 0.03% and 0.01% of time exceedance, accordingly.

Table 4.5 Annual Rainfall Rate and Annual Rain Attenuation of the C-band at 0.1%, 0.3%, 0.01% and 0.03% of Time Exceedance

Annual CDF	Time Exceedance (%)			
	0.3	0.1	0.03	0.01
Rainfall rate (mm/hr)	13	50	80	103
C-band (dB)	NA	NA	0.6	0.8

4.2.2.3 Rain Attenuation at the Ku-band

From the annual CDF of the Ku-band, the Ku-band attenuation is 8 dB at a time exceedance of 0.1%, as shown in Figure 4.20. The annual rain attenuation values of the Ku-band at 0.01% and 0.001% of unavailability links were 30 dB and 41 dB, respectively. The attenuation amount of 30 dB detected in the Ku-band link was higher than at the C-band link. It strengthens the literature that rain attenuation in tropical regions is acute at a frequency above 10 GHz.

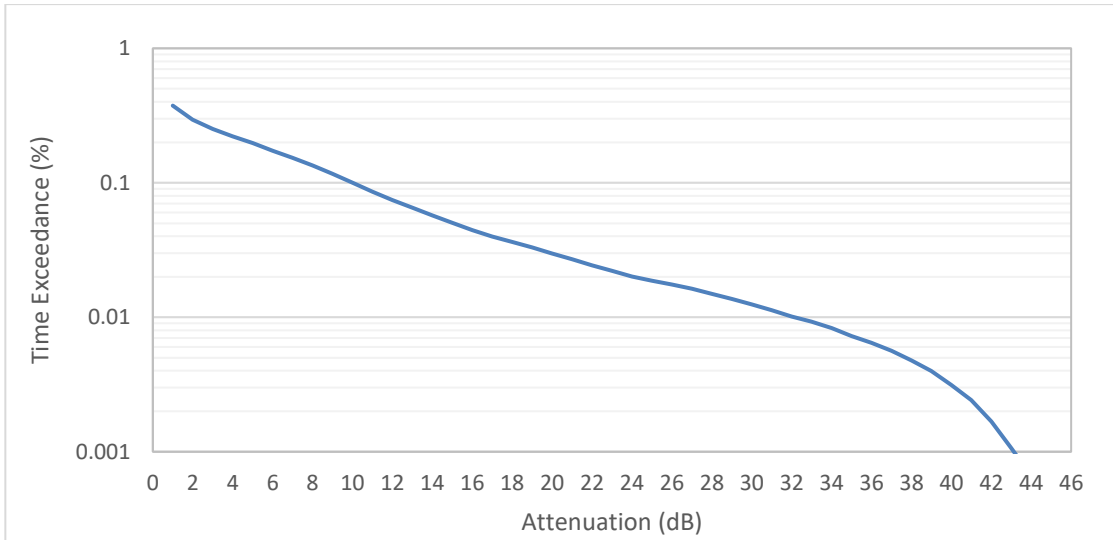


Figure 4.20 Annual CDF of Ku-band Rain Attenuation for 2016 in Cyberjaya

Table 4.6 lists the annual rainfall rate and annual rain attenuation of the Ku-band at 0.1%, 0.3%, 0.01% and 0.03% of time exceedance. From Table 4.6, it can be seen that the Ku-band link experienced attenuation values of 8 dB, 17 dB and 30 dB, occurring at 0.1%, 0.03% and 0.01% of time exceedance, respectively.

Table 4.6 Annual Rainfall Rate and Annual Rain Attenuation of the Ku-band at 0.1%, 0.3%, 0.01% and 0.03% of Time Exceedance

Annual CDF	Time Exceedance (%)			
	0.3	0.1	0.03	0.01
Rainfall rate (mm/hr)	13	50	80	103
Ku-band (dB)	0	8	17	30

Figure 4.21 displays the rain attenuation of the Ku-band which increases almost proportionally with the rainfall rate. It can be seen that rain attenuation became higher as the rainfall rate intensified. Attenuation can reach up to 43 dB at a rainfall rate of more than 120 mm/hr.

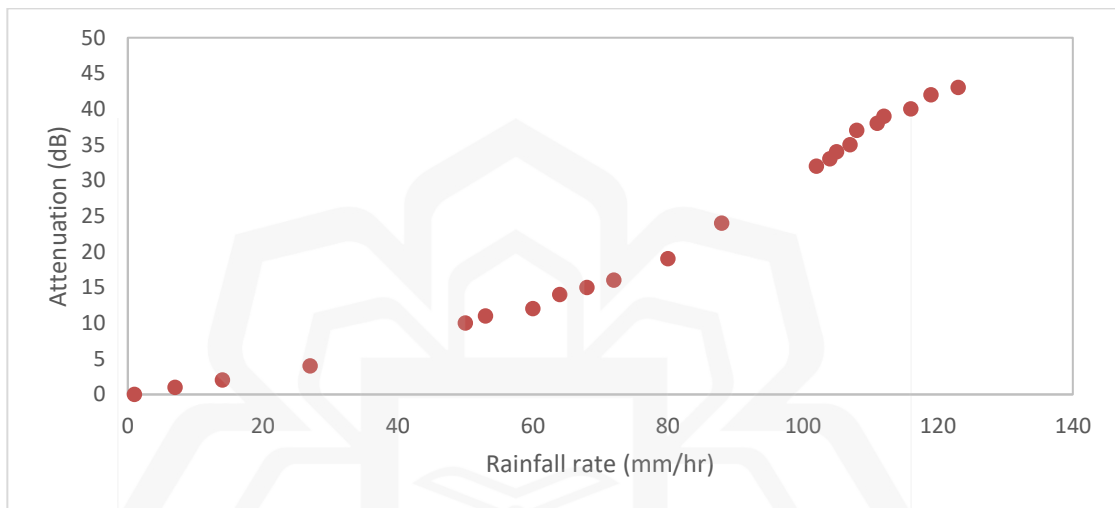


Figure 4.21 Ku-band Rain Attenuation Correlated to Rainfall Rate in Cyberjaya's Rain Gauge

Yaacop (2016) modified the ITU-R model with the implementation of local parameters (the rain height and specific coefficients) which offered a similar rain attenuation value as the current study. According to Yaacop (2016), the rain attenuation values for the Ku-band at 99.9% and 99.99% of link availability are 12.58 dB and 24.16 dB, respectively.

4.2.2.4 Rain Attenuation at the Ka-band

The annual CDF of Ka-band rain attenuation is portrayed in Figure 4.22. The cumulated rain-induced attenuation for one year at 0.1% of time exceedance was 25 dB. No attenuation was captured for 0.01% and 0.001% of time exceedance. The graph indicates that the data-saturated at 0.05% of time exceedance when rain attenuation values exceeded 33 dB.

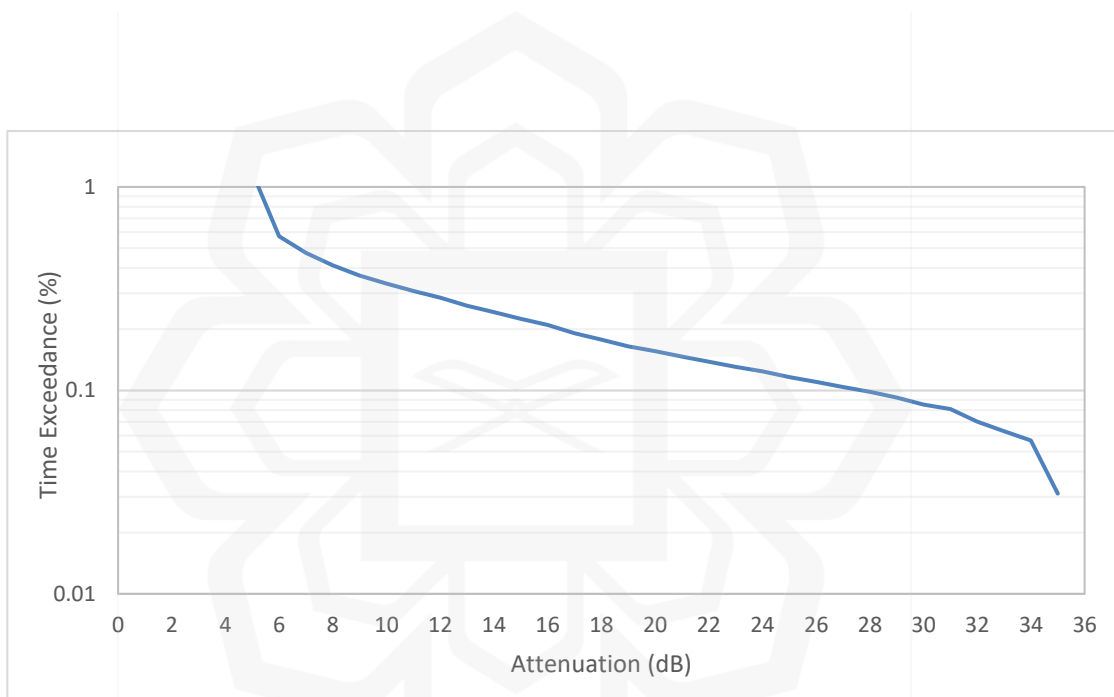


Figure 4.22 Annual CDF of Ka-band Rain Attenuation for 2016 in Cyberjaya

Figure 4.23 demonstrates how the Ka-band rain attenuation correlates to the rainfall rate. Ka-band rain attenuation uniformly increases with the rainfall rate. It was noted that rain attenuation consistently increases as the rainfall rate intensifies. Rain attenuation can only be correlated to the rainfall rate of 68 mm/hr due to the receiver's level saturation. The rain attenuation of the Ka-band at a higher rainfall rate value can

be extrapolated by using the trendline technique. Table 4.7 lists the attenuation value of the Ka-band at 0.1%, 0.3%, 0.01% and 0.03% of time exceedance.

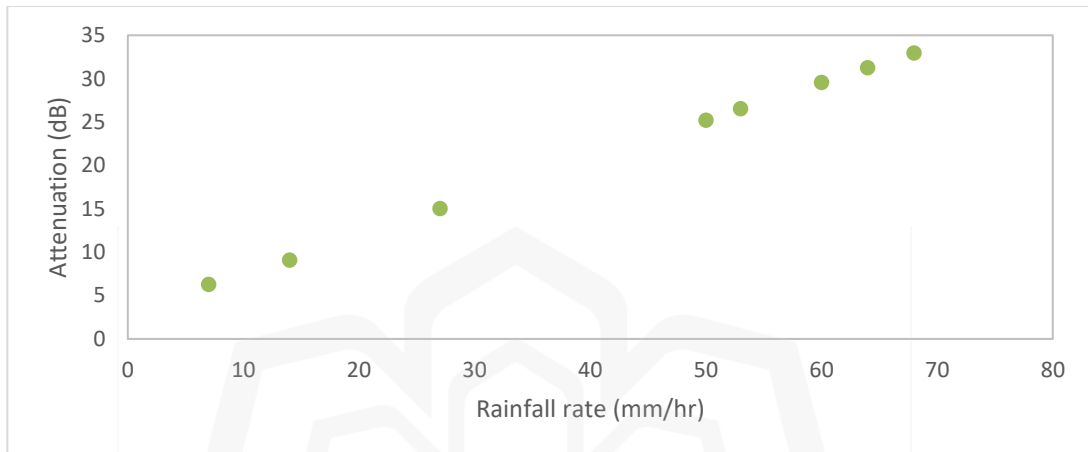


Figure 4.23 Ka-band Rain Attenuation Correlated to Rainfall Rate in Cyberjaya's Rain Gauge

Table 4.7 Annual Rainfall Rate and Annual Rain Attenuation of Ka-band at 0.1%, 0.3%, 0.01% and 0.03% of Time Exceedance

Annual CDF	Time Exceedance (%)			
	0.3	0.1	0.03	0.01
Rainfall rate (mm/hr)	13	50	80	103
Ka-band (dB)	9	25	NA	NA

4.2.2.5 Extrapolation of Rain Attenuation at the Ka-band

All extrapolation models performed in Chapter Three were plotted in Figures 4.24-4.28. The extrapolation results were compared with the measured value of the annual Ka-band rain attenuation.

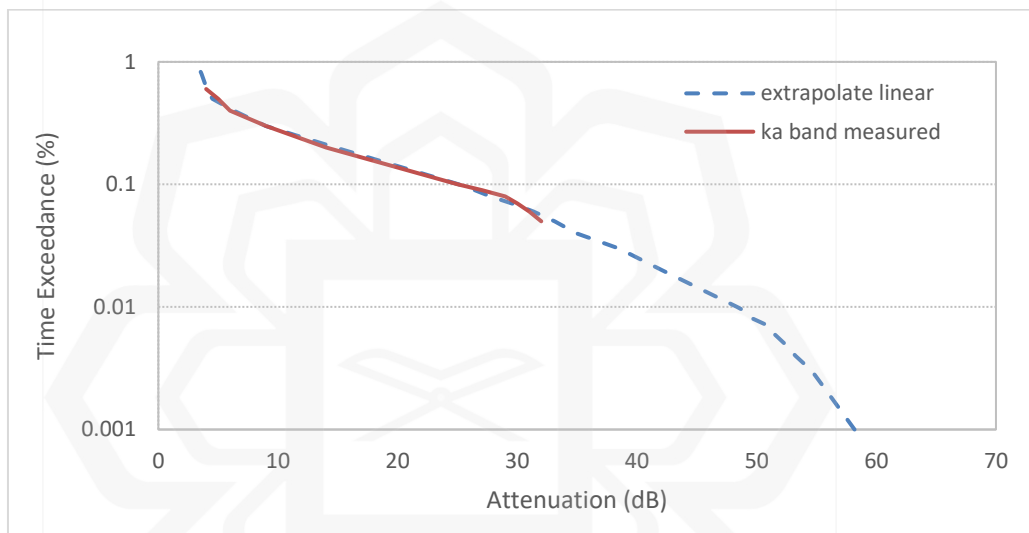


Figure 4.24 Measured Plotted Values with Linear Extrapolation Model

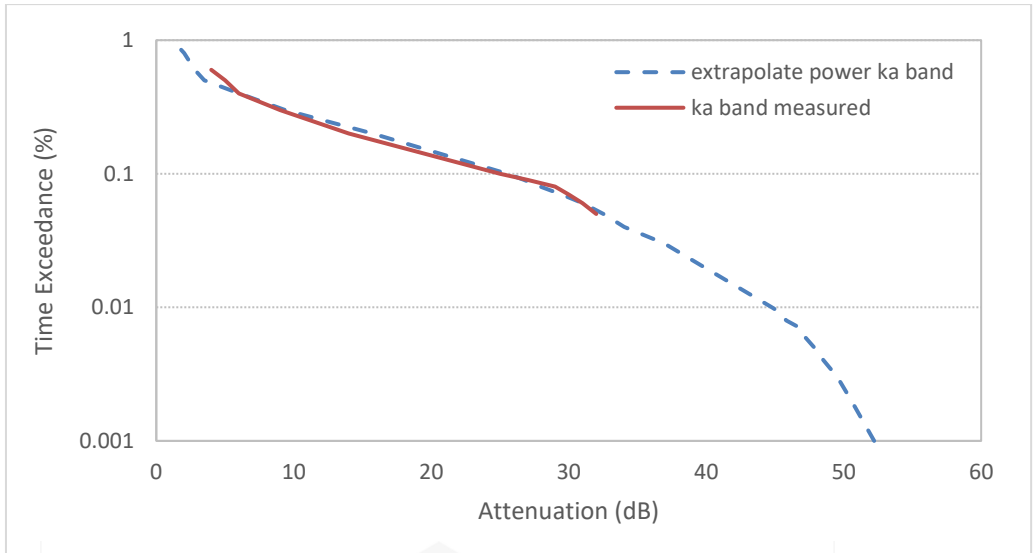


Figure 4.25 Measured Plotted Values with First-Order Power Law Extrapolation Model

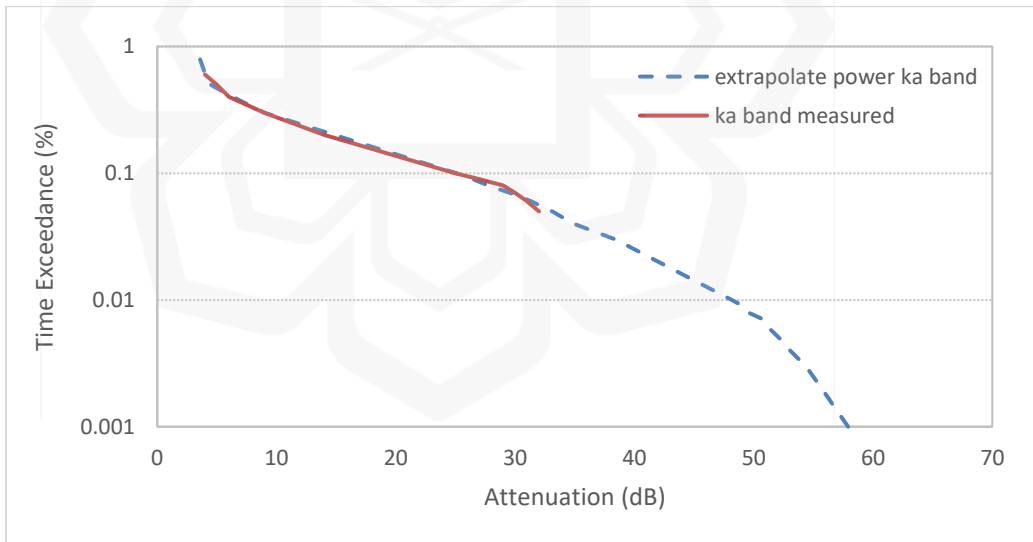


Figure 4.26 Measured Plotted Values with Second-Order Power Law Extrapolation Model

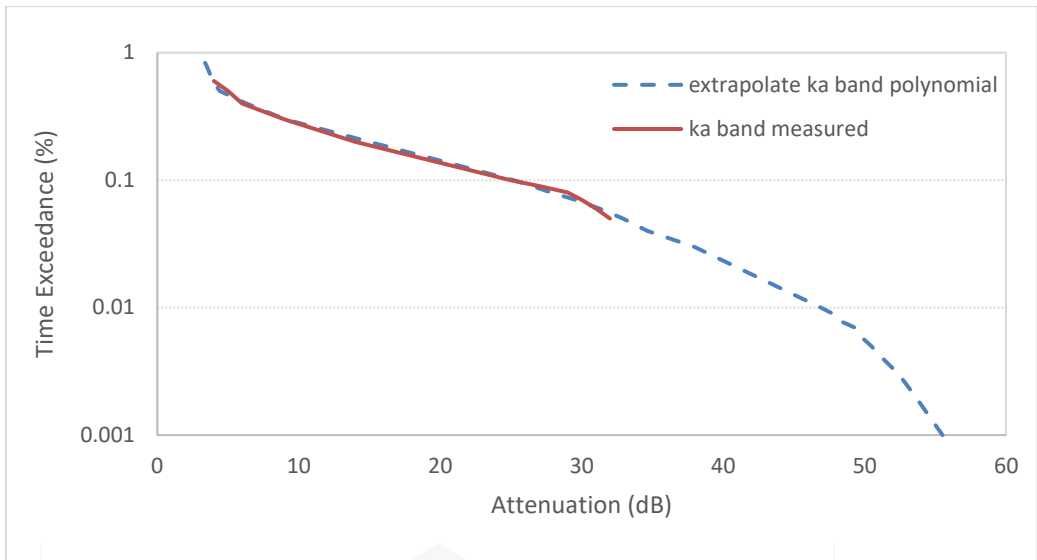


Figure 4.27 Measured Plotted Values with Second-Degree Polynomial Extrapolation Model

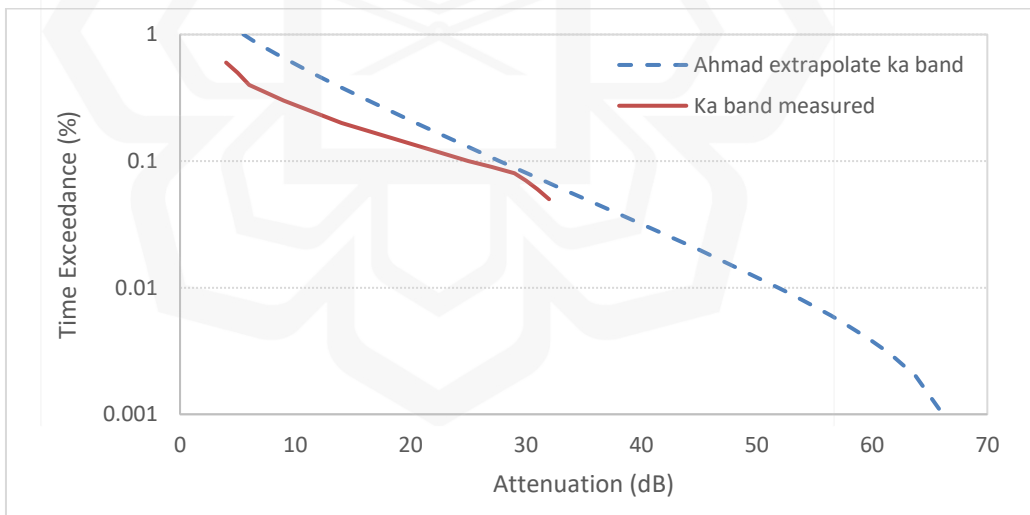


Figure 4.28 Measured Plotted Values with Ahmad's (2019) Extrapolation Model

All extrapolation models were evaluated using four evaluation methods: R-squared, Correlation, Root Means Square Error (RMSE) and percentage of error, as shown in Table 4.8. RMSE and relative error analyses are the predictive capabilities of the models suggested by (P.311-13, 2009). The second-degree polynomial model was selected for the Ka-band data extrapolation since the model offers a small value of RMSE (0.62).

Table 4.8 Summary of Techniques Used to Determine the Best Extrapolation Graph for Extended Ka-band

Model	Linear Extrapolation	First-Order Power Law Extrapolation	Second-Order Power Law Extrapolation	Second-Degree Polynomial extrapolation	Ahmad's Extrapolation
Correlation	0.998	0.997	0.998	0.998	0.978
R-squared	0.997	0.994	0.997	0.997	0.956
RMSE	0.63	0.90	0.63	0.62	4.97

After applying the second-degree polynomial model to extrapolate the annual CDF of Ka-band rain attenuation, the attenuation values obtained at 0.01% and 0.001% of time exceedance are 47 dB and 56 dB, respectively. Table 4.9 displays the summation of attenuation results by comparing the extrapolation data with a previous model, Ahmad (2019) and ITU-R 618-13. From Table 4.9, at all percentages of time exceedance, it was noted that Ahmad suggested higher values while the ITU-R model recommended lower values.

Table 4.9 Comparison of Measured Rain Attenuation at 0.1%, 0.01% and 0.001% of Time Exceedance with Ahmad's (2019) Model and ITU-R 618-13 (2017)

Time Exceedance (%)	Ka-band with extrapolation data (dB)	Ahmad prediction model with revised specific attenuation (dB)	ITU-R 618-13 prediction attenuation (dB)
0.1	25	28	22
0.01	47	53	43
0.001	56	66	55

From Figure 4.29, it can be seen that the Ka-band rain attenuation uniformly increases with the rainfall rate, starting from the lower rainfall rate. It was observed that rain attenuation evenly increases as the rainfall rate rises. Attenuation can reach up to 56 dB at a rainfall rate of more than 120 mm/hr. The limitation of the Ka-band receiver's sensitivity can be countered by employing a larger-sized antenna (Kalai, 2020). To operate the Ka-band at 99.99% of link availability in tropical regions, the considered fade margin values are approximately 45 dB and 55 dB for $R_{0.01\%}$, equal to 103 mm/hr and 194 mm/hr, respectively.

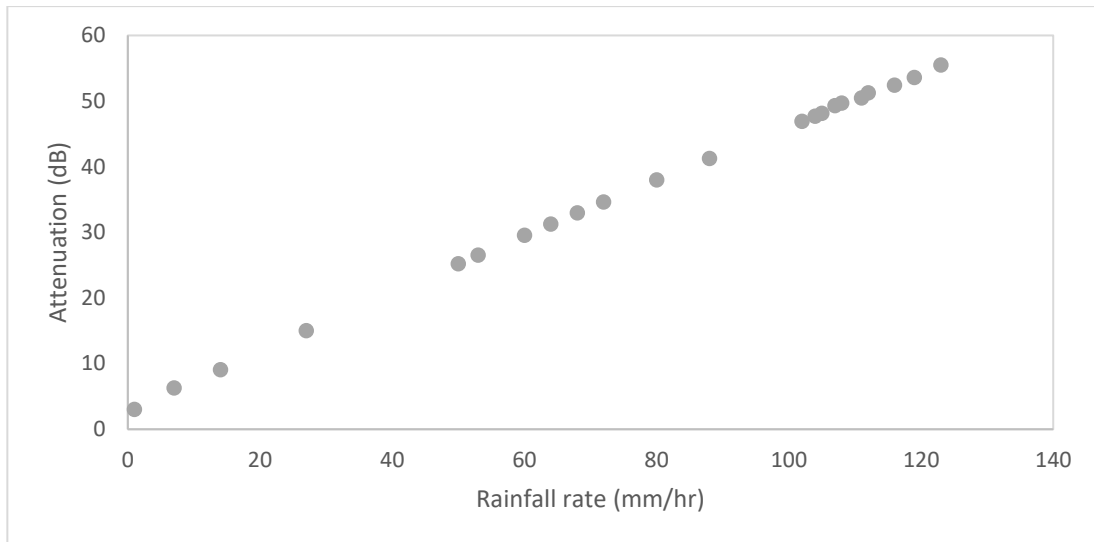


Figure 4.29 Extrapolated Ka-band Rain Attenuation Correlated to Rainfall Rate in Cyberjaya’s Rain Gauge

Renju (2021) noted that the significant factor that affects Ka-band attenuation is raindrop size. Intense convective rain causes higher rain attenuation within the range of 10 dB to 30 dB. The light stratiform rain can attenuate the signal below 12 dB in tropical regions.

4.3 DETERMINATION OF FADE MARGIN

This section provides the results that accomplish the first objective of the study. An exceedance at a specific point or link availability can be determined from the annual CDF. The rain attenuation values attained at the desired link performance can be implied as the system fade margin. The CDF provides information on the required estimation of rain attenuation margins for given link reliability. It is typically conveyed in percentage and represents the given link reliability expressed in minutes per year. Figures 4.30 to

4.33 display the annual CDFs of rain attenuation for the C, Ku and Ka-bands at 0.10%, 0.30%, 0.01% and 0.03% of time exceedance.

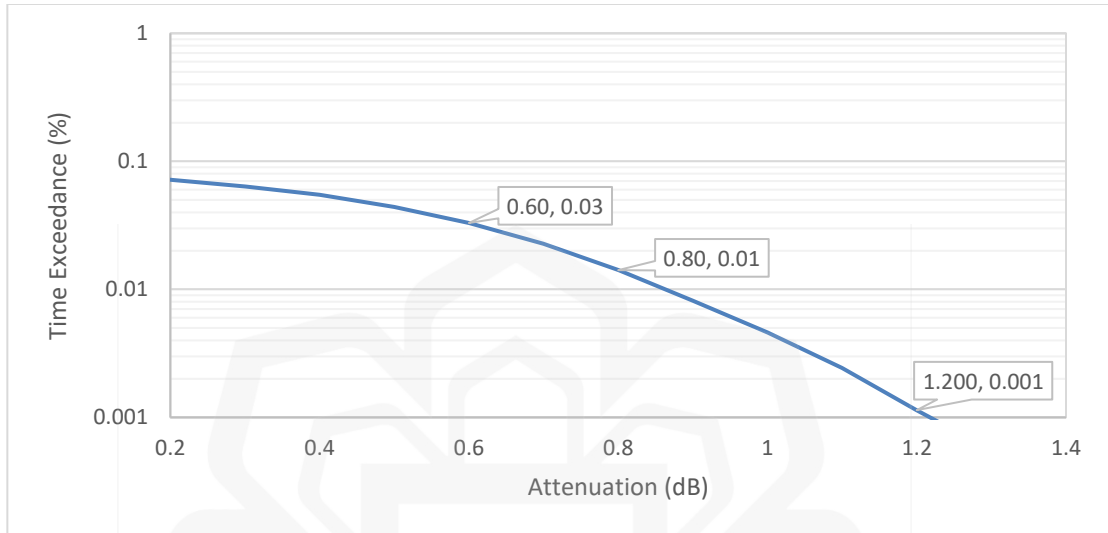


Figure 4.30 Annual CDF of C-band Rain Attenuation

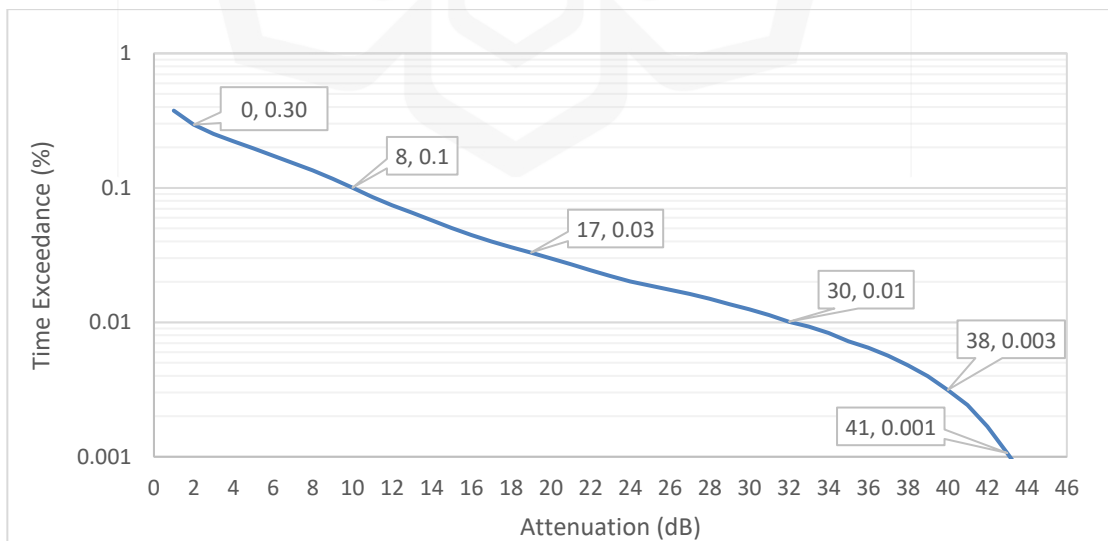


Figure 4.31 Annual CDF of Ku-band Rain Attenuation

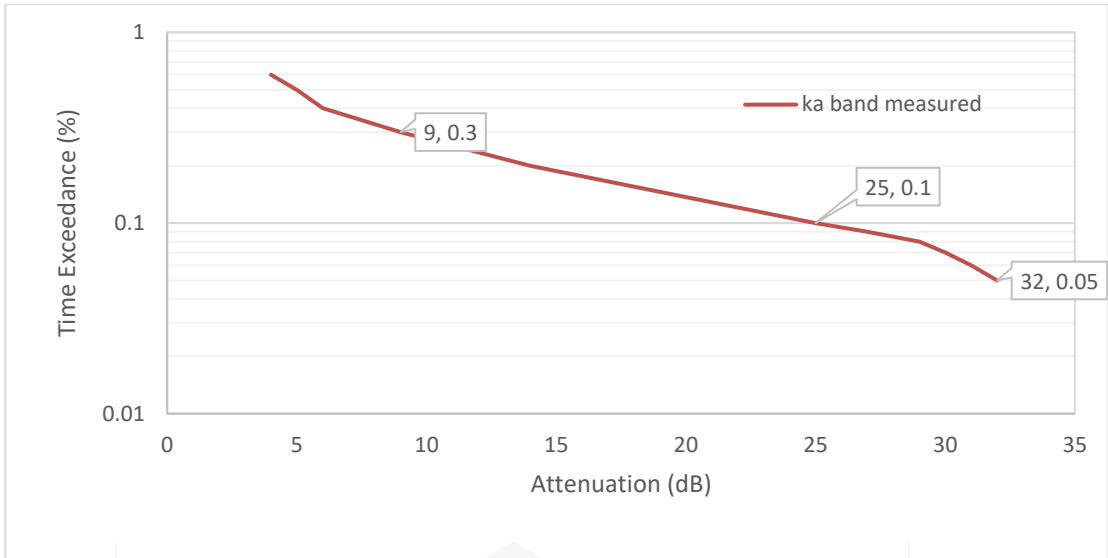


Figure 4.32 Annual CDF of Measured Ka-band Rain Attenuation

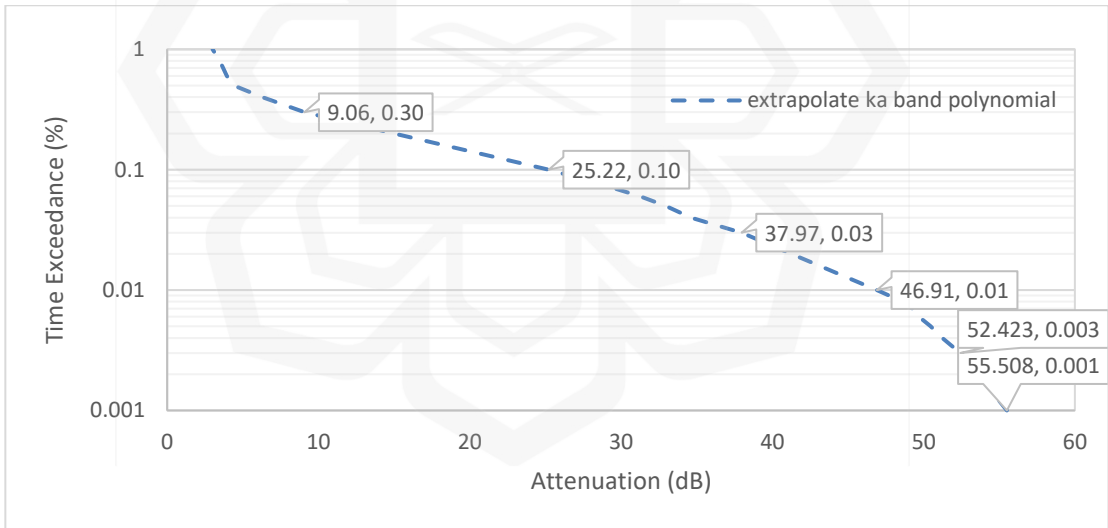


Figure 4.33 Annual CDF of Extrapolated Ka-band Rain Attenuation

The satellite link's quality of service (QoS) can be determined from the time exceedance plots. Service availability is measured in the percentage of availability per year. It is a network-related parameter that measures the performance of a service for a

particular application. It is defined as the ability of the service provider to efficiently deliver to the customer its required function over a given period. The minimum requirements of link availability to achieve QoS for communication and broadcasting services are 99.90% and 99.99% according to the Malaysian Communications and Multimedia Commission (MCMC) and the ITU-R G.1028, respectively (MCMC, 2022)

The fade margins for C, Ku and Ka-band links that operate at 99.70%, 99.90%, 99.97% and 99.99% of link availability in 2016 are listed in Table 4.10. It is clear that attenuation at 0.1%, 0.3%, 0.01% and 0.03% of link unavailability increases as frequency increases. Higher frequencies are more susceptible to rainfall, degrading the performance of link signal availability. The best QoS for delivering the expected broadcasting service is 99.99% link availability corresponding to attenuation at 0.01% of time exceedance. The required fade margins to enable system performance of Ku and Ka-band links and achieve the required level are 30 Db and 47 Db, respectively. The margin values of 8 Db and 25 Db are required for Ku and Ka-band to achieve the suggested QoS standard for communication services, respectively.

Table 4.10 Fade Margins for C, Ku and Ka-Band Links Operating at 99.70%, 99.90%, 99.97% and 99.99% in 2016

Link Availability (%)	Time Exceedance (%)	Attenuation (dB)			
		C-band	Ku-band	Ka-band	Extrapolated Ka-band
99.70	0.3	NA	0	9	9
99.90	0.1	NA	8	25	25
99.97	0.03	0.6	17	NA	38
99.99	0.01	0.8	30	NA	47

Satellites operating at frequencies above 10 GHz are generally vulnerable to rain-induced attenuation and will therefore require a measurement approach to improve design parameters. The fade margin value obtained from the time exceedance plot is important in satellite-Earth link systems that target cost-efficiency, including the implementation of suitable antenna size as well as power consumption at the receiver. It was noticed that high fade margins of 30 dB and 17 dB (more than 10 dB) are required to enable the Ku-band to achieve 99.99% and 99.97% link availability, respectively. The fade margin required for the Ka-band link is larger than the Ku-band for any percentage of link availability. From Figure 4.33, it can be seen that an approximately 38 dB fade margin would have been required at 0.03% link outage corresponding to 2.6 hours per year. This is equivalent to 99.97% link availability in the year 2016. It was also noted that the fade margins of 25 dB and 9 dB would have been needed for outages of 8.7 hours (0.1% of time exceedance) and 26.3 hours (0.3% of time exceedance), respectively. The high-quality link has been characterised by the national telephone system as the link with only one-hour outage per year (Ismail, 2001).

4.4 COMPARISON WITH ITU-R

Figures 4.34 and 4.35 present a CDF comparison of the predicted and measured values of rainfall measurements and rain attenuation, respectively. The rain rate prediction model by ITU-R overpredicts the rainfall rate time at time exceedance of more than 0.2% and less than 0.02%. The ITU-R model underpredicts the rainfall rate value even at 0.1% of time exceedance. The ITU-R proposes a value of 40 mm/hr, whereas the measured value is 51 mm/hr. The ITU-R model underpredicts the measured rainfall rate values within the range of $0.2\% < \text{time exceedance} < 0.03\%$. The measured rainfall rate is still higher than the predicted rain value by ITU-R (P.837-6 2012). The proposed rainfall rate by ITU-R for Malaysia is 100 mm/hr, which can be considered inaccurate and impractical since the point of rainfall measurement is unique for each location. Rainfall rate varies with climate and location. Marzuki (2020) tested the ITU-R rain

prediction model 837-7 for various areas throughout Indonesia, such as Kototabang, Padang, Sicincin, Pontianak and Bandung. The ITU-R tested in Cyberjaya produced a similar result to the ITU-R tested in Padang. Both Padang and Cyberjaya are tropical areas that experience annual precipitation of 1868.1 mm and 1493.0 mm, respectively. It is important to use precise rainfall rates in predicting rain attenuation in a particular area. In the year 2016, the rainfall rate at 0.01% of time exceedance, the $R_{0.01}$ obtained at Cyberjaya was 103 mm/hr, while at Puncak Niaga, it was about 136 mm/hr (Ahmad 2019). Tropical regions experienced a combination of stratiform and convective rain types throughout the year. This can be the factor that limits the ITU-R's accuracy in predicting rain attenuation since it uses only a single rainfall rate at 0.01% of time exceedance ($R_{0.01}$ value) for producing an annual CDF.

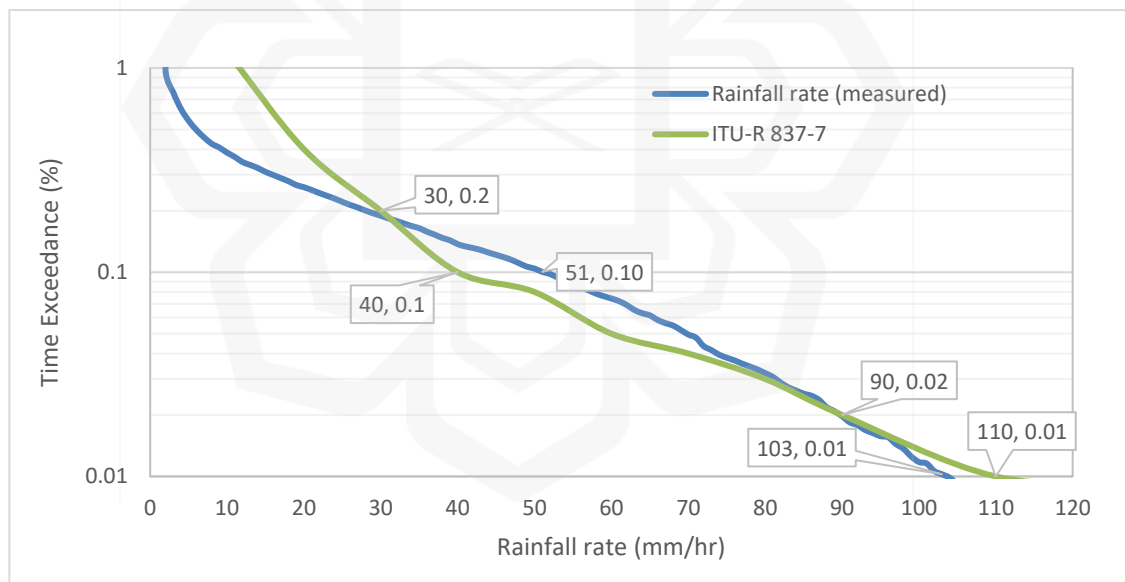


Figure 4.34 Annual CDF of the Measured Rain Rate Value in 2016 compared to ITU-R 837-7 Rainfall Prediction

From the rain attenuation, the ITU-R prediction model overpredicts the attenuation values for the time exceedance of more than 0.2% and underpredicts the attenuation for the time exceedance of less than 0.2%. It can be seen that no consistency is present in the ITU-R prediction model. The exact parameters that influence rainfall intensity in tropical regions must be extensively examined. The ITU-R prediction model to be used for tropical regions must be meticulously developed based on the tropical climate data. This is critical in predicting rain attenuation in areas that suffer frequent heavy rainfall as well as various types of rainfall throughout the year.

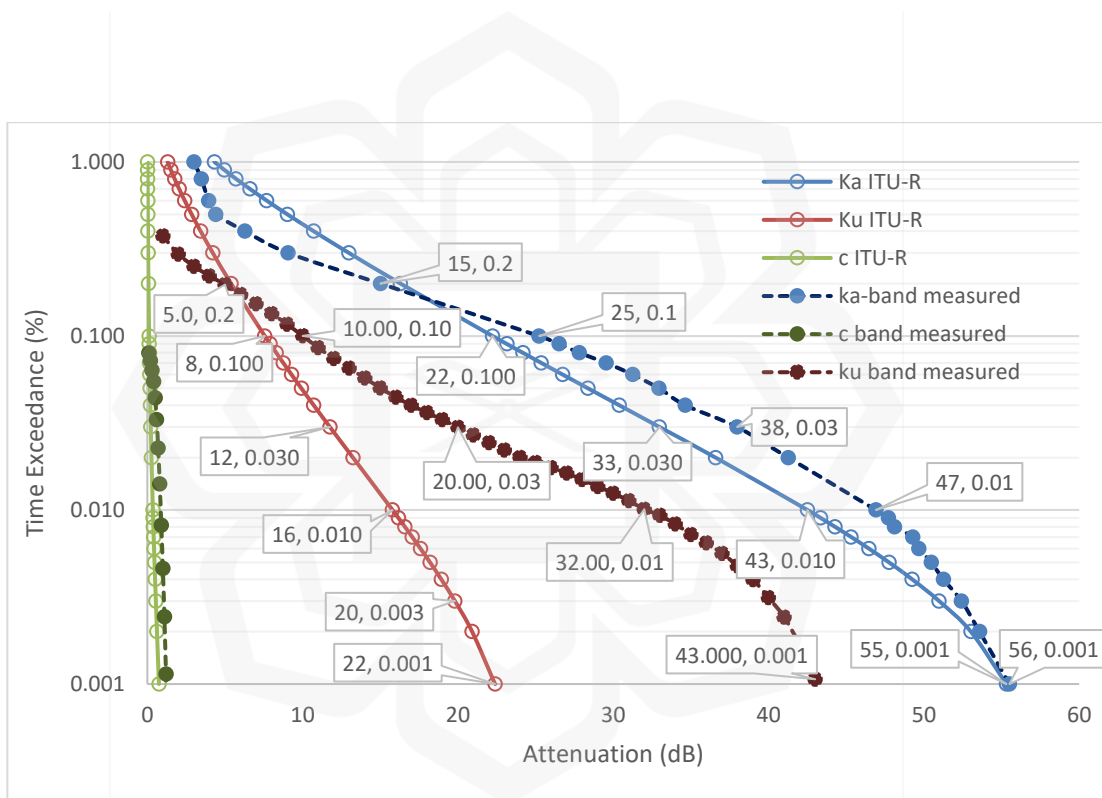


Figure 4.35 Annual CDF of Measured Values compared to ITU-R Prediction Values of Rain Attenuation for C, Ku and Ka-band Links

4.5 WORST MONTH ANALYSIS

The worst month analysis for rainfall and rain attenuation conducted in the previous chapter is discussed in this section. From Figure 4.36, the worst month for the rainfall rate at Cyberjaya in the year 2016 was identified as November with a rainfall rate of 120 mm/hr.

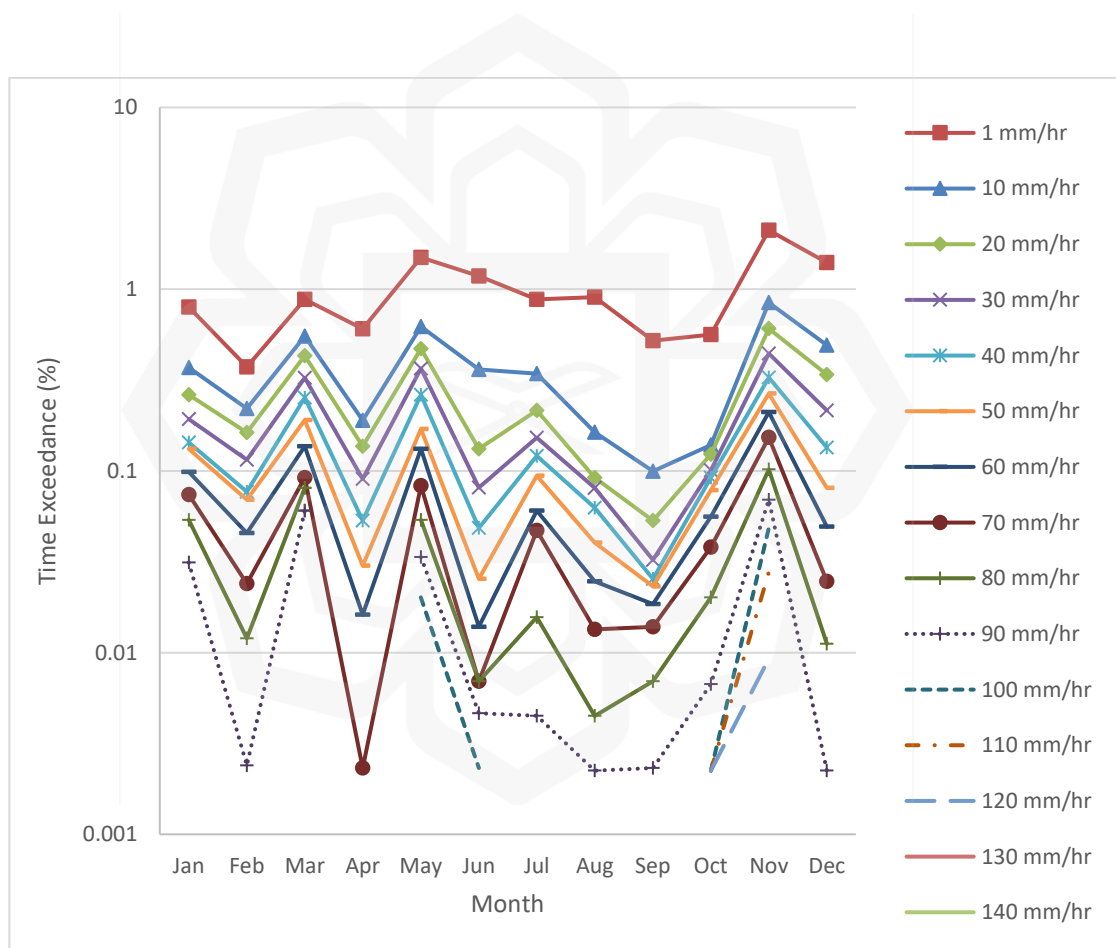


Figure 4.36 The Probability of a Specific Threshold of Rainfall Rate Exceeded for the year 2016 at Cyberjaya

The values for Q_I and β parameters, as mentioned by the ITU-R P.841-6, for tropical climate areas with frequent rain are 2.82 and 0.15, respectively. The recommended values of $Q_I=2.85$ and $\beta=0.13$ are for global planning purposes or terrestrial or slant path rain attenuation propagation. From the table of ITU-R P.841-6, in tropical regions section, the provided coefficient values of Q_I and β were adapted from a test involving the rain effect on terrestrial microwaves conducted in Indonesia. ITU-R has recommended that the values of β and Q_I should be 0.22 and 1.7, respectively, for determining the worst month analysis for rain attenuation effect on terrestrial propagation links in Indonesia. There is no available value for the slant-path rain attenuation propagation effect in tropical regions. The annual CDF of rainfall intensity and the worst month analysis were obtained from the measured data and then plotted in Figure 4.37. ITU-R's predicted worst month was determined and plotted in the same figure for comparison.

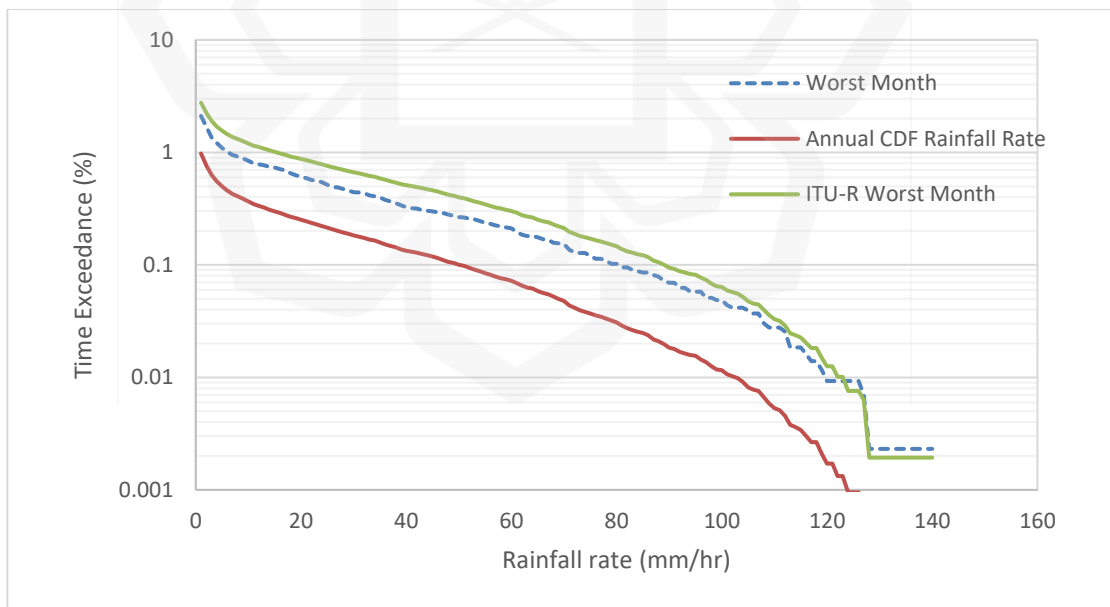


Figure 4.37 Annual and Worst Month Rain Rate Exceedance Curve

The variable Q represents the ratio of time exceedances between the average year and the average worst month and was derived from the measured data. The ratio can be extracted from a regression fit, as shown in Figure 4.38. Figure 4.38 presents the ratio of time exceedance between the annual rainfall rate and the average worst month at probabilities of 0.001% up to 1% of time exceedance. The ratio of time exceedance between the annual rain attenuation at Ku-band compared to the average worst month at the same probabilities is portrayed in Figure 4.39. As can be noticed from both figures, the values for the regression parameters of Q_I and β were derived from the measured data by applying a trendline or the least square method of the power law equation. The values of the obtained parameters Q_I and β for the slant path rain effect as well as for the rain rate propagation in tropical climate regions are presented in Table 4.11. From the analysis, the worst month for the Ku-band slant path at Cyberjaya in the year 2016 is the month of May, as shown in Figure 4.13.

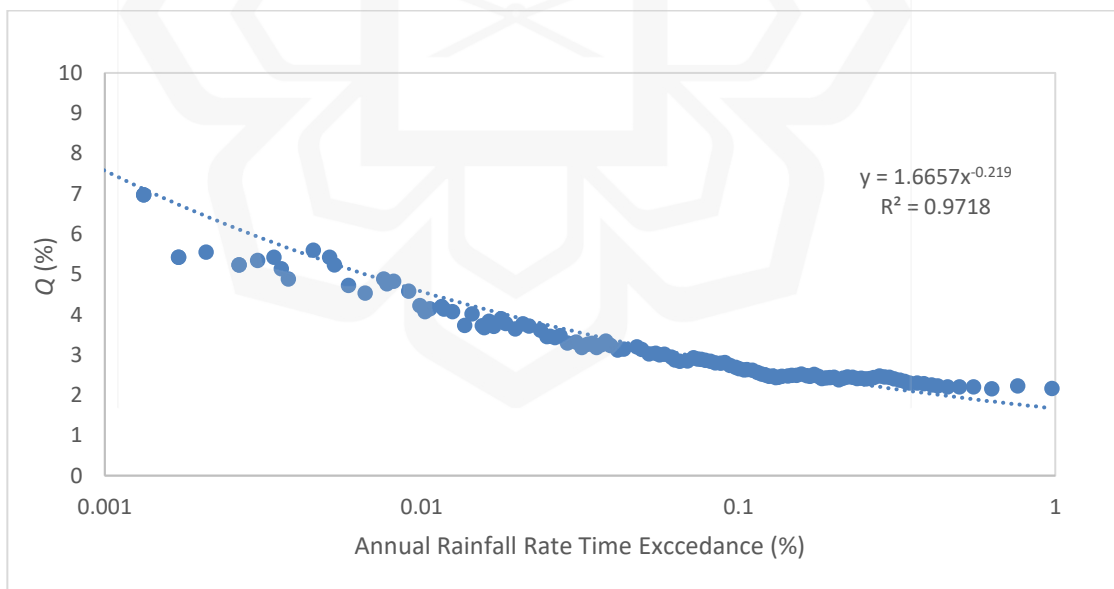


Figure 4.38 Q as a Function of Annual Rainfall Rate Exceedance Percentage

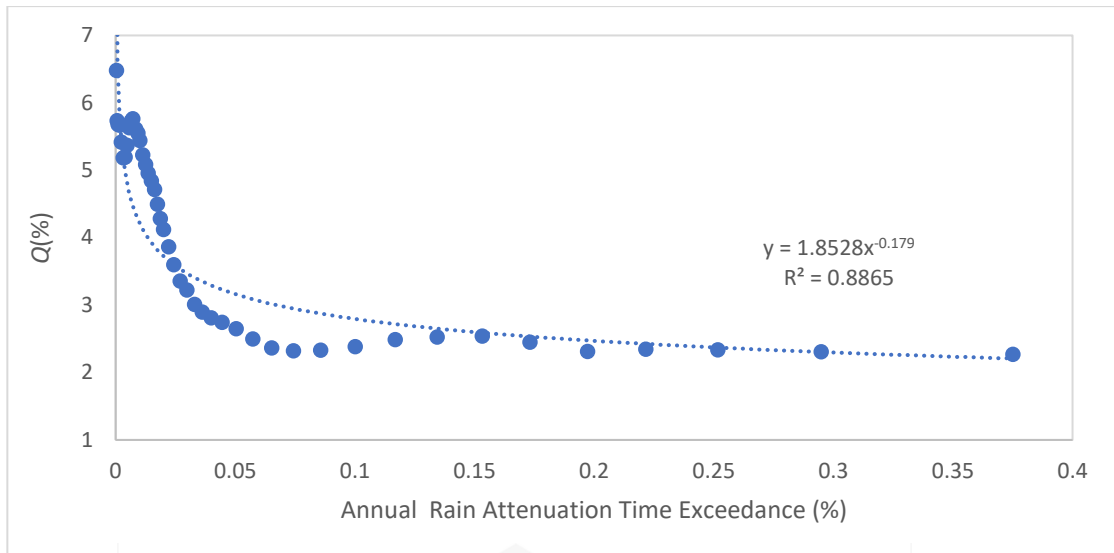


Figure 4.39 Q_1 as a Function of Annual Rain Attenuation at Ku-Band Exceedance Percentage

The proposed values of $Q_1 = 1.85$ and $\beta = 0.18$ were applied for rain attenuation at the Ku-band slant path link. The $Q_1 = 1.67$ and $\beta = 0.22$ values were suggested for the rain rate. From the measured data, the rain-induced attenuation and CDF of the Ku-band for a year and the worst month analysis were obtained and plotted in Figure 4.40. Figure 4.40 displays the identified worst month graph for Ku-band rain attenuation compared to the annual rain attenuation, and the worst month graph proposed by ITU-R for the terrestrial links in Indonesia, as well as the recommended ITU-R for general purposes. It was noticed that there is a slight difference in the attenuation value at 0.1% of time exceedance when compared to ITU-R. The new parameter values of Q_1 and β acquired during this research are similar to those recommended in previous research. These parameters can be used to attain a better estimation of any slant path rain attenuation for the worst month statistics in tropical regions.

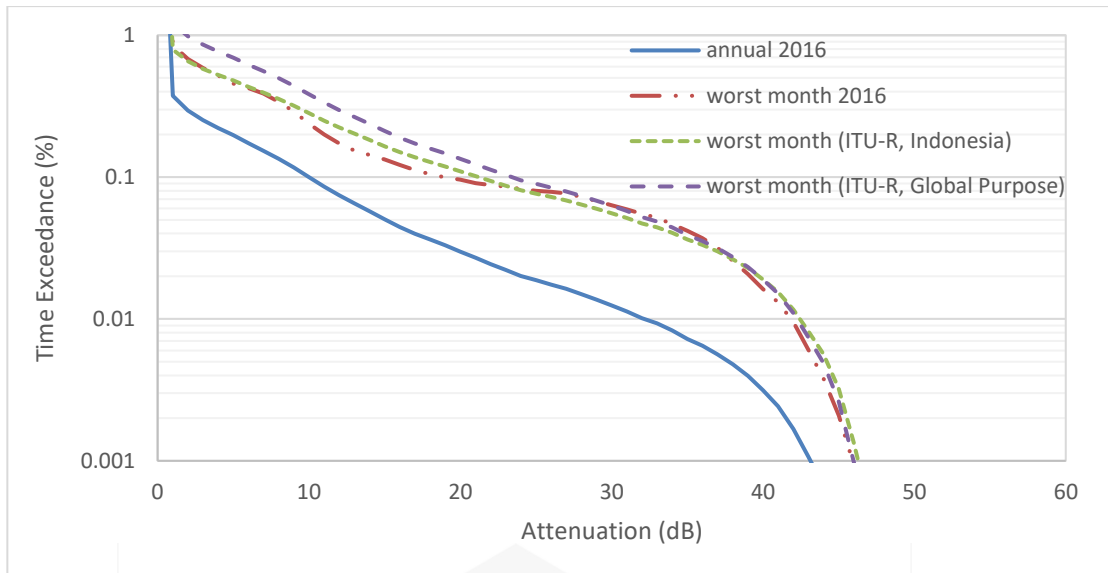


Figure 4.40 Worst Month Model Comparison of Ku-band Rain Attenuation

Table 4.11 summarises the Q_1 and β values at Cyberjaya and other tropical locations in comparison to the ITU-R values. The measured values of Q_1 and β for Cyberjaya are similar to the values proposed by ITU-R for Indonesia. This is probably because Indonesia and Malaysia are located in the same tropical and equatorial regions. The Q factor depends on the climate, thus different climate regions will have different Q factors. The values of $Q_1 = 2.59$ and $\beta = 0.07$ were proposed for rain attenuation at the Ka-band slant path link in tropical regions. The values can be observed in Figure 4.41.

Table 4.11 Measured Values and Proposed Values for Q_I and β in Tropical Regions for Slant Path and Rain Rate Propagation

Source	Propagation Type	Location	Q_I	β
ITU-R P.841-6	General Purpose	Tropical regions	2.85	0.13
Drudola (2017)	Rain rate	Nigeria	1.06	0.37
Ismail (2016)	Rain Attenuation at Ku-band	Johor Bahru, Malaysia	1.69	0.22
Marzuki (2016)	Rain rate	Indonesia	1.39	0.24
Mandeep (2008)	Rain Attenuation at Ku-band	Malaysia	1.7	0.10
Ting & Mandeep (2014)	Rain Attenuation at Ku-band	Penang, Malaysia	1.68	0.07
Islam et.al, (2003)	Rain Attenuation at Ku-band, Ka-band	Johor, Malaysia	0.95, 0.91	0.3, 0.32
Yagasena (2000)	Rain Attenuation at Ku-band, Ka-band	Perak, Malaysia	1.39	0.30
Yagasena (2000)	Rain rate	Perak, Malaysia	1.40	0.29
Measured	Rain rate	Cyberjaya, Malaysia	1.67	0.21
Measured	Rain Attenuation at Ku-band	Cyberjaya, Malaysia	1.85	0.18
Measured	Rain Attenuation at Ka-band	Cyberjaya, Malaysia	2.59	0.07

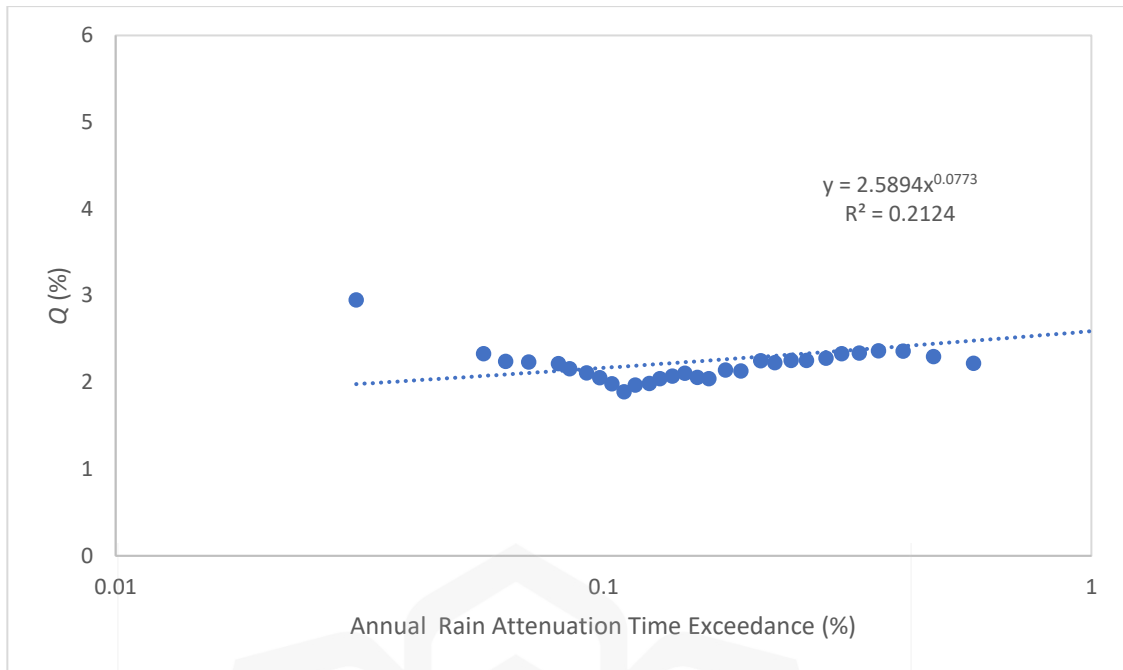


Figure 4.41 Q as a Function of Annual Rain Attenuation at Ka-band Exceedance Percentage

The annual and worst month analyses of rain attenuation for the Ka-band link in Malaysia are presented in Figure 4.42. The figure also provides a comparison with the ITU-R model for general purposes. The worst-month statistics of rainfall rate and rain attenuation are very beneficial in offering high-quality communication networks. The degradation of the signal at the satellite link is expected to be higher during the worst month due to the maximum occurrence of rain events. The worst month analysis in tropical regions can be assumed to have a less critical impact compared to that in temperate regions. Tropical regions experience heavy rain throughout the year and this is not exclusively influenced by a specific month or a particular season.

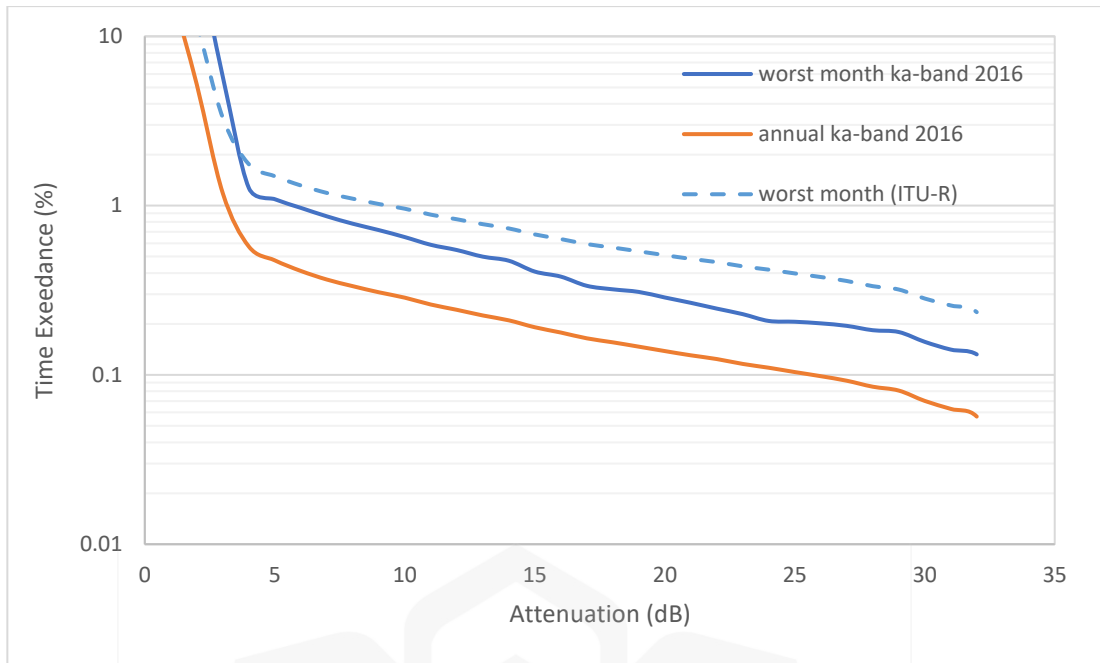


Figure 4.42 Worst Month Model Comparison of Ku-band Rain Attenuation

4.6 FREQUENCY SCALING

Several existing statistical frequency scaling techniques have been tested using the acquired rain attenuation information. This section presents the results.

4.6.1 ITU-R 618-13 Frequency Scaling

The ITU-R 618-13 has proposed a frequency scaling model in equations (2.30) – (2.32). Figure 4.43 presents the results of ITU-R 618-13 frequency scaling rain attenuation prediction. By applying the frequency scaling model proposed by ITU-R, the following occurred:

- i. For pairs f_2/f_1 of Ku-band/C-band and Ka-band/C-band, ITU-R underpredicted the measured value of rain attenuation at all percentages of time exceedance.
- ii. For pairs f_2/f_1 of Ka-band/Ku-band, ITU-R underpredicted the value of rain attenuation at a time exceedance of more than 0.1% and overpredicted the value of rain attenuation at a time exceedance of less than 0.07%.

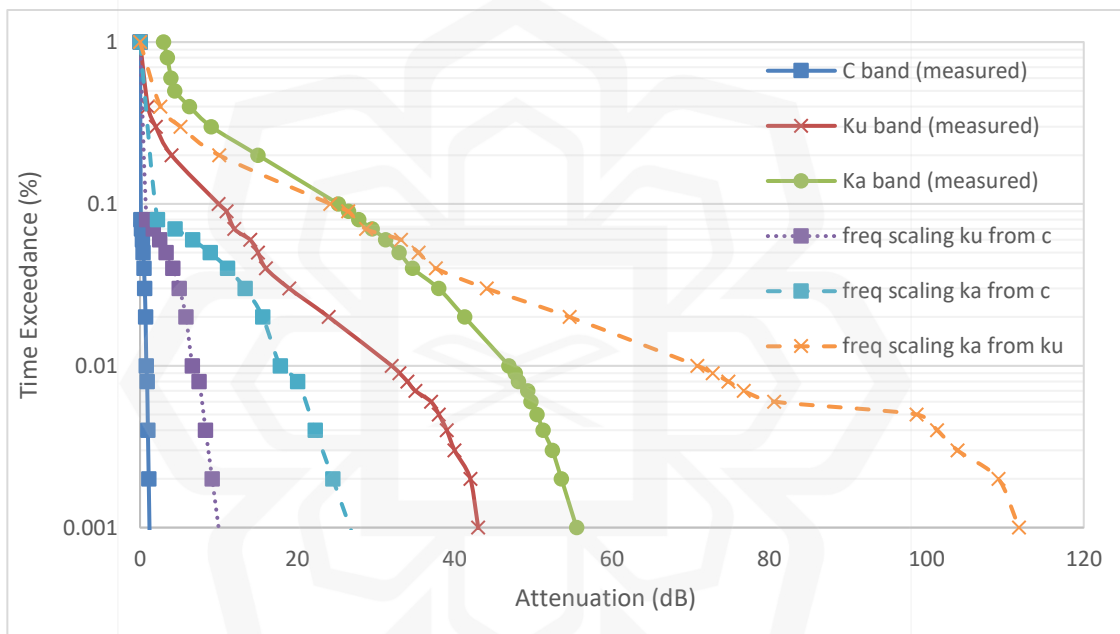


Figure 4.43 ITU-R 618-13 Frequency Scaling

4.6.2 Hodge

Hodge proposed a frequency scaling technique that can be expressed as equation (2.34). The constants a and b were derived from the specific attenuation-rain rate relationships provided in equation (2.35). The results of Hodge's frequency scaling rain attenuation

prediction model are shown in Figure 4.44. By applying the frequency scaling model proposed by Hodge, the following can be seen:

- i. For pairs f_2/f_1 of Ku-band/C-band, the Hodge model overpredicted the measured value of rain attenuation at less than 0.07% of time exceedance.
- ii. For pairs f_2/f_1 of Ka-band/C-band, the Hodge model overpredicted the measured value of rain attenuation at less than 0.06% of time exceedance.
- iii. For pairs f_2/f_1 of Ka-band/Ku-band, the Hodge underpredicted the value of rain attenuation at a time exceedance of more than 0.03% and overpredicted the value of rain attenuation at a time exceedance of less than 0.03%.

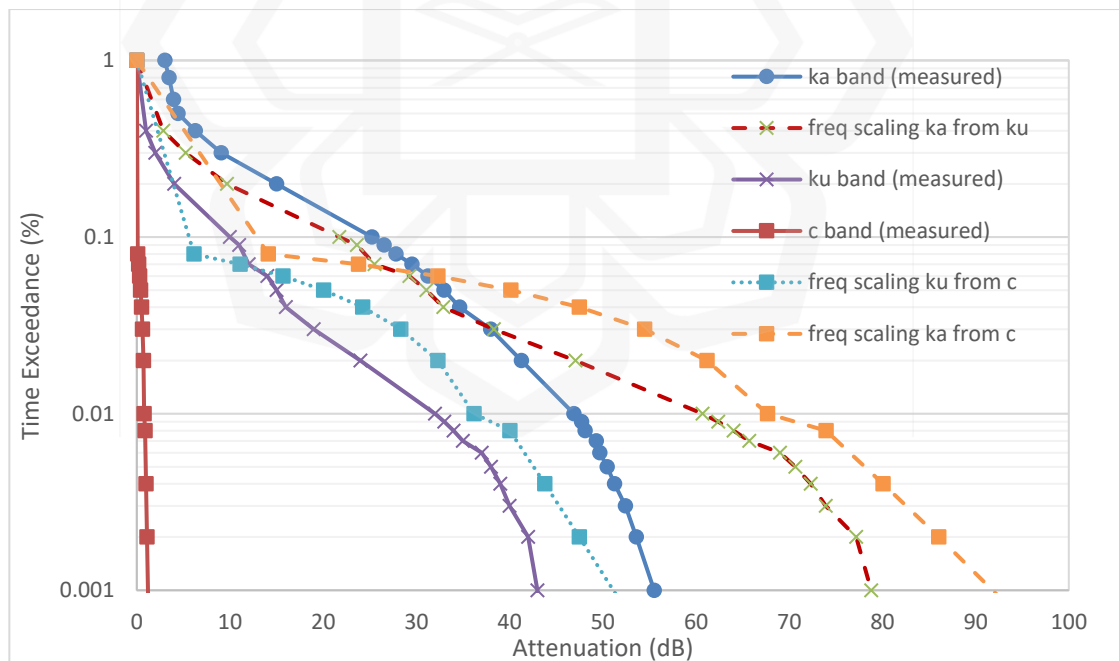


Figure 4.44 Hodge Frequency Scaling Model

4.6.3 Battesti

Battesti's model proposed a frequency scaling method, as represented by equations (2.36) – (2.38). This model emphasised that attenuation is proportional to a linear function of the frequency models. The results of Battesti's frequency scaling rain attenuation prediction model are shown in Figure 4.45.

- i. For pairs f_2/f_1 of Ku-band/C-band and Ka-band/C-band, the Battesti model cannot provide an accurate prediction since the results are of negative values.
- ii. For pairs f_2/f_1 of Ka-band/Ku-band, the Battesti model underpredicted the value of rain attenuation at a time exceedance of more than 0.07% and overpredicted the value of rain attenuation at time exceedance less than 0.04%.

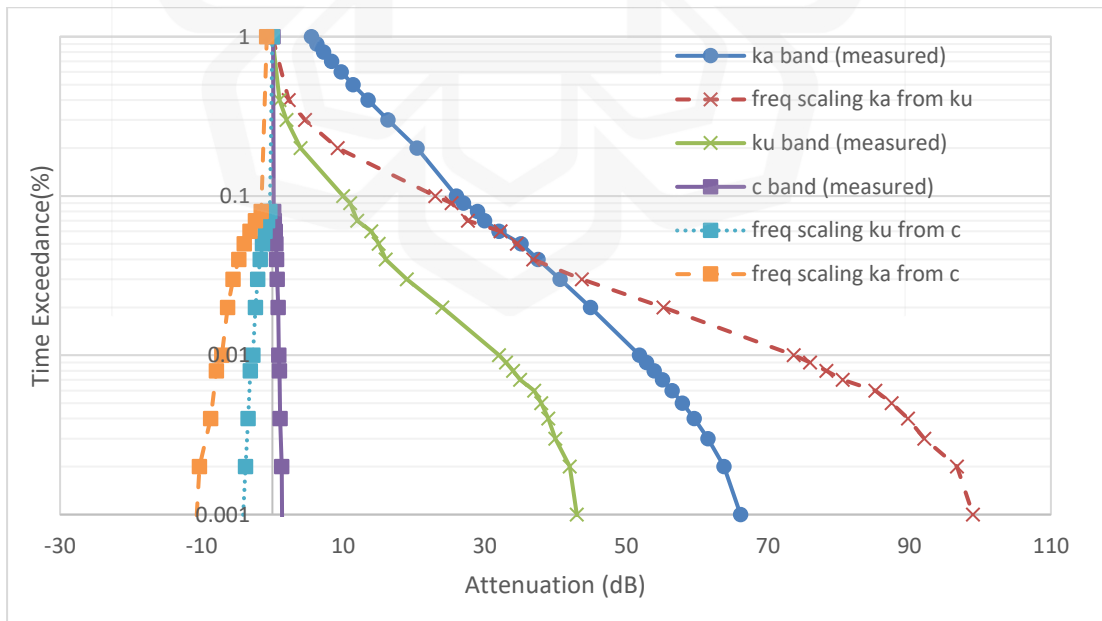


Figure 4.45 Battesti Frequency Scaling Model

4.6.4 Kheirallah

Kheirallah's model proposed a frequency scaling technique, as given in equation (2.41). The results of Kheirallah's frequency scaling rain attenuation prediction model are shown in Figure 4.46.

- i. For pairs f_2/f_1 of Ku-band/C-band, Kheirallah's model adequately predicted the percentage of exceedance less than 0.01%, overpredicted at exceedance percentage from 0.01% to 0.06% and underpredicted at exceedance percentage from 0.06% to 0.08%.
- ii. For pairs f_2/f_1 of Ka-band/C-band, Kheirallah's model overpredicted the measured rain attenuation value at less than 0.06% of time exceedance and more than 0.08% of time exceedance.
- iii. For pairs f_2/f_1 of Ka-band/Ku-band, Kheirallah's model underpredicted the rain attenuation value at a time exceedance of more than 0.02% and overpredicted the value of rain attenuation at a time exceedance of less than 0.02%.

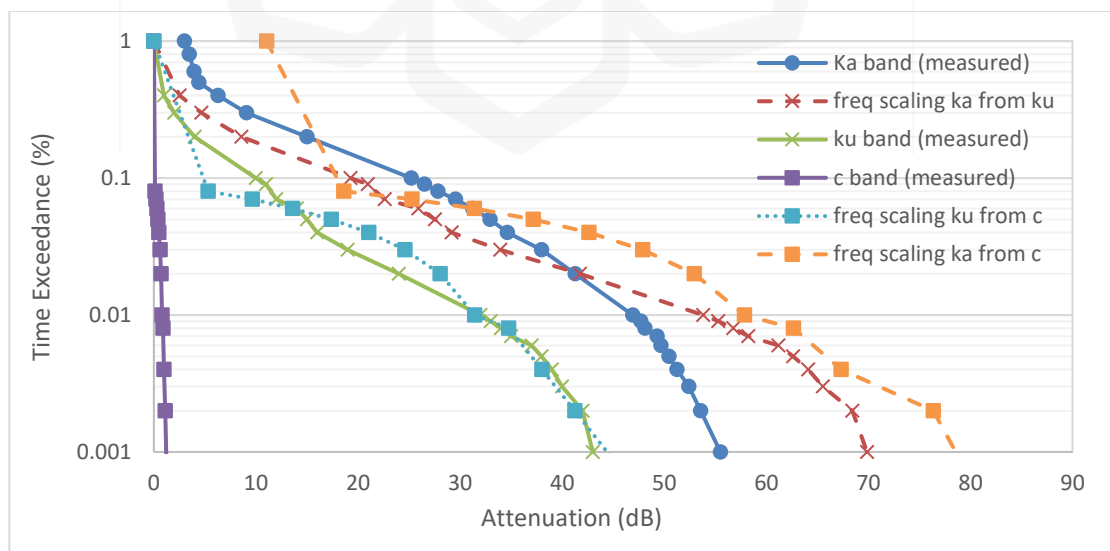


Figure 4.46 Kheirallah Frequency Scaling Model

4.6.5 CCIR

The results of the International Radio Consultative Committee (CCIR) model, given in equations 2.42 and 2.43, are provided in Figure 4.47. By applying the frequency scaling model proposed by CCIR, the result was similar to ITU-R.

- i. For pairs f_2/f_1 of Ku-band/C-band and Ka-band/C-band, the CCIR underpredicted the measured value of rain attenuation at all percentages of time exceedance.
- ii. For pairs f_2/f_1 of Ka-band/Ku-band, the CCIR underpredicted the value of rain attenuation at the time exceedance of more than 0.1% and overpredicted the value of rain attenuation at the time exceedance of less than 0.06%.

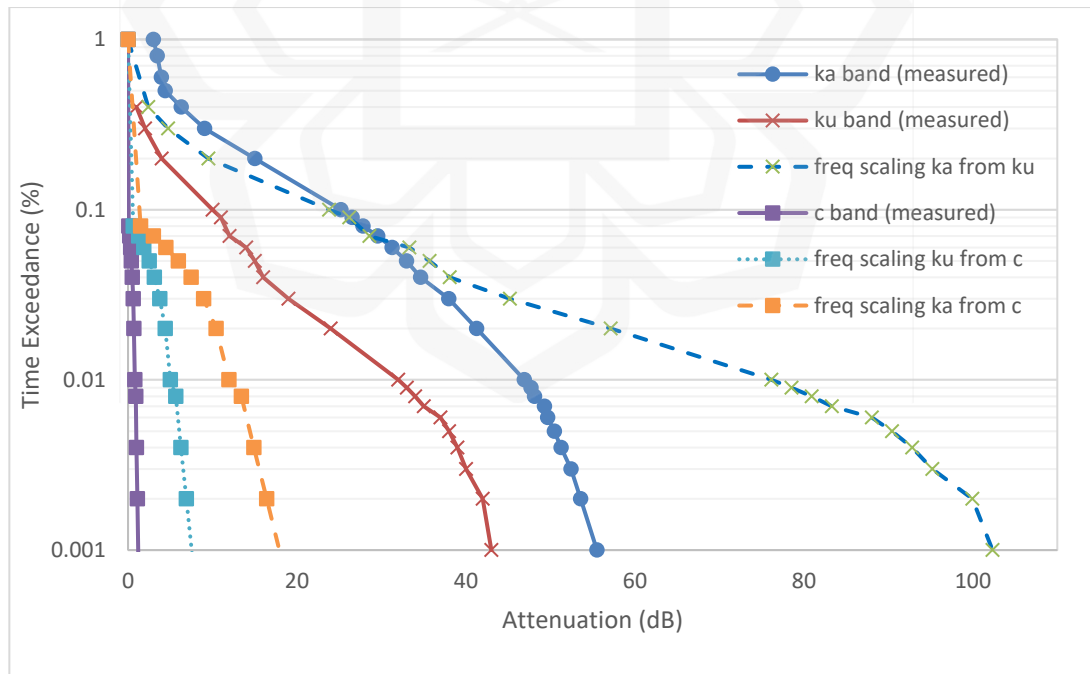


Figure 4.47 CCIR Frequency Scaling Model

4.6.6 Simple Power Law

The Simple Power Law frequency scaling model applied a power law relationship in predicting rain attenuation at the desired frequency. The results of simple power scaling proposed by Dintelman, Owalabi and Olympus are presented in Figures 4.48 and 4.49.

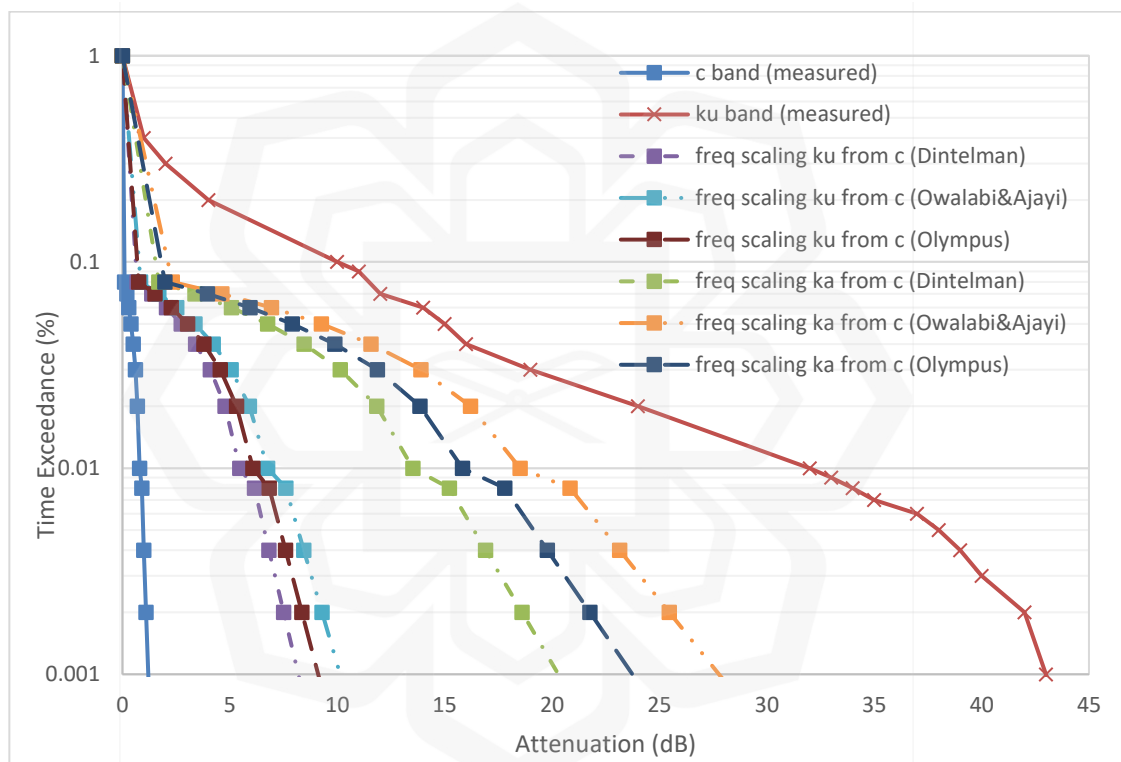


Figure 4.48 Simple Power Law Frequency Scaling for Pairs Ku-band/C-band and Ka-band/C-band

By applying the simple power law frequency scaling model:

- i. For pairs f_2/f_1 of Ku-band/C-band and Ka-band/C-band, all models of simple power law underpredicted the measured value of rain attenuation for all percentages of time exceedance.
- ii. For pairs f_2/f_1 of Ka-band/Ku-band, all models of simple power law underpredicted the value of rain attenuation at a time exceedance of more than 0.1% and overpredicted the value of rain attenuation at a time exceedance of less than 0.1%.

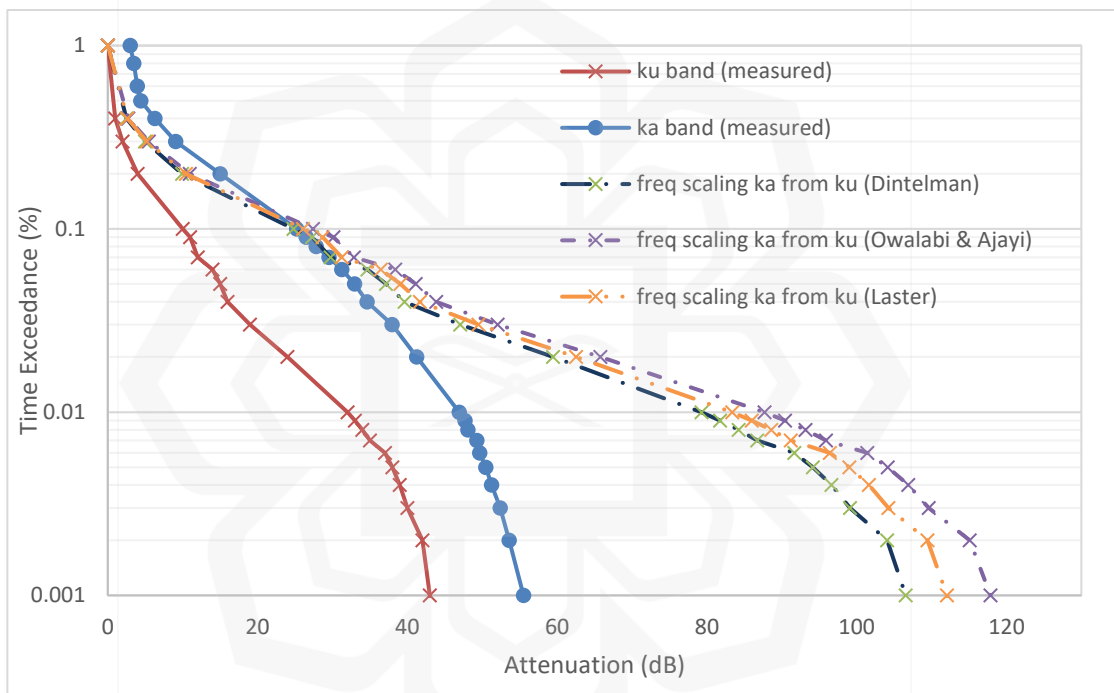


Figure 4.49 Simple Power Law Frequency Scaling for Pairs Ka-band/Ku-band

Drafuca (1974) is another simple power law frequency scale, as shown in Figure 4.50. It has been empirically found that the rain attenuation scales can be established, as shown in the following equation:

$$\frac{A_2}{A_1} = \left(\frac{f_2}{f_1}\right)^{(1.72)} \quad (4.1)$$

- i. For pairs f_2/f_1 of Ku-band/C-band and Ka-band/C-band, Drafuca underpredicted the measured value of rain attenuation at all percentages of time exceedance.
- ii. For pairs f_2/f_1 of Ka-band/Ku-band, Drafuca underpredicted the value of rain attenuation at a time exceedance of more than 0.1% and overpredicted the value of rain attenuation at a time exceedance of less than 0.07%.

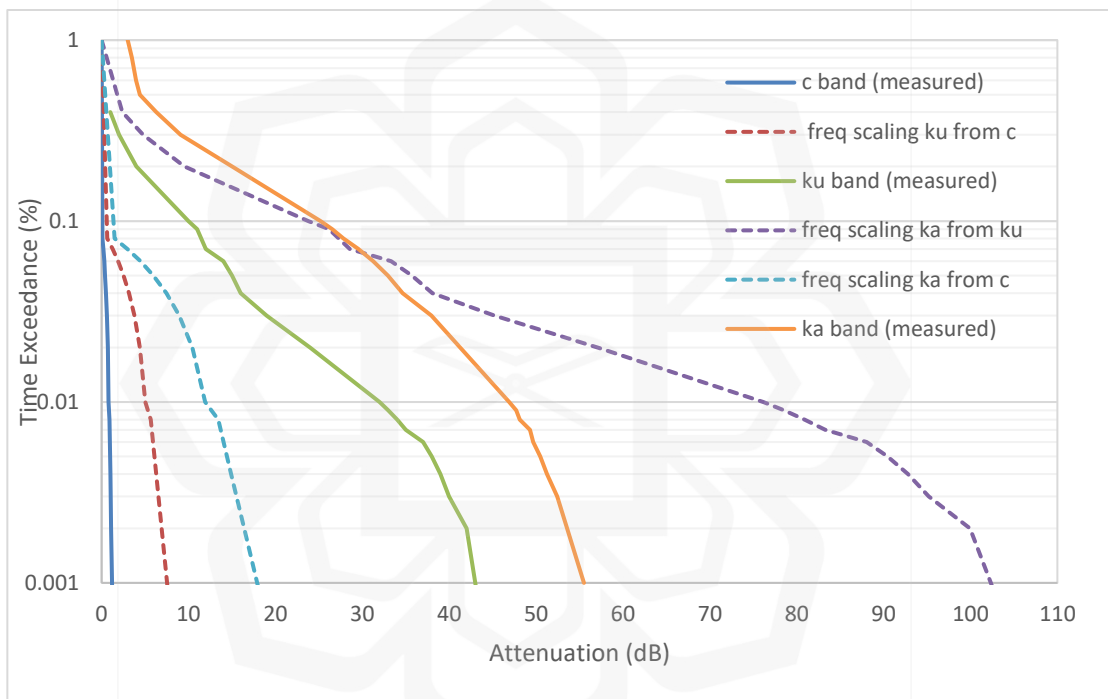


Figure 4.50 Drafuca Frequency Scaling Model

4.6.7 Boithias

Boithias (1989) proposed an empirical expression for a scaling factor that directly produces an attenuation ratio as a function of frequency and measured attenuation, as shown in equations (2.45) – (2.47). The results are illustrated in Figure 4.51. By applying the frequency scaling model proposed by Boithias, the results are as follows:

- i. For pairs f_2/f_1 of Ku-band/C-band and Ka-band/C-band, Boithias underpredicted the measured value of rain attenuation at all percentages of time exceedance.
- ii. For pairs f_2/f_1 of Ka-band/Ku-band, Boithias underpredicted the value of rain attenuation at a time exceedance of more than 0.02% and overpredicted the value of rain attenuation at a time exceedance of less than 0.02%.

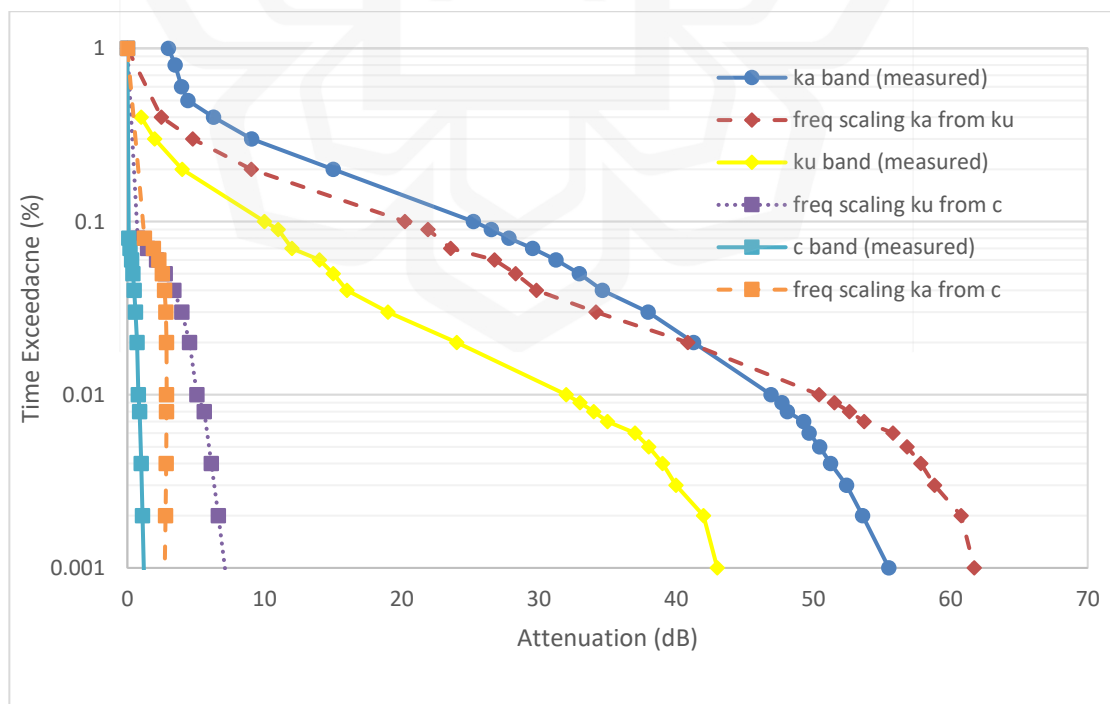


Figure 4.51 Boithias Frequency Scaling Model

4.6.8 Zhou

Figure 4.52 presents the results of the scaled attenuation at the desired frequency compared to the measured attenuation at the base frequency, as proposed by Zhou.

By applying the frequency scaling model, the results are as follows:

- i. For pairs f_2/f_1 of Ku-band/C-band and Ka-band/C-band, the Zhou model overpredicted the Ku-band rain attenuation at more than 0.4% of time exceedance and underpredicted the measured value of rain attenuation of Ku and Ka-band at all percentages of time exceedance.
- ii. For pairs f_2/f_1 of Ka-band/Ku-band, the Zhou model underpredicted the value of rain attenuation at a time exceedance of more than 0.2% and less than 0.4%, while it overpredicted the value of rain attenuation at time exceedance of less than 0.02%.

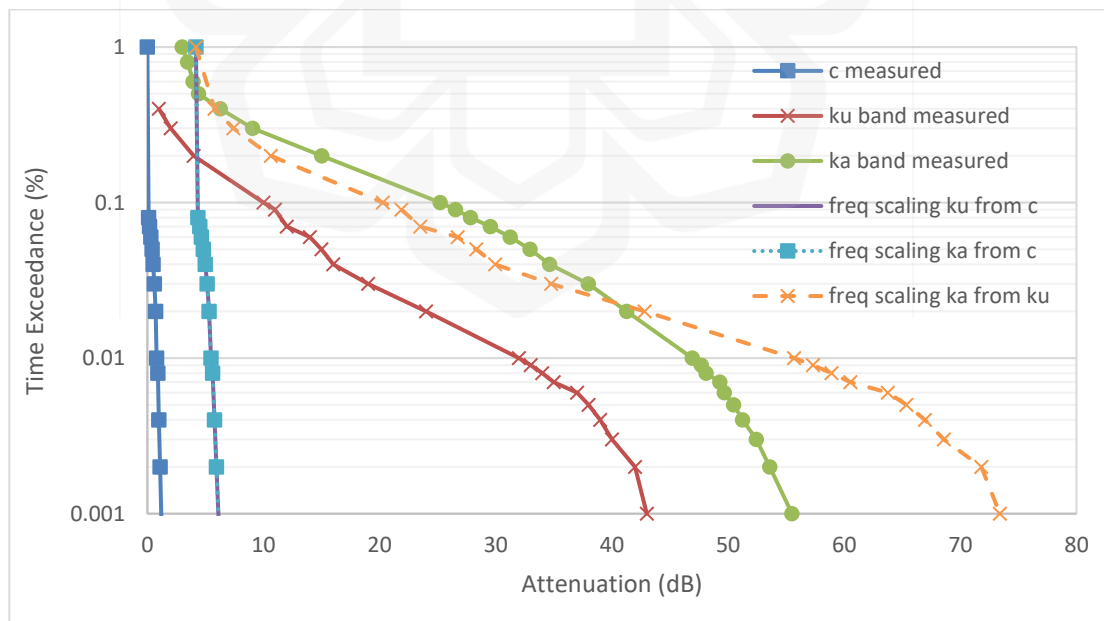


Figure 4.52 Zhou Frequency Scaling Model

The error analysis was performed on all eleven existing models for further assessment. Table 4.12 presents the results. From the obtained RMSE and percentage error, it can be identified that all models produce very high RMSE values as well as large percentage error rates. The model that offers the smallest RMSE value of 5 and the second-lowest percentage error is the Boithias model. From these findings, a new frequency scaling model with reduced RMSE value and low percentage error rates was developed.

Table 4.12 RMSE and Percentage Error of Available Model over the Interval [0.001% to 1%]

Model	Parameters	
	RMSE	ϵ (%)
Dintelman	29.0	32.3
Owalabi	35.9	39.6
Drufuca	26.5	30.9
Olympus data	32.4	35.7
Hodge	13.2	25.6
Battesti	24.5	30.1
Kheirallah	8.5	30.4
CCIR	26.5	30.9
Boithias	5.0	28.2
Zhou	9.9	17.3
FS ITU-R	28.3	28.0

4.7 PROPOSED FREQUENCY SCALING TECHNIQUE

The second aim of the research was achieved by the findings presented in this section. The frequency scaling technique did not utilise the C-band rain attenuation measurement as a base frequency since the C-band is minimally affected by rain. The CDF of rain attenuation from the year 2016 for C, Ku and Ka-band with their mutual time base were simultaneously plotted with the rainfall rate throughout the year 2016 in Figure 4.53. Figure 4.53 exhibits that rain attenuation at the Ku and Ka-band gets higher as the rainfall rate increases. It can be seen that the different values between rain attenuation amounts of the Ku and Ka-band are consistently equal to 15 dB at 0.1% and 0.01% of time exceedance, respectively. Rain attenuation at a higher frequency is proportional to the rainfall rate. Rain attenuation of the Ka-band is indeed more severe compared to that of the Ku-band.

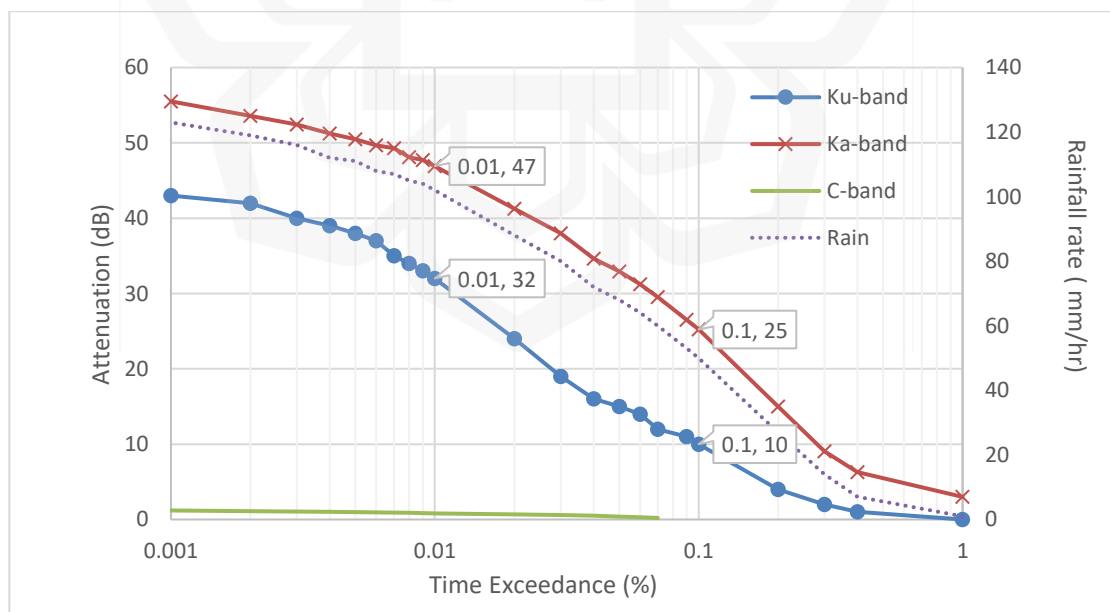


Figure 4.53 Time Percentage Exceedance Curve of Measured Rain Rate and Rain Attenuation of C, Ku and Ka-band Links for 2016

Figure 4.54 displays the graph of the Ratio of Statistical Attenuation (RAS) for the year 2016. The graph outlines the function of lower frequency attenuation for the frequency pair of Ka-band/Ku-band where the logarithmic equation was fitted to RAS within the percentage interval of $0.05\% < P < 0.4\%$. The relationship between the RAS at two frequencies with attenuation at the base frequency is represented by the following equation:

$$\frac{A_{f_2}}{A_{f_1}} = -1.425 \times \ln(A_{f_1}) + c \quad (4.2)$$

where A_{f_1} refers to attenuation at a base frequency or reference frequency or lower frequency, while A_{f_2} refers to attenuation at the upper frequency. The frequency of f_1 and f_2 are 12 GHz and 20 GHz, respectively. The parameter, c , obtained from the graph in Figure 4.54 is 5.9006.

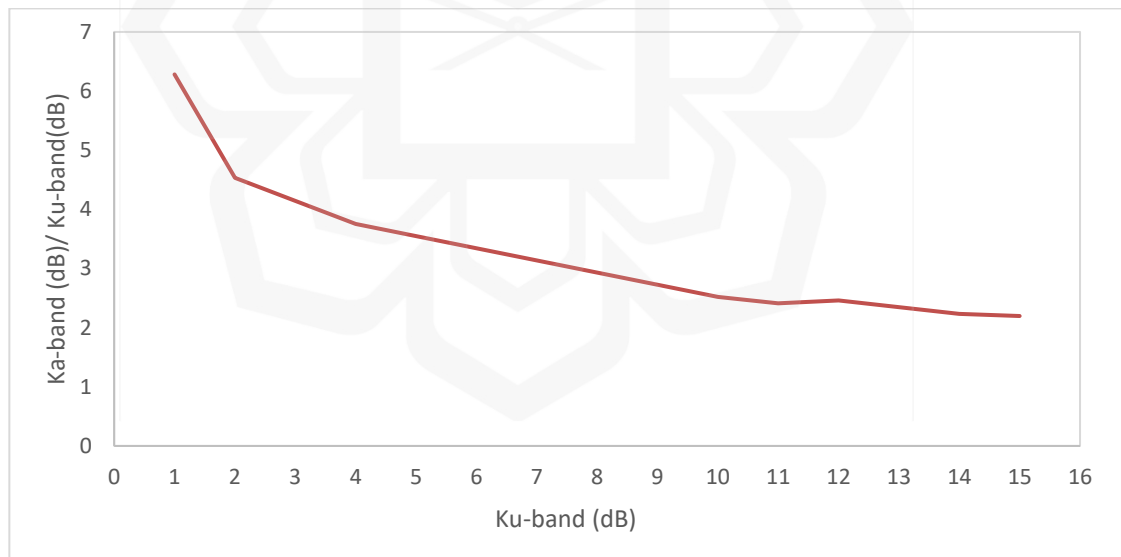


Figure 4.54 RAS for the Year 2016 as a Function of Lower Frequency Attenuation for the Frequency Pairs of 20/12 GHz

Another important parameter in deriving frequency scaling values was obtained from the correlation of A_{f_2} and A_{f_1} . The correlation graph of attenuation at the Ka-band and Ku-band was plotted within the percentage interval of $0.05\% < P < 0.4\%$ in Figure 4.55. The following power equation was fitted to the values:

$$A_{f_2} = \alpha \times A_{f_1}^\beta \quad (4.3)$$

The acquired α and β are 6.1685 and 0.6175, respectively.

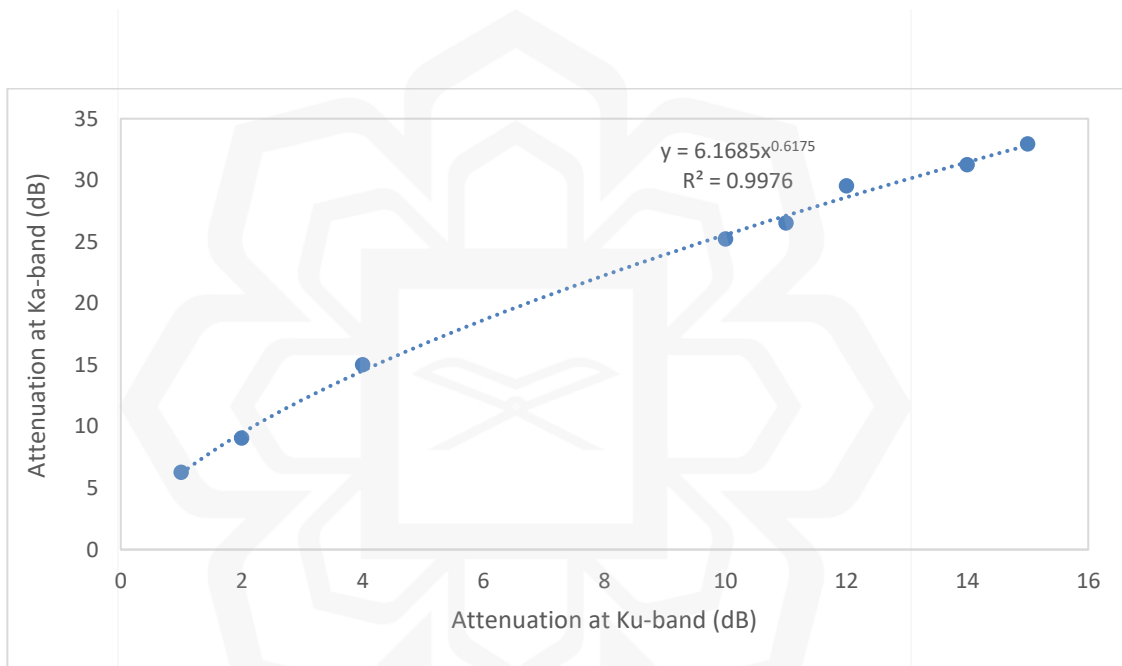


Figure 4.55 Graph of Attenuation at the Ku-band versus Attenuation at the Ka-band

Figures 4.56 and 4.57 present the attenuation at the Ku-band versus that of the C-band as well as the attenuation at the Ka-band compared to that of the C-band, respectively. The correlation plots of frequency pairs (Ka-band/C-band) and (Ku-band/C-band) demonstrate that there is no uniform relationship between both frequencies. The C-band link cannot be set as the base frequency. It can be seen in Figures 4.56 and 4.57 that attenuation at the C-band has no uniform relationship with

attenuation at the Ku and Ka-band links. The C-band link is less likely to suffer from rain since its frequency has a 74 mm wavelength which is longer than the wavelength of the Ku and Ka-band links. Signal attenuation of the C-band link is mainly due to absorption since its wavelength is greater than the diameter of convective rain, which is approximately 60 mm. The wavelengths for the Ku and Ka-band links are 24.5 mm and 14.8 mm, respectively. These wavelengths are significantly shorter than the raindrop size diameter and therefore greatly influenced by absorption and scattering effects. These effects contribute to greater loss in signal propagation. When scaling attenuation at higher frequencies, it is important to consider attenuation at lower frequencies that have a consistent relationship since they have similar characteristics.

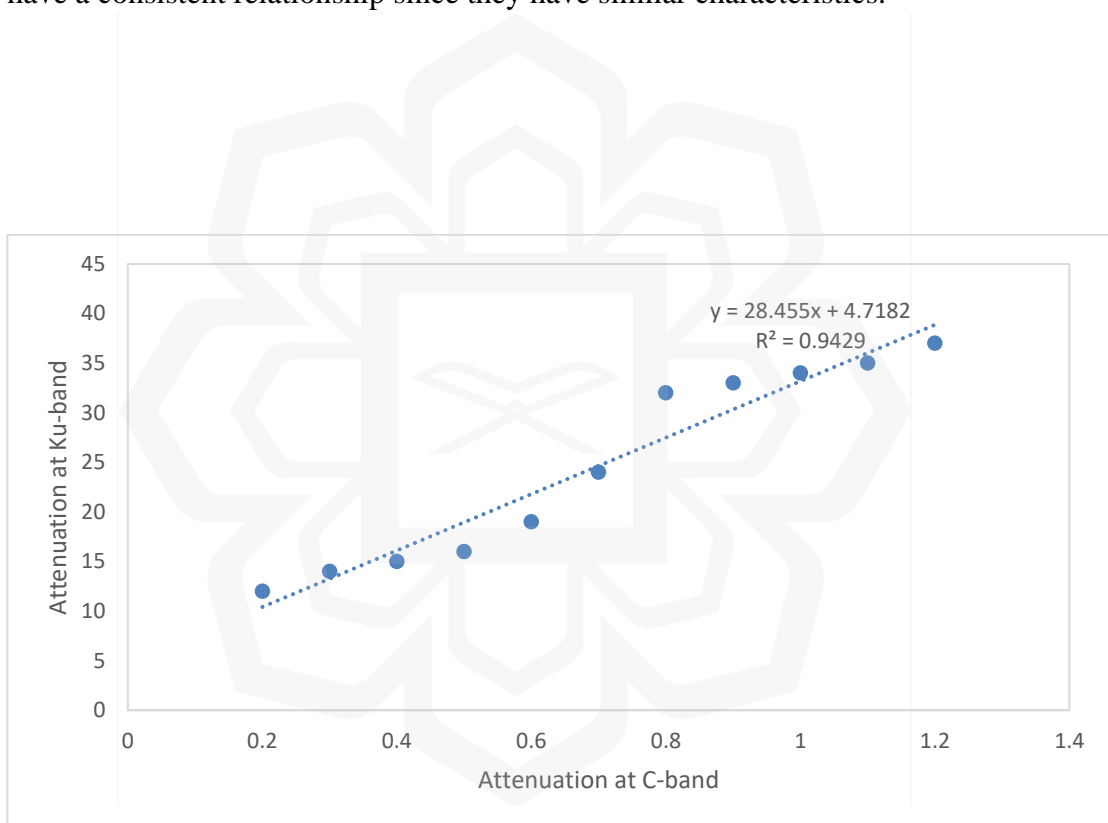


Figure 4.56 Graph of Attenuation at the Ku-band versus Attenuation at the C-band

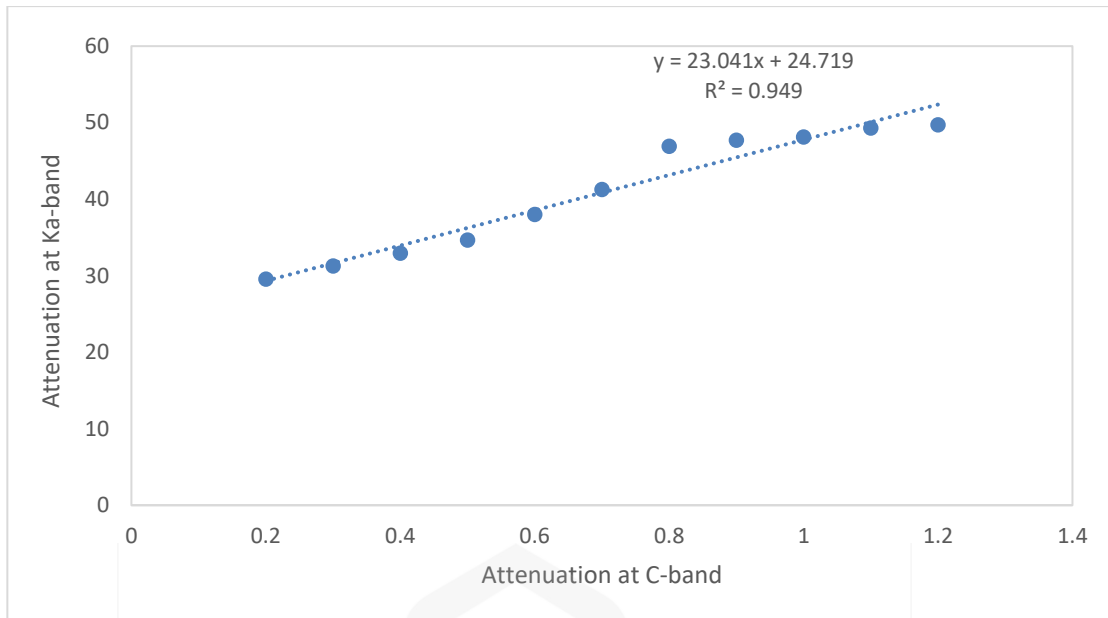


Figure 4.57 Graph of Attenuation at the Ka-band versus Attenuation at the C-band

The study proposed a new frequency scaling model based on the correlation of two rain attenuation information within Cyberjaya. The technique employed the Ka-band as the upper frequency and the Ku-band as the base frequency. The newly derived model can be said suitable to be used for tropical regions since the model was developed using data from tropical areas.

The proposed frequency scaling of rain attenuation for tropical-equatorial regions is provided in equation 4.4 which combines equations (4.2) and (4.3) with some modifications.

$$A_2 = (\alpha \times A_1^{0.669}) - (1.425 \times \ln b + (2 \times b)) \quad (4.4)$$

$$b = \frac{f_2}{f_1} \quad (4.5)$$

The coefficient c in equation (4.2) was modified, as follows:

$$c = 2 \times b \quad (4.6)$$

where b is the ratio of f_2 and f_1 . The variable coefficients α and β in equation (4.3) were modified with the upper and lower frequency values. A has the following formation:

$$\alpha = \sqrt{f_2 - f_1} + 1.38 \quad (4.7)$$

and β is 0.669. β was derived from the modified power value of the power model that fit the graph of attenuation at the Ka-band versus attenuation at the Ku-band with the same time exceedance percentage.

The proposed model was tested to estimate attenuation at the Ka-band in the year 2016 by using attenuation at the Ku-band in Cyberjaya as the base frequency. The proposed frequency scaling model for the year-wise estimation of rain attenuation at the Ka-band is depicted in Figure 4.58 and compared with the measured value of Ka-band rain attenuation in that year.

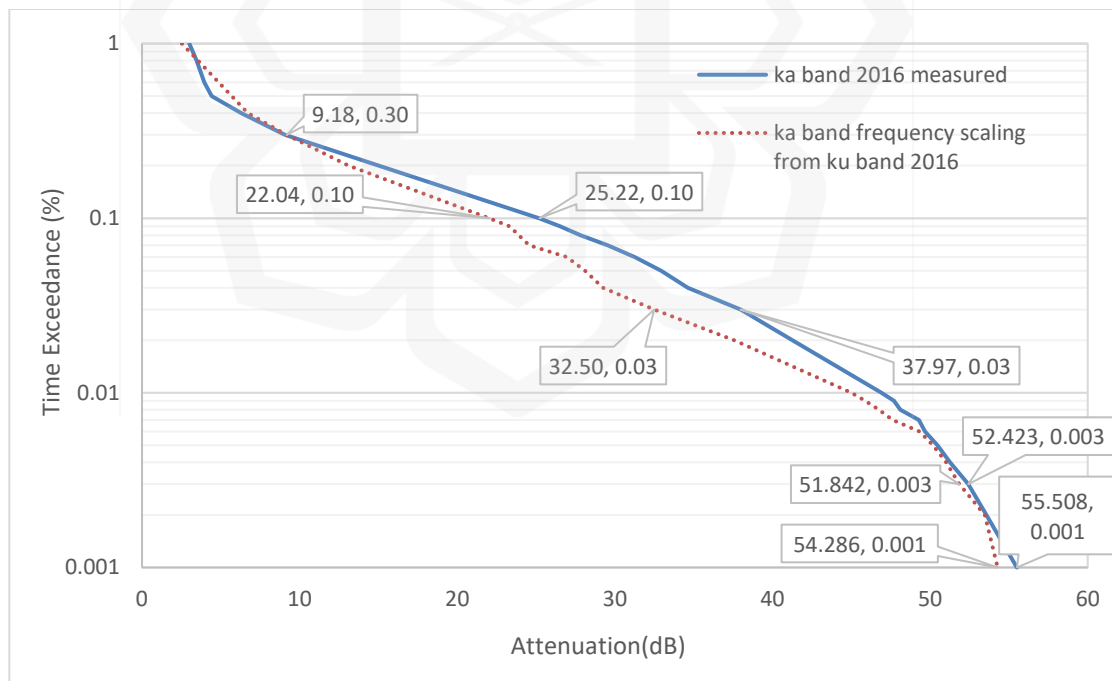


Figure 4.58 Comparison of Scaled-up Ka-band Rain Attenuation Using the Proposed Frequency Scaling Model with Measured Rain Attenuation at the Ka-band in 2016

The performance of the proposed frequency scaling model derived from this research was compared with various well-known statistical frequency scaling methods for rain attenuation. Most models perform poorly in tropical areas. This is because these models were developed in different climatic regions. The comparison of the available model with the proposed model is portrayed in Figure 4.59.

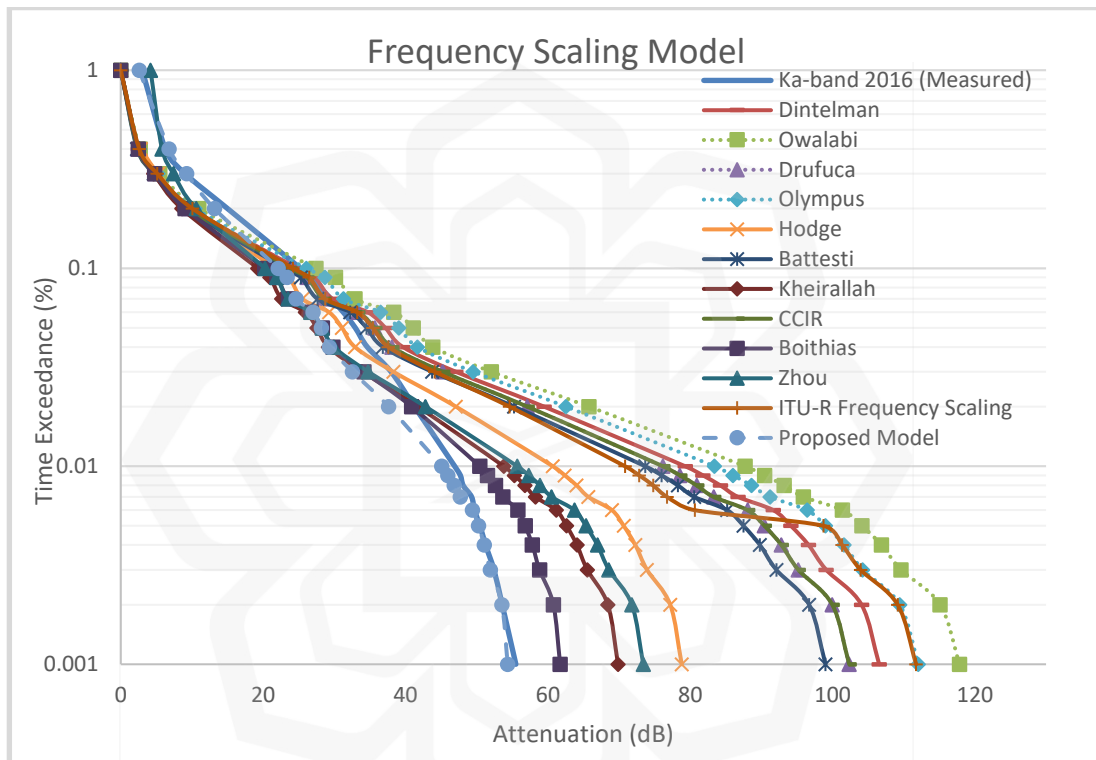


Figure 4.59 Comparison of the Derived Frequency Scaling Technique and Available Frequency Scaling Models, including ITU-R at Frequency Pair of Ka/Ku-band

All models were evaluated using the Root Means Square Error (RMSE) and Relative Error Analysis (ϵ). RMSE represents the average difference between the predicted values and the measured values. The RMSE equation is given in equation (4.9). At the same probability level, the percentage errors of ϵ between the measured

rain attenuation data ($A_{\%p}$, measured) and the model's predictions ($A_{\%p}$, predicted) are evaluated within the percentage interval of $0.001\% < P < 1\%$, shown as follows:

$$\text{Percentage error, } \varepsilon = (A_{\%p} \text{ predicted} - A_{\%p} \text{ measured}) / (A_{\%p} \text{ measured}) \times 100 [\%] \quad (4.8)$$

$$\text{RMSE} = \sqrt{\frac{\sum (P_i - M_i)^2}{n}} \quad (4.9)$$

Σ refers to the summation of the particular variable. P_i is the predicted value for the percentage of time exceedance in the percentage interval of $0.001\% < P < 1\%$. M_i is the measured value for the percentage of time exceedance in the percentage interval of $0.001\% < P < 1\%$. N is the number of samples in the percentage interval of $0.001\% < P < 1\%$.

Table 4.13 presents the error matrixes, which consist of the RMSE value and average relative percentage error. From the table, the percentage error and RMSE of the proposed frequency scaling model were the lowest as compared to previous models for all-time exceedance values. The proposed model produced an RMSE value of 2.8 and an average relative error of 11.3%. The measured rain attenuation at the Ka-band link was compared with the proposed model and previous models. These values are the lowest compared to other available models, including ITU-R. A lower RMSE value in a model will ensure a greater fit of measured data. The lowest number of statistical parameters implies that the best prediction model has been determined.

Table 4.13 RMSE and Percentage Error Obtained after Testing the Proposed Model over the Intervals [0.001% to 1%]

Model	Parameters	
	RMSE	ε (%)
Proposed Frequency Scaling Model	2.8	11.3

This result proves that the proposed model is more practical for use in tropical regions such as Malaysia. The frequency scaling model proposed by ITU-R can therefore be regarded as inaccurate for application in tropical regions since it has a high RMSE value and huge percentage error (28.3 and 28%, respectively). The newly proposed model achieves 88.7% accuracy, which is significantly higher compared to the frequency scaling technique proposed by ITU-R (only 72% accuracy).

The proposed model was further examined by forming a ratio of the predicted attenuation and measured attenuation at each percentage of exceedance, RMSE, and percentage error as compared to the recommended frequency scaling method from ITU-R. The ratio of predicted attenuation, A_{pre} (dB), to measured attenuation, A_{mea} (dB), for each percentage of time was calculated, as shown in the following equation:

$$S_i = A_{pre,I}/A_{mea,I} \quad (4.10)$$

S_i is the above ratio calculated for each percentage of time exceedance:

$$V_i = \ln S_i \times (A_{mea,I} / 10)^{0.2} \quad \text{for } A_{mea,I} < 10 \text{ dB} \quad (4.11)$$

$$V_i = \ln S_i \quad \text{for } A_{mea,I} \geq 10 \text{ dB} \quad (4.12)$$

The RMSE, ratio of S_i and percentage error values of the proposed model and ITU-R method are tabulated in Table 4.14. It can be seen from the table that for the rain attenuation dataset in the year 2016 at Cyberjaya, the RMSE and percentage error obtained from the new technique were significantly lower than the ITU-R model. The ITU-R frequency scaling calculation seems to be overestimating the measured values by almost double (at 0.003% and 0.001% of time exceedance). Therefore, it can be regarded that the proposed technique can be applied to predict rain attenuation in tropical regions. The results indicate that the newly derived model can produce better estimation values than the ITU-R recommendation 618-9.

Table 4.14 Comparison of Statistical Parameters between the Proposed Frequency Scaling Model and the ITU-R Frequency Scaling Method

Time Exceedance (%)	Ka-band (2016)	Proposed Frequency Scaling Model			FS ITU-R		
Statistical Parameter	Measured Attenuation (dB)	Predicted Attenuation (dB)	S_i	E(%)	Predicted Attenuation (dB)	S_i	E(%)
0.1	25.22	22.10	0.88	Predicted	24.20	0.96	70.74
0.05	32.95	28.18	0.86	52.59	35.41	1.07	74.53
0.03	37.97	32.57	0.86	47.79	44.09	1.16	78.13
0.02	41.26	37.64	0.91	49.94	54.62	1.32	91.11
0.01	46.91	45.07	0.96	49.16	70.85	1.51	104.11
0.005	50.47	50.25	1.00	49.08	98.75	1.96	145.19
0.003	52.42	51.91	0.99	46.60	103.95	1.98	145.87
0.002	53.59	53.55	1.00	46.34	109.15	2.04	150.11
0.001	55.51	54.35	0.98	42.41	111.75	2.01	145.81
RMSE value		2.98			36.56		

4.8 IMPLEMENTATION OF FREQUENCY SCALING TECHNIQUE FOR Q-BAND AND V-BAND

The proposed model has been applied to scale up attenuation at millimetre-wave (mm-wave) frequency bands, such as the Q-band (30 GHz) and V-band (40 GHz), for exceedance probabilities of 0.001% to 1%. The attenuation variations at different frequencies are portrayed in Figure 4.60.

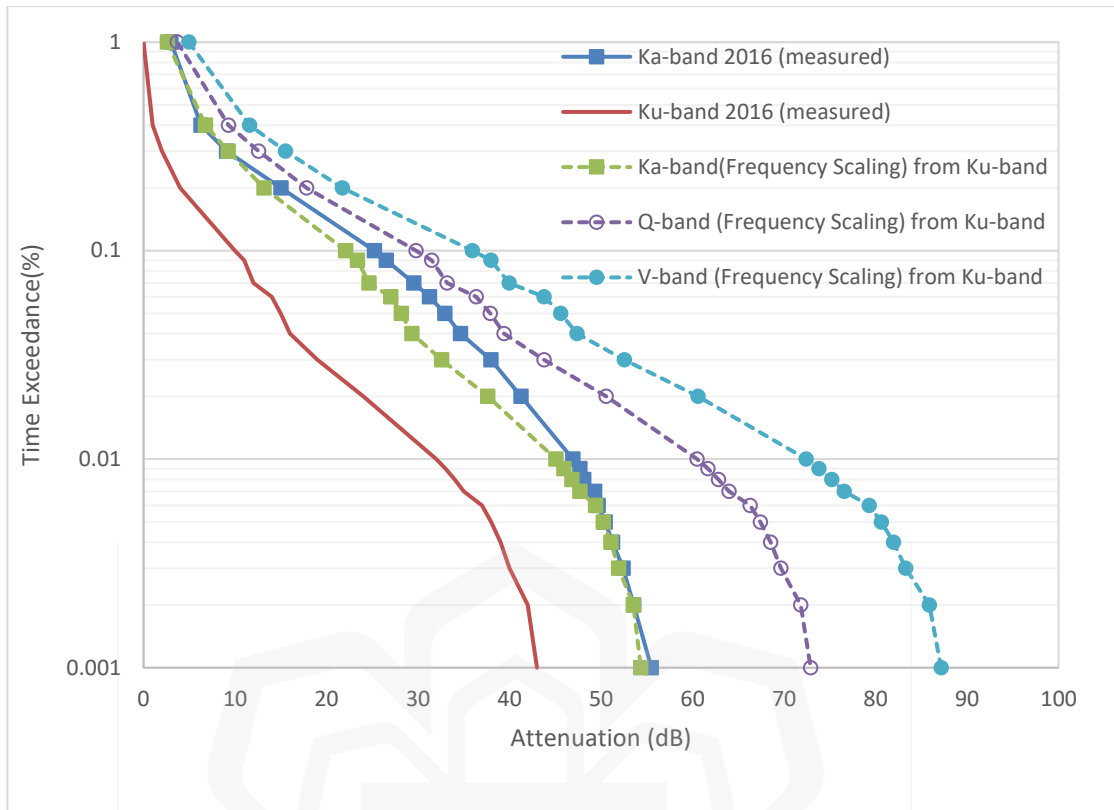


Figure 4.60 Scale-up of Ka, Q and V-band links using the Proposed Frequency Scaling Model

The summarised attenuation of Ku, Q and V-band at the desired time exceedance is shown in Table 4.15. At 0.1% of time exceedance, the estimated values of rain attenuation of both the Q-band and V-band are 29.73 dB and 41.68 dB, respectively. Malaysia is estimated to suffer frequent severe attenuation observed at the Q-band and V-band with attenuation values reaching up to 60.39 dB and 83.33 dB, respectively, at 99.99% of link availability in a year. In tropical regions with frequent heavy rain volumes such as Malaysia, it is expected that a larger fade margin is required to achieve high link availability.

The postulated signal loss values during rainfall at the Ka and Q-band in Cyberjaya were between 25.22 to 55.51 and 29.73 dB to 72.91 dB, respectively. The V-band is expected to suffer attenuation levels in the range of 35.94 dB to 87.17 dB. The findings strengthen the theory that mm-wave frequencies are very susceptible to rain. A

greater fade margin will be required to overcome rain attenuation, especially to obtain high link availability of 99.99% and above. The estimated fade margins that permit Q and V-band links to have better system performance at that level are 61 dB and 72 dB, respectively. The required fade margins at the desired time outage of Ku, Ka, Q and V-band links are presented in Table 4.15. Omotosho et al. (2017) suggested increasing the antenna power to counter the signal loss due to rainfall and achieve the desired link availability.

Table 4.15 Tabulated Values of Scaled Attenuation at Ka, Q and V-band links

Time Exceedance (%)	Measured Attenuation Value in the Year 2016 (dB)		Predicted Attenuation Value Proposed Frequency Scaling Model (dB)		
	Ku-band	Ka-band	Ka-band	Q-band	V-band
0.1	10	25.22	22.10	29.78	35.94
0.05	15	32.95	28.18	37.91	45.59
0.03	19	37.97	32.57	43.77	52.56
0.02	24	41.26	37.64	50.55	60.61
0.01	32	46.91	45.07	60.50	72.42
0.005	38	50.47	50.25	67.42	80.64
0.003	40	52.42	51.91	69.64	83.28
0.002	42	53.59	53.55	71.83	85.88
0.001	43	55.51	54.35	72.91	87.17

Nandi (2019) noted that rain attenuation greatly rises with the increase in frequency or path length. Rain attenuation is very high for mm-wave frequency bands, even for very low rain rates only applicable to short-distance communication.

Otomosho (2019) claimed that rain attenuation at 99.99% link availability is between 79.2 dB to 121.7 dB. At 99.9% link availability, the losses at the V-band were within the range of 20 dB to 41 dB. Badron (2014) also proposed a model that predicts rain attenuation at the V-band. At 0.1% and 0.01% of link availability, the rain attenuations were estimated to be 43.54 dB and 75.11, respectively. The value of the required fade margin for the V-band link proposed by the new model of frequency scaling is slightly lower than the values proposed by Otomosho (2019) and Badron (2014). Table 4.16 represents the comparison values of V-band rain attenuation at 99.9% and 99.99% of link availability between the existing model and the new model.

Table 4.16 Comparison Values of V-band Rain Attenuation at 99.9% and 99.99% of Link Availability Between the Existing Model and the New Model.

Link Availability (%)	Attenuation (dB)		
	Model		
	Otomosho (2019)	Badron (2014)	New model
99.9	20 to 41	43.54	35.94
99.99	79.2 to 121.7	75.11	72.42

4.9 VALIDATION OF THE PROPOSED FREQUENCY SCALING TECHNIQUE

The third objective of the study was fulfilled with the outcomes presented in this section. The model was validated using two rain attenuation datasets in Malaysia. The first dataset was Ka-band rain attenuation retrieved in Cyberjaya for the year 2015. Attenuation measured at the backup station in Rawang for the year 2016 was applied as

the second dataset. The assessment of the proposed model using the first dataset is shown in Figure 4.61.

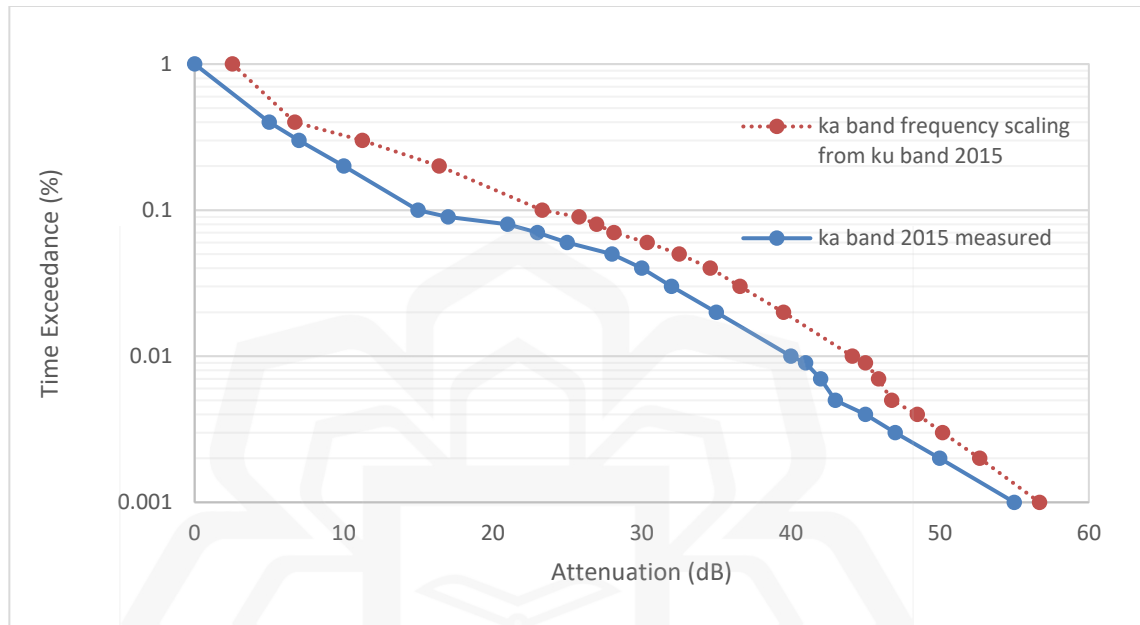


Figure 4.61 Comparison of Measured Rain Attenuation of the Proposed Model at Cyberjaya in 2015

The result of the proposed model was evaluated and weighed against the frequency scaling method recommended by the ITU-R model. From Table 4.17, it can be seen that the proposed model acquired a significantly lower RMSE value in contrast to the ITU-R model. The RMSE value of the derived technique is 4.56 as compared to the ITU-R value of 38.39.

Table 4.17 RMSE and Percentage Error Value of Rain Attenuation Predicted at Cyberjaya in the year 2015 using the Proposed Model

Link Availability (%)	Time Exceedance (%)	Measured (dB)	ITU-R Frequency Scaling Model (dB)	% Error	Proposed Model (dB)	% Error
99.9	0.1	15	26.48	161.52	23.39	140.92
99.95	0.05	28	44.09	129.46	32.57	88.31
99.97	0.03	32	52.54	132.19	36.65	82.54
99.98	0.02	35	58.75	132.85	39.56	78.04
99.99	0.01	40	68.86	132.15	44.18	70.45
99.995	0.005	43	74.80	130.95	46.83	65.91
99.997	0.003	47	98.75	163.11	50.25	59.91
99.998	0.002	50	106.55	163.10	52.73	55.46
99.999	0.001	55	119.54	162.35	56.74	48.17
	RMSE		26.48		4.56	

As shown in Figure 4.62, validations included the use of the second rain attenuation dataset from Rawang. At 0.1% of time exceedance, the predicted attenuation value was 22 dB, which is lower compared to the measured value of 31 dB. The predicted and measured attenuation values are 45 dB and 46 dB, respectively, once the time exceedance approached 0.01%. At 0.001% of time exceedance, the difference between the predicted and measured attenuation values was 3 dB.

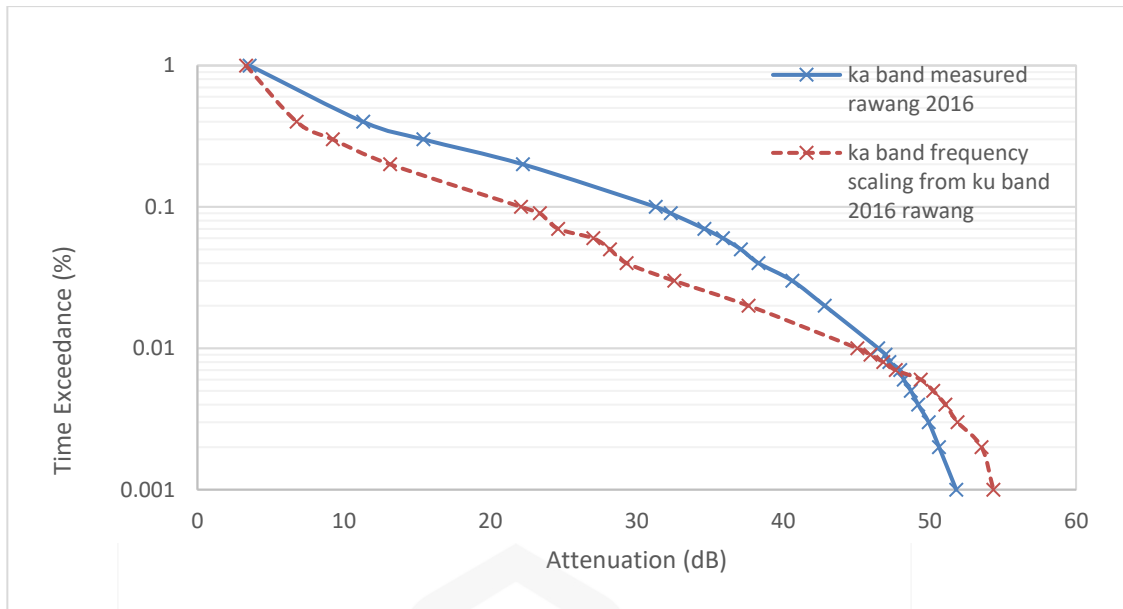


Figure 4.62 Comparison of Measured Rain Attenuation of the Proposed Model at Rawang in 2016

The RMSE and percentage error of the new prediction model were presented and compared with the frequency scaling method suggested by the ITU-R model in Table 4.18. From the table, it can be denoted that the RMSE value and percentage error of the proposed model was 5.57 and 47.75%, respectively. They are considerably lower in comparison to the ITU-R frequency scaling model.

Table 4.18 RMSE and Percentage Error Value of Rain Attenuation using the Proposed Model Predicted at Rawang in the year 2016

Time Exceedance (%)	Measured Ka-band Rain Attenuation at Rawang (dB)	ITU-R FS prediction	Error (%)	Rain Attenuation by Proposed Model (dB)	Error (%)
0.1	31.30	24.20	46.02	22.10	39.33
0.05	37.12	35.41	58.27	28.18	38.79
0.03	40.63	44.09	67.89	32.57	39.53
0.02	42.83	54.62	84.70	37.64	45.03
0.01	46.49	70.85	105.91	45.07	50.45
0.005	48.73	98.75	153.92	50.25	54.39
0.003	49.93	103.95	158.26	51.91	54.02
0.002	50.65	109.15	164.85	53.55	55.08
0.001	51.82	111.75	163.83	54.35	53.08
RMSE		38.34		5.57	

The future annual statistics of rain attenuation were estimated for the V-band link operating in Malaysia. The result was validated with the V-band rain attenuation data at Akure, Nigeria for a time availability of 99–99.99%. Nigeria is a tropical region with a wet climate. The rain height and annual rainfall volume are 4.75 km and 1314 mm, respectively. The rain attenuation data was obtained from Omotosho & Oluwafemi (2009). The data was retrieved from NigComSat-1 (Nigerian communication satellite) located at 42.5° E. The slant path length of rain attenuation of the V-band at Akure was denoted as 6.13 km, which is longer than Cyberjaya (5.32 km). The effective path length of rain attenuation of the V-band was 5.22 km, which is slightly longer than in Akure (4.59 km) (Badron, 2014). Attenuation is very dependable on effective path length.

The scaled-up rain attenuations at the V-band using the proposed model were plotted in Figure 4.63, together with the measured values at Akure. The results were

compared with ITU-R 618-13 rain attenuation prediction model to analyse the percentage error.

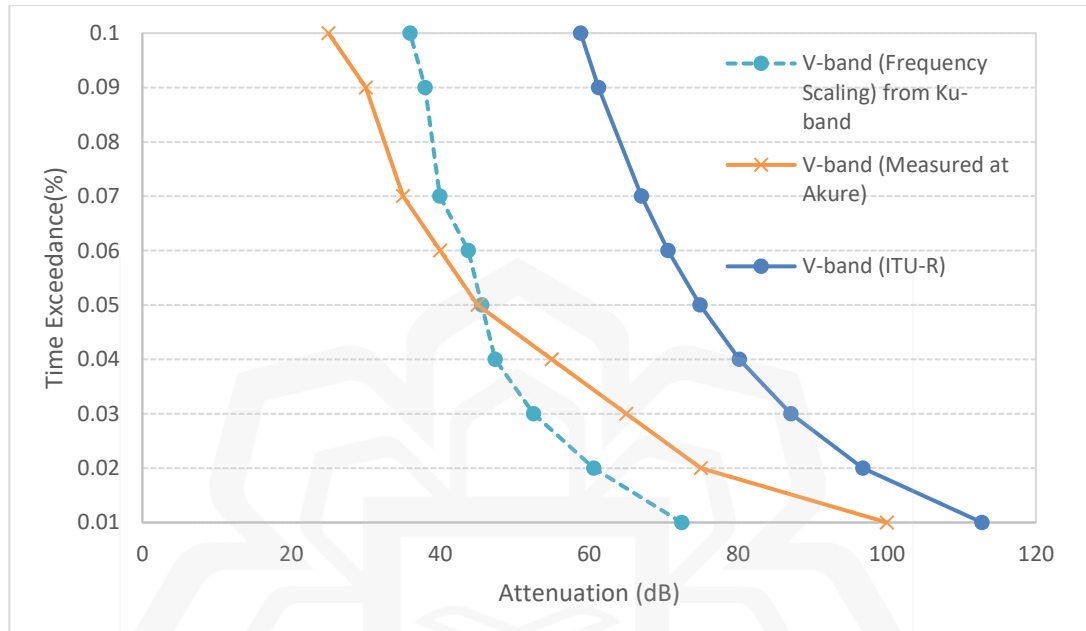


Figure 4.63 Comparison of the Proposed Model with the Measured Rain Attenuation at the V-band Link in Nigeria

The error analysis, including RMSE and average percentage error for specific time exceedance, is displayed in Table 4.19. The attained RMSE and average percentage error were 3.24 and 43.88%, respectively.

Table 4.19 RMSE and Average Percentage Error Value of Rain Attenuation at the V-band (40 GHz) Predicted in Nigeria using the Proposed Model

Time Exceedance (%)	Link Availability (%)	V-band (40 GHz)				
		Measured	ITU-R 618-13 Rain Attenuation Prediction	% Error	New model	% Error
0.1	99.9	25	58.86	210.46	35.94	118.75
0.09	99.91	30	61.25	174.16	37.98	96.59
0.07	99.93	35	67.02	156.47	39.96	79.16
0.06	99.94	40	70.61	136.52	43.76	69.40
0.05	99.95	45	74.90	121.44	45.59	56.32
0.04	99.96	55	80.20	90.82	47.39	31.16
0.03	99.97	65	87.08	68.97	52.56	15.86
0.02	99.98	75	96.76	54.01	60.61	5.81
0.01	99.99	100	112.76	12.76	72.42	27.58
RMSE			27.36		12.48	

The new frequency scaling model and the ITU-R model were compared using the RMSE analysis, as shown in Figure 4.64. Table 4.20 presents the percentage reduction of RMSE for the proposed frequency scaling model.

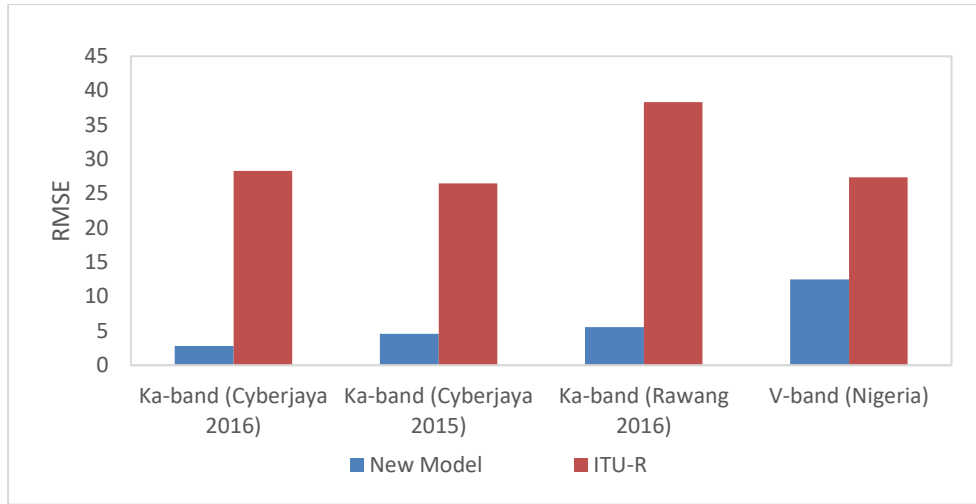


Figure 4.64 RMSE Comparison between the New Model and ITU-R model

Table 4.20 RMSE Percentage Improvement for the Ka-band using the Proposed Model as compared to the ITU-R Frequency Scaling Technique

	Ka-band (Cyberjaya 2016)	Ka-band (Cyberjaya 2015)	Ka-band (Rawang 2016)
New Model	2.8	4.56	5.57
ITU-R Frequency Scaling Technique	28.3	26.48	38.34
RMSE Improvement	90%	83%	85%

For all datasets, the improvement in the RMSE value is very large, approximately 80% to 90%. Table 4.21 represents the RMSE percentage improvement for estimating V-band rain attenuation using the proposed model as compared to the ITU-R rain attenuation prediction model.

Table 4.21 RMSE Percentage Improvement for Estimating V-band Rain Attenuation using the Proposed Model as compared to the ITU-R Rain Attenuation Prediction Model

	V-band (Nigeria)
New Model	12.48
ITU-R 618-13 Rain Attenuation Prediction Model	27.36
RMSE Improvement	54%

4.10 SUMMARY

This chapter deliberates the research findings that successfully achieved all the objectives. This section further discusses the results from the adopted methodologies. The research findings were highlighted concerning the attenuation characteristics due to heavy precipitation in tropical-equatorial regions. The findings of the measured rainfall rate in Cyberjaya as well as the rain attenuation for C, Ku and Ka-band frequencies were examined in terms of the CDF. Determining the required fade margin was obtained from the annual CDF for specific exceedance values. The first objective was satisfied by the CDF analysis results. The worst month statistics of rainfall rate and rain attenuation were also revealed. These elements are extremely essential in establishing high-quality communication networks. Severe signal degradation was expected to be in the worst month due to the high occurrence of rain events. The correlation between rainfall rate and rain attenuation for each frequency (C, Ku and Ka-band links) was accomplished to develop a new frequency scaling model. This successfully answered the second objective. The best prediction method was derived from a model that produced the lowest statistical parameter values when compared to the ITU-R and other available prediction methods. Attenuation at higher frequencies, such as Q-band and V-band, was also estimated using the proposed model. Validation methods were executed to establish a reliable model. The validation approach was

accomplished using datasets consisting of different years and locations throughout tropical regions. The validation step completes the last objective of this research. The results revealed an improvement in the frequency scaling technique which can be applied in tropical regions. The derived model can be considered the best prediction model since it has the lowest RMSE value (a value close to zero).



CHAPTER FIVE

DISCUSSION AND CONCLUSION

5.1 DISCUSSION

The results presented in previous Chapter Four are discussed in this section. The findings were guided by the five research questions highlighted in Chapter One. The discussion emphasized significant findings and their theoretical contributions as well as methodological influences on the existing body of knowledge on the satellite system's propagation effect. The accurate and reliable rain attenuation prediction methods are essential in the Earth-space telecommunication systems design.

In addressing the first research question, it had been identified from the study that the rainfall rate distribution at the ASTRO station varied from 89.8 mm/hr to 140 mm/hr throughout 2016. From the obtained annual CDF, the rainfall intensity at 0.01% of the time exceedance, $R_{0.01}$ was 103 mm/hr. The suggested value of $R_{0.01}$ by the ITU-R for tropical areas was 100 mm/hr which was lower than the measured value. Other previous research at a different location in tropical regions acquired a value of 126 mm/hr of $R_{0.01}$, which was also greater than ITU-R's recommendation (Ahmad, 2019). The statistical analyses of the rainfall intensity are important findings in studying the effect of signal attenuation on the satellite-Earth link during rainfall conditions.

From the study, it can be observed that accurate rainfall rates can be determined by deploying several rain gauges over a wide area. Future rain models should consider the inclusion involving the combination of different rain types such as convective and stratiform rain during rain events throughout the year. Most countries in tropical regions suffer frequent rain because many of them are water-logged areas. Such instances involve the evaporation of water from the sea and/or river. The monthly and annual CDF of rainfall rates less than 1% of time exceedance are presented and explained in

section 4.2. The value could be used to estimate the rain attenuation at various time exceedances using applicable prediction techniques in tropical climate areas including Cyberjaya.

To answer the second research question, the analyses involving the rain attenuations experienced by the C, Ku, and Ka-band beacon signals transmitted from MEASAT-3 and MEASAT-5 were carried out. The statistical characteristics were computed from the analysis to determine the required fade margin for links operating in tropical-equatorial regions. The methodologies involving measurement and data processing were elaborated on in Chapter Three. The monthly and annual CDFs of less than 1% unavailability for the C, Ku, and Ka-band are also presented in Section 4.2. The annual rain attenuation values at 0.01% time exceedance for the C and Ku-bands are 0.8 dB and 30 dB respectively. The attenuation amount of the C-band was small indicating that rain attenuation in tropical-equatorial regions was manageable for the C-band link. In contrast to C-band, Ku-band on the other hand suffered a larger rain attenuation with a value of 30 dB at the same time exceedance. The value of 30 dB loss corresponded to the 103 mm/hr of annual rainfall rate. The rain attenuation faced by the Ka-band was much more severe than Ku-band. It denotes that rain attenuation increased significantly with the increment of the frequency band. In the study, the time exceedance of 0.01% could not be compiled for the Ka-band. The rain attenuation value was capped at 0.05% of unavailability with a value of 33 dB. This was due to the saturation effect encountered by the receiver. The rain attenuation at the Ka-band had to be extrapolated to attain the desired value at 0.01% of time exceedance. The selected extrapolation technique offering the lowest RMSE was the second-degree polynomial.

The correlation between the measured rain attenuation and the rainfall rate distribution in Cyberjaya was carried out. It can be concluded that as the wavelength of the deployed frequency became shorter, the rain attenuation, therefore, became more severe. This was due to the absorption and a more intense scattering of the signal's particles. The latest ITU-R prediction model (ITU-R P.618-13, 2017) offered had underestimated the rain-induced attenuation values for Cyberjaya, as shown in Figure 4.35.

Dealing with research question three, applicable fade margins were determined from the rain attenuation annual CDFs for time exceedances of 0.10%, 0.30%, 0.01%, and

0.03%. The service availability of Quality of Service (QoS) requirements for Broadcast Satellite Services (BSS) applications is not less than 99.99% availability accordingly to the recommendation by MCMC. The QoS required for communication applications as recommended by ITU-R G.1028 is 99.9% of link availability. From the study involving the C, Ku and Ka-band link analysis, it had been determined that the required fade margins to operate at 99.99% of link availability were 0.8 dB, 30 dB, and 47 dB respectively. To achieve the QoS for communication services, the required fade margin values for Ku and Ka-band links were 8 dB and 25 dB correspondingly.

The findings concluded that when availability increases, the required rain fade margin also had to be increased. In future millimetre-wave frequency applications, these fade margin values are needed to be embedded in the design consideration to mitigate rain attenuation. Such analyses will provide wide-ranging ideas of rain attenuation to communication engineers and designers to facilitate a more relevant link budget for improved signal propagation. Mentioned elements in the previous paragraphs fulfilled the first research objective.

In specifying the best performance of a satellite link system, anticipated link margin values should be adequate to compensate for the rain attenuation. The underestimation of the fade margin would affect the link availability, while overestimation would inflict greater costs on investment. The best QoS and reliable signal availability for satellite link transmission can be obtained from proper planning. The implementation of fade mitigation techniques such as power control, diversity, coding, and resource sharing can also be taken into consideration to overcome the attenuation due to rain effects at higher frequency bands. The physical characteristic of a raindrop, rain height, statistics of rainfall, and geometrical parameters related to satellite information are essential elements in performing rain attenuation estimation.

To tackle the fourth research question as well as the second research objective, an alternative rain attenuation prediction technique was ascertained. The frequency scaling technique can be a reliable optional method to predict rain attenuation when there is no available meteorological data. The acquired findings from the evaluation of the previously available frequency scaling methods, including the ITU-R, indicated unreliable outcomes. This led to the motivation of the research and the derivation of a

new revised model. The new model was evaluated by using statistical parameters, such as RMSE and percentage error. It presented the smallest and lowest error values when compared with the earlier proposed models. The newly proposed model possessed an RMSE value of 2.8 and an average relative error of 11.3%. The frequency scaling recommended by the ITU-R 618.13 should be used with caution for predicting rain attenuation in tropical regions as it produces an extra-large value of RMSE and error.

In achieving the third objective, a new frequency scaling model proposed in the study was validated with various datasets in the evaluation of the RMSE and percentage error. The model showed a great improvement of 80% to 90% in the percentage of RMSE reduction compared to the frequency scaling method recommended by ITU-R, as well as the rain attenuation prediction model of ITU-R. The best model should be the one with the smallest number of statistical parameters as well as the least percentage error. As for the fifth research question, the study established a newfound frequency scaling model that can considerably improve the prediction of rain attenuation for satellite communication links in tropical regions.

5.2 CONCLUSION AND FUTURE WORKS

In conclusion, reliable fade margins are crucial elements in rain attenuation studies on satellite-Earth link communication. This is applicable in applying the best mitigation technique with an economically viable cost. The fade margin derived from annual CDF is essential in providing information concerning the suitable and reliable fade margin to be adapted in the higher frequencies' communication link designs. This study significantly contributes to the improvement in achieving desired link availability for telecommunication as well as a broadcasting application in heavy frequent rainfall areas. The rainfall characteristics in tropical regions are different from those of temperate regions due to geographical location.

The correlations between rainfall rate and rain attenuation at C, Ku, and Ka-band were conducted. It is noted that the rain attenuation is strongly dependent on the operating frequency except for the C-band. Rain attenuation detected at C-band is very small and can be neglected. Rain attenuations at Ku-band and above are severe and very significant as they degraded the satellite system performance. In tropical regions, high rainfall volume throughout the year and severe rain-induced attenuation are the big challenges in implementing frequencies above 10 GHz. Throughout the study that had been conducted, several recommendations are offered for future works in contributing new knowledge involving rain attenuation prediction for the satellite-Earth link.

For future works, it is recommended that more measurements at different frequencies above 10 GHz with different rain characteristics should be made available. It is recognized that tropical regions experience heavy rainfall volume throughout the year with a combination of stratiform and convective rain. The understanding of the physics of rain and accurate characterization of rain that produces the impairment also need to be enhanced. Future research on satellite-Earth propagation that concerns the effect of different types of rain can produce a highly accurate model. Extensive data is required for the development of satisfactory physically based models for prediction with the variety of rain events to be characterized. A comprehensive study on the investigation of relevant rain height in tropical areas with a different drop size distribution of rain can be explored. It is envisaged that the inclusion of these future findings can significantly improve the accuracy of rain attenuation estimation for satellite communications systems in tropical regions.

REFERENCES

- Abdulrahman, Y., Rahman, T. A., Islam, R. M., Olufeagba, B. J., & Chebil, J. (2015). Comparison of measured rain attenuation in the 10.982-GHz band with predictions and sensitivity analysis. *International Journal of Satellite Communications and Networking*, 33 (3), 185–195.
- Abubakar, I., Din, J. Bin, Yin, L. H., & Alhilali, M. (2019). Rain attenuation in broadband satellite service and worst month analysis. *Indonesian Journal of Electrical Engineering and Computer Science*, 15 (3), 1443–1451.
- Acharya, R. (2017). Tropospheric impairments: Measurements and mitigation. *Satellite Signal Propagation, Impairments and Mitigation*, Academic Press, 195–245.
- Acharya, R. (2019). A simple real-time frequency scaling technique for rain attenuation and its performance. *International Journal of Satellite Communications and Networking*, 38 (4), 329–340.
- Afahakan, I. E., Udofia, K. M., & Umoren, M. A. (2016). Analysis of Rain Rate And Rain Attenuation for Earth- Earth - Space Communication Links over Uyo - Akwa Ibom State. *Nigerian Journal of Technology (NIJOTECH)*, 35 (1), 137–143.
- Ahmad, Y. A. (2019). Determination of specific attenuation for satellite links in equatorial-tropical region. Kulliyyah of Engineering, International Islamic University Malaysia.
- Ahmad, Y. A., Ismail, A. F., & Badron, K. (2019). Two-Year Rain Fade Empirical Measurement and Statistics of Earth-Space Link at Ka-Band in Malaysia. *ASM Science Journal*, 12 (2), 35–46.
- Ahmad, Y. A., Suhaimi, N. H. S., Ismail, A. F., & Badron, K. (2022). Assessment of Monthly Rain Fade in the Equatorial Region at C & Ku-band Using MEASAT-3 Satellite Links. *Lecture Notes in Electrical Engineering*, 829 LNEE, 72–79.
- Al-Saman, A. M., Cheffena, M., & Ai, Y. U. N. (2020). Statistical Analysis of Rain at Millimeter Waves in Tropical Area. *IEEE Access*, 8, 51044–51061.
- Al-Samman, A. M., Mohamed, M., Ai, Y., Cheffena, M., Azmi, M. H., & Rahman, T. A. (2020). Rain Attenuation Measurements and Analysis at 73 GHz E-Band Link in Tropical Region. *IEEE Communications Letters*, 24 (7), 1368–1372.
- Albendag, A. A. M., & Zain, A. F. M. (2020). Improving the estimation of the Earth-space link in the ITU rain attenuation model. *ACM International Conference Proceeding Series*, March.
- Athanasios D. Panagopoulos, Pantelis-Daniel M. Arapoglou, A. P. G. C. (2004).

Satellite Communications at Propagation Impairments and Ku, Ka, And V Bands: Mitigation Techniques. *IEEE Communications Surveys & Tutorials*, 2–14.

- Badron, K., Ismail, A. F., Asnawi, A. L., Malek, N. F. A., Abidin, S. Z., & Islam, M. R. (2015). Estimations of fade margin for the new Malaysian MEASAT-3B Ku-band link. *Lecture Notes in Electrical Engineering*, 344, 95–103.
- Badron, K., Ismail, A. F., Din, J., & Tharek, A. R. (2011). Rain-induced attenuation studies for V-band satellite communication in tropical regions. *Journal of Atmospheric and Solar-Terrestrial Physics*, 73 (5–6), 601–610.
- Badron, K., Ismail, A. F., Islam, M. R., Abdullah, K., Din, J., & Tharek, A. R. (2015). A modified rain attenuation prediction model for tropical V-band satellite earth link. *International Journal of Satellite Communications and Networking*, 33 (1), 57–67.
- Bahri, R., Hosseini, S. H. M., Mohammadi, L., & Yarmohammadi, H. (2013). Rain Attenuation Prediction at Ku Band Using Satellite Signal Beacon Measurement in Iran. *AUT Journal of Electrical Engineering*, 45 (2), 29-42.
- Baldotra, A. K., & Hudiara, I. S. (2004). Rain attenuation statistics over terrestrial microwave link at 19.4 GHz at Amritsar. *IEEE Transactions on Antennas and Propagation*, 52 (6), 1505-1508, June 2004.
- Bertorelli, S., & Paraboni, A. (2007). Modelling of short-term frequency scaling for rain attenuation using ITALSAT data. *International Journal of Satellite Communications and Networking*, 25 (3).
- Brisseau, O., Mallet, C., Barthes, L., & Marsault, T. (2006). Frequency scaling of rain attenuation based on microphysical characteristics for SatCom links. *IEEE Proceedings: Microwaves, Antennas and Propagation*, 153 (6), 523–532.
- Brisseau, Olivier, Barthes, L., Mallet, C., & Marsault, T. (2003). Effect of microphysical characteristics of rain on frequency scaling in the microwave band. *International Geoscience and Remote Sensing Symposium (IGARSS)*, 7 (C), 4121–4125.
- Chakraborty, S., Chakraborty, M., & Das, S. (2021). Experimental Studies of Slant-Path Rain Attenuation Over Tropical and Equatorial Regions. *IEEE Antennas & Propagation Magazine*, March 2020.
- Choi, M. A. S. and D.-Y. (2021). Scaling of Rain Attenuation Models: A Survey. *Journal of Applied Sciences*, 18 (11).
- Christensen, J. (2012). ITU Regulations for Ka-band Satellite Networks. *30th AIAA International Communications Satellite System Conference (ICSSC)*, 1–8.
- COST project 205. (2011). Influence of the atmosphere on radio propagation on satellite earth paths at frequencies above 10 GHz. *Commission Of The European*

Communities (3).

- Cuervo, Felix, Lam, H. Y., Din, J. Bin, Castro, J. R., Schmidt, M., & Schonhuber, M. (2017). The JOANNEUM RESEARCH SatCom Ka and Q band campaigns in Europe and Malaysia. *2017 11th European Conference on Antennas and Propagation, EUCAP 2017*, 1476–1480.
- Cuervo, Felix, Plimon, K., Schonhuber, M., Martellucci, A., & Castro, J. R. (2016). Alphasat Aldo Paraboni propagation experiment in Graz - Frequency scaling analysis. *2016 10th European Conference on Antennas and Propagation, EuCAP 2016*, 1–5.
- Cuervo, Félix, Schönhuber, M., Capsoni, C., Yin, L. H., Jong, S. L., Din, J. Bin, & Martellucci, A. (2016). Ka-band propagation campaign in Malaysia - First months of operation and site diversity analysis. *2016 10th European Conference on Antennas and Propagation, EuCAP 2016*.
- Dao, H., Islam, md rafiquel, Khalid, A., & Sheroz, K. (2011). Preliminary Analysis of Ku-Band Rain Fade Data for Earth to-Satellite Path Measured in Malaysia. *2011 IEEE 10th Malaysia International Conference on Communications, Sabah, Malaysia, 2011*, 93-96,
- Das, D., & Maitra, A. (2015). Journal of Atmospheric and Solar-Terrestrial Physics Rain attenuation prediction during rain events in different climatic regions. *Journal of Atmospheric and Solar-Terrestrial Physics*, 128, 1–7.
- Das, S., Maitra, A., & Shukla, A. (2010). Rain attenuation modelling in the 10-100 GHz frequency using drop size distributions for different climatic zones in tropical India. *Progress In Electromagnetics Research B*, June 2014.
- Das, S., Maitra, A., & Shukla, A. K. (2013). Diurnal variation of slant path Ka-band rain attenuation at four tropical locations in India. *Indian Journal of Radio & Space Physics*, 42 (February), 34–41.
- De, A., & Maitra, A. (2020). Radiometric Measurements of Atmospheric Attenuation Over a Tropical Location. *American Geophysical Union*, 55 (10), 0–2.
- Durodola, O., Ojo, J., & Ajewole, M. (2017). Characterization of Worst Month Statistics for Satellite-Earth Links Performance in Tropical Locations. *Physical Science International Journal*, 13 (3), 1–9.
- Ebert, J., Plimon, K., Schmidt, M., & Rivera-Castro, J. (2015). Measurement of instantaneous frequency scaling for Q/V-band. *2015 9th European Conference on Antennas and Propagation, EuCAP 2015*, 7–10.
- El-Shami, I. F., Lam, H. Y., Din, J., & Jong, S. L. (2015). Clear sky diurnal behaviour of tropospheric scintillation at Ku-band satellite communication in equatorial Malaysia. *Jurnal Teknologi*, 77 (10), 25–33.

- El-shami, I. F., Yin, L. H., Din, J., Elgayar, A. I., & Alhilali, M. (2018). Tropospheric scintillation with rain attenuation of Ku band at tropical region. *Telkomnika (Telecommunication Computing Electronics and Control)*, 16 (5), 1982–1987.
- Elbert, B. R. (2008). *Introduction to Satellite Communication*. Third Edition. Artech.
- Fadilah, N., & Pratama, R. (2018). Comparison of rain attenuation estimation in high frequency in Indonesia region for LAPAN communication satellite. *Journal of Physics: Conference Series*, 1130 (1).
- Ghanim, M., Alhilali, M., Din, J., & Lam, H. Y. (2018). Rain attenuation statistics over 5G millimetre wave links in Malaysia. *International Conference on Electrical Engineering, Computer Science and Informatics (EECSI), 2018-October*, 266–269.
- Grabner, M., Fiser, O., Pek, V., Pechac, P., & Valtr, P. (2017). Analysis of one-year data of slant path rain attenuation at 19 and 39 GHz in Prague. *2017 11th European Conference on Antennas and Propagation, EUCAP 2017*, 2361–2364.
- Green, H. E. (2004). Propagation impairment on Ka-band SATCOM links in tropical and equatorial regions. *IEEE Antennas and Propagation Magazine*, 46 (2), 31–45.
- Hassan, M. R., Islam, M. R., Habaebi, M. H., Alam, M. M., Suriza, A. Z., Badron, K., & Basahel, A. (2021). Time Diversity Analysis Based on Predicted Rain Attenuation at Ku, Ka and V-Bands using Synthetic Storm Technique. *Proceedings of the 8th International Conference on Computer and Communication Engineering, ICCCE 2021, 1*, 401–405.
- Haule, P., Iddi, H., & Kissaka, M. (2019). Rain attenuation distribution for satellite microwave links application in Tanzania. *Indonesian Journal of Electrical Engineering and Computer Science*, 17 (2), 982–987.
- Hidayat, S., Ramdani, T., Alam, I. F., Sfenrianto, S., & Kaburuan, E. R. (2019). The Role of High Throughput Satellite as Sky Highway Infrastructure to Support The Acceleration of Internet. *International Journal of Mechanical Engineering and Technology (IJMET)*, 10 (03), 1447–1455.
- Hodge, D. B. (1977). Frequency Scaling of Rain Attenuation. *IEEE Transactions on Antennas and Propagation*, 25 (3), 446–447.
- IEEI. (2014). *IEEI __ World Map*. Retrieve from <https://www.ieei.com/worldmap.shtml>.
- IEEE (2002). IEEE Standard Letter Designations for Radar-Frequency Bands. *IEEE Std 521-2002 (Revision of IEEE Std 521-1984)*, 1-10, 8 Jan. 2003.
- Igwe, K. C., Oyedum, O. D., Ajewole, M. O., & Aibinu, A. M. (2019). Evaluation of some rain attenuation prediction models for satellite communication at Ku and Ka bands. *Journal of Atmospheric and Solar-Terrestrial Physics*, 188 (February), 52–

61.

- IRCC. (1986). *RECOMMENDATIONS AND REPORTS OF THE CCIR*. Retrieve from <https://www.itu.int/en/history/Pages/AssemblyRadio.aspx?conf=4.281>.
- Islam, Chebil, J., & Tharek, A. R. (1999). Frequency Scaling of Rain Attenuation From 23- to 38-GHz Microwave Signals Measured in Malaysia. *Asia Pacific Microwave Conference. APMC'99. Microwaves Enter the 21st Century. Conference Proceedings*.
- Islam, M R, Rahman, T., Khan, S., Khalifa, O., & Rashid, M. M. (2004). The Rain Attenuation Prediction Methods from 10- To 37-GHz Microwave Signals Based on Data Measured in Malaysia. *3rd International Conference on Electrical & Computer Engineering, December, 28–30*.
- Islam, Md R., Rahman, T. A., & Karfaa, Y. (2003). Worst-month rain attenuation statistics for radio wave propagation study in Malaysia. *APCC 2003 - 9th Asia-Pacific Conference on Communications, in Conjunction with 6th Malaysia International Conference on Communications, MICC 2003, Proceedings, 3, 1066–1069*.
- Islam, Md Rafiqul, Ali Hussein Budalal, A., Habaebi, M. H., Badron, K., & Ismail, A. F. (2017). Performance analysis of rain attenuation on earth-to-satellite microwave links design in Libya. *IOP Conference Series: Materials Science and Engineering, 260 (1)*.
- Islam, R. M., Abdulrahman, Y. a, & Rahman, T. a. (2012). An improved ITU-R rain attenuation prediction model over terrestrial microwave links in tropical regions. *EURASIP Journal on Wireless Communications and Networking, 2012 (1), 189*.
- Ismail, A. F., Badron, K., Yaccop, A. A. H., & Yao, Y. D. (2013). Determination of Ku-band specific attenuation parameters based on measurements in the tropics. *IEEE Antennas and Propagation Society, AP-S International Symposium (Digest), 2008–2009*.
- Ismail, A. F., Rashid, N. E. A., Din, J., Tharek, A. R., & Islam, M. R. (2012). Analyses of worst-month rain fade statistics for Ku-band (26GHz) in the tropics. *2012 7th International Conference on Telecommunication Systems, Services, and Applications, TSSA 2012, 14–17*.
- ITU-R P.618-13. (2017). *Recommendation ITU-R P.618-13 Propagation data and prediction methods required for the design of Earth-space telecommunication systems. 13*. Retrieve from <http://www.itu.int/ITU-R/go/patents/en>.
- ITU-T G.1028. (2016). *End-to-end quality of service for voice over 4G mobile networks*. Retrieve from <https://www.itu.int/itu-t/recommendations/rec.aspx?rec=12748>
- Jalel Chebil, T. A. R. (2003). Study Of Worst-Month Rain Statistic Effect On

Radiowave Propagation In Malaysia. *APCC 2003 - 9th Asia-Pacific Conference on Communications, in conjunction with 6th Malaysia International Conference on Communications, MICC 2003, Proceedings*, 3 (March 2015).

- Jong, S. L., Lam, H. Y., D'Amico, M., Cuervo, F., Yunus, M. M., & Din, J. (2017). Impact of link elevation angles on rain attenuation statistics in heavy rain region predicted using the synthetic storm technique. *Journal of Telecommunication, Electronic and Computer Engineering*, 9 (3–8), 17–20.
- Jong, S. L., Lam, H. Y., Din, J., & D'Amico, M. (2015). Investigation of Ka-band satellite communication propagation in equatorial regions. *ARPN Journal of Engineering and Applied Sciences*, 10 (20), 9795–9799.
- Kalaivaanan, P. M., Sali, A., Raja Abdullah, R. S. A., Yaakob, S., Jit Singh, M., & Al-Saegh, A. M. (2020). Evaluation of Ka-band rain attenuation for satellite communication in tropical regions through measurement of multiple antenna sizes. *IEEE Access*, 8, 18007–18018.
- Kamruzzaman, M., & Islam, M. S. (2014). Rain attenuation prediction for satellite communications link at Ku and Ka bands over Bangladesh. *1st International Conference on Electrical Engineering and Information and Communication Technology, ICEEICT 2014*.
- Karagiannis, G. A., Panagopoulos, A. D., & Kanellopoulos, J. D. (2013). Short-term rain attenuation frequency scaling for satellite up-link power control applications. *IEEE Transactions on Antennas and Propagation*, 61 (5).
- Kestwal, M. C., Joshi, S., & Garia, L. S. (2014). Prediction of rain attenuation and impact of rain in wave propagation at microwave frequency for tropical regions (Uttarakhand, India). *International Journal of Microwave Science and Technology, 2014*.
- Khairolanuar, M. H., Ismail, A. F., Badron, K., Jusoh, A. Z., Islam, M. R., & Abdullah, K. (2015). Assessment of ITU-R predictions for Ku-Band rain attenuation in Malaysia. *ISTT 2014 - 2014 IEEE 2nd International Symposium on Telecommunication Technologies*, 389–393.
- Kheirallah, H. N., KNIGHT, J. P., SEGAL, R. L., S., O. K., & B., M. (1980). Frequency Dependence of Effective Path Length in Prediction of Rain Attenuation. *Electronics Letters*, 16 (12), 448–450.
- Kubista, E., Fontan, F. P., Castro, M. A. V., Buonomo, S., Arbesser-Rastburg, B. R., & Baptista, J. P. V. P. (2000). Ka-band propagation measurements and statistics for land mobile satellite applications. *IEEE Transactions on Vehicular Technology*, 49 (3), 973–983.
- Kvicera, V., Grabner, M., & Fiser, O. (2012a). Frequency and path length scaling based on long-term statistics of rain attenuation on terrestrial paths at 38 GHz and 58 GHz. *Proceedings of 6th European Conference on Antennas and Propagation*,

EuCAP 2012, 497–499.

- Kvicera, V., Grabner, M., & Fiser, O. (2007). Frequency and polarization scaling of rain attenuation on 58 and 93 GHz terrestrial links. *Proceedings of the 37th European Microwave Conference, EUMC, December 2005*, 759–762.
- Kvicera, V., Grabner, M., & Fiser, O. (2012b). Frequency scaling of rain attenuation based on 4-year statistics obtained on two parallel terrestrial paths at 58 GHz and 93 GHz. *European Microwave Week 2012: “Space for Microwaves”, EuMW 2012, Conference Proceedings - 7th European Microwave Integrated Circuits Conference, EuMIC 2012*, 932–935.
- Lam, H. Y., Luini, L., Din, J., Capsoni, C., & Panagopoulos, A. D. (2010). Application of the SC EXCELL model for rain attenuation prediction in tropical and equatorial regions. *2010 IEEE Asia-Pacific Conference on Applied Electromagnetics, APACE 2010 - Proceedings*, May 2014.
- Lam, Hong Yin, Din, J., & Jong, S. L. (2015). Statistical and Physical Descriptions of Raindrop Size Distributions in Equatorial Malaysia from Disdrometer Observations. *Advances in Meteorology*. 2015. 1-14.
- Laster, J.D., & Stutzman, W. L. (1995). Frequency Scaling of Rain Attenuation for Satellite Communication Links. *IEEE Transactions on Antennas and Propagation*, 43 (11), 1207.
- Lee, Y. H., & Winkler, S. (2011). Effects of Rain Attenuation on Satellite Video Transmission. *2011 IEEE 73rd Vehicular Technology Conference (VTC Spring)*.
- Lin, D. P., & Chen, H. Y. (2002). An empirical formula for the prediction of rain attenuation in the frequency range 0.6-100 GHz. *IEEE Transactions on Antennas and Propagation*, 50 (4), 545–551.
- Luini, L., Panzeri, A., & Riva, C. G. (2021). Frequency Scaling Model for the Prediction of Total Tropospheric Attenuation Time Series at EHF. *IEEE Transactions on Antennas and Propagation*, 69 (3), 1569–1580.
- Lutz, E., Bischl, H., Ernst, H., Giggenbach, D., Holzbock, M., Jahn, A., & Werner, M. (2004). Development and future applications of satellite communications. *IEEE International Symposium on Personal, Indoor and Mobile Radio Communications, PIMRC*, 4, 2342–2346.
- Lwas, A. K., Islam, R., Habaebi, M. H., Mandeep, S. J., Ismail, A. F., Daoud, J. I., & Zyoud, A. (2015). A Modified Effective Path Length for Predicting Penang-Malaysia. *ARPN Journal of Engineering and Applied Sciences*, 10 (21), 10096–10100.
- Lyras, N. K., Kourogiorgas, C. I., Panagopoulos, A. D., & Rutherford, S. (2016). Rain Attenuation Statistics at Ka and Q band in Athens using SST and Short Scale Dynamic Diversity Gain Evaluation. *2016 Loughborough Antennas &*

Propagation Conference (LAPC), 2–6.

- Malinga, S. J., Owolawi, P. a, & Afullo, T. J. O. (2013). Estimation of Rain Attenuation at C, Ka, Ku and V Bands for Satellite Links in South Africa. *Proceedings of PIERS in Taipei*, March 25-28, 2013.
- Mandeep, J. S. (2009). Slant path rain attenuation comparison of prediction models for satellite applications in Malaysia. *Journal of Geophysical Research Atmospheres*, 114 (17), 1–12.
- Mandeep, J. S., Hassan, S. I. S., & Tanaka, K. (2008). Rainfall measurements at Ku-band satellite link in Penang, Malaysia. *IET Microwaves, Antennas and Propagation*, 2 (2), 147–151.
- Mandeep, J. S., Hui, O. W., Abdullah, M., Tariqul, M., Ismail, M., Suparta, W., Yatim, B., Menon, P. S., & Abdullah, H. (2011). Modified ITU-R rain attenuation model for the equatorial climate. *2011 IEEE International Conference on Space Science and Communication: "Towards Exploring the Equatorial Phenomena", IconSpace 2011 - Proceedings*, July, 89–92.
- Mandeep, J. S., & Ng, Y. Y. (2008). The worst month analysis of ka-band in Penang, Malaysia. *Journal of Electromagnetic Waves and Applications*, 22 (17–18), 2373–2378.
- Mandeep, J. S., Ng, Y. Y., Abdullah, H., & Abdullah, M. (2010). The study of rain specific attenuation for the prediction of satellite propagation in Malaysia. *Journal of Infrared, Millimeter, and Terahertz Waves*, 31 (6), 681–689.
- Mao, Z. (2021). Basic Principles of Microwave Communication. *Journal of Physics: Conference Series*.
- Maruddani, B., Kurniawan, A., Sugihartono, & Munir, A. (2014). Prediction method for rain rate and rain propagation attenuation for K-band satellite communications links in Tropical areas. *Journal of ICT Research and Applications*, 8 (2), 85–96.
- Marzuki, Hashiguchi, H., Shimomai, T., & Randeu, W. L. (2016). Cumulative distributions of rainfall rate over Sumatra. *Progress In Electromagnetics Research M*, 49 (July 2016), 1–8.
- Matricciani, E., & Paraboni, A. (1985). Instantaneous Frequency Scaling of Rain Attenuation at 11.6-17.8 GHz with SIRIO Data. *IEEE Transactions on Antennas and Propagation*, 33 (3), 335–337.
- MCMC. (2022). *Malaysian Communications And Multimedia Commission (MCMC) – Suruhanjaya Komunikasi dan Multimedia Malaysia (SKMM) - Quality of Service*. Retrieve from <https://www.mcmc.gov.my/en/sectors/broadcasting/quality-of-service>.
- MEASAT. (2022). *Satellite Details - MEASAT*. Retrieve from <http://www.measat.com/>

satellite-details/.

- Mishra, M. K., Renju, R., Mathew, N., Suresh Raju, C., Sujimol, M. R., & Shahana, K. (2020). Characterization of GSAT-14 Satellite Ka-Band Microwave Signal Attenuation Due to Precipitation Over a Tropical Coastal Station in the Southern Peninsular Region of the Indian Subcontinent. *Radio Science*, 55 (2), 0–3.
- Mitra, M. (2008). Advanced Satellite Communications Systems & Services. *Academic Journal of Engineering Studies*, January, 513–516.
- MMD. (2016). *Malaysian Meteorological Department*. Retrieve from <https://www.met.gov.my/penerbitan/laporan-tahunan/>
- Mohamed, N. E., & Nadir, Z. (2005). Microwave attenuation studies due to rain for communication links operating in Malaysia. *Georgian Electronic Scientific Journal: Computer Science and Telecommunications*, January.
- Mom, J., Tyokighir, S., & Igwe, G. (2021). Modification of the ITU-R P . 530-17 Rain Attenuation Prediction Model. *International Journal of Engineering Research & Technology (IJERT)*, 10 (09), 119–125.
- Momin, M., Alam, M. M., Hasan Mahfuz, M. M., Islam, M. R., Hadi Habaebi, M., & Badron, K. (2021). Prediction of Rain Attenuation on Earth-To-satellite Link using Rain Rate Measurement with Various Integration Times. *Proceedings of the 8th International Conference on Computer and Communication Engineering, ICCCE 2021*, 385–390.
- Montera, L. De, Mallet, C., & Barth, L. (2008). Short-term prediction of rain attenuation level and volatility in Earth-to-Nonlinear Processes in Geophysics Short-term prediction of rain attenuation level and volatility in Earth-to-Satellite links at EHF band. *Nonlinear Processes in Geophysics*, May 2014.
- Mustafa, K., Arzu, K., & Cennet, O. (2017). Ecosystem-Based Approach to Combat Drought and Desertification and Their Relation with Rural Development. In *Current Trends in Science and Landscape Management* (Issue January, 319–342).
- Nalinggam, R., Ismail, W., & Mandeep, J. S. (2012). Rain-induced attenuation for Ku-band satellite communications in the west coast of Peninsular Malaysia, Penang. *Annales Des Telecommunications/Annals of Telecommunications*, 67 (11–12), 569–573.
- Nazrul, M., Nordin, H., Yih, L. E. E. C., & Mahmoudbeik, A. (2013). Analysis of Rain Attenuation Model for Ku Band in Cameron Highland, Malaysia 2 Literature Review. *Recent Advances in Automatic Control, Information and Communications Analysis*, 287–290.
- Nizhanthi, T. S. P. and T. (2012). A Study on The Effects of Rain Attenuation For an X-Band Satellite System over Malaysia. *Progress In Electromagnetics Research B*, 45 (August), 37–56.

- Nuroddin, A. C. M., Ismail, A. F., Badron, K., Zulkurnain, N. F., Ismail, M., & Salim, H. (2013). Rain-induced attenuation studies using RazakSAT space-earth links. *International Conference on Space Science and Communication, IconSpace, July*, 402–406.
- Ojo, J. S., Ajewole, O., & Sarkar, S. K. (2008). Rain rate and rain attenuation prediction for Satellite Communication in Ku and Ka Bands Over Nigeria. *Progress In Electromagnetics Research B*, 5, 207–223.
- Ojo, J. S., & Rotimi, O. C. (2015). Diurnal and Seasonal Variations of Rain Rate and Rain Attenuation on Ku-Band Satellite Systems in a Tropical Region : A Synthetic Storm Techniques Approach. *Journal of Computer and Communications, April*, 1–10.
- Oluwayemisi, O. O., Victor, O. T., Akinloye, A. S., Oladimeji Mustapha, A., Eterigho, E. M., & Adenike, B. (2019). Proposed Model for the Estimation of Rain Attenuation: At Ku-Band at Ota, a Tropical Location. *International Conference on Space Science and Communication, IconSpace, 2019-July(July)*, 172–176.
- Oluwayemisil, O. O., Victor, O. T., Mustapha, A. O., Akinloye, A. S., Moses Eterigho, E., & Adenike, B. (2019). Rainfall Attenuation Measurement at Ota, a Tropical Location. *International Conference on Space Science and Communication, IconSpace, 2019-July(July)*, 91–95.
- Omosho, T. V, Akinwumi, S. A., Ometan, O. O., Adewusi, M. O., & Mandeep, J. S. (2017). Earth-Space Rain Attenuation Prediction : Its Impact at Ku, Ka and V-band Over Some Equatorial Stations. *Journal of Informatics and Mathematical Sciences*, 9 (2), 359–374.
- Osahenvemwen, O. ., & Omorogiuwa, O. (2017). Rain Attenuation Analysis from System Operating at Ku and Ka Frequencies. *American Journal of Advanced Research*, 9829, 7–12.
- Ozuomba, S., & Kalu, C. (2015). Determination of The Dominant Fading and The Effective Fading for The Rain Zones in the ITU-R P . 838-3 Recommendation. *European Journal of Mathematics and Computer Science*, 2 (December).
- P.311-13, I.-R. (2009). *Acquisition, presentation and analysis of data in studies of tropospheric propagation*. 13. Retrieve from <https://www.itu.int/rec/R-REC-P.311/en>.
- P.530-18, I.-R. (2021). *Propagation data and prediction methods are required for the design of terrestrial line-of-sight systems*. 18. Retrieve from <https://www.itu.int/rec/R-REC-P.530-18-202109-I/en>.
- P.838-3, I.-R. (2005). *RECOMMENDATION ITU-R P.838-3 Specific attenuation model for rain for use in prediction methods*. Retrieve from <https://www.itu.int/rec/R-REC-P.838/en>.

- P.841-6, I.-R. (2019). *Conversion of annual statistics to worst-month statistics*. 6. Retrieve from <https://www.itu.int/rec/R-REC-P.841-7-202208-I/en>.
- Patra, T., & Mitra, S. K. (2020). Rain Attenuation Predicted Model for 5G Communication in Tropical Regions. *International Journal of Engineering and Advanced Technology*, 9 (3), 1151–1158.
- Pek, V., Brazda, V., & Fiser, O. (2016). First Ka and Q band results of atmospheric attenuation measurements using Alphasat receiver in the Czech Republic. *2016 26th International Conference Radioelektronika, RADIOELEKTRONIKA 2016*, 470–474.
- Pinder, J., Ippolito, L. J., Horan, S., & Feil, J. (1999). Four Years of Experimental Results from the New Mexico ACTS Propagation Terminal at 20.185 and 27.505 GHz. *IEEE Journal on Selected Areas in Communications*, 17 (2), 153–162.
- Pontes, M. S., Mello, L. da S., Souza, R. S. L. de, & B.C., E. M. (2015). Review of Rain Attenuation Studies in Tropical and Equatorial Regions in Brazil. *ICICS 2005*, 55 (1), 103–113.
- Rafiqul, I. M., Alam, M. M., Lwas, A. K., & Mohamad, S. Y. (2018). Rain rate distributions for microwave link design based on long-term measurement in Malaysia. *Indonesian Journal of Electrical Engineering and Computer Science*.
- Rahim, N. A., Mulop, H. N. A., & Badron, K. (2020). Study of tropospheric scintillation effects in Ku-band frequency for the satellite communication system. *International Journal of Electrical and Computer Engineering*, 10 (3), 3136–3144.
- Ramana, Y. R. T. V. (2015). Modeling Aspects of Fade at Ku Band of Frequencies. *International Journal of Research in Electronics*, 2 (2), 13–15.
- Renju, R., C., S. R., Mishra, M. K., Kirankumar, N. V. P., & Mathew, N. (2021). Attenuation Characteristics of GSAT-14/Ka-Band Signals over the Tropical Coastal Region. *IEEE Transactions on Antennas and Propagation*, 69 (11), 7805–7810.
- Saad, N. W. M., Ismail, A. F., Badron, K., & Isa, F. (2013). Proposed Rain Fade Mitigation Technique for Ka-band Space-Earth Links in Tropical Climate. *2013 IEEE 11th Malaysia International Conference on Communication, November*, 511–516.
- Samad, A., Diba, F. D., & Choi, D.-Y. (2021). Rain Attenuation Scaling in South Korea: Experimental Results and Artificial Neural Network. *Journal of Electronic*, 1–16.
- Samad, M. A., & Choi, D. Y. (2021). Scaling of rain attenuation models: A survey. *Applied Sciences*, 11 (18).

- Samad, M. A., Diba, F. D., & Choi, D.-Y. (2021). A Survey of Rain Fade Models for Earth – Space Telecommunication Links — Taxonomy, Methods, and Comparative Study. *Journal of Remote Sensing*.
- Samat, F., & Jit Singh, M. S. (2020). Impact of Rain Attenuation to Ka-Band Signal Propagation in Tropical Region: A Study of 5-Year MEASAT-5's Beacon Measurement Data. *Wireless Personal Communications*, 112 (4), 2725–2740.
- Samat, F., & Singh, M. J. (2020). Site diversity performance in Ka-band using a 7.3-m antenna diameter at tropical climate: a comparison of prediction models. *Acta Geophysica*, 68 (4), 1213–1221.
- Samat, F., & Singh, M. S. J. (2019). Rain attenuation at tropical region-site diversity gain models' sensitivity. *Indonesian Journal of Electrical Engineering and Informatics*, 7 (3), 472–483.
- Samat, F., Singh, M. S. J., & Sountharapandian, T. (2019). Rain Attenuation Prediction Model Assessment on 3-Year Ka-Band Signal of MEASAT-5 at Tropical Region Using 7.3-m Antenna. *Journal of Metrology Society of India*.
- Sany, S. B. T., Tajfard, M., Rezayi, M., Rahman, M. A., & Hashim, R. (2018). The west coast of peninsular Malaysia. *World Seas: An Environmental Evaluation Volume II: The Indian Ocean to the Pacific* (Second Edi). Elsevier Ltd.
- SatFinder. (2018). *SatFinder - Apps on Google Play*.
- Semire, F. A., Mohd-Mokhtar, R., Ismail, W., Mohamad, N., & Mandeep, J. S. (2013). Improved rain attenuation reduction factors for tropical regions. *International Conference on Space Science and Communication, IconSpace*.
- Shrestha, S., & Choi, D.-Y. (2017a). Characterization of Rain Specific Attenuation and Frequency Scaling Method for Satellite Communication in South Korea. *International Journal of Antennas and Propagation*.
- Shrestha, S., & Choi, D. (2017b). Rain attenuation statistics over millimetre wave bands in South Korea. *Journal of Atmospheric and Solar-Terrestrial Physics*, 1–10.
- Shrestha, S., & Choi, D. Y. (2019). Rain Attenuation Study at Ku-Band over Earth-Space Path in South Korea. *Advances in Astronomy*, 2019, 29–34.
- Shrestha, S., & Choi, D. Y. (2018). Diurnal and monthly variations of rain rate and rain attenuation on Ka-band satellite communication in South Korea. *Progress In Electromagnetics Research B*, 80 (February), 151–171.
- Shrestha, S., Nadeem, I., Ghimire, J., Kim, S. W., Yu, H. G., & Choi, D. Y. (2017). Seasonal and diurnal variations of rain attenuation measured with the Koreasat 6 at 20.73 GHz. *International Conference on Information and Communication Technology Convergence: ICT Convergence Technologies Leading the Fourth Industrial Revolution, ICTC 2017, 2017-Decem*, 935–940.

- Singh, E. S., Singh, E. I., & Singh, E. J. (2018). A Review on Rain Fade and Signal Attenuation by Rain in Ku and Ka-Band Satellite Communication at MGC Campus Punjab India. *International Journal of Trend in Scientific Research and Development, Volume-2*(Issue-6), 825–828.
- Singh, M. J., & Saleh, W. (2021). Comparison of Rain Attenuation Model for Equatorial Climate. *7th International Conference on Space Science and Communication (IconSpace)*, 275–280.
- Stutzman, W. L., & Dishman, W. K. (1982). A Simple Model for The Estimation Of Rain-Induced Attenuation Along Paths At Millimetre Wavelengths Lowing Was Identified. *Radio Science*, 17 (6), 1465–1476.
- Sudarshana, K. P. S., & Samarasinghe, A. T. L. K. (2011). Rain rate and rain attenuation estimation for Ku band satellite communications over Sri Lanka. *2011 6th International Conference on Industrial and Information Systems, ICIIIS 2011 - Conference Proceedings*, 1–6.
- Sujimol, M. R., Acharya, R., & Shahana, K. (2019). *Prediction and Estimation of Rain attenuation of Ka-Band signals*. 46 (March), 2019.
- Sujimol, M. R., Acharya, R., Singh, G., & Gupta, R. K. (2015). Rain attenuation using Ka and Ku band frequency beacons at Delhi Earth Station. *Indian Journal of Radio and Space Physics*, 44 (March), 45–50.
- Suryana, J., Utoro, S., Tanaka, K., Igarashi, K., & Iida, M. (2005). Study of prediction models compared with the measurement results of rainfall rate and Ku-band rain attenuation at Indonesian tropical cities. *2005 Fifth International Conference on Information, Communications and Signal Processing, 2005*, 1580–1584.
- Tashan, W., Shayea, I., Aldirmaz-Colak, S., Rahman, T. A., El-Saleh, A. A., & Roslee, M. (2021). Rain Rate and Rain Attenuation Over Millimeter Waves in Tropical Regions Based on Real Measurements. *15th IEEE Malaysia International Conference on Communications: Emerging Technologies in IoT and 5G, MICC 2021 - Proceedings*, 120–125.
- Timeanddate. (2022). *Weather for Cyberjaya, Malaysia*. Retrieve from <https://www.timeanddate.com/weather/@6930887>
- Ting, T. S., & Mandeep, J. S. (2014). Analysis of worst-month relationship with annual rain attenuation in Malaysia. *Research Journal of Applied Sciences, Engineering and Technology*, 7 (7), 1267–1269.
- Tomaz, L. M., Capsoni, C., & Luini, L. (2018). Scaling Rain Attenuation as a Function of the Link Elevation. *2018 2nd URSI Atlantic Radio Science Meeting, AT-RASC 2018, June*, 1–4.
- Toriola, W. A., Ojo, J. S., & Ashidi, A. G. (2021). Characterization of rain specific

- attenuation and frequency scaling technique for satellite communication systems in a tropical location. *Journal of Physics: Conference Series*, 2034 (1).
- Ulaganathen, K., & Assis, M. S. (2015). Rain attenuation measurements in Malaysia. *2015 1st URSI Atlantic Radio Science Conference (URSI AT-RASC)*, 1–1.
- Ulaganathen, K., Islam, M. R., Abdullah, K., & Tharek, A. R. (2015). Rain attenuation prediction for higher frequencies in microwave communication using frequency scaling technique. *Proceedings - 5th International Conference on Computer and Communication Engineering: Emerging Technologies via Comp-Unication Convergence, ICCCE 2014*, 217–219.
- Ulaganathen, K., Rahman, T. A., Rahim, S. K. A., & Islam, R. M. (2013). Review of rain attenuation studies in tropical and equatorial regions in Malaysia: An overview. *IEEE Antennas and Propagation Magazine*, 55 (1), 103–113.
- Ulaganathen, K., Tharek, A. R., Islam, R. M., & Abdullah, K. (2016). Case study of rain attenuation at 26 GHz in tropical regions (Malaysia) for the terrestrial link. *2015 IEEE 12th Malaysia International Conference on Communications, MICC 2015, Micc*, 252–257.
- Ulaganathen, K., Tharek, A. R., & Rafiqul Islam, M. (2013). Rain attenuation prediction using frequency scaling technique at tropical region for the terrestrial link. *Progress in Electromagnetics Research Symposium*, 191–194.
- Usha, A., & Karunakar, G. (2020). Preliminary analysis of rain attenuation and frequency scaling method for satellite communication. *Indian Journal of Physics*.
- Vidal, O., Verelst, G., Lacan, J., Albery, E., Radzik, J., & Bousquet, M. (2012). Next generation high throughput satellite system. *Proceedings - 2012 IEEE 1st AESS European Conference on Satellite Telecommunications, ESTEL 2012*, 1–7.
- Vidyardhi, A., Biswas, R., Jassal, B. S., & Shukla, A. K. (2017). Frequency scaling of slant path rain attenuation for fade mitigation in satellite communication. *2016 International Conference on Emerging Trends in Communication Technologies, ETCT 2016*.
- Vilhar, A., & Hrovat, A. (2016). First Year Analysis of ALPHASAT KA- and Q-BAND beacon Measurements in Ljubljana, Slovenia. *Ka and Broadband Communications Conference*, 1–4.
- Walter, U. (2018). *Astronautics The Physics of Space Flight -Orbit Determination*. Springer Nature Switzerland AG.
- Widjanarko, D. I., & Gunawan, D. (2017). A hybrid C/Ku-band high throughput satellite system as an optimal design for Indonesia. *Proceedings - International Conference on Signals and Systems, ICSigSys 2017*, 168–174.
- Wong, C. L., Venneker, R., Uhlenbrook, S., Jamil, a. B. M., & Zhou, Y. (2009).

- Variability of rainfall in Peninsular Malaysia. *Hydrology and Earth System Sciences Discussions*, 6 (4), 5471–5503.
- Yaccop, A. A. H., Yao, Y. D., Ismail, A. F., & Badron, K. (2013). Comparison of Ku-band satellite rain attenuation with ITU-R prediction models in the tropics. *IEEE Antennas and Propagation Society, AP-S International Symposium (Digest)*, 2006–2007.
- Yaccop, A. H., Yao, Y. D., Ismail, A. F., Khairayu, B., & Hasan, M. K. (2016). Refining Ku-Band Rain Attenuation Prediction using Local Parameters in Tropics. *Indian Journal of Science and Technology*, 9 (25).
- Yagasena. (2016). Satellite-earth rain attenuation prediction in tropical regions using the Two-Part model. *ARPJ Journal of Engineering and Applied Sciences*, 11 (5), 3236–3238.
- Yagasena, & Hassan, S. I. S. (2000). Worst-month rain attenuation statistics for satellite-earth link design at Ku-band in Malaysia. *IEEE Region 10 Annual International Conference, Proceedings/TENCON, 1*(September).
- Yee, O. S., Shafikah, N., & Mire, M. (2007). Terrestrial Microwave Link Design. Retrieve from <https://www.scribd.com/document/474666919/Terrestrial-Microwave-Link-Design-pdf#>
- Yeo, J. X., Lee, Y. H., & Ong, J. T. (2009a). Ka-band satellite beacon attenuation and rain rate measurements in Singapore comparison with ITU-R models. *IEEE Antennas and Propagation Society, AP-S International Symposium (Digest)*, 8–11.
- Yeo, J. X., Lee, Y. H., & Ong, J. T. (2009b). Modified ITU-R slant path rain attenuation model for the tropical region. *ICICS 2009 - Conference Proceedings of the 7th International Conference on Information, Communications and Signal Processing*, 40–43.
- Yeo, Jun Xiang, Lee, Y. H., & Ong, J. T. (2014). Rain attenuation prediction model for satellite communications in tropical regions. *IEEE Transactions on Antennas and Propagation*, 62 (11), 5775–5781.
- Yunus, M. M., Din, J., Jong, S. L., & Lam, H. Y. (2018). Slant Path Ka-Band rain attenuation statistics in equatorial Malaysia obtained using the stratiform convective-synthetic storm technique. *International Journal of Engineering and Technology(UAE)*, 7 (2), 22–25.
- Yunus, M. M., Din, J., Lam, H. Y., & Jong, S. L. (2016). Estimation of inter-fade duration for Ku- and Ka-band satellite communication system in equatorial Malaysia. *2016 URSI Asia-Pacific Radio Science Conference, URSI AP-RASC 2016*, 1967–1970.
- Yussuff, A. I., & Khamis, N. H. H. (2014). Rain attenuation prediction model for Lagos at millimetre-wave bands. *Journal of Atmospheric and Oceanic Technology*, 31

(3), 639–646.

- Yussuff, Abayomi I. O., & Khamis, N. H. H. (2013). Modified ITU-R Rain Attenuation Prediction Model for a Tropical Station. *Journal of Industrial and Intelligent Information*, 1 (3), 155–159.
- Yussuff, Abayomi I.O., Khamis, N. H. B. H., & Yahya, A. (2014). Performance evaluation of rain attenuation models in a tropical station. *International Journal of Electrical and Computer Engineering*, 4 (5), 782–789.
- Yussuff, Abayomi Isiaka O., Tavwo, G., & Khamis, N. H. H. (2019). Rain attenuation models at ka band for selected stations in the southwestern region of Nigeria. *Indonesian Journal of Electrical Engineering and Informatics*, 7 (1), 130–137.
- Zhou, Z. X., Li, L. W., Yeo, T. S., & Leong, M. S. (1999). Analysis of experimental results on microwave propagation in Singapore's tropical rainfall environment. *Microwave and Optical Technology Letters*, 21 (6), 470–473.
- Zhou, Z. X., Li, L. W., Yeo, T. S., & Leong, M. S. (2000). Cumulative distributions of rainfall rate and microwave attenuation in Singapore's tropical region. *Radio Science*, 35 (3), 751–756.

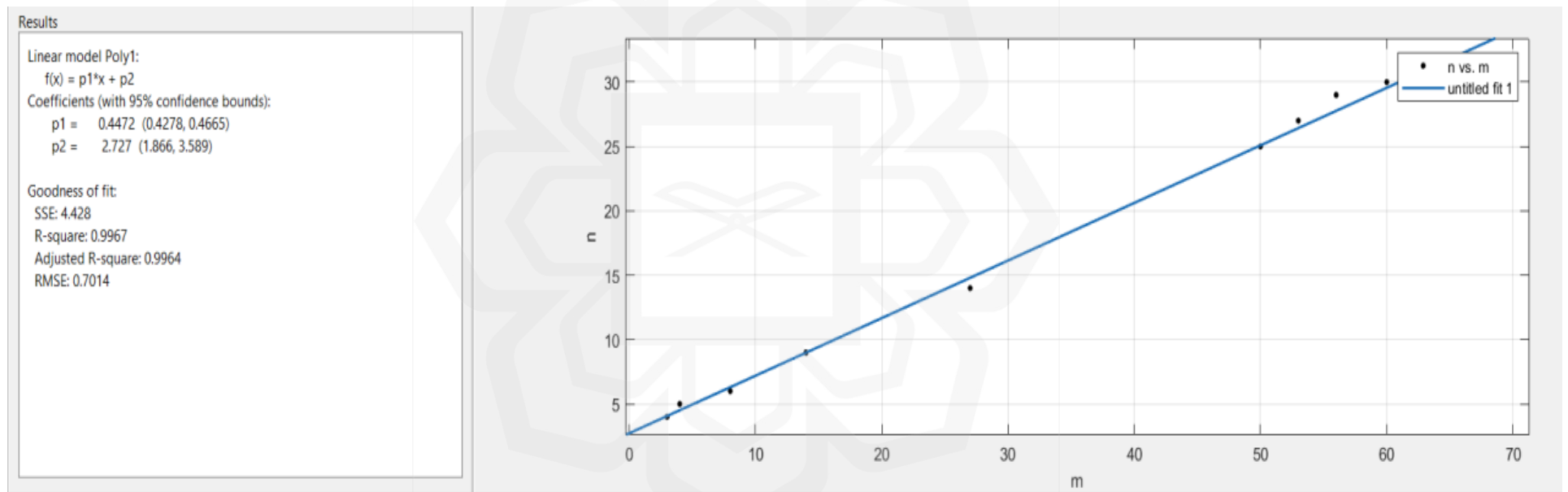
APPENDIX I: SAMPLE PDF OF KA-BAND RAIN ATTENUATION

Attenuation	Jan	Feb	Mar	Apr	May	Jun	Jul	Aug	Sep	Oct	Nov	Dec
0	30568	38880	37188	34696	28436	38880	39167	39013	38384	36014	25869	36016
1	1706	1764	6522	7723	13930	3600	2671	5311	4467	6618	15942	6349
2	9794	1016	595	486	1577	498	2438	197	153	1781	779	1782
3	2181	27	50	73	129	63	146	28	52	88	162	209
4	104	8	32	26	81	25	35	13	27	17	92	59
5	45	10	23	28	54	22	21	13	11	13	55	40
6	29	5	19	17	47	19	19	5	11	10	35	23
7	15	1	16	18	37	5	10	1	12	10	27	15
8	5	0	16	11	29	8	12	3	15	10	20	11
9	9	3	9	11	29	4	7	4	7	4	19	9
10	13	0	16	12	29	6	8	3	7	7	20	13
11	5	2	14	3	18	6	3	1	7	6	15	15
12	7	0	12	7	21	5	10	3	6	4	13	7
13	5	3	10	3	12	3	6	3	2	3	17	9
14	9	2	6	2	29	10	7	0	7	5	15	7
15	7	1	8	3	12	2	2	8	4	3	8	12
16	11	0	2	5	20	4	3	1	1	2	11	11
17	10	0	3	3	7	0	2	4	6	2	4	5
18	7	2	4	0	5	3	4	3	4	2	8	5
19	4	1	2	0	10	2	3	3	3	3	5	9
20	4	1	3	5	9	2	3	1	3	3	5	2
21	2	1	2	2	9	0	3	2	5	1	4	3
22	5	1	2	2	8	4	9	0	2	2	4	3
23	3	2	1	1	9	1	4	0	1	2	4	3
24	0	5	4	5	5	2	2	0	2	1	5	2
25	2	1	4	2	5	4	4	0	0	2	2	4
26	3	1	4	1	3	0	7	1	1	3	7	0
27	5	2	4	4	3	1	10	0	0	3	4	2
28	2	0	3	2	3	0	6	1	0	1	2	3
29	10	2	5	4	9	3	6	3	0	3	7	4
30	7	1	6	4	4	0	4	3	0	2	6	1
31	4	2	6	6	5	1	2	2	0	1	3	1
32	48	10	8	12	19	2	1	10	0	7	18	0
33	11	6	41	23	37	15	5	0	0	7	13	6
34	0	0	0	0	0	0	0	0	0	0	0	0

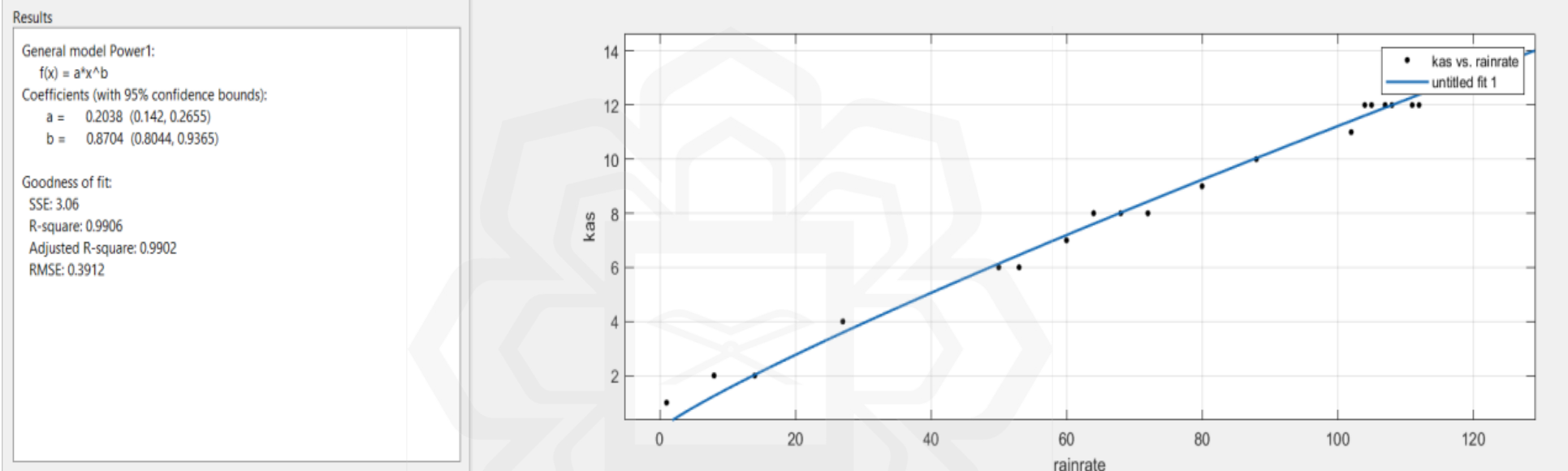
APPENDIX II: SAMPLE CDF OF KA-BAND RAIN ATTENUATION

Attenuation	Jan	Feb	Mar	Apr	May	Jun	Jul	Aug	Sep	Oct	Nov	Dec
0	44640	41760	44640	43200	44640	43200	44640	44640	43200	44640	43200	44640
1	14072	2880	7452	8504	16204	4320	5473	5627	4816	8626	17331	8624
2	12366	1116	930	781	2274	720	2802	316	349	2008	1389	2275
3	2572	100	335	295	697	222	364	119	196	227	610	493
4	391	73	285	222	568	159	218	91	144	139	448	284
5	287	65	253	196	487	134	183	78	117	122	356	225
6	242	55	230	168	433	112	162	65	106	109	301	185
7	213	50	211	151	386	93	143	60	95	99	266	162
8	198	49	195	133	349	88	133	59	83	89	239	147
9	193	49	179	122	320	80	121	56	68	79	219	136
10	184	46	170	111	291	76	114	52	61	75	200	127
11	171	46	154	99	262	70	106	49	54	68	180	114
12	166	44	140	96	244	64	103	48	47	62	165	99
13	159	44	128	89	223	59	93	45	41	58	152	92
14	154	41	118	86	211	56	87	42	39	55	135	83
15	145	39	112	84	182	46	80	42	32	50	120	76
16	138	38	104	81	170	44	78	34	28	47	112	64
17	127	38	102	76	150	40	75	33	27	45	101	53
18	117	38	99	73	143	40	73	29	21	43	97	48
19	110	36	95	73	138	37	69	26	17	41	89	43
20	106	35	93	73	128	35	66	23	14	38	84	34
21	102	34	90	68	119	33	63	22	11	35	79	32
22	100	33	88	66	110	33	60	20	6	34	75	29
23	95	32	86	64	102	29	51	20	4	32	71	26
24	92	30	85	63	93	28	47	20	3	30	67	23
25	92	25	81	58	88	26	45	20	1	29	62	21
26	90	24	77	56	83	22	41	20	1	27	60	17
27	87	23	73	55	80	22	34	19	0	24	53	17
28	82	21	69	51	77	21	24	19	0	21	49	15
29	80	21	66	49	74	21	18	18	0	20	47	12
30	70	19	61	45	65	18	12	15	0	17	40	8
31	63	18	55	41	61	18	8	12	0	15	34	7
32	59	16	49	35	56	17	6	10	0	14	31	6
33	11	6	41	23	37	15	5	0	0	7	13	6
34	0	0	0	0	0	0	0	0	0	0	0	0

APPENDIX III: EXTRAPOLATIONS FORMULA FOR THE KA-BAND LINK



Linear Model of Extrapolation Method by MATLAB



First-order Power Law Model of Extrapolation Method by MATLAB

Results

General model Power2:

$$f(x) = a \cdot x^b + c$$

Coefficients (with 95% confidence bounds):

a = 0.4638 (0.06625, 0.8613)

b = 0.9917 (0.7963, 1.187)

c = 2.659 (0.795, 4.524)

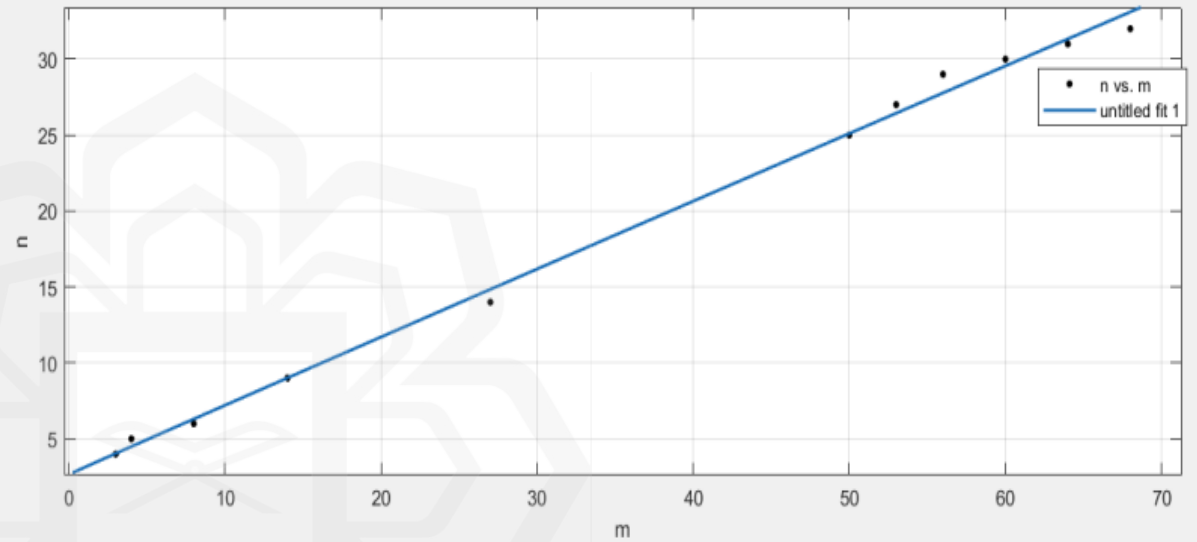
Goodness of fit:

SSE: 4.422

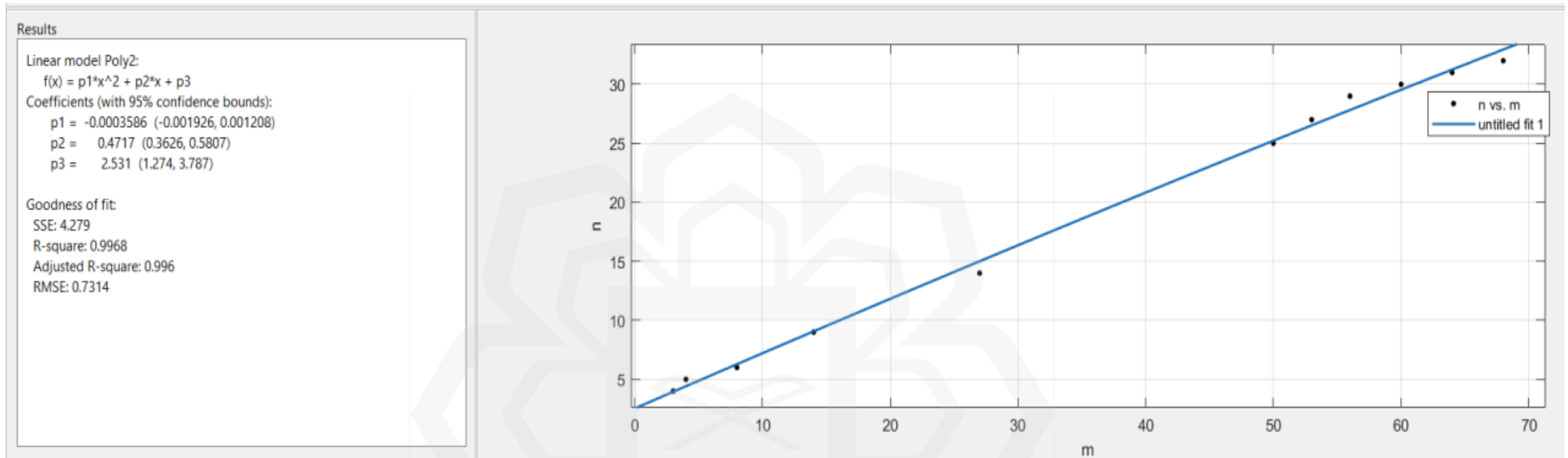
R-square: 0.9967

Adjusted R-square: 0.9959

RMSE: 0.7435



Second-order Power Law Model of Extrapolation Method by MATLAB



Second-degree Polynomial Model of Extrapolation Method by MATLAB